Geophysical Monitoring for Climatic Change

No. 16

Summary Report 1987

U.S. DEPARTMENT OF COMMERCE

NATIONAL OCEANIC AND ATMOSPHERIC ADMINISTRATION

ENVIRONMENTAL RESEARCH LABORATORIES

Geophysical Monitoring for Climactic Change No. 16

Summary Report 1987

Barry A. Bodhaine, Editor
Rita M. Rosson, Assistant Editor

Air Resources Laboratory
Geophysical Monitoring for Climatic Change

Boulder, Colorado

December 1988

U.S. DEPARTMENT OF COMMERCE
C. William Verity, Secretary

National Oceanic and Atmospheric Administration
William E. Evans, Under Secretary for Oceans and Atmosphere/Administrator

Environmental Research Laboratories
Vernon E. Derr, Director

NOTICE

Mention of a commercial company or product does not constitute an endorsement by NOAA Environmental Research Laboratories. Use for publicity or advertising purposes of information from this publication concerning proprietary products or the tests of such products is not authorized.

For sale by the National Technical Information Service, 5285 Port Royal Road
Springfield, VA 22161

Contents

GMCC Staff, 1987

Director's Office

James Peterson, Director
Bernard Mendonca, Deputy Director
Ellen Hardman, Secretary
Howard Bridgman, Guest Scientist
Dale Gillette, Physical Scientist
Jon Kahl, NRC Post Doctorate
Everett C. Nickerson, Meteorologist
Dana Roper, Summer Aid
Rita Rosson, Clerk-Typist
Pedro Sancho, Guest Scientist
Russell Schnell, CIRES
Patrick Sheridan, NRC Post Doctorate
Elizabeth Shuey, Scientific Data Clerk
Paul Stockton, Physical Science Technician
Denise Theede, Program Clerk
Thomas Watson, Physical Science Aid
Chi Zhou, CIRES

Acquisition and Data Management Group

Gary Herbert, Chief
Dee Dee Giebelhaus, Secretary
Richard Clark, Computer Programmer
Richard Cook, Physical Science Aid
Michael Ellis, Physical Science Aid
Joyce Harris, Computer Specialist
Steve Roughton, Computer Assistant
Kenneth Thaut, Electronic Technician

Aerosols and Radiation Monitoring Group

John DeLuisi, Chief
Marilyn Van Asche, Secretary
Christa Anderson, Physical Science Aid
Barry Bodhaine, Meteorologist
Mickey Cronin, Physical Science Aid
Ellsworth Dutton, Meteorologist
Rudy Haas, Mathematician
Bradley Halter, Meteorologist
David Kanzer, Physical Science Aid
Fred Kreiner, Physical Science Aid
David Longenecker, CIRES
David Massey, Physical Science Aid
Donald Nelson, Meteorologist
Timothy Quakenbush, Physical Science Aid
Patrick Reddy, CIRES
Michael Shanahan, Physical Science Aid
Lois Stearns, Meteorologist
Robert Stone, CIRES

Air Quality Group

Joseph Boatman, Chief
Dee Dee Giebelhaus, Secretary
Mark Cichy, CO-OP
Laureen Gunter, Meteorologist
Helmut Horvath, Guest Scientist
Young Kim, CIRES
Menachem Luria, NRC Post Doctorate
John Ray, CIRES
Herman Sievering, CIRES
Kurt Shallenberger, CIRES
Karen Stamminger, Physical Science Aid
Charles Van Valin, Research Chemist
Dennis Wellman, Engineer
Stan Wilkison, Computer Programmer

Carbon Cycle Group

Pieter Tans, CIRES
Lee Prendergast, Secretary
Craig Averman, CO-OP
Thomas Conway, Research Chemist
Ronald Garrett, Physical Science Aid
Thomas Greaney, CIRES
Darryl Kaurin, CO-OP
Duane Kitzis, CIRES
Patricia Lang, CIRES
Russell Martin, CIRES
Kenneth Masarie, CIRES
Paul Novelli, CIRES
Vernon Preston, CO-OP
L. Paul Steele, CIRES
John Taylor, CIRES
Kirk Thoning, CIRES
James Todd, CIRES
Lee Waterman, Research Chemist
Glen Weiler, Physical Science Aid

Monitoring Trace Gases Group

Walter Komhyr, Chief
Lee Prendergast, Secretary
Mark Anderson, Physical Science Aid
Maureen Ballard, CIRES
Sean Coleman, Physical Science Aid
Robert Evans, CIRES
Leigh Fanning, Physical Science Aid
Paul Franchois, CIRES
Robert Grass, Physicist
Timothy Kauffman, Physical Science Aid
Gloria Koenig, Computer Programmer
Laura Landrum, CIRES
Kent Leonard, CIRES
Michael O'Neill, CO-OP
Samuel Oltmans, Physicist
Frank Polacek, III, Meteorological Technician
Ronald Thorne, Engineering Technician
LaRae Williams, Physical Science Aid

Nitrous Oxide and Halocarbons Group

James Elkins, Chief
Marilyn Van Asche, Secretary
Christina Brunson, Physical Science Aid
James Butler, CIRES
Ellen DeMoney, CIRES
Keith Egan, CIRES
Brad Hall, Physical Science Technician
Thayne Thompson, Physicist

Barrow Observatory

Daniel Endres, Station Chief
James Wendell, Electronic Technician

Mauna Loa Observatory

Elmer Robinson, Director
Judith Pereira, Program Support Technician
Arne Austring, Physical Scientist
Lynne Borman, Physical Science Aid
John Chin, Physicist
Thomas DeFoor, Electronic Engineer
Thomas Garcia, Meteorological Technician
Barbara Kerecman, Data Clerk
Darryl Kuniyuki, NOAA Jr. Fellow
Mamoru Shibata, Electronic Technician
Alan Yoshinaga, Chemist

Samoa Observatory

Steven Ryan, Station Chief
M. Emily Wilson, Electronic Technician

South Pole Observatory

Clifford Wilson, NOAA Corps, Station Chief
Scott Kuester, NOAA Corps, Station Chief
Ted Mullen, Electronic Technician
Patrick Reitelbach, Electronic Technician

GMCC Station Information

Name:	**Barrow (BRW)**	**Mauna Loa (MLO)**
Latitude:	71.3233	19.533
Longitude:	156.6067	155.578
Elevation:	0 km	3.4 km
Time Zone:	GMT -9	GMT -10
Office Hours:	8:00 am-5:00 pm	8:00 am-5:00 pm
Telephone		
Office hours:	(907) 852-6500	(808) 961-3788
After hours:	(907) 852-6500	(808) 961-3788
Postal Address:	Officer in Charge NOAA/ERL/ARL/GMCC Pouch 8888 Barrow, AK 99723	U.S. Dept. of Commerce NOAA - Mauna Loa Observatory P.O. Box 275 Hilo, HI 96720
Freight Address:		U.S. Dept. of Commerce NOAA - Mauna Loa Observatory 154 Waianuenue Ave. Hilo, HI 96720

Name:	**Samoa (SMO)**	**South Pole (SPO)**
Latitude:	-14.2522	-90.000
Longitude:	170.5628	0.000
Elevation:	0.03 km	2.8 km
Time Zone:	GMT -11	GMT +12
Office Hours:	8:00 am-5:00 pm	8:00 am - 5:00 pm
Telephone:		
Office hours:	011-(684) 622-7455	Relayed through GMCC Boulder
After hours:	011-(684) 699-9953	
Postal Address:	U.S. Dept. of Commerce NOAA - GMCC Samoa Observatory P.O. Box 2568 Pago Pago, American Samoa 96799	Officer in Charge, GMCC Program Box 400 USARP C/O NAVSUPPFORANTARCTICA FPO San Francisco, CA 96692 ATTN: South Pole #S-257 E. Crozer

GEOPHYSICAL MONITORING FOR CLIMATIC CHANGE

NO. 16

SUMMARY REPORT 1987

1. Summary

At MLO, major additions were gas chromatographs for continuous in situ measurements of methane and certain halocarbons. The staff supported 24 cooperative projects from university and other-agency investigators. Lidar measurements of stratospheric aerosol showed continued decay toward background and no major new injections of volcanic dust. At BRW, the frequency of ozonesonde balloon profiles was enhanced during winter-spring to look for stratospheric ozone depletion. Numerous improvements were made to facilities at BRW, SMO, and SPO. The major change at SPO was to raise the Clean Air Facility by about 3.7 m, thus lengthening its lifetime by some 10 years before it becomes covered by drifting snow.

The ongoing GMCC core measurement programs continued. They include CO_2 and CH_4 from the flask network and observatories; total column ozone; ozone vertical distribution by ECC sonde and Umkehr technique; surface ozone; stratospheric water vapor by balloon soundings at Boulder; CFC-11, CFC-12 and N_2O from flask samples and observatory analyzers; stratospheric aerosols at MLO using lidar; aerosol light scattering; CN concentration; direct and diffuse solar and infrared radiation; meteorological variables; and chemistry of precipitation.

In the Aerosols and Radiation Monitoring Group, linear trends of CN concentration and particle scattering for the full records (up to 14 years in length) at the four observatories are all not statistically significant from zero. The major features in the measurements of aerosol optical depth, turbidity and incident solar radiation over the last 10 years are the very notable effects beginning in 1982 from the eruption of El Chichon. Two active cavity radiometers were characterized for U.S. representation in the world standard group maintained by WMO. An objective method of calculating errors to Umkehr ozone profiles due to stratospheric aerosol interference was developed and applied to a selected set of global Umkehr data. Results from the analysis, which are in agreement with theoretical model output from Lawrence Livermore Laboratory, show average ozone depletion at 35 km altitude for the period 1979-1986 of about 8%.

The Carbon Cycle Group continued regular atmospheric sampling of CO_2 and CH_4 at the observatories and another 22 cooperative sites with in situ analyzers and flask samples. Concentrations in 1987 increased compared with 1986, by about 1.7 ppm and 12 ppb for CO_2 and CH_4, respectively. Continuous measurements of CH_4 at BRW during springtime showed it to be correlated with CO_2 and aerosol black carbon, suggesting a common source or source region for all three species. Installation of an in situ CH_4 analyzer at MLO yielded intriguing results, showing rather large variability corresponding to time periods of 12-14 days.

The Monitoring Trace Gases Group continued Dobson total ozone measurements at 16 sites and international Dobson calibration work. Assessment of the calibration history of the World Primary Standard Dobson instrument showed very high stability since 1976, having calibration uncertainty of only ± 0.5%. Reassessment of the complete Dobson record from MLO showed increasing total ozone from 1964 to 1974 at about 0.37% per year, and decreasing amounts since then at about the same rate. Ozonesonde and total ozone measurements from SPO throughout the year gave clear definition of the Antarctic ozone hole; record low total ozone amounts were measured during September-November. The Group also continued regular balloon ozonesonde profiles at BRW, MLO, SMO, and Boulder; Umkehr ozone profiles at six locations; surface ozone at the observatories; and in situ stratospheric water vapor profiles at Boulder.

The Acquisition and Data Management Group continued regular meteorological measurements at the observatories. Annual surface wind rose patterns were similar to long-term climatologies, but the mature stage of the 1987 ENSO event evidently did cause some anomalous weather patterns and extreme events at the observatories. Numerous isobaric and isentropic air mass trajectories were calculated for NOAA and affiliate researchers. A special trajectory project supported the SPO aerosol study whereby measured aerosol variability was clearly linked to changes in air mass transport over Antarctica.

The Air Quality Group continued participation in the National Acid Precipitation Assessment Program and several other field programs making use of their NOAA King Air research aircraft, which they have extensively modified and modernized for meteorological and chemical airborne research. Highlights included new characterization of H_2O_2 concentrations by long latitudinal sampling profiles and measurements of DMS over the Gulf of Mexico and southern United States that suggested DMS is the principal source of SO_2 in the marine atmosphere.

The Nitrous Oxide and Halocarbons Group continued flask sampling of CFC-11, CFC-12, and N_2O, and improvement of performance of newly installed automated gas chromatographs for in situ sampling of halocarbons and N_2O at the observatories. The rate of increase of CFC-11 and CFC-12 continued at about 4% per year. The Group undertook a major expeditionary effort through participation in SAGA II, a joint US-USSR sea cruise over the western Pacific and Indian

Oceans. More than 1000 measurements were made of a variety of trace gases in the air and surface water, yielding a high-quality data set that is giving new information on the spatial distribution and air-sea exchange of these species.

Within the Director's Office, NAPAP research included development of a model to estimate the flux of dust to the atmosphere, primarily via wind erosion, for use in an inventory of alkaline elements in acid/base balance studies of precipitation. Areas of maximum dust production in the United States include the region from western Texas to western Nebraska, the valley of the Red River of the North, and northern Montana. Analyses of AGASP measurements led to numerous publications. A follow-on study incorporating BRW surface ozone and solar radiation data indicated that bromine plays an important role in Arctic ozone photochemistry and the very low ozone measured there during March-May. Many scientists used the observatories for cooperative research; several of their projects are summarized.

2. Observatory Reports

2.1. Mauna Loa

2.1.1. Facilities

The 1987 observational year was especially notable for several important upgrades of observatory instrumentation. In April an automated Carle GC was installed to provide ambient air samples each 24 minutes for CH_4, CO, and CO_2. A second complex automated halocarbon GC system was installed in June for 3-hourly concentration measurements of the halocarbons CFC-11, CFC-12, CCl_4, and CH_3CCl_3, as well as for N_2O. The Carle GC system replaced an earlier GC that provided only CO_2 and CH_4 concentration measurements. The halocarbon-N_2O system supplements the ongoing weekly flask sampling program, which has provided data since 1977.

The MLO CO_2 sampling program was upgraded in August when a Siemens Ultramat-3 replaced the URAS-2 instrument system. The Siemens system is also a nondispersive infrared system, but with improved design and electronic systems it provides a much improved CO_2 concentration record. The URAS-2 had been in essentially continuous operation at MLO since the spring of 1974.

In September an electronic engineer joined the MLO staff. He is responsible for ozonesonde operations and for the calibration and maintenance of the MLO Dobson spectrophotometer and the Dasibi surface ozone system; he also has observing and engineering duties.

Data tapes from the three main CAMS units are changed once or twice a month. Before these tapes are sent to GMCC Boulder, copies are made and kept at MLO. The copies are used to prepare monthly plots of hourly provisional CAMS data. These provisional data plots provide a "quick look" review of the month's data from which the general trends of the observations can be ascertained and periods warranting special review can be identified. The plots of provisional data are included in the MLO monthly activity reports, but they are not for general publication.

Lidar operations and ozonesonde flights were carried out on an approximately weekly schedule. Both programs provide ground-truth data for NOAA NESDIS satellite observational systems. The lidar data showed that stratospheric aerosol concentrations gradually decreased during the year and that there were no identifiable new volcanic episodes.

In late April the Soviet oceanographic research ship *Akademik Korolev* called at Hilo to load a contingent of American atmospheric and oceanographic scientists for a joint U.S.-U.S.S.R. scientific study. The U.S. scientific party included GMCC and other NOAA scientists as well as a number of university researchers. After about a 3-mo cruise with port calls in Wellington, New Zealand, and Singapore, the *Korolev* returned to Hilo in late July to disembark the U.S. scientific team and their equipment.

The installation and instrumentation of the 40-m tower at MLO has resulted in considerable reconfiguration of the air sampling intake lines to various monitoring instruments. Table 2.1 shows the number, location, and composition of the inlet lines for the GMCC and SIO monitoring instruments. For most instruments sampling from the 40-m tower, inlet lines of Dekoron 3/8-in-OD tubing have replaced the aluminum tubing previously used. The MLO air intake stack has been described by Komhyr (1983).

2.1.2. Programs

The principal programs conducted at MLO during 1987 are listed in Table 2.2. The programs that are carried out at MLO for non-GMCC scientists are listed under Cooperative Programs. Brief comments on some of the individual GMCC programs follow.

TABLE 2.1. MLO Air Sampling Intake Lines, Locations and Composition (as of early 1988)

No.	Height	Location	Composition
		GMCC Siemens CO_2 Analyzer	
1	40 m (126 ft)	E side of tower	Dekoron*
2	24 m (80 ft)	NE corner of tower	Dekoron*
		SIO Appied Physics CO_2 Analyzer	
1	24 m (80 ft)	NE corner of tower	Dekoran*
2†	6 m (20 ft)	300 m W of building	Dekoron*
3‡	15 m (50 ft)	150 m SE of building	Dekoron*
4	40 m (126 ft)	E side of tower	Dekoron*
5	24 m (80 ft)	NE corner of tower	Aluminum
		Carle CH_4-CO-CO_2 Gas Chromatograph	
1, 2	40 m (126 ft)	NE corner of tower	Dekoron*
		Halocarbon-N_2O Gas Chromatograph	
1	12.2 m (40 ft)	GMCC main building stainless-steel stack	Stainless steel
		Dasibi O_3 Analyzer	
1	12.2 m (40 ft)	GMCC main building stainless-steel stack	Teflon tube
		G.E. CNC	
1	12.2 m (40 ft)	GMCC main building aluminum stack	Teflon tube
		Four-Wavelength Nephelometer	
1	12.2 m (40 ft)	GMCC main building aluminum stack	1.5-in-OD plastic inlet

*Dekoron refers to Eaton Dekoron Type 1300, 3/8-in-OD tubing. The outer surface is a rugged plastic; inside is a light aluminum tube lined with a thin plastic material. The Dekoron lines appear to be non-reactive for the gaseous constituents sampled at MLO.

†Daytime intake.

‡Nighttime intake.

TABLE 2.2. Summary of Sampling Programs at MLO in 1987

Program	Instrument	Sampling Frequency	Remarks
Gases			
CO_2	URAS-2 IR analyzer*	Continuous	MLO; discontinued Aug. 5
	Siemens Ultramat-3 IR analyzer*	Continuous	MLO; installed Aug. 5
	3-L glass flasks	1 pair wk^{-1}	MLO and Kumukahi
	0.5-L glass flasks, through analyzer	1 pair wk^{-1}	MLO
CO_2, CH_4	0.5-L glass flasks, P3	1 pair wk^{-1}	MLO and Kumukahi
	GC	Continuous	MLO; discontinued April
CH_4, CO, CO_2	Carle automated GC	1 sample (24 min)$^{-1}$	MLO; installed April
Surface O_3	Dasibi ozone meter*	Continuous	MLO
Total O_3	Dobson spectrophotometer no. 76	3 day^{-1}	Weekdays
O_3 profile	Dobson spectrophotometer no. 76	2 day^{-1}	Umkehr method
	Balloonborne ECC sonde	1 wk^{-1}	From Hilo Airport
CFC-11, CFC-12, N_2O,	300-mL stainless steel flasks	1 pair wk^{-1}	MLO
CFC-11, CFC-12, N_2O CCl_4, CH_3CCl_3	HP5890 automated GC	1 sample (3 hr)$^{-1}$	MLO; installed June
N_2O	Shimadzu automated GC	1 sample (3 hr)$^{-1}$	MLO; installed June
SO_2	Flame photometric analyzer	Continuous	MLO; Installed Aug.
Aerosols			
Condensation nuclei	Pollak CNC	1 day^{-1}	Weekdays
	G.E. CNC*	Continuous	
Optical properties	Four-wavelength nephelometer*	Continuous	450, 550, 700, 850 nm
Stratospheric aerosols	Lidar	Discrete	694.3 nm; average 1 profile wk^{-1}
Solar Radiation			
Global irradiance	Eppley pyranometers (3) with Q, OG1, and RG8 filters*	Continuous	
Direct irradiance	Eppley pyrheliometers (2) with Q filter*	Continuous	
	Eppley pyrheliometer with Q, OG1, RG2, and RG8 filters	3 day^{-1}	
	Eppley /Kendall active cavity radiometer	1 mo^{-1}	
Diffuse irradiance	Eppley pyranometer with shading disk and Q filter*	Continuous	
Turbidity	J-series sunphotometers, J-202 and J-314	3 day^{-1}	380, 500, 778, 862 nm; narrowband; discontinued July
	Mainz II sunphotometer, M119 and M120	3 day^{-1}	380, 412, 500, 675, 862 nm; M119 operational July-Oct.; M120 installed Oct.
	PMOD three-wavelength sunphotometer*	Continuous	380, 500, 778 nm; narrowband
Meteorology			
Air temperature	Aspirated thermistor*	Continuous	2- and 40-m heights
	Max.-min. thermometers	1 day^{-1}	Standard shelter
	Hygrothermograph	Continuous	MLO and Kulani Mauka
Temperature gradient	Aspirated thermistors*	Continuous	2- and 40-m heights
Dewpoint temperature	Depoint hygrometer*	Continuous	2-m height
Relative humidity	Hygrothermograph	Continuous	MLO and Kulani Mauka
Pressure	Capacitance transducer*	Continuous	
	Microbarograph	Continuous	
	Mecurial barometer	1 day^{-1}	
Wind (speed and direction)	Bendix Aerovane*	Continuous	8.5- and 40-m heights
Precipitation	Rain gauge, 8-in	1 day^{-1}	
	Rain gauge, 8-in	1 wk^{-1}	Kulani Mauka
	Rain gauge, weighing bucket	Continuous	Weekly chart record
	Rain gauge, tipping bucket*	Continuous	
Total precipitable water	Foskett IR hygrometer*	Continuous	
	HAO IR hygrometer*	Continuous	Discontinued July

TABLE 2.2. (continued)

Program	Instrument	Sampling Frequency	Remarks
Precipitation Chemistry			
pH	pH meter, Hilo lab.	Weekly	Rainwater collections, 3 sites
Conductivity	Conductivity bridge, Hilo lab.	Weekly	Rainwater collections, 3 sites
Chemical components	Ion chromatograph, Hilo lab.	Weekly	Rainwater collections, 3 sites
Cooperative Programs			
CO_2 (SIO)	IR analyzer (Applied Physics)	Continuous	
CO_2, ^{13}C, N_2O (SIO)	5-L evacuated glass flasks	1 pair wk^{-1}	MLO and Kumukahi
Surface SO_2 (EPA)	Chemical bubbler system	Every 12 days	24-h (0000-2400) sample
CO_2, CO, CH_4, $^{13}C/^{12}C$ (CSIRO)	Pressurized glass flask sample	1 mo^{-1}	MLO
CO_2, CH_4, and other trace gases (NCAR)	Evacuated stainless steel flasks	1 pair wk^{-1}	MLO and Kumukahi
Total suspended particles (DOE)	High-volume sampler	Continuous	1 filter wk^{-1}
Total O_3, SO_2 (AES Canada)	Brewer spectrophotometer, MK-I	1-3 day^{-1}	MLO, discontinued March
	Brewer spectrophotometer, MK-II; Umkehr-automated	Continuous	MLO, installed March
Turbidity (AES Canada)	Sonotek sunphotometer no. 5698	1-3 day^{-1}	MLO
CH_4 ($^{13}C/^{12}C$) (Univ. of Washington)	35-L evacuated flask	1 mo^{-1}	MLO
Total suspended particles (EPA)	High-volume sampler	Every 12 days	24-h (0000-2400) sample
Ultraviolet radiation (Temple Univ.)	UV radiometer (erythema)	Continuous	Radiation responsible for sunburning of skin
Ultraviolet radiation (Smithsonian)	8-wavelength UV radiometer	Continuous	290-325 nm, narrowband
Solar variability (Univ. of Arizona)	Solar spectroradiometer	Discrete	Program began Sept. 1985
Solar aureole intensity (CSU)	Multi-aperture tracking photometer	Continuous	2, 5, 10, 20, 30° fields of view
Precipitation collection (DOE)	Exposed collection pails	Continuous	MLO
Precipitation collection (ISWS)	Aerochemetric automatic collector	Continuous	Analysis for ^{7}Be and ^{10}Be
Precipitation collection (Univ. of Virginia)	Aerochemetric automatic collector	Continuous	Organic acid analysis
Wet-dry deposition (ISWS)	Aerochemetric automatic collector	Continuous	NADP
Aerosol chemistry (Univ. of Washington)	Nuclepore filters	Continuous	Upslope-downslope discrimination
^{13}C (USGS, Denver)	10-L stainless steel flasks	Biweekly	MLO
Various trace gases (OGC)	Stainless steel flasks	1 set wk^{-1} (3 flasks)	MLO and Kumukahi
HNO_3, HCl vapor, and aerosols (URI)	Filter system	Four 2-wk periods yr^{-1}	MLO
IR solar spectra (Univ. of Denver)	Interferometer	Feb. and July 1987 1 wk each	MLO
Sunphotometery (NASA Goddard)	Sunphotometer calibrations	Oct. 1987, 1 wk	MLO

*Data from this instrument recorded and processed by CAMS.

Carbon Dioxide

The GMCC and the SIO Applied Physics NDIR analyzers were operated in parallel without major problems during the year. The average CO_2 concentration for the year was about 348.6 ppm, and the rate of CO_2 increase was approximately 1.9 ppm yr^{-1}. This provisional value is noticeably larger than the long-term MLO CO_2 rate of increase of 1.42 ppm yr^{-1} [*Schnell and Rosson*, 1987].

A Siemens Ultramat-3 IR analyzer replaced the URAS-2 IR analyzer on August 5, 1988. The URAS-2 analyzer had been in use at MLO since May 1974. A series of comparisons between the two analyzers was performed before the removal of the

URAS-2 analyzer. The analyzers were first operated independently but using the same synthetic air as reference gases, sharing the same 25-m (80-ft) air intake, and using the same freeze trap at -60° to -70°C. After this side-by-side operation indicated a possible accuracy problem, a second test was run using a double freeze trap connected in series. In these tests URAS-2 values were 0.3 ppm higher than the Siemens values. When the analyzers were interchanged with all the plumbing configuration remaining untouched, the URAS-2 values were still consistently 0.3 ppm higher than the Siemens'. However, when a set of natural air standards was used to replace the usual operational synthetic air as the reference gases, the Siemens and URAS-2 values showed no consistent concentration difference. Experiments are being undertaken in Boulder GMCC laboratories to explain the differences in ambient air response observed for the two instruments.

The weekly CO_2 flask samplings at MLO and Cape Kumukahi were continued without problems and with no changes in protocol.

As in previous years, outgassing from several volcanic vents near the summit and along the northeast rift of Mauna Loa caused observable disturbances in some of the CO_2 records. These occur during the nocturnal downslope wind regime, most frequently between 0000 and 0800 LST. Visual scanning of the recorder chart records showed the frequency of disturbed periods; these have been accumulated into monthly totals (Table 2.3). Note that these frequencies indicate only the number of days of occurrence and not the number or percentage of hours of data that are affected. Periods when the MLO CO_2 record is affected in this manner by volcanic events are not included in the determination of background CO_2 concentrations.

The 1987 average frequency of outgassing episodes was 38%, which continues the downward trend of venting influences seen in prior years (e.g., 1984, 61%; 1985, 48%; 1986, 44%). The 5-yr average prior to the March 25, 1984, Mauna Loa eruption was 27%. The lower frequencies observed in February and March are probably due to lower frequencies of southeasterly winds during those 2 months.

Surface Ozone

The Dasibi ozone monitor samples directly from the air intake stack and is recorded by the CAMS. In 1987 the instrument was out of service from April 10 to July 25 because of the nonavailability of replacement electronic components. Otherwise continuous ambient data were obtained.

Total Ozone

The regular program of Dobson measurements and Umkehr profiles using Dobson spectrophotometer no. 76 was augmented in May, June, and July by a program of Langley plot calibrations of the WMO world standard Dobson instrument, no. 83. During this calibration program, intercomparison calibrations with no. 83 were also carried out on the MLO Dobson no. 76 and the SMO Dobson no. 42.

Ozone Profiles

In the MLO ozonesonde program there were 53 launches, approximately weekly, from the NWS Hilo airport station. Of these, 48 produced satisfactory profile data. Of the five that were unsuccessful, four were due to instrument failure after launch and one was due to the weather. The average flight altitude for the 48 successful flights was 41.4 km (2.5 mb) and ranged between 39.6 km (3.3 mb) and 44.9 km (1.6 mb). All but three of the 48 profiles exceeded the target altitude of 40 km (3.0 mb).

Aerosols

As in prior years, the MLO aerosol program consisted of both surface and stratospheric aerosol measurements. Continuous measurements of CN concentration and aerosol scattering extinction were made by the G.E. CNC and the four-wavelength nephelometer, respectively. Both systems were recorded by the CAMS. Operation of both instruments was essentially continuous through the year, having only minor periods of downtime. The Pollak CNC was operated daily to provide a calibration check for the G.E. CNC.

Lidar data were obtained on 45 nights during the year. Weather permitting, observations were coordinated with overpasses of the SAGE II satellite. Stratospheric aerosol concentrations continued to decay toward background, as shown by the decrease in average non-Rayleigh backscatter (NRBS) from an average of 1.4×10^{-4} sr^{-1} in January 1987 to an average value of 1.0×10^{-4} sr^{-1} in December. Prior to the eruption of the Columbian volcano Ruiz in November 1985, the NRBS was averaging 1.1×10^{-4} sr^{-1}. No new volcanic stratospheric aerosol clouds were observed by the MLO lidar in 1987.

Solar Radiation

In July the older J-series sunphotometers were replaced with a single Mainz II (M119) five-channel sunphotometer. The new instrument is easier to use and has more accurate aiming optics than the J-series units. The five filters in the Mainz II units are narrowband filters at approximately 380, 412, 500, 675, and 862 nm. In October, a Mainz II M120 replaced the M119 when the filter rotation mechanism malfunctioned.

The other components of the MLO solar radiation program were continued with little change from the previous year. These, as shown in Table 2.2, include normal incidence pyrheliometers and global pyranometers for total and diffuse radiation measurements. In the solar dome a variety of solar

TABLE 2.3. Monthly Occurrences of Outgassing from Volcanic Vents on Mauna Loa

	Jan.	Feb.	March	April	May	June	July	Aug.	Sept.	Oct.	Nov.	Dec.	Year
Number of days	10	2	5	9	8	12	18	19	10	16	11	18	138
Percent of days	32	7	16	30	26	40	58	61	33	52	37	30	38

measurement instruments were mounted on the active solar-tracking spar. The dome and shutter controllers malfunctioned occasionally, but repairs could generally be made readily and downtime was kept to a minimum.

The MLO solar radiation program was used frequently by non-GMCC groups for assistance in instrument calibrations and as a source for information to assist in data interpretation. Specialized long-term cooperative programs, especially in the shorter wavelength bands, augmented the MLO radiation program.

Meteorology

The MLO program of meteorological measurements was continued without major problems other than a 1-mo period of downtime for the dewpoint hygrometer. The CAMS record of weather factors was expanded with the addition of the temperature gradient between 2 m and the top of the 40-m tower and of the wind gradients between 8.5 m and 40 m; thus a continuous measure of boundary layer stability is now available for use in data interpretation.

Precipitation Chemistry

The 1987 precipitation chemistry program consisted of collections from three local sites: Hilo, 22-mile on the Saddle Road, and MLO. Collections and collector equipment changes were made at each of these sites each weekday to provide an approximation of precipitation event sampling. These samples plus rain and snow samples from the other three GMCC observatories were analyzed in the MLO Hilo laboratory. As shown in Table 2.2, the precipitation analysis protocol includes pH, conductivity, and a variety of anions and cations. Ion chromatography is used for the latter analysis. Several cooperative programs in precipitation chemistry are also carried out at MLO and serve to augment the GMCC program.

Cooperative Programs

Table 2.2 lists 24 cooperative projects supported by the GMCC MLO program. Most of these programs are long-term monitoring and sampling studies in which MLO staff assume the rudimentary housekeeping chores to maintain the operations, and the P.I. does the sample and data analysis. Classic in this cooperation between P.I. and MLO staff is the SIO CO_2 program involving both flask samples and the operation of a CO_2 analyzer. This program completes 30 years of operation at MLO in 1988, and thus this program predates the establishment of the GMCC program in 1972. The other type of cooperative program is one in which the P.I. and colleagues use MLO facilities to carry out specific short-term studies without any significant involvement of MLO staff members. The 1987 URI studies of HNO_3 and HCl, and the University of Denver IR solar spectra research are examples of this latter type of program.

All of the MLO cooperative programs listed in the 1986 *Summary Report* [*Schnell and Rosson,* 1987] were active in 1987. The SIO CO_2 analyzer was upgraded with the addition of a new data acquisition system and new sample lines. The inlet line that had been on the old high (25-m) tower was moved to a similar height on the new 40-m tower (see Table 2.1). The Canadian Atmospheric Environment Service program of total ozone and SO_2 measurements using the Brewer spectrophotometer was upgraded in March with the installation of a fully automated Brewer MK-II in place of the older, manually oriented and initiated Brewer MK-I instrument. The MK-I had been in operation at MLO since April 1982.

The program of infrared solar absorption spectra measurements made by the University of Denver in February and July showed that MLO is a favorable site for this type of measurement [*Rinsland et al.,* 1988]. The results of this program provided total vertical column amounts of 13 atmospheric gases and average tropospheric concentrations of CO_2, N_2O, CH_4, and $CHClF_2$ (CFC-22). The diurnal variations of the total column amounts of NO and NO_2 were also obtained. Spectral measurements of this type provide a permanent record of the observed atmospheric solar spectra and can be compared with spectra taken at other times and in other locations. Such comparisons can provide geographic distributions and temporal trends of a wide variety of minor and trace atmospheric constituents. As more basic information becomes available on the IR spectra of other trace constituents such as the CFCs these spectra can be reanalyzed to provide additional information.

The sampler used by URI for aerosol particle studies was moved from a surface location to the 23-m level on the new tower. Boundary layer profiles and possible surface deposition effects will be examined in this continuing program.

2.2. Barrow

2.2.1. Facilities

Another year of data was successfully collected at BRW in 1987. Scientific interest in BRW and the Arctic increased in 1987. This was manifested by visits to BRW by the NOAA Administrator in February, the NSF Polar Research Board in April and September, the Director of the Geophysical Institute of the University of Alaska in February, and others throughout the year who looked into ways to increase U.S. involvement in Arctic science. The visits focused on reviewing present Arctic research and in determining what more is needed and could be done in the Arctic in the future.

Station personnel were called on several times by the North Slope Borough/Wildlife Management for technical expertise. On several occasions GMCC personnel were also used by NWS to repair equipment. There was a change in the GMCC staff in December when one staff member was temporarily assigned to Boulder; a new electronics technician was recruited and was assigned to BRW in his place. BRW's administrative support was transferred from WASC in Seattle to MASC in Boulder at the beginning of 1987. This included hooking BRW up to the FIDO communication network in ERL, Boulder.

The BRW vehicles underwent major changes in 1987. The GSA Dodge truck was relegated to standby status early in the year after numerous problems made it too unreliable. In the summer it was replaced by a new 1985 Chevrolet Suburban provided by GSA. At year's end the new Suburban was still working well. A new Skandic 503 snowmobile was purchased in February. By the end of the year, all the old snowmobiles

and the historic Bombi were excessed and removed from the station inventory. The 1979 GMC truck, which has served as the most durable observatory transportation vehicle, received a new engine in February but needed further repairs. By the end of the year, thanks to a third-party support agreement with the Dew Line Station for vehicle maintenance on a noninterference basis, it was running better.

The Dew Line Station supply of electrical power to BRW observatory was cut off in April 1987 when a fire at the Dew Line Station destroyed more than one-third of its electrical power plant. Emergency action was required to locate and hook up an alternate power supply to the GMCC observatory. In a matter of days power was obtained to continue the measurements at BRW with minimum instrument downtime, and in a matter of months a working agreement was in place to receive commercial power from the Eskimo Corporation (UIC), which had taken over the day-to-day operation of NARL. By the end of the year, good and reliable power was still being supplied to BRW by UIC through NARL using the Barrow Borough Power Plant.

The phone lines to the observatory continue to work marginally. Every spring, during breakup, water can infiltrate into the lines feeding to the observatory and cause noisy conditions. GTE has worked on the lines several times during the year to bring temporary relief, but the problem remains. The observatory computer continues to be used as an alternate communication link with Boulder. Computer data transfer between BRW and Boulder is being planned.

The clean room at the observatory had acoustic foam installed on the remaining walls this year, helping with the noise problem at the station. The clean room was also rearranged to make better use of the small amount of room left for expansion. An air conditioning unit arrived to help with the cooling/humidity problems at the station.

The arrangement between NWS and GMCC for shared housing in BRW continued throughout 1987. Several upgrades and repairs were done in the units occupied by GMCC staff. A water heater was installed, along with a new front door, in the double-wide housing unit. Corroded fixtures were replaced in both houses. The heater system in the double-wide unit is marginal and is scheduled for replacement.

2.2.2. Programs

Table 2.4 summarizes the programs at BRW. Further discussion of some of the programs follows.

Carbon Dioxide

Several problems this year were power related and solved with simple restarts. Tanks of compressed gas were sent to BRW on the cool barge; this continues to be a good system for shipping large amounts of heavy goods to the station.

Methane

The methanizer was reconditioned early in the year and replaced in May. The HP integrator locked up twice and had to be replaced. The pure air generator also died and was replaced with canned air sent from Boulder. The results seem to be better using the canned air, so we may continue using it. The stream selection valve had to be replaced when it stopped flow on channel 3.

Surface Ozone

A new lamp was installed in the Dasibi ozone meter along with a different LED display. The old display had several burned out segments, making it hard to read. The only other occurrence of note was replacement of the pump.

Total Ozone

Observations continued without any major problems this year.

Ozone Profiles

The ozonesonde program in BRW was enhanced this spring to look for stratospheric depletion of ozone in the Arctic. A total of 54 balloons were launched this year. A member of the MTG Group was here from Boulder during the spring to launch ozonesondes during the spring Arctic haze episode.

Halocarbons and Nitrous Oxide

A new Epson printer was installed to replace the troublesome HP Think-jet printer. Bad power led to several problems this year. Several times outages were long enough that the UPS could not keep things running. The problems were solved by use of the town power. A new disk drive was installed because the old one tried to write continually to the disk even though there was nothing to write. A member of the NOAH group came from Boulder to upgrade the RITS GC and make some programming changes. He installed a Shimadzu GC, the plumbing to run it, and two tanks of calibration gas. Earlier in the year a new compressor was installed to take the place of the tanks of compressed air that turn the pneumatic valves in the GC.

Aerosols

The vacuum pump for the GE CNC was rebuilt this year. A cracked O-ring was found in the GE CNC causing erroneous readings. This was repaired and the unit ran properly the rest of the year. The Pollak CNC operated normally all year. The print head in the Leeds and Northrup recorder started sticking and causing poor-quality chart records. The trouble was traced to a worn bearing in the print head carriage; a new one was ordered and sent from Boulder.

Solar and Terestrial Radiation

The sun rose on January 24 and set on November 18, both as expected. A Teflon cable was installed on the Li-Cor tracker because the old plastic one had cracked. The HP data acquisition system was moved to a rack this year to make more space in the clean room.

Meteorology

This year's weather at BRW was characterized by extremes. Blizzards and blowing snow closed the observatory road for portions of January, February, March, and April. A new 24-h rainfall record was set in July: 1.48 in. The old record was 1 in set in October 1926. A new 24-h snowfall record was also set

Table 2.4. Summary of Sampling Programs at BRW in 1987

Program	Instrument	Sampling Frequency
Gases		
CO_2	URAS-2T IR analyzer	Continuous
	3-L glass flasks	1 pair wk^{-1}
	0.5-L glass flasks, through analyzer	1 pair wk^{-1}
CO_2, CH_4	0.5-L glass flasks, P[3]	1 pair wk^{-1}
CH_4, CO, CO_2	Carle automated GC	1 sample $(24\ min)^{-1}$
Surface O_3	Dasibi ozone meter	Continuous
Total O_3	Dobson spectrophotometer no. 91	3 day^{-1}
O_3 profile	Balloonborne ECC sonde	1 wk^{-1}
CFC-11, CFC-12, N_2O	300-mL stainless steel flasks	1 pair wk^{-1}
CFC-11, CFC-12, N_2O, CCl_4, CH_3CCl_3	HP5890 automated GC	1 sample $(3\ hr)^{-1}$
N_2O	Shimadzu automated GC	1 sample $(3\ hr)^{-1}$
Aerosols		
Condensation nuclei	Pollak CNC	1 day^{-1}
	G.E. CNC	Continuous
Optical properties	Four-wavelength nephelometer	Continuous
Solar and Terrrestrial Radiation		
Albedo	Eppley pyranomter	Continuous
Global irradiance	Eppley pyranometers with Q and RG8 filters	Continuous
Direct irradiance	Tracking NIP	Continuous
	Eppley pyrheliometer with Q, OG1, RG2, and RG8 filters	Discrete
Terrestrial (IR) radiation	Eppley pyrgeometer	Continuous
Turbidity	Sunphotometers with 380-, 500-, 778-, and 862-nm narrowband filters	Discrete
Meteorology		
Air temperature	Thermistor, 2 levels	Continuous
	Max.-min. thermometers	1 day^{-1}
Dewpoint temperature	Dewpoint hygrometer	Continuous
Pressure	Capacitance transducer	Continuous
	Mercurial barometer	Discrete
Wind (speed and direction)	Bendix Aerovane	Continuous
Precipitation	Rain gauge, tipping bucket	
Precipitation Chemistry		
pH	pH meter (samples analyzed at MLO)	Discrete
Conductivity	Conductivity bridge (samples analyzed at MLO)	2 mo^{-1}
Cooperative Programs		
Total surface particulates (DOE)	High-volume sampler (1 filter wk^{-1})	Continuous
Aerosol chemistry (URI)	High-volume sampler (2 filters wk^{-1})	Continuous
Aerosol chemistry (Univ. of Alaska)	Hi-volume filters filters wk^{-1}	Continuous
Ultraviolet radiation (Temple Univ.)	UV radiometer	Continuous
Precipitation gauge (ASCS)	Wyoming shielded precipitation gauge	2 mo^{-1}
Magnetic fields (USGS)	Magnetometer	1 station check wk^{-1})
^{13}C (USGS)	10-L stainless steel flasks	1 pair mo^{-1}
Various trace gases (OGC)	Stainless steel flasks	1 set wk^{-1} (3 flasks set^{-1})
CO_2, CH_4 and other trace gases (NCAR)	3-L stainless steel flasks	1 pair wk^{-1}
^{13}C, ^{18}O, CO_2 (CSIRO)	5-L glass flasks	1 pair $(2\ wk)^{-1}$
CO_2, ^{13}C, N_2O (SIO)	5-L evacuated glass flasks	1 pair wk^{-1}
Halocarbon monitoring (Univ. of Calif., Irvine)	Various stainless steel flasks	1 set $(3\ mo)^{-1}$
Earthquake detection (Univ. of Alaska)	Seismograph	Continuous; check site 1 wk^{-1} change tape 1 mo^{-1}
$^{13}CH_4$ ($^{13}C/^{12}C$) (Univ. of Washington)	35-L stainless steel flasks	1 $(2\ wk)^{-1}$
Atmospheric tracer experiment (ARL/Idaho Falls)	Air sample	1 wk^{-1}

this year: 5.2 in in September. The old record was 5.0 in. The total for September was 16.2 in, beating the old September record of 12.9 in. Several new low-temperature records were also set. Routine calibrations were performed, and all instruments operated normally during the year.

Precipitation Chemistry

Precipitation samples were collected this year according to instructions from ARL. After collection they were sent to MLO for analysis.

Cooperative Programs

After running for only 7 months, the pump for the DOE filter collector seized a bearing and had to be replaced.

The ANATEX project was run in cooperation with ARL/ Field Research.

The USGS equipment was checked on a regular basis. A CRT was installed to replace the one that stopped working this year.

The University of California, Irvine continues to send a person to BRW four times per year to collect air samples for CH_4 analysis.

The Soil Conservation Service rain gauge continues to operate, although it needs some repairs.

A flag was flown for NWS to check the wear resistance. The GMCC site was chosen because it is far enough away from town to determine a more accurate wear rate.

The Temple University UV meter was calibrated this year.

Some repairs were made in September to the University of Alaska filter hut.

A long-standing problem with shipping the CSIRO flasks has finally been solved. The flasks will be sent to MLO and then mailed to BRW. This solves the problems with customs in Anchorage.

2.3. Samoa

2.3.1. Facilities

SMO had a year of fairly trouble-free operation in 1987, and several construction and upgrade projects were completed. In May, a 24-ft square carport was built in front of the observatory entrance, providing shelter for the government vehicles during the day and making freight and mail loading easier during rainy periods. The upper sampling tower was primed and painted in July. Both of these projects provided jobs for people of nearby Tula village.

The station's main air conditioner was replaced in April, and a second small air conditioner was installed in the GMCC room of the EKTO building in May. With the recent addition of a gas chromatograph, the single EKTO air conditioner was unable to maintain room temperature on the hottest days; with the two units working together the room temperature can be kept stable to within 2°F.

As the solar photovoltaic system entered its fourth year of operation, a few of the 60 battery cells began to fail, and two six-cell replacement batteries were ordered to replace them. Apart from this, the system continued to perform well throughout the year.

Other projects included the paneling of the Dobson dome in August, application of wood preservative to the shingles of housing unit T-7, and installation of a plastic bed liner in the Toyota pickup. Concrete landings were poured in front of both EKTO building doors in November. In December, a sump pump was installed in series with the observatory pressure pump to eliminate the occasional priming problems with that pump. Both the Ford van and the Toyota gave a year of trouble-free service.

On January 17, a hundred-year hurricane devastated the Manua Islands 70 mi to the east, leaving over 90% of the residents homeless, and stripping all of the vegetation down to ground level. Luckily, Tutuila Island was spared, and the observatory escaped damage.

2.3.2. Programs

Table 2.5 summarizes the programs for 1987. New programs this year include the addition of a Shimadzu automated GC by GMCC to improve N_2O measurements, and the initiation of flask sampling for the U.S. Bureau of Mines to measure atmospheric helium.

Carbon Dioxide

The URAS-2T analyzer and its system operated without problems all year with the exception of the Cryocool freezer. The old unit and two spares were used throughout the year, maintaining -60°C or cooler temperatures except for a period in June and July, when the trap warmed to -30°C. By early 1988, a heavy-duty Cincinnati Sub Zero freezer was delivered; it has maintained -80°C temperatures. An experiment was performed in May to compare the effect of using a small, low-flow-volume glass freezeout trap with that of a larger, high-flow-volume trap.

In September, a special intercomparison was conducted between 0.5-L P^3 flasks with greased stopcocks and with stopcocks having a new type of O-ring.

Surface Ozone

In January, the Teflon intake line was shortened and wrapped with heat tape to eliminate condensation. Dasibi ozone meter no. 1326 was replaced by no. 1323 in October, resulting in a much improved data set.

Total Ozone

After spending 1 year in Samoa, Dobson instrument no. 65 was returned to Boulder in July and replaced by no. 42. Dobson no. 42 arrived in May, and a side-by-side comparison with no. 65 was run for 3 weeks. In early July, no. 42 was sent to MLO where it was calibrated against the world standard instrument before being returned to service in Samoa on July 29. The frequency of daily observations was increased to 4-5 per day in 1987.

Ozone Profiles

Weekly ozonesonde flights from the NWS facility in Tafuna continued in 1987, resulting in 43 total launches and a 96%

TABLE 2.5. Summary of Sampling Programs at SMO in 1987

Program	Instrument	Sampling Frequency
Gases		
CO_2	URAS-2T IR analyzer	Continuous
CO_2, CH_4	3-L glass flasks	1 pair wk^{-1}
	0.5-L glass flasks, through analyzer	1 pair wk^{-1}
	0.5-L glass flasks, P[3]	1 pair wk^{-1}
Surface O_3	Dasibi ozone meter	Continuous
Total O_3	Dobson spectrophotometer no. 42 or 65	3 day^{-1}
O_3 profile	Balloon borne ECC sonde	1 wk^{-1}
CFC-11, CFC-12, N_2O	300-mL stainless steel flasks	1 pair wk^{-1}
CFC-11, CFC-12, N_2O, CCl_4, CH_3CCl_3	HP5890 automated GC	1 sample $(3\ hr)^{-1}$
N_2O	Shimadzu automated GC	1 sample $(3\ hr)^{-1}$
Aerosols		
Condensation nuclei	Pollak CNC	1 day^{-1}
	G.E. CNC	Continuous
Optical properties	Four-wavelength nephelometer	Continuous
Solar Radiation		
Global irradiance	Eppley pyranometers with Q and RG8 filters	Continuous
	Eppley pyranometers with Q filters on tilted mounts	Continuous
Direct irradiance	Eppley pyrheliometer with Q filter	Continuous
	Eppley pyrheliometer with Q, OG1, RG2, and RG8 filters	Discrete
Turbidity	Sunphotometers with 380-, 500-, 778-, and 862-nm narrowband filters	Discrete
Meteorology		
Air temperature	Thermistors (2)	Continuous
	Max.-min. thermometers	1 day^{-1}
Pressure	Capacitance transducer	Continuous
	Microbarograph	Discrete
	Mercurial barometer	1 wk^{-1}
Wind (speed and direction)	Bendix Aerovane	Continuous
Precipitation	Rain gauge, weighing bucket	Continuous
	Rain guage tipping bucket	Continuous
	Plastic bulk rain guage	1 day^{-1}
Precipitation Chemistry		
pH	Fisher model 805 meter	1 day^{-1} (GMCC); 1 wk^{-1} (NADP)
Conductivity	Beckman model RC-16C meter	1 day^{-1} (GMCC); 1 wk^{-1} (NADP)
Cooperative Programs		
CO_2, ^{13}C, N_2O (SIO)	5-L evacuated glass flasks	3 flasks wk^{-1}
ALE project: CFC-11, CFC-12, N_2O, CH_3CCl_3, CCl_4 (OGC)	HP5880 gas chromatograph	1 h^{-1}
Various trace gases (OGC)	Stainless steel flasks	3 flasks wk^{-1} (3 flasks set^{-1})
^{13}C, ^{18}O, CO_2 (CSIRO)	5-L glass flasks	1 pair mo^{-1}
^{13}C (USGS)	10-L stainless steel flasks	2 pair mo^{-1}
Wet-dry deposition (NADP)	HASL Chemetrics wet-dry collector	1 wk^{-1}, wet; discrete, dry
Bulk deposition (EML)	Plastic bucket	Continuous (1 bucket mo^{-1})
Hi-vol sampler (EML)	Hi-volume sampler	Continuous (1 filter wk^{-1})
Hi-vol sampler (SEASPAN Project)	Hi-volume sampler	Continuous (1 filter wk^{-1})
CO_2, CH_4, trace gases (NCAR)	Evacuated stainless steel flasks	1 pair wk^{-1}
^{13}C, $^{13}CH_4$ (Argonne Lab.)	30-L evacuated steel cylinders	1 pair discrete
^4He (U.S. Bureau of Mines)	1-L pressurized steel cylinder	2 yr^{-1}

launch success rate. The program at SMO has been standardized with 2000-g balloons that reach typical heights of 6-8 mb. In July, hypsometer radiosondes began to be used to improve pressure determinations at high altitudes.

Halocarbons and Nitrous Oxide

The GMCC halocarbon program continued to be upgraded in 1987. An HP5890 GC operated throughout the year and was augmented in June by a Shimadzu GC. At the same time, the system was converted from using one calibration gas to using two and had a software upgrade installed.

Flask sampling continued on a weekly basis. Once per month, flask pairs were filled through a chemical dryer to test the effect of humidity in the exposed flasks.

Aerosols

Condensation nuclei were measured continuously except for a 6-wk period centered around November when the GE CNC was sent to Boulder for repair. The four-wavelength nephelometer ran well all year until November, when a board replacement and microswitch contacts on a rotary valve needed adjustment.

Solar and Terrestrial Radiation

The solar radiation program at SMO continued without any changes in 1987. The program consists of a continuous tracking pyrheliometer, global pyranometers at two wavelengths, a pyrheliometer at four wavelengths for making discrete measurements, and sunphotometers at four wavelengths.

Meteorology

The complement of meteorological measurements continued in 1987 with the exception of dewpoint temperature. In April, the standard plastic rain gauge at the observatory was relocated when it was discovered that droplets could bounce off a nearby wall into the gauge, causing an average 14% increase in the measured amounts when compared with measurements at an unsheltered location.

Precipitation Chemistry

Collection of samples, using a plastic funnel and bottle, was carried out on a daily basis. After on-site measurement of pH and conductivity, selected samples were sent to the MLO Hilo laboratory for further analyses.

Cooperative Programs

Table 2.5 lists 14 cooperative projects supported by the GMCC SMO program. The U.S. Bureau of Mines atmospheric helium program involved the pressurization of a small steel cylinder and was conducted twice in 1987.

The largest cooperative project at SMO is the ALE project run by OGC consisting of an HP5880 gas chromatograph and associated equipment. In March, a new UPS was installed for the project, along with a compressor pneumatic air source and a new version of software for the IBM PC data acquisition system. A second upgrade to the software was installed in October. The IBM PC suffered several periods of down time during the year due to program and communication problems.

In May, an SIO scientist visited to discover the cause of excessive scatter between the CO_2 concentrations measured during the three weekly 5-L glass flask exposures. The problem was found to be caused by sunlight striking the grease in the glass stopcocks, liberating trace amounts of CO_2. Canvas "boots" sent from La Jolla to cover the stopcocks while the flasks are carried from the observatory to the exposure point and back corrected the problem.

2.4. South Pole

2.4.1. Facilites

The GMCC SPO program is situated in the NSF's CAF (Figure 2.1). After an unsuccessful attempt to raise the CAF building during the summer of 1985-1986, it was raised 3.7 m during December 1986. A hydraulic jacking system composed of a central pumping station, ten jacks, and associated hosing was used. The only major incident that occurred during the building raising involved the main CAF power cable, which was gouged by a bulldozer. Power to the CAF was not lost, however, and the cable was spliced later. A new stairway was constructed of timber and aluminum to reach from the CAF front porch to the snow surface, and a new iron ladder was constructed to reach from the CAF back porch to the snow surface.

Electric power was very reliable this year except for a few concentrated, problematical periods. Once again frequency fluctuations were virtually nonexistent.

SPO operations continued to be good this year. Three new projects were undertaken: a special aerosol measurement program, a Smithsonian-NOAA cooperative project to monitor and record UV radiation levels, and a U.S. Department of Interior cooperative project to collect a single sample of air for eventual ^4He content analyses. The most significant operating problem encountered during the year was with the halocarbon program's GC. Additionally the surface ozone program's Dasibi ozone monitor was inoperable at various times.

The CAMS units worked very well again this year. One BRAM loss was due to equipment failure. All other BRAM losses were due to maintenance. The ASR automatically restarted frequently (and inexplicably) in periods of high winds. The MO3 did not always resume logging surface ozone data after scheduled calibrations. The root of this problem was never determined. On all occasions all three CAMS systems automatically restarted following power outages and failures.

Data transfer by satellite continued this year in much the same form as initiated last year. There were some losses of message traffic, which hampered some programs. Most of these losses were due to an addressing problem, which was subsequently discovered and corrected. At the SPO end of communication, high winds and auroral activity disrupted message receipt and transmission capabilities at times.

2.4.2. Programs

Table 2.6 lists the sampling programs carried out during

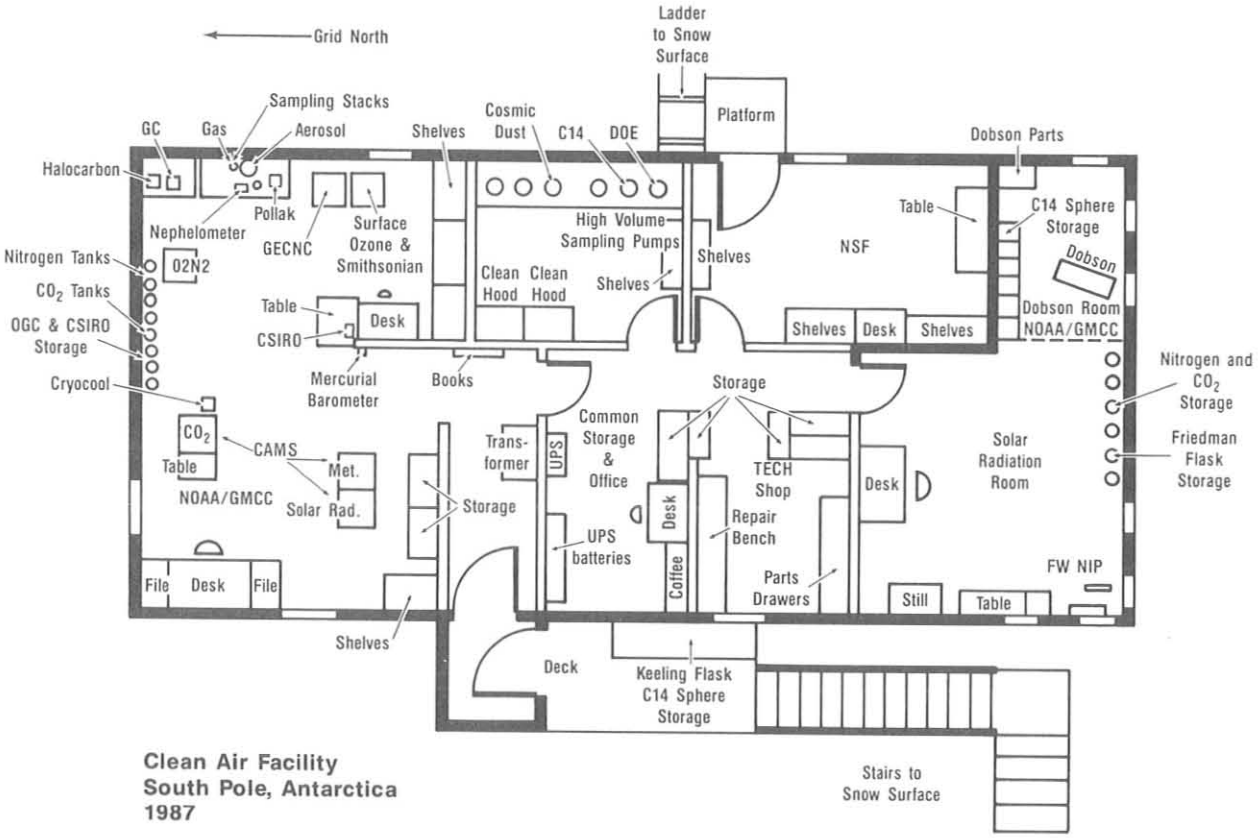

Fig. 2.1. Clean Air Facility at SPO, 1987

1987. Comments on some of the programs follow.

Carbon Dioxide

There were a few problems with this program last year; perhaps most significant was the apparent deterioration of the IR light source and heater/blower unit in the analyzer. Both units were replaced, and after a period of internal temperature stabilization, the analyzer resumed normal operation.

Surface Ozone

Problems with this program included logging difficulties in the MO3 CAMS and the failure of the Dasibi ozone meter on August 4. The logging problem seemed to be in the CAMS hardware and/or software. The Dasibi logic/display board failed and could not be replaced until opening flight. Therefore, no surface ozone data were collected from August 4 until after station opening.

Ozone Profiles

The ozonesonde program continued this year as a major element of GMCC. The biggest problem encountered with this program was high wind. When winds were in excess of approximately 15 knots, it was virtually impossible to launch successfully. A sustained period of high winds permitted only three successful launches in April 1987; otherwise, there were more than 60 successful launches through the year, with a concentration in the austral spring. The standard balloon used was a 19,000-ft^3 plastic balloon, but 3000-g rubber and 141,770-ft^3 plastic balloons were also used occasionally.

Halocarbons and Nitrous Oxide

The most significant operating problem encountered this year was with this program. After a period of variable data quality, the gas chromatograph failed in February 1987. Despite considerable effort made to return the instrument to operation, it was still not operating when the station opened the following November.

Aerosols

The Pollak CNC, GE CNC, and nephelometer performed well all year. The GE CNC required the usual maintenance; problems with this instrument normally occurred very shortly after maintenance, having resulted from overgreasing the valves, etc.

The equipment for the special aerosol project consisted of two stepping streakers, a diffusion battery with a TSI CN counter, and an aethelometer. The project was designed to investigate aerosol chemistry, size, concentration, and scattering properties in relation to large-scale meteorology in order to understand source regions and transport paths to the South Pole.

TABLE 2.6. Summary of Sampling Programs at SPO in 1987

Program	Instrument	Sampling Frequency
Gases		
CO_2	URAS-2T IR analyzer	Continuous
CO_2, CH_4	0.5-L glass flasks, through analyzer	1 pair twice mo^{-1}
	0.5-L glass flasks, P[3]	1 pair twice mo^{-1}
Surface O_3	Dasibi ozone meter	Continuous
Total O_3	Dobson spectrophotometer no. 82	3 day^{-1}
Ozone profile	Balloonborne ECC sonde	1 wk^{-1} summer, autumn, winter 1 $(3\ day)^{-1}$ spring
CFC-11, CFC-12, N_2O	300-mL stainless steel flasks	3 wk^{-1} summer
CFC-11, CFC-12, N_2O	Shimadzu automated GC	2 analyses wk^{-1}
Aerosols		
Condensation nuclei	Pollak CNC	2 day^{-1}
	G.E. CNC	Continuous
Optical properties	Four-wavelength nephelometer	Continuous
Carbon aerosols	Aethalometer	Continuous
Aerosol chemistry	Stepping streakers	1 sample day^{-1}
Solar and Terrestrial Radiation		
Global irradiance	Eppley pyranometers with Q and RG8 filters	Continuous, summer
Direct irradiance	Eppley pyrheliometer with Q, OG1, RG2, and RG8 filters	Discrete, summer
Turbidity	Sunphotometers with 380-, 500-, 778-, and 862-nm narrowband filters	Discrete, summer
Albedo	Eppley pyranometers with Q and RG8 filters, downward-facing	Continuous, summer
Terrestrial (IR) radiation	Eppley pyrgeometers, upward- and downward-facing	Continuous
Meteorology		
Air temperature	Platinum resistor, 2- and 20-m heights	Continuous
Snow temperature	Platinum resistor, 0.5 cm	Continuous
Pressure	Capacitance transducer	Continuous
	Mercurial barometer	2 times wk^{-1}
Wind (speed and direction)	Bendix Aerovane	Continuous
Cooperative Programs		
CO_2, ^{13}C, N_2O (SIO)	5-L evacuated glass flasks	2 mo^{-1} (3 flasks $sample^{-1}$)
Total surface particulates (DOE)	High-volume sampler	Continuous (4 filters mo^{-1})
Aerosol physical properites (SUNYA)	Pollak CNC with diffusion battery	Discrete
	Nuclepore filters	Continuous
Various trace gases (OGC)	Stainless steel flasks	Twice mo^{-1} $(3\ flasks\ set)^{-1}$
$^{13}C/^{12}C$, CH_4 (USGS)	10-L stainless steel cylinder	1 mo^{-1} (2 cylinders $sample^{-1}$)
^{14}C (NOAA/ARL)	3,000 psi spheres	500 psi day^{-1}
Snow acidity (NOAA/ARL)	125-mL Nalgene flasks	1 $(2\ wk)^{-1}$
Interhemispheric $^{13}C/^{14}C$ (CSIRO)	5-L glass flasks	1 or 2 flasks mo^{-1}
NO_2, O_3 (NZARP)	Spectrophotometer, data logger	Continuous for 6 wk at sunrise and sunset, and control periods in summer
He (Dept of Interior)	1-L steel cylinder	One time
CH_4, CO_2, CO (NCAR)	2.5-L steel flasks	Daily (seasonally)
Ultraviolet radiation (Smithsonian-NOAA)	UV radiometer, data logger	Continuous, summer

Solar and Terrestrial Radiation

Once again there were a few problems associated with pre-amps, but downtime was short. All cables with the exception of one leading from CAF to the albedo rack were replaced with single-run, longer cables to facilitate the raising of the CAF building. Additionally, the cables were suspended above the snow surface to prevent their future burial by blowing snow.

Meteorology

The problems encountered with this program were relatively minor and infrequent. An extended period of data loss occurred

when the wires near the snow temperature sensor probe broke and went unnoticed for approximately 3 months. This affected only the snow surface temperature readings.

Cooperative Programs

Most of the cooperative programs listed in Table 2.6 were continued from previous years. However, two new projects began. One, the Smithsonian-NOAA UV radiometer project will be an ongoing program; the other, a U.S. Department of Interior project to reassess global ^{4}He levels, was a one-time sample. The Smithsonian-NOAA instrument went offline due to a failed tape-drive unit, but a new unit was received by airdrop and the system was returned to operation.

2.5. REFERENCES

Komhyr, W. D., An aerosol and gas sampling apparatus for remote observatory use, *J. Geophys. Res., 88*, 3913-3918, 1983.

Rinsland, C. P., A. Goldman, F. J. Murcray, R. D. Blatherwick, F. H. Murcray, and D. G. Murcray, Infrared measurements of atmospheric gases above Mauna Loa, Hawaii, in February 1987, *J. Geophys. Res.*, 1988.

Schnell, R. C., and R. M. Rosson (Eds.), *Geophysical Monitoring for Climatic Change No. 15, Summary Report 1986,* 155 pp., NOAA Environmental Research Laboratories, Boulder, Colo. 1987.

3. Aerosols and Radiation Monitoring Group

3.1. Continuing Programs

3.1.1. Surface Aerosols

The GMCC aerosol monitoring program continued during 1987 as in previous years. CN concentration and aerosol scattering extinction coefficient (σ_{sp}) were measured continuously at BRW, MLO, SMO, and SPO. A G.E. automatic CN counter operates continuously, and a Pollak CN counter provides daily calibration points for the automatic CN counter at each station. A four-wavelength nephelometer at each station continuously measures σ_{sp} at 450-, 550-, 700-, and 850-nm wavelengths.

No major changes were made to the routine monitoring program at the GMCC stations during 1987. The MLO nephelometer exhibited low sensitivity on channel four (850 nm) during the early part of 1987. Therefore, only 450-, 550-, and 700-nm scattering extinction data for MLO are shown here until September 5 (DOY 248), the date when the photomultiplier tube in the MLO nephelometer was replaced. The BRW, SMO, and SPO aerosol monitoring programs operated essentially trouble free during 1987.

A special aerosol experiment was conducted at SPO during 1987. A Nuclepore-filter diffusion battery apparatus for measurement of particle size distribution in the Aitken size range, a TSI alcohol-based CN counter, an aethalometer for the measurement of soot carbon, two stepping streaker samplers, and an HP data acquisition and control system were installed in the Clean Air Facility. The streaker samplers were programmed to take 24-h filter samples for each day of the year for subsequent aerosol chemistry analysis using the PIXE technique.

Monthly geometric means of the data for 1987 are listed in Table 3.1. Figure 3.1 shows daily geometric means of CN concentration (lower portion of each plot), σ_{sp} (middle portion of each plot), and Angstrom exponent (upper portion of each plot) at the GMCC stations for 1987. Three independent values of Angstrom exponent were calculated from the σ_{sp} data. Monthly geometric means of the entire data record for each station are shown in Figure 3.2.

The BRW data in Figure 3.1 show a maximum in σ_{sp} of about 2×10^{-5} m^{-1} during the middle of March, typical of the well-known springtime Arctic haze. After a decrease during the last week of March, the σ_{sp} data again show high Arctic haze values during the first 3 weeks of April 1987. The high springtime values of σ_{sp} decrease rapidly in May and June, reaching values well below 10^{-6} m^{-1}. The BRW long-term record presented in Figure 3.2 clearly shows this annual cycle in σ_{sp}, having monthly means above 10^{-5} m^{-1} in the spring and occasionally below 10^{-6} m^{-1} in the summer. The BRW CN data in Figure 3.1 show an apparent semiannual cycle and a secondary maximum

TABLE 3.1. Monthly Geometric Means of CN Concentration (cm^{-3}) and σ_{sp} (m^{-1}) at 450, 550, 700, and 850 nm for BRW, MLO, SMO, and SPO During 1987

	Jan.	Feb.	March	April	May	June	July	Aug.	Sept.	Oct.	Nov.	Dec.
BRW												
CN	251	292	426	321	161	145	330	347	190	181	89	157
σ_{sp} (450)	1.07-05	1.37-05	1.50-05	1.96-05	1.09-05	3.57-06	2.76-06	2.80-06	3.63-06	4.74-06	6.82-06	1.11-05
σ_{sp} (550)	1.00-05	1.28-05	1.34-05	1.66-05	8.90-06	3.11-06	2.50-06	2.74-06	3.55-06	4.50-06	5.81-06	1.08-05
σ_{sp} (700)	7.28-06	9.09-06	8.90-06	1.03-05	5.23-06	2.06-06	1.84-06	2.18-06	2.81-06	3.50-06	3.80-06	8.26-06
σ_{sp} (850)	5.42-06	6.69-06	6.29-06	6.90-06	3.39-06	1.49-06	1.40-06	1.85-06	2.30-06	2.92-06	2.65-06	6.44-06
MLO												
CN	242	250	252	298	271	320	295	293	258	252	247	207
σ_{sp} (450)				3.48-06	2.33-06	2.66-06	2.47-06	1.75-06	2.47-06	1.36-06	1.10-06	1.21-06
σ_{sp} (550)				2.97-06	1.84-06	2.06-06	1.83-06	1.28-06	1.80-06	9.79-07	7.99-07	8.98-07
σ_{sp} (700)				2.77-06	1.52-06	1.66-06	1.42-06	9.86-07	1.22-06	6.76-07	5.39-07	6.11-07
σ_{sp} (850)									9.95-07	6.25-07	5.17-07	5.87-07
SMO												
CN	310	255	234	198	233	197	190	211	208	218		303
σ_{sp} (450)	1.10-05	8.66-06	1.50-05	1.88-05	1.31-05	1.18-05	1.02-05	1.69-05	1.31-05	2.00-05	1.96-05	2.44-05
σ_{sp} (550)	1.06-05	8.40-06	1.41-05	1.84-05	1.30-05	1.18-05	1.02-05	1.73-05	1.29-05	2.03-05	1.80-05	2.36-05
σ_{sp} (700)	1.06-05	8.59-06	1.41-05	1.91-05	1.34-05	1.21-05	1.05-05	1.82-05	1.32-05	2.13-05	1.74-05	2.36-05
σ_{sp} (850)	1.14-05	9.09-06	1.47-05	2.05-05	1.43-05	1.30-05	1.11-05	1.98-05	1.47-05	2.34-05	1.80-05	2.47-05
SPO												
CN	100	100	102	32	24	16	11	15	27	89	121	115
σ_{sp} (450)	4.49-07	3.04-07	3.35-07	2.53-07	2.45-07	3.93-07	3.49-07	5.02-07	3.85-07	5.52-07	5.37-07	
σ_{sp} (550)	2.66-07	1.84-07	2.18-07	1.67-07	1.61-07	2.65-07	2.55-07	4.03-07	3.12-07	4.31-07	3.75-07	
σ_{sp} (700)	1.19-07	7.78-08	1.19-07	8.91-08	9.29-08	1.56-07	1.36-07	2.58-07	1.85-07	2.68-07	2.21-07	
σ_{sp} (850)	6.40-08	4.15-08	6.10-08	5.60-08	5.19-08	8.61-08	8.37-08	1.72-07	1.22-07	1.78-07	1.45-07	

A compact exponential format is used for σ_{sp} such that 1.07-05 = 1.07×10^{-5}.

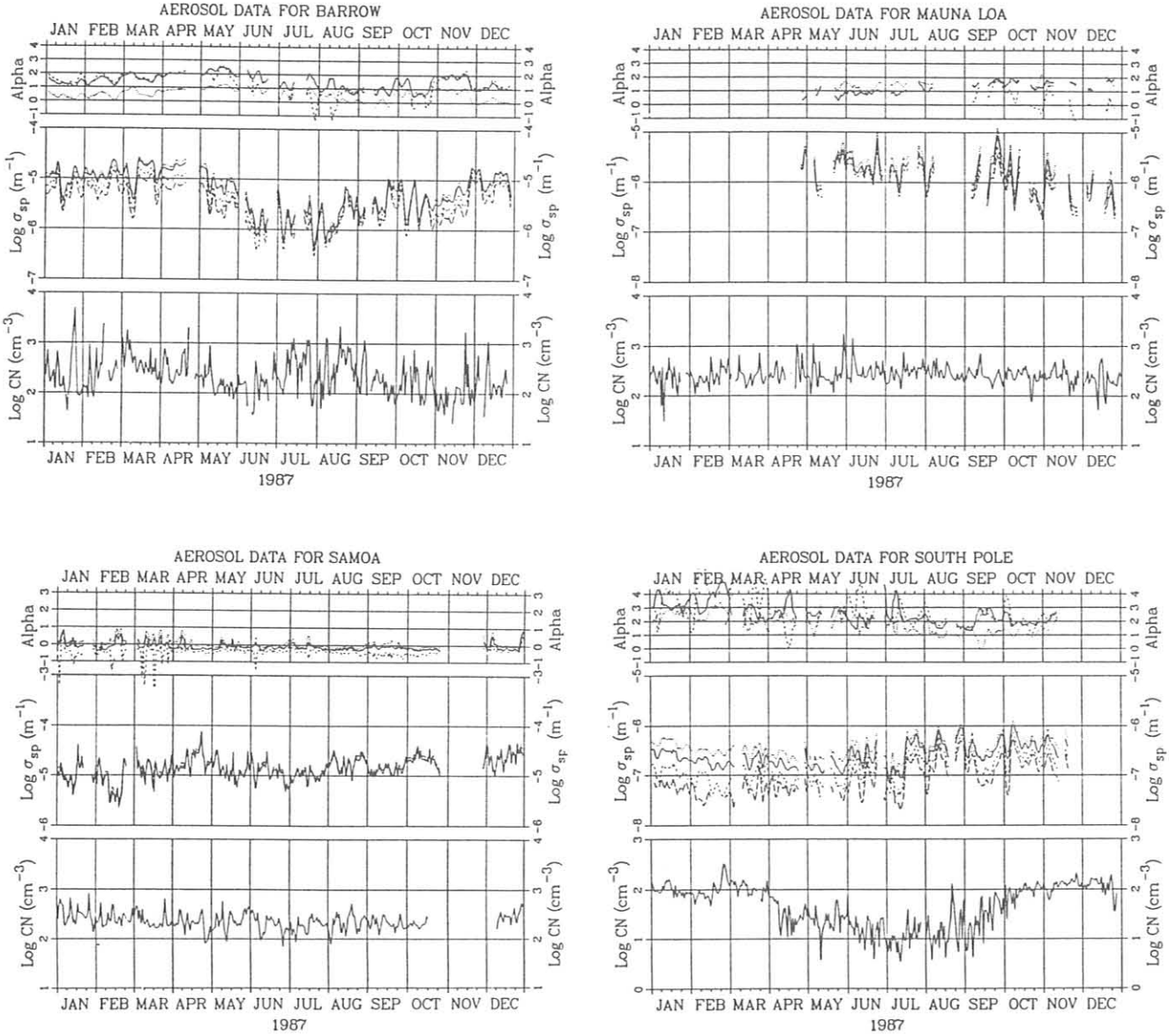

Figure 3.1. Daily geometric means of σ_{sp} and CN data at BRW, MLO, SMO, and SPO for 1987. Data for MLO are included only for 0000-0800 LST. For each station, CN concentration (lower) is shown as a solid line. σ_{sp} data (middle) are shown for 450 (dotted), 550 (solid), 700 (dashed), and 850 nm (long-dashed). Angstrom exponents (alpha) were calculated from 450- and 550-nm (dotted), 550- and 700-nm (solid), and 700- and 850-nm (dashed) σ_{sp} data. σ_{sp} data for 850 nm and Angstrom exponent data for 700-850 nm are not shown for MLO.

in July-August. The BRW long-term CN record shows a more variable semiannual cycle, having maxima usually in March and August, and minima usually in June and November. *Quakenbush and Bodhaine* [1987] presented the Barrow aerosol record graphically in the form of hourly means for 1976-1986.

The MLO σ_{sp} data shown in Figure 3.1 are fairly typical for MLO but do not clearly show the expected annual cycle because of instrument problems and missing data. A maximum is expected in April-May that is caused by the long-range transport of Asian desert dust in the upper troposphere to the vicinity of Hawaii. The Angstrom exponent data show a minimum in April-May, indicating larger particle sizes during that time. The MLO CN data shown in Figures 3.1 and 3.2 average about 250 cm^{-3} and are probably representative of the background troposphere in this region. The desert dust events in the spring do not significantly affect the CN concentration because the dust particles contribute only a small percentage to the total numbers. However, because of their larger size, they contribute significantly to the scattering coefficient. The MLO long-term aerosol record presented in Figure 3.2 shows significantly higher wintertime values during 1985-1987 than during 1974-1980. It is not known whether this is a real change or if it

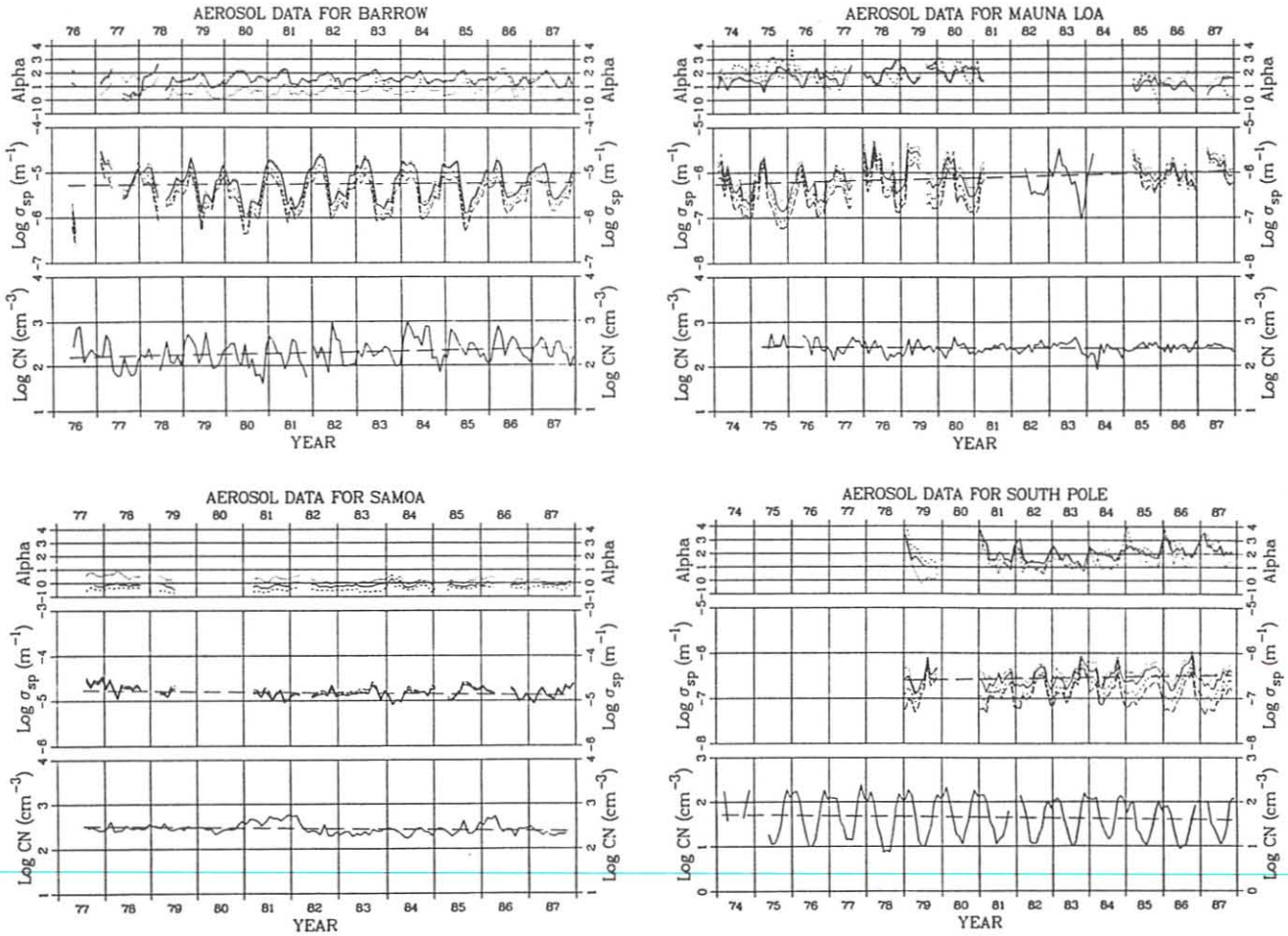

Figure 3.2. Monthly geometric means of σ_{sp} and CN data for the entire data record, as in Figure 3.1. Details of the trend lines are given in Table 3.2.

is because of the new nephelometer installed at MLO in 1985.

The SMO σ_{sp} and CN data (Figures 3.1 and 3.2) continue as in previous years, showing no significant annual cycle or long-term trend. The SMO aerosol is representative of the background marine boundary layer in this region. The long-term mean at SMO is about 1.5×10^{-5} m^{-1} for σ_{sp} and about 270 cm^{-3} for CN concentration. A detailed analysis of the entire SMO data record was presented by *Bodhaine and DeLuisi* [1985].

The SPO σ_{sp} data (Figures 3.1 and 3.2) show intermediate values in the summer, a minimum in May, and a record dominated by large events, sometimes exceeding 10^{-6} m^{-1}, in late winter. These large aerosol events are caused by the transport of sea salt in the middle troposphere from stormy regions near the coast to the interior of the continent. Analyses of the SPO data were presented by *Bodhaine et al.* [1986, 1987]. The SPO CN data show an annual cycle strikingly different from that of the σ_{sp} data. The CN data show a strong annual cycle, reaching a maximum of about 200 cm^{-3} in the austral summer and a minimum of about 10 cm^{-3} in the winter.

Preliminary results from the 1987 SPO aerosol experiment show that aerosol carbon has an annual cycle with a minimum concentration of about 0.1 ng m^{-3} in May and a maximum of about 10 ng m^{-3} in the austral summer. The general shape and phase of the carbon annual cycle most resembles that of σ_{sp}. Time-height cross sections of temperature show no surface temperature inversion in summer and a strong, shallow inversion in winter. Large surface aerosol events often occur during a decrease in the strength of the surface temperature inversion. Trajectories calculated backward from the South Pole show periods of rapid transport from the Weddell and Ross Seas corresponding to sea-salt events in the aerosol data. This experiment was described in more detail by *Bodhaine et al.* [1988] and *Hansen et al.* [1988].

The least-squares trend lines shown in Figure 3.2 were calculated using the common logarithms of the monthly means of the entire data record, and the results are given in Table 3.2. Similar trend lines have been calculated and presented in previous GMCC Summary Reports. The long-term trends are

TABLE 3.2. Least-Squares Trend Analysis of the Common Logarithms of the Data Shown in Figure 3.2*

	Parameter	Slope	Intercept	S.E.	Trend (% yr^{-1})
BRW	CN	0.0164	0.954	0.290	3.9
	σ_{sp}	0.00553	-5.70	0.370	1.3
MLO	CN	-0.00457	2.79	0.127	-1.05
	σ_{sp}	0.0210	-7.81	0.321	5.0
SMO	CN	-0.0113	3.38	0.113	-2.6
	σ_{sp}	-0.0107	-3.94	0.116	-2.4
SPO	CN	-0.00917	2.39	0.432	-2.1
	σ_{sp}	0.0124	-7.58	0.187	2.9

*The time axis is in fractional years, with a data point centered at the middle of a month; e.g., Jan. 1974 = 74.042, Feb. 1974 = 74.125, etc.

TABLE 3.3. Current Radiation Measurements at GMCC Observatories

	SWD	SWU	LWD	LWU	RG8D	DIRQ	FWNIP	SPHTM	MISC
BRW	X	X	X	X	X	X	X	X	O
MLO	X	O	O	O	X	X	X	X	X
SMO	X	O	O	O	X	X	X	X	O
SPO	X	X	X	X	X	X	X	X	X

X, measurements made; O, measurements not made; SWD, downward solar irradiance; SWU, upward (reflected) solar; LWD, downward longwave (sky emitted); LWU, upward longwave (earth emitted); RG8D, downward solar (RG8 filter, 0.7 to 3.0 μm) irradiance; DIRQ, direct solar; FWNIP, filter wheel normal incidence pyrheliometer (discrete observations, four solar bands); SPHTM, multi-wavelength sunphotometer; MISC, miscellaneous—MLO: global diffuse solar, downward solar (OG1 filter, 0.53 to 3.0 μ), 2-channel sunphotometer (water vapor), 3-channel sunphotometer (calibration standard); SPO: RG8 albedo, direct sun (RG8 filter).

not statistically significant compared with the standard error about the regression line, suggesting that there is no long-term trend in the background aerosol measured at these four stations.

3.1.2. Solar and Thermal Radiation

The purpose of the GMCC solar and thermal radiation measurement project is to establish the surface radiation budget components at the GMCC sites. From this data set two major research areas are addressed: (1) the explanation of observed variations on multiple time scales and (2) understanding the influence of surface radiation budget variations on global and regional climate. A major effort in the project is spent on the acquisition and quality control of the radiation data, thereby facilitating a research-quality data base. In addition to measurements of the principal components of the radiation budget, assorted spectral radiation measurements are made at solar wavelengths. These spectral measurements, obtained by remote-sensing techniques, support radiation budget research by providing data on different atmospheric constituents, such as water vapor and aerosols.

Current Measurements

Table 3.3 shows the radiation measurements currently being made at the four GMCC observatories. This suite of measurements has remained unchanged for the previous 3 years. The long-term goal of the measurements is to provide an understanding of phenomena on a multiyear time scale.

Filter Wheel NIP Analysis

Two sources of day-to-day and long term variations in the radiation budget are water vapor and to a lesser extent aerosols. Recently the 11-yr records of the FWNIPs from all four sites were analyzed in an effort to determine the aerosol optical depth and precipitable water information contained in the observation results. This analysis was accomplished, observation-by-observation, by repeatedly adjusting the aerosol and water vapor amounts in a spectral atmospheric transmission model [*Bird and Riordan*, 1986] until agreement with the observations in several spectral bands was achieved. Preliminary results from this effort are shown in Figures 3.3 and 3.4. Identical scales were used for the different locations in Figures 3.3 and 3.4 for easy comparison. Only SPO water vapor values, which range from 0.02 to about 0.1 cm with an average of 0.05 cm, are not easily discernible on the plots. The uncertainty in these results is larger than in results from more traditional techniques for measuring these quantities. Although it is difficult to estimate the magnitude of the errors in the FWNIP derived values, the absolute values are reasonable when compared with other measurements.

The FWNIP record is exceptionally consistent and stable. However, on a few occasions in the 44-station-year record, as yet unexplained, step discontinuities have appeared in the raw data, which are most likely observational artifacts. For this reason and the fact that the derived values are wholly dependent on the absolute calibration of the instrument, model, and extraterrestrial solar spectrum, the results shown in Figures 3.3 and 3.4 are best considered to be only model inputs that force the model to agree with FWNIP observations. Both the model and raw data need to be examined further to refine the results and define error bounds.

Aerosol Optical Depth

Other than the absolute levels and short term variability the most obvious feature in the aerosol optical depth data (Figure 3.3) is the peak starting in 1982 due to debris from El Chichon. The exact arrival time of the maximum in El Chichon debris at BRW and SPO cannot be easily determined because of the seasonality of the measurements. However, the peak magnitude and multiyear decay time for the event is well depicted in the plots.

Each station's aerosol record exhibits characteristics unique to that station's latitude and elevation. The annual cycles at BRW and MLO are due to the springtime Arctic haze and Asian desert dust respectively. The higher frequency variability at SMO is due to boundary layer sea salt.

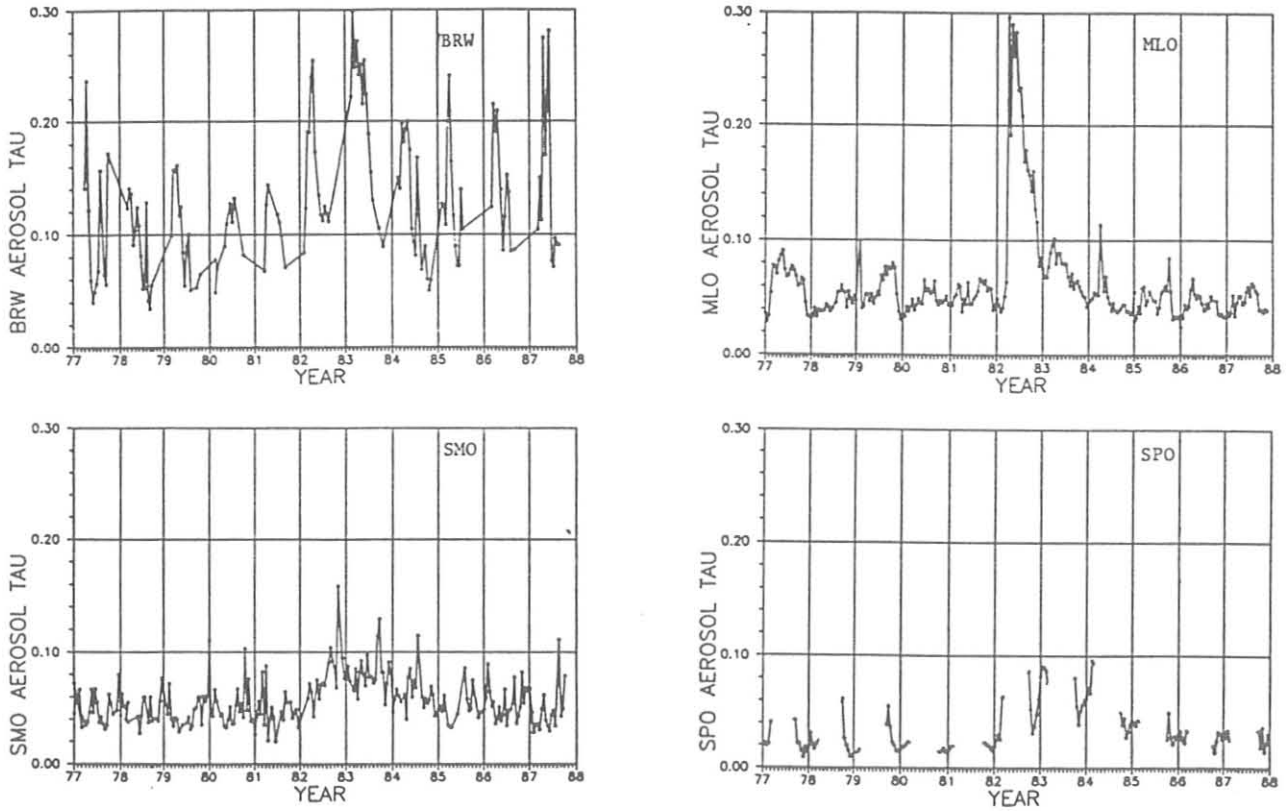

Fig. 3.3. Two-week averages of aerosol optical depth values (averaged over the visible) that, when input to a solar transmission model, result in the model solar irradiances best agreeing with FWNIP observations at the GMCC observatories.

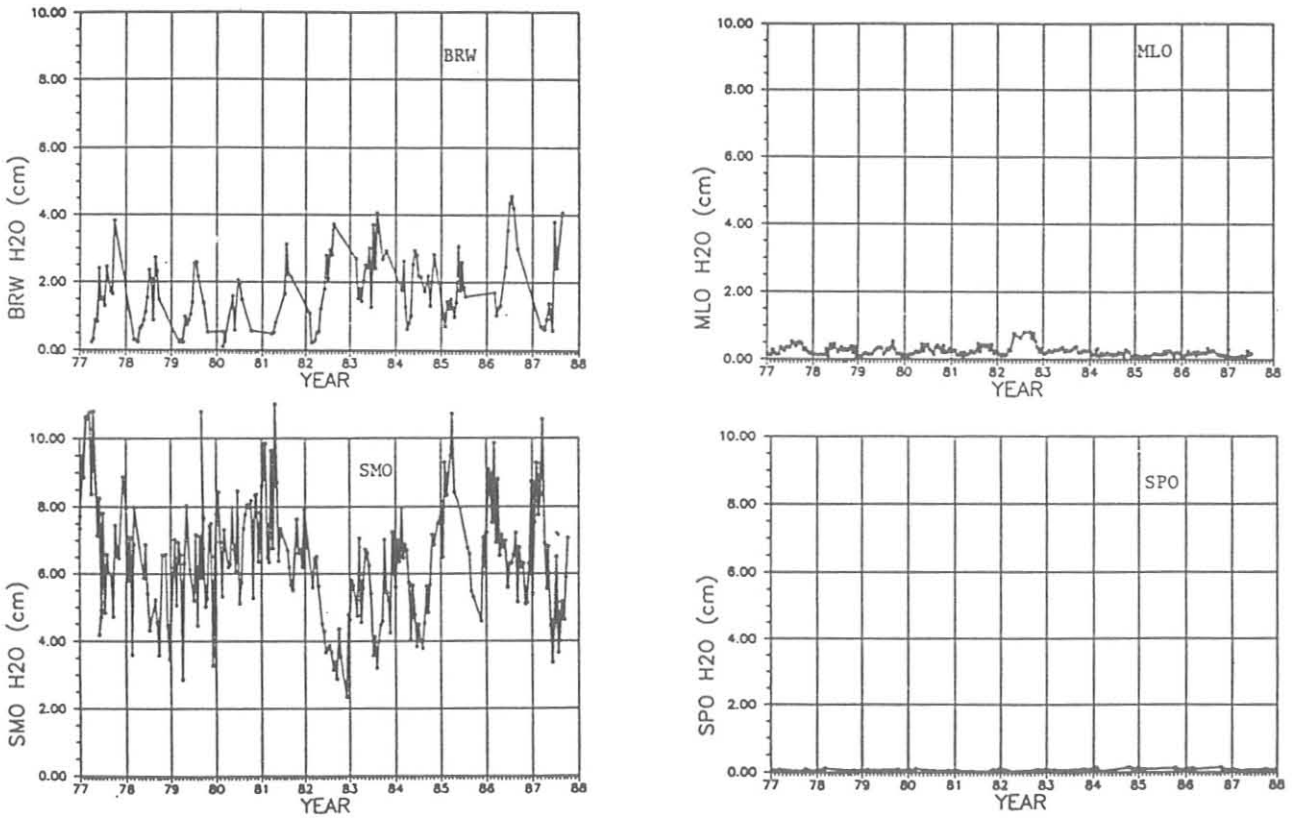

Fig. 3.4. Two-week averages of precipitable water (cm), as in Figure 3.3. Some aerosol contamination is evident in 1982 (see text).

Precipitable Water

The precipitable water values in Figure 3.4 show a minor interference from the El Chichon event, due to aerosol contamination of the water vapor retrieval algorithm. This interference is most evident in the last two-thirds of 1982 at MLO. The precipitable water values shown in Figure 3.4 cover 4 orders of magnitude but in general agree to much better than a factor of 2 with other observations from radiosondes and a sunphotometer.

Downward Solar Irradiance

The downward solar component of the radiation budget has been most consistently measured and processed for all GMCC sites. Monthly averages of this component are shown in Figure 3.5. These data were manually edited once and data gaps of up to several minutes were filled by interpolation. Only complete or nearly complete days were used to form the monthly averages. Missing days may adversely affect the monthly average if the missing days are concentrated at the beginning or the end of particular "transition" months, but this is not typically the case. Most months have just random missing days.

Many interesting features are seen in the solar irradiance data in Figure 3.5. The most obvious are annual and station-to-station variations that are caused largely by sun-earth geometry. Year-to-year and seasonally dependent variations caused by the atmosphere are seen best by comparing individual months of consecutive years. For example at BRW, April irradiances have varied less than ±10% over the 11 years; however, July values decreased by 40% in the first 6 years, only to recover half that loss in 1 year and then steadily decrease again for the past 5 years. The BRW July variability is of a magnitude that can only be caused by cloudiness changes associated with multiyear-time-scale climate fluctuations.

The effect of the eruption of El Chichon is not obvious in Figure 3.5. This is because these data include all cloudy times as well as clear, and the effect is masked. The dip at MLO in 1982 may be related to El Chichon, but similar dips not evident at other stations are evident at MLO for different times.

No sustained trends are discernible. There is an apparent slight decrease at SMO during the past 3 years, which is believed to be due to instrument detector deterioration common in the tropics and not fully corrected in this presentation. The SMO pyranometer is scheduled to be replaced in 1988, and the detector drift can then be corrected.

Radiation Budget

Nearly 3 years of complete radiation budget data have been acquired at three GMCC locations: SPO, BRW, and Erie, Colo. These records are considerably shorter than most GMCC data sets because of the relatively recent development of a suitable instrument for monitoring longwave radiation. The new instrument, an Eppley pyrgeometer with a silicon dome, has just enough increased complexity that it was incompatible with the data-logging capabilities at the observatories and with the data validation and processing procedures used in the project. These problems have since been solved, but the data are not ready for presentation at this time.

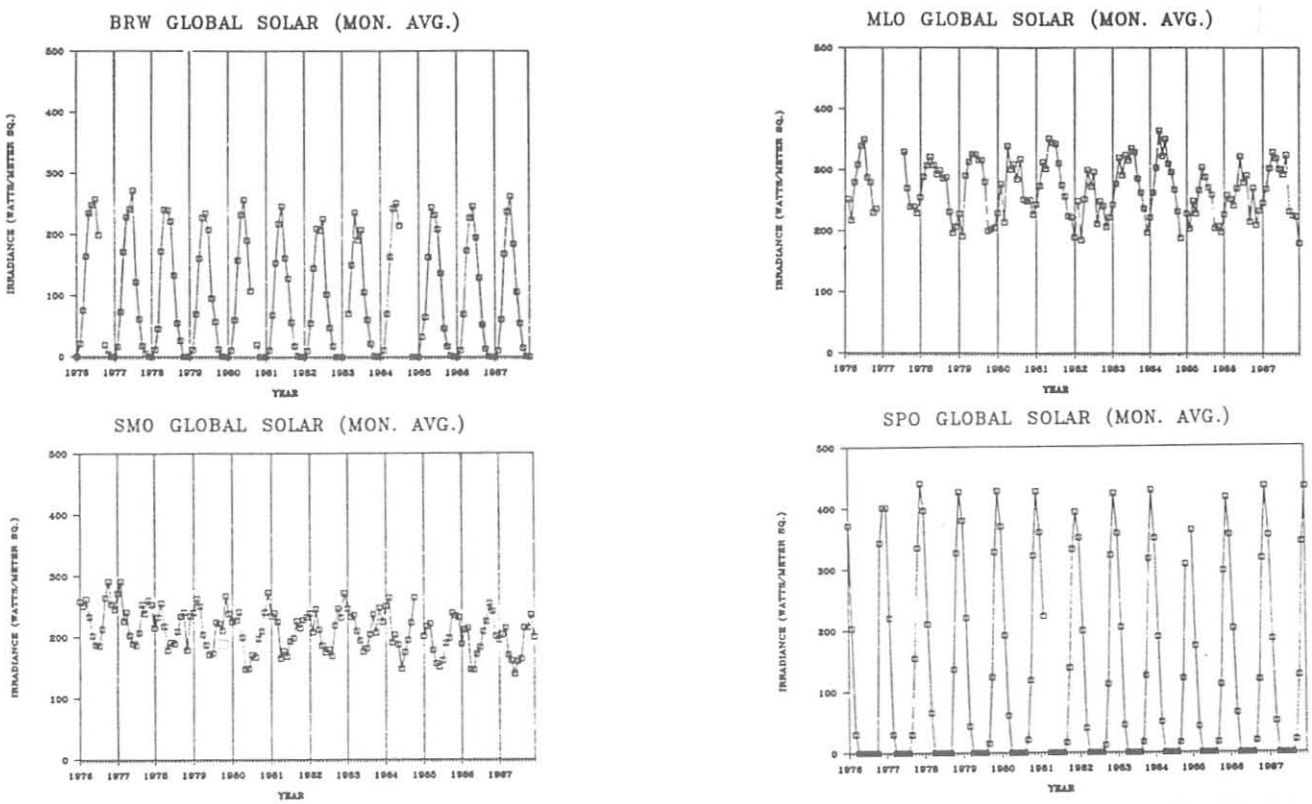

Fig. 3.5. Monthly average downward solar irradiance (W m^{-2}, averaged over 24 hours a day) observed at the four GMCC observatories. The slight downward trend at SMO is most likely a measurement artifact (see text).

3.1.3. Solar Radiation Facility

SRF activities during 1987 were devoted to the following areas: recalibration of a set of pyranometers for resupply of the 31 NOAA SOLRAD sites, other support of SOLRAD sites, completion of the new automated tracker purchase contract, installation of multiple automated tracker testing and operational capability in the SRF, development of data processing software for the SRF computer installation, coordination of and funding for a precision measurement of two view-limiting apertures for two ACRs designated to become the U.S. representative sensors in the World Standard Group of ACRs maintained in Davos, Switzerland, comparisons of NOAA reference ACRs with SERI ACRs as a check for consistent operation, and publication of a report summarizing the Seventh New River Intercomparison of ACRs.

SOLRAD Network

As part of the preparations for resuming measurements of global and direct beam solar radiation at NOAA SOLRAD sites in the United States, a group of 30 recalibrated pyranometers was prepared for exchange with sensors last calibrated in 1984 (1982 for five of the sensors). Attempts were made to send the same sensor back to a given site if at all possible. Table 3.4 lists the sites and serial numbers of the sensors sent to them. Additionally, the calibration histories of each sensor are listed so that the long-term stability may be examined. It should be noted that rather-detailed histories of all NOAA sensors have been developed during the past 12 years and that, overall, the NOAA complement of thermopile sensors is quite well characterized. For this reason the reestablishment of the SOLRAD network with its new data acquisition capabilities and quality control should do well in collecting a high-quality data set in the years ahead.

Although the calibration values in Table 3.4 are not strictly comparable because not all are normalized to the same zenith angle, particularly for the earlier years, information about the long-term stability of the NOAA group of thermopile-based pyranometers is present.

Each SOLRAD site also has a direct-beam sensor, an Eppley pyrheliometer (NIP), but an insufficient number of sensors prevents a complete exchange of field instruments. This is not a serious problem because of better long-term stability of the NIP compared with that of a global sensor.

Automated Tracker Project

Final production design of the new Eppley automated trackers was achieved during the summer of 1987. Design changes were incorporated that will ensure better long-term tracker performance and minimize maintenance requirements. Delivery of the first group of 15 production units was completed by the end of the year. The remainder of the units will be delivered in early 1988. Installation of the trackers at the SOLRAD sites should be accomplished during 1988.

The SRF facility was fitted with permanently installed control cabling sufficient to operate up to five of the new trackers simultaneously for monitoring and testing purposes in preparation for SOLRAD site installation activity. Each unit will be tested in Boulder prior to shipment to the field sites.

SRF Standards Activity

SRF primary and working standards were routinely checked during the year. Shade calibrations of the SRF primary reference pyranometer, Eppley PSP 19917F3, were performed using the SRF ACR reference, TMI67502. Regular comparisons of reference NIPS were also performed. Historical scale factors were reproduced, and no significant departures from past performance were observed.

A comparison of SRF and SERI ACR reference instruments was also held on 4 days during August and September. The SRF reference ACRs, manufactured by Technical Measurements Inc. and by Eppley Laboratory, were compared with the SERI references. Significant departures from the historical record date back over 10 years.

ACR Aperture Measurements

Two ACRs manufactured in the United States have been selected as representative sensors in the WMO World Standard Group of ACRs maintained in Davos, Switzerland. To fulfill requirements set forth by the WMO regarding the admission of these ACRs to the World Standard Group, the instruments' view-limiting aperture areas had to be measured. The NBS Dimensional Metrology Laboratory was contracted to perform high-precision diameter determinations of the two apertures. These measurements were completed in late August and early September, and two U.S. ACRs were forwarded to the World Radiation Center in Davos.

The two ACRs sent were manufactured by the Eppley Laboratory and by Technical Measurements Inc. They are essentially on permanent loan to the World Radiation Center by their respective owners, the Eppley Laboratory and SERI.

Analysis of the data and discussion of final results of the Seventh New River Intercomparison of ACRs (NRIP7) were published by *Nelson et al.* [1987].

3.1.4. Turbidity

The number of monitoring sites in GMCC's U.S. Turbidity Network remained constant at 17 during 1987. Of these, 13 continued to send data to GMCC in Boulder for reduction and processing. Sunphotometers at Sterling, Madison, Raleigh, and Lander, however, were used solely for quality control of pyrheliometric data. These locations are not yet reporting sunphotometer observations as part of the turbidity network. Turbidity measurements also continued at the four GMCC baseline stations during 1987. A five-channel Mainz II hand-held sunphotometer was put into service at MLO in July. This was the first of several Mainz II sunphotometers scheduled to be sited at ADN stations. A Mainz II sunphotometer was also shipped to the ADN station at Haute Provence in France during November. Table 3.5 lists the 22 stations and the wavelengths at which turbidity was measured during 1987.

In 1987, 123 sunphotometer calibrations were completed. Of these, 14 were not of sufficient quality to be recorded in the calibration history files for the respective instruments. Eighty-six calibrations were completed in the mountains west of

TABLE 3.4. NOAA Calibration Histories (Scale Factors) of Pyranometers Currently in the SOLRAD Network

Site	Serial Number	1976	1977	1978	1980	1982	1983	1984	1987	Average	Std. Dev.
Lander, Wyo.	73-19	8.43		8.62		8.50		8.72	8.67	8.59	0.11 ± 0.33%
Guam	73-23	9.47		9.58		9.50		9.40	9.45	9.48	0.06 ± 0.63%
Salt Lake City, Utah	73-31	9.06		8.81		8.87		8.81	8.82	8.87	0.10 ± 1.08%
El Paso, Tex.	73-38	9.91		10.09		9.70		9.71	9.68	9.82	0.16 ± 1.62%
Omaha, Nebr.	73-41	8.97		8.75		8.57		8.58	8.71	8.72	0.15 ± 1.67%
Dodge City, Kans.	73-40	8.84		8.74		8.75		8.67	8.70	8.74	0.06 ± 0.66%
Fresno, Calif.	73-44	8.89		8.80		8.74		8.70	8.71	8.77	0.07 ± 0.80%
Raleigh, N.C.	73-48	10.63*		8.61		8.62		8.49	8.64	8.59	0.06 ± 0.68%
Brownsville, Tex.	73-50	9.72		9.35		9.22		9.04	9.04	9.27	0.25 ± 2.72%
Midland, Tex.	73-55	8.50*		8.26*		10.08			9.97	10.03	0.06 ± 0.55%
Boise, Idaho	73-60	8.67				8.79		8.60	8.57	8.66	0.08 ± 0.98%
Tallahassee, Fla.	73-62	9.50		9.78		9.55		9.48	9.54	9.57	0.11 ± 1.13%
Montgomery, Ala.	73-63	8.38*		8.40*		7.54		7.47	7.50	7.50	0.03 ± 0.38%
Phoenix, Ariz.	73-65	10.07		10.07		10.02			9.97	10.03	0.04 ± 0.41%
Columbia, Mo.	73-66	9.89		9.80		9.67		9.72	9.80	9.78	0.08 ± 0.77%
Great Falls, Mont.	73-82	8.78				8.54		8.44	8.50	8.57	0.13 ± 1.51%
Nashville, Tenn.	73-83	8.47		8.33		8.29		8.21	8.30	8.32	0.08 ± 1.02%
Coraopolis, Pa.	73-84	8.24		8.16		8.06		7.98	8.04	8.10	0.09 ± 1.14%
Lake Charles, La.	73-89					8.65		8.62	8.62	8.63	0.01 ± 0.16%
Albuquerque, N. Mex.	73-92	8.41		8.28		8.13		8.02	8.06	8.18	0.15 ± 1.77%
Long Beach, Calif.	73-98	9.49		9.35				9.03	9.03	9.23	0.20 ± 2.18%
Madison, Wis.	73-99	9.88		9.79		9.73			9.63	9.76	0.09 ± 0.93%
Avg. Std. Dev.											0.10 ± 1.09%
Grand Junction, Colo.	10095			6.92		6.90		6.82	6.83	6.87	0.04 ± 0.63%
Ely, Nev.	11441		9.73			9.33		9.26	9.26	9.40	0.20 ± 2.08%
Burlington, Vt.	11916			9.15		8.67	8.74	8.79	8.79	8.83	0.17 ± 1.89%
Las Vegas, Nev.	11939				9.61	9.47		9.29	9.25	9.41	0.15 ± 1.55%
Bismarck, N. Dak.	12258			9.39			8.80	8.78	8.66	8.91	0.28 ± 3.19%
Seattle, Wash.	12687		9.05	9.01	9.02	8.90			8.57	8.91	0.18 ± 1.99%
Caribou, Maine	15130					10.18			10.01	10.10	0.08 ± 0.84%
Sterling, W. Va.	15952			10.09		9.67		9.52	9.50	9.70	0.24 ±2.45%
Avg. Std. Dev.											0.17 ± 1.83%

Scale factors are in units of $\mu V\ W^{-1}\ m^{-2}$.
*Rebuilt sensor (not used in computation).

Boulder, Colorado, and 37 were performed at MLO. Langley plot measurements were made at elevations of 2.7-3.5 km above sea level. This method of calibration was the only one used in 1987 and has proved to be accurate and reliable for the majority of cases.

Plots of typical calibration histories for NOAA J-series sunphotometers are presented in Fig. 3.6. The calibration constant for the 500-nm channel of sunphotometer J202 shows little variance and no significant drift. The 380-nm channels for J204 and J203, however, show a more common pattern of downward drift with time and more substantial variance. Calibration drift is generally linear for the J-series sunphotometers. The estimated uncertainty in optical depth computations resulting from uncertainty in calibration trends is typically on the order of 0.005 to 0.04 optical depth units at a relative air mass of 1.0. This uncertainty is inversely proportional to the relative air mass, and would be half the amount indicated, for example, if the relative air mass were 2.0.

Software for acquisition of Mainz II sunphotometer data from the ADN sites was developed and tested in 1987. Logistical considerations and problems with the filter mechanisms on some of the Mainz II suphotometers contributed to delays in the deployment of these instruments at ADN stations. Two of the nine Mainz II sunphotometers were put into service in 1987.

The turbidity project staff began the design of a new five-wavelength sunphotometer to replace the aging J-series sunphotometers at the baseline observatories. The new sunphotometers will use a detector-filter-amplifier (DFA) module developed by EG&G. Digital panel meters, chips, and 55 of these DFA modules were purchased. The new instruments will be more accurate and more rugged, and will have more features than the J-series sunphotometers.

Data have been processed for 1982 through the end of 1987 for Boulder (see Figure 3.7) and for 1983 through mid-1986 for Atlantic City, Bismarck, Caribou, Huron, Salem, Tallahassee, Alamosa, and Meridian. Data are complete for 1983 through November of 1986 for Victoria. Data for 1986, the first year of operation for Ely, Las Vegas, and Salt Lake City, have also been processed. MLO and SPO data have been processed through 1987. BRW and SMO data have been processed through 1987; however, priods of questionable data from these sites have not yet been corrected or deleted.

TABLE 3.5. GMCC Turbidity Monitoring Sites and Filter Wavelengths for Sunphotometers Used at Each Site

Site	Sunphotometer Wavelength (nm)
BRW*	380, 500, 778, 862
MLO*	380, 412, 500, 675, 778, 862
SMO*	380, 500, 778, 862
SPO*	380, 500, 778, 862
Alamosa, Colo.*	380, 500
Atlantic City, N.J.	380, 500
Boulder, Colo.	380, 500, 778, 862
Bismarck, N. Dak.	380, 500
Caribou, Maine *	380, 500
Ely, Nev.	380, 500
Haute Provence, France	380, 412, 500, 675, 862
Huron, S. Dak.	380, 500
Lander, Wyo.†	380, 500
Las Vegas, Nev.	380, 500
Madison, Wis.†	380, 500
Meridian, Miss.*	380, 500
Raleigh, N.C.†	380, 500
Salem, Ill.*	380, 500
Salt Lake City, Utah	380, 500
Sterling, Va.†	380, 500
Tallahassee, Fla.	380, 500
Victoria, Tex.*	380, 500

* BAPMoN station.
†Not yet reporting data as part of the Turbidity Network.

Data for Boulder and other continental U.S. stations continue to show a clear annual cycle, having maxima in the spring or summer months and minima during November, December, or January. The impact of El Chichon is evident at many stations. The decay of the El Chichon signal appears as a slow downward trend in optical depths since the beginning of the record in early 1983.

SPO aerosol optical depths for a sample of wavelengths are shown in Figures 3.8 and 3.9. The first graph in figure 3.8 presents the 380-nm data record after it has been edited to remove observations made through clouds and thick ice fogs. This record has also been edited to remove negative aerosol optical depths, which are generally artifacts caused by errors in the measurement process or errors in the calibration constants. A perturbation of 0.04 to 0.05 optical depth units is apparent in late 1982 and early 1983. This marks the arrival of the El Chicon stratospheric aerosol cloud.

The second graph in Figure 3.8 shows the 380-nm data set prior to editing. Negative aerosol optical depths and the effects of clouds and ice fogs are evident. The magnitude of the negative aerosol optical depths is too great to be due to errors in the calibration constants alone. The instruments used at SPO are some of the most carefully and frequently calibrated of GMCC's sunphotometers. It is believed that the large negative values are caused in part by measurement techniques and in part by the peak-hold feature on the sunphotometers.

The SPO staff have usually taken sunphotometer observations through an open window in the CAF. The readings are made from a table top within the facility. Cold air pouring into

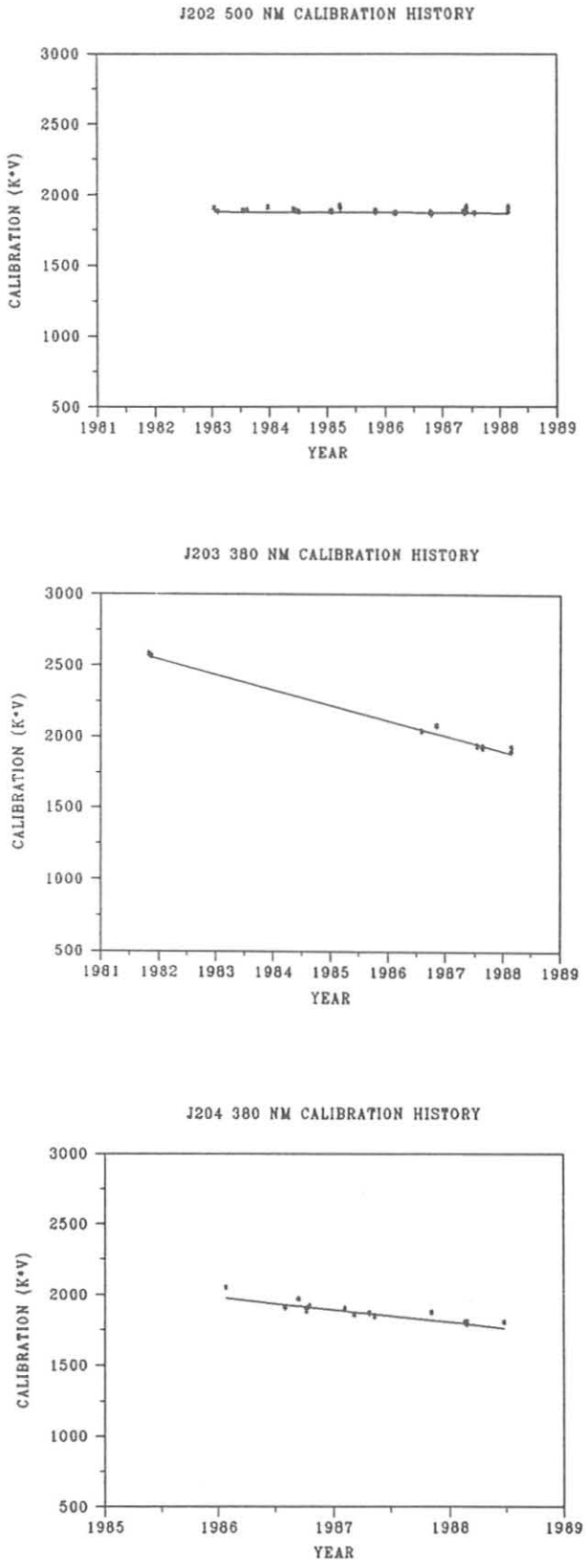

Fig. 3.6. Typical calibration histories for NOAA J-series sunphotometers.

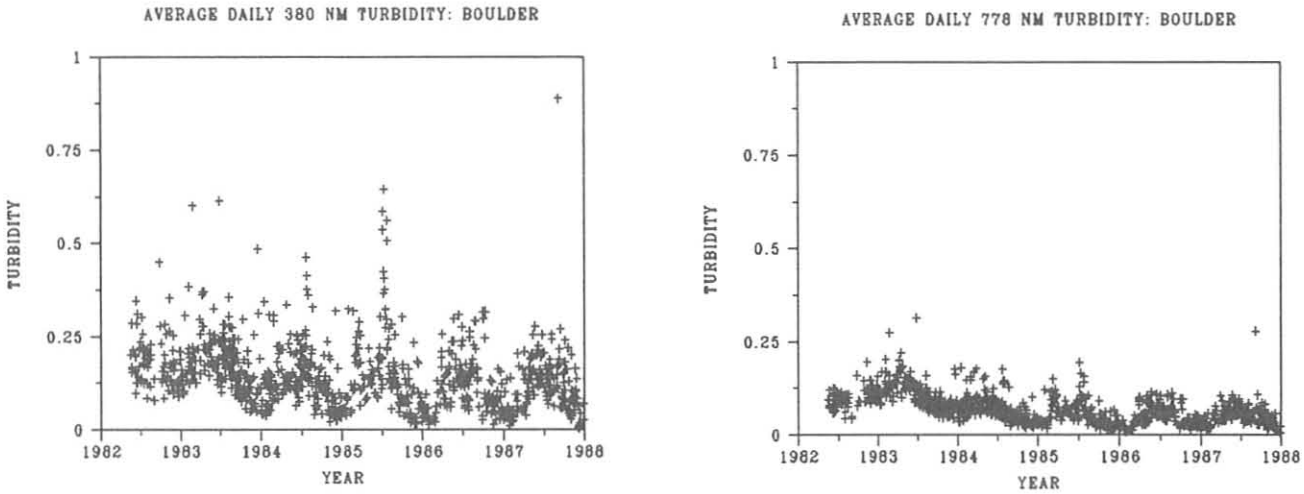

Fig. 3.7. Daily average aerosol optical depths at Boulder at 380 nm and 778 nm.

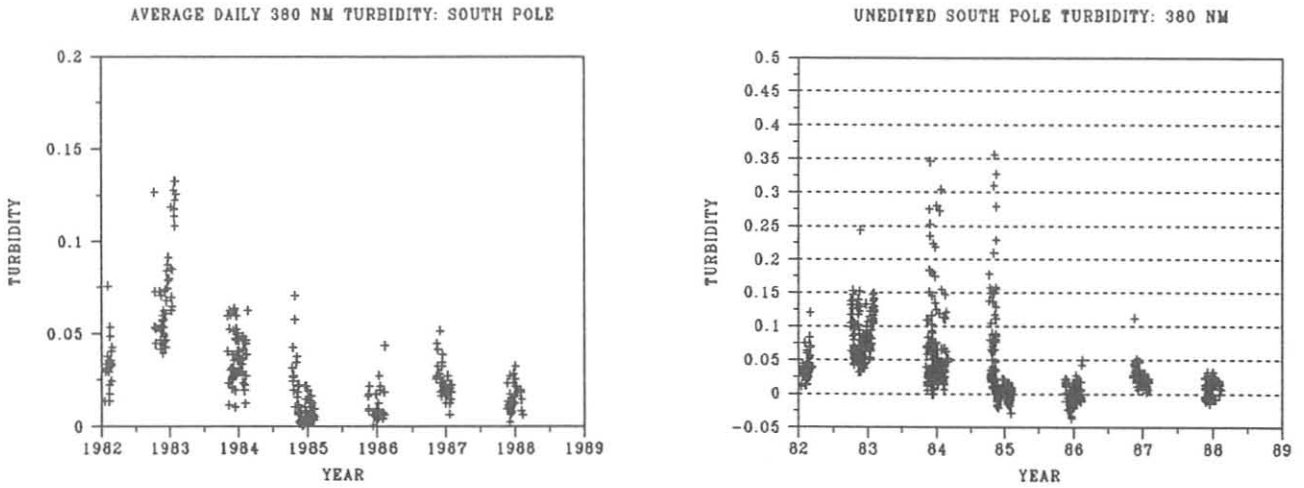

Fig. 3.8. Aerosol optical depths at SPO: daily averages at 380 nm and unedited instantaneous 380-nm data.

the heated room causes density discontinuity waves in the air around the window. Sunlight is apparently focused in some areas of the wave field, and the peak-hold feature stores the maximum signal received within the measurement period. An artificially high reading and correspondingly low computed optical depth result. This phenomenon has been duplicated at Boulder during observations made in subfreezing weather near a building air exit vent on the roof of the ERL building.

During the 1987-1988 austral summer, the SPO crew made sunphotometer observations outside the facility, and no negative optical depths were observed. The 1988-1989 crew will be asked to take readings from inside the facility as well as outside in the hopes that this will provide some quantitative measure of the impact of past measurement practices on the South Pole record.

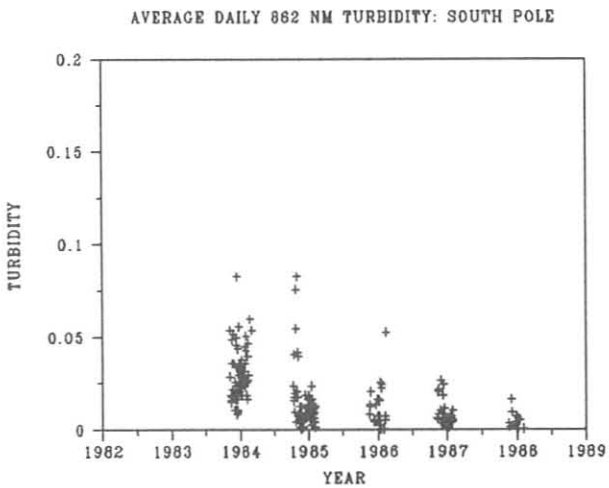

Fig. 3.9. Daily average aerosol optical depths at SPO at 862 nm.

3.2. Special Projects

3.2.1. Zenith-Sky Cloud Detection for Automated Dobson Umkehr Measurements

The seven automated Dobson instruments of the GMCC program operate in the Umkehr mode without the presence of an operator [*Komhyr et al.*, 1984]. In the absence of an onsite observer it is necessary to have an independent measure of zenith-sky conditions, because the large-particle scattering condition (primarily clouds) of the zenith sky is manifested in the Umkehr measurement, which is accepted or rejected on the basis of the smoothness of the Umkehr curve. Erroneous Umkehr data could be due either to such cloud interference or to instrumentation malfunction. Large-particle scatterers such as cirrus clouds present the most serious problem because of their optical thickness and variability over short periods of time. Atmospheric aerosols in the troposphere are less serious because they are more homogeneously distributed in the lower atmosphere where the Umkehr sensitivity is low and their optical thickness is considerably less than that of cirrus clouds.

To monitor the zenith-sky brightness as an indicator of cloud presence during an Umkehr measurement, GMCC constructed a special photometer--a zentih-sky cloud detector (ZSCD)--to view essentially the same sky as the Dobson instrument does. Figure 3.10 is a drawing of the design of the ZSCD. The lens and aperture fix the field of view at 0.060 sr. The filter bandpass is 10 nm centered at 862 nm. The collimator tube is protected with a dust- and rain-resistant glass cover, and the shade tube prevents the sun's direct rays from reaching the glass cover. Water drain holes are located in the block holding the shade tube. A stable EG & G silicon photodiode is used with an amplifier that is adjusted to give an output of 0-10 V. The system dark current is obtained each time the hatch cover of the Dobson housing dome is automatically closed between observation times. The output is adjusted to give a voltage reading of a few volts for a cloud-free zenith sky. All field instruments were compared simultaneously, and amplifiers were adjusted to give the same readings.

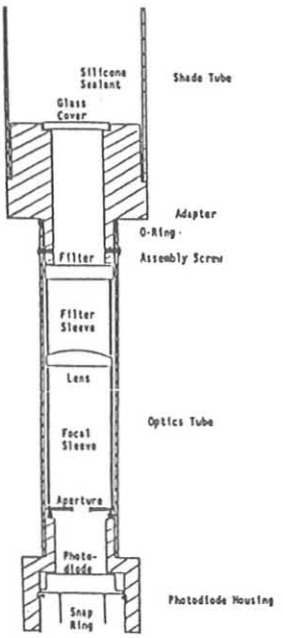

Fig. 3.10. A schematic of the zenith-sky cloud detector.

At the automated Dobson field sites the output of the ZSCD was fed to the data acquisition system. During the data processing procedure, which was carried out at Boulder, the digitized cloud detector signal and a plot of the signal strength versus time were automatically recorded.

Figure 3.11 shows an example of zenith-sky signals at MLO received under conditions completely free of clouds on the morning of March 21, 1988, during the time that the Umkehr observation (solid line) was made. Note the low value of the ZSCD signal and the very smooth continuity in the fitted curve (dashed line). On March 19, 1988, during the afternoon Umkehr measurement, clouds interfered severely. The interference effects are shown in Figure 3.12.

These examples serve to illustrate the sensitivity of the zenith-sky cloud observations and the ability to quantify the quality of the zenith-sky conditions during an Umkehr measurement. The Umkehr, being a ratio measurement, does not clearly display direct relationships between cloud presence and error, other than to produce a noisy observation. However, in general, thin cloud cover will cause the Umkehr observation N-values to become erroneously high at the smaller zenith angles. At the larger zenith angles, interference effects become less than at the smaller zenith angles.

3.2.2. An Objective Method of Correcting Umkehr Measurements for Volcanic Aerosol Error

An objective method of calculating errors to Umkehr measurements for stratospheric aerosol interference was developed and used on a selected set of Umkehr data. The

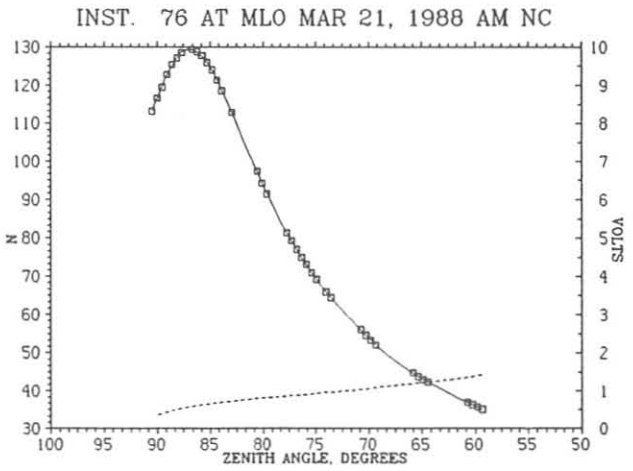

Fig. 3.11. Umkehr observation N-values versus solar zenith angle (solid line), taken at MLO. The dashed line represents the zenith-sky signal observation from the ZSCD versus zenith angle at the same time as the Umkehr observation. These results, obtained during the morning of March 21, 1988, are typical of completely cloud-free conditions.

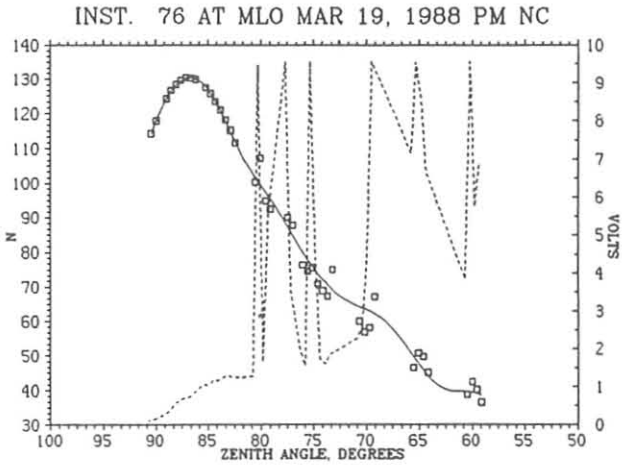

Fig. 3.12. N-values and zenith-sky signals, both versus zenith angle, as in Figure 3.11 but for the afternoon of March 19, 1988, and under conditions of severe cloud interference for part of the observation.

method involves theoretical calculations that include observations of stratospheric ozone and aerosols. Stratospheric ozone and aerosol profile data used to calculate the errors to the Umkehr measurements are derived from ozonesonde observations and from observations provided by five lidar stations in the northern hemisphere middle latitudes. Optical properties of the stratospheric aerosol are deduced from photometric observations and in situ observations of aerosol size distribution. The calculated errors are used to correct Umkehr data for several stations in the northern middle-latitude region. The corrected data display noteworthy variations, one of which is an obvious decrease in ozone concentration in the upper stratosphere during the first half of the 1980 decade. However, the decrease does not appear to be out of the range of variations seen in the long-term data set.

Calculations of the Stratospheric Aerosol Error

A schematic diagram that gives the sequence of steps for correcting Umkehr ozone profiles is shown in Figure 3.13. The following subsections contain a discussion of those steps.

Data sources. To calculate the error for a given month, it is necessary to acquire the following data:

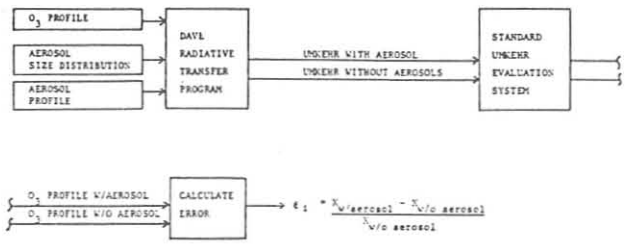

Fig. 3.13. Scheme of the steps to calculate the stratospheric aerosol error to the Umkehr ozone profile.

- Stratospheric aerosol profile information from lidar sites and from satellites such as in the Stratospheric Aerosol and Gas Experiment (SAGE).
- Optical thickness information from lidar and satellite measurement systems as well as ground-based turbidity measurements.
- Aerosol size distribution from in situ aircraft and dustsonde systems.

Theoretical Computation. The procedure for calculating aerosol errors to the Umkehr profile is as follows:

- Use the *Dave et al.* [1979] multiple-scattering code with pseudo-spherical atmosphere approximation to calculate an Umkehr profile.
- Use monthly average lidar observations of the stratospheric aerosol profile for input to Dave's code [*DeLuisi et al.*, 1988].
- Use monthly average ozonesonde profile data [*Tiao et al.*, 1986] for input to Dave's code.
- Assume surface reflectance = 0 for the present study. The error is small.
- Calculate Umkehr N-values for atmospheres with and without aerosols separately. N_A and N_C stand for N-values with and without aerosol effects, respectively. $\Delta N_A = N_A - N_C$.
- Invert the results of calculated Umkehr measurements following the procedure given next.

The monthly averaged stratospheric optical thickness observed by lidar at five northern middle-latitude sites is shown in Fig. 3.14 [*DeLuisi et al.*, 1988]. Note the abrupt change caused by the eruption of El Chichon. The corresponding vertical profiles to the optical thickness results were used in the theoretical calculations for error.

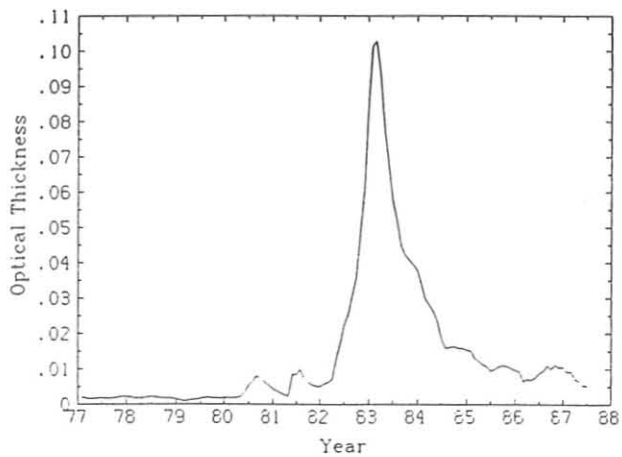

Fig. 3.14. Monthly averaged (smoothed) stratospheric aerosol optical thickness observed by lidar at five northern middle latitude sites vs. time. The sites were Langley, Virginia, U.S.A.; Aberystwyth, Wales; Haute Provence, France; Boulder, Colorado, U.S.A.; and Garmisch-Partenkirchen, F.R.G. (figure from *DeLuisi et al.* [1988]).

Inversion of Umkehr. The procedure for estimating the ozone profile error due to aerosols is as follows:

- Use the WMO Uniform Evaluation System (conventional Umkehr) to invert the Umkehr measurement.
- Use a monthly average *actually observed Umkehr* profile acquired during conditions of stratospheric quiescence. Invert this Umkehr profile. Then, invert the same Umkehr profile, but with ΔN_A added to it.
- Calculate the ozone error profile by taking the difference between the two cases (with aerosol and without aerosol) and dividing by the without aerosol case.

Results and Discussion

Figure 3.15 shows the unweighted average ozone profiles for 1970-1986, in Umkehr layers, for four of the five Umkehr stations: Belsk, Arosa, Lisbon, and Tateno. It is obvious that amounts for layers 5 through 9 were lower than normal during the passage of the major mass of the El Chichon cloud.

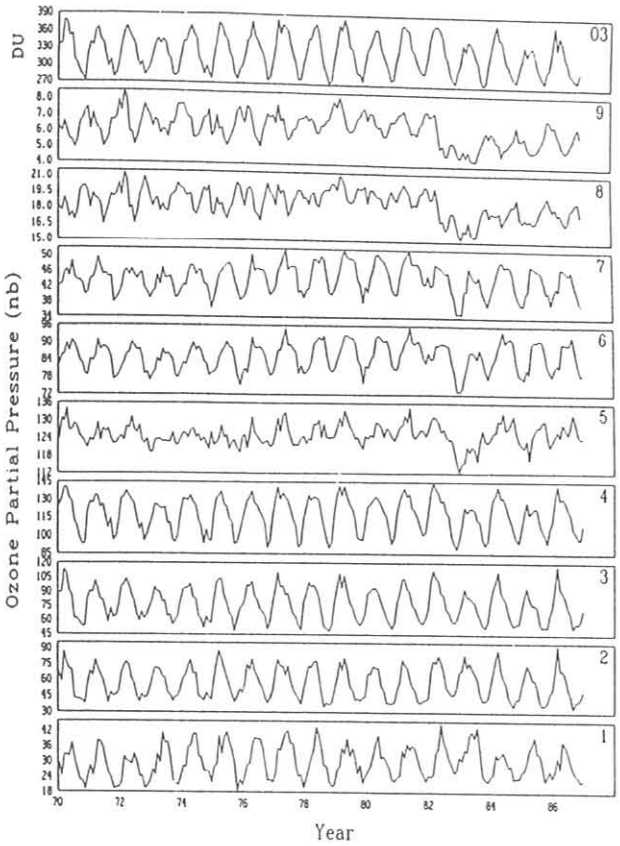

Fig. 3.15. Monthly average ozone partial pressure vs. time, in Umkehr layers 1-9 for Belsk, Arosa, Lisbon, and Tateno, for 1970-1986. Also shown (top) is a plot of total ozone (in Dobson units, DU) corresponding to the ozone profile data. Data were supplied courtesy World Ozone Data Center at Toronto. These data have not been corrected for stratospheric aerosol error. Note the error effects of El Chichon during the winter of 1982-1983.

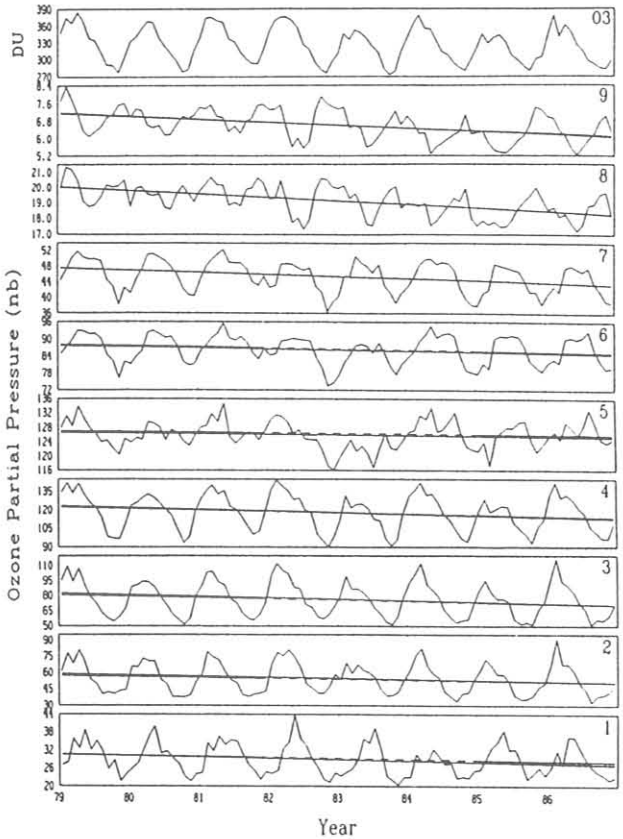

Fig. 3.16. Monthly average ozone partial pressure vs. time as in Figure 3.15, but including data from Boulder and beginning in 1979. Also, the data have been corrected for stratospheric aerosol errors throughout the entire length of record. The solid lines are the least-squares linear fits for slope. The dashed segments are the fit excluding the years 1982-1984.

The corrected profiles are shown in Figure 3.16. (The figure also includes data from Boulder station and is for 1979-1986.) We estimate an uncertainty of the calculated correction to be in the range of 10% to 20%. The maximum estimated error was 38% ± 6% in layer 9 during the winter of 1982-1983. The lower values seen in layer 5 during years 1983 and 1985 and after correction are thought to be due to strong quasibiennial effects [see *Bojkov*, 1987]. In 1983 the increased error is due to the imperfect coincidence of the aerosol and Umkehr data. A 12-mo running average was used to smooth the data of Figure 3.16 and a least-squares linear fit was applied to estimate a linear change, excluding the years 1983-1985. The results are shown in Figure 3.17. This figure shows the 8-yr ozone change in percent for each Umkehr layer (dashed line with 2σ confidence level). In addition, the change for the same time period given by the Lawrence Livermore two-dimensional model [*DeLuisi et al.*, 1988] that includes photochemical depletion due to fluorocarbons and solar cycle variations is shown (solid line). The corrected Umkehr observations will be used to validate satellite SBUV measurements of ozone profile.

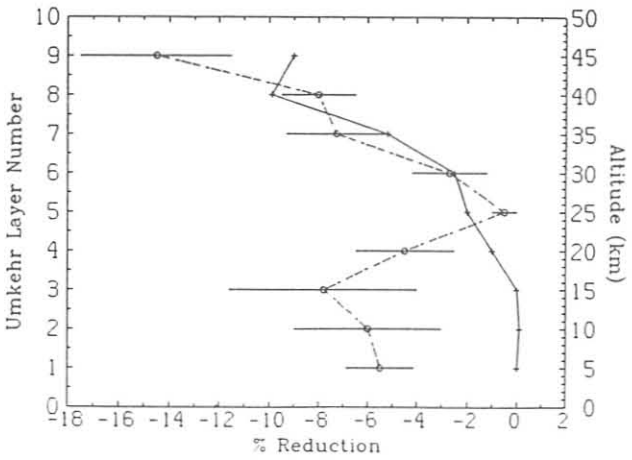

Fig. 3.17. Plot of Umkehr ozone concentration reduction (dashed line) and modeled ozone concentration reduction (solid line) in Umkehr layers 1-9, during 1979-1986. The bars represent the 2σ confidence level.

3.3. REFERENCES

Bird, R.E., and C. Riordan, Simple solar spectral model for direct and diffuse irradiance on horizontal and tilted planes at the earth's surface for cloudless atmospheres. *J. Clim. Appl. Meteorol., 25*, 87-97, 1986.

Bodhaine, B.A., and J.J. DeLuisi, An aerosol climatology of Samoa, *J. Atmos. Chem., 3*, 107-122, 1985.

Bodhaine, B.A., J.J. DeLuisi, J.M. Harris, P. Houmere, and S. Bauman, Aerosol measurements at the South Pole, *Tellus, 38B*, 223-235, 1986.

Bodhaine, B.A., J.J. DeLuisi, J.M. Harris, P. Houmere, and S. Bauman, PIXE analysis of South Pole aerosol, *Nucl. Instrum. Methods, B22*, 241-247, 1987.

Bodhaine, B.A., E.G. Dutton, J.J. DeLuisi, J.M. Harris, G.E. Shaw, and A.D.A. Hansen, South Pole aerosol measurements during 1987, *Proceedings of the Twelfth International Conference on Atmospheric Aerosols and Nucleation*, August 22-27, 1988, Vienna, Austria, Springer-Verlag, 225-228, New York, 1988.

Bojkov, R.D., The 1983 and 1985 anomalies in ozone distribution in perspective, *Mon. Wea. Rev., 115*, 2187-2201, 1987.

Dave, J.V., J.J. DeLuisi, and C.L. Mateer, Results of a comprehensive theoretical examination of the optical effects of aerosols on the Umkehr measurement, *Spec. Environ. Rep. 14*, World Meteorological Organization, Geneva, 15-22, 1979.

DeLuisi, J.J., D.U. Longenecker, C.L. Mateer, and D. J. Wuebbles, An analysis of northern middle latitude Umkehr measurements corrected for stratospheric aerosols for the years 1979-1986, *J. Geophys. Res*, submitted, 1988.

Hansen, A.D.A., B.A. Bodhaine, E.G. Dutton, and R.C. Schnell, Aerosol black carbon measurements at the South Pole: Initial results, 1986-1987, *Geophys. Res. Lett., 15*, 1193-1196, 1988.

Komhyr, W.D., R.D. Grass, R.D. Evans, R.K. Leonard, and G.M. Seneniuk, Umkehr observations with automated Dobson spectrophotometers, *Proceedings of the Quadrennial Ozone Symposium*, September 3-7, 1984, Halkidiki, Greece, D. Reidel, Dordrecht, Holland, 316-320, 1985.

Nelson, D., R. Haas, J. DeLuisi, G. Zerlaut, Results of the NRIP intercomparison November 18-21, 1985, *NOAA Tech. Memo. ERL ARL-161*, 108 pp., Air Resources Laboratory, Silver Spring, Md., 1987.

Tiao, G.C., G.C. Reinsel, J.H. Pedrick, G.M. Allenby, C.L. Mateer, A.J. Miller, and J.J. DeLuisi, A statistical trend analysis of ozonesonde data, *J. Geophys. Res., 91*, 13,121-13,136, 1986.

Quakenbush, T.K., and B.A. Bodhaine, Surface aerosols at the Barrow GMCC Observatory: Data from 1976 through 1985, *NOAA Data Rep. ERL ARL-10*, 230 pp., NOAA Air Resources Laboratory, Boulder, Colo., 1987.

4. Carbon Cycle Group

4.1. Continuing Programs

4.1.1. Continuous In-Situ CO_2 Measurements

The in situ NDIR CO_2 analyzers at the four GMCC observatories continued to operate in 1987. The preliminary monthly and annual means for 1987 are shown in Table 4.1, expressed in the WMO 1985 mole fraction scale (X85). The complete record of the growth rate observed at each station is shown in Figure 4.1. Calibration and data acquisition procedures remained the same as in previous years. A digital-filtering technique [*Thoning et al.*, 1988] was used to separate the seasonal cycle and the long-term trend signals. The latter were plotted as the smooth curves in Figure 4.1. The differences between the annual means of 1987 and 1986 are 1.1 ppm for BRW, 1.8 ppm for MLO, 1.7 ppm for SMO, and 1.6 ppm for SPO. The complete record at MLO has recently been described by *Komhyr et al.* [1988].

In August a new Siemens Ultramat 3 analyzer was installed at MLO parallel to the URAS analyzer that has been in use since the beginning of the program in 1974. To our surprise, the Siemens results were consistently 0.3 ppm lower than the URAS results when they were both analyzing the same air stream and using the same tanks of working standards. Further comparative tests showed that both analyzers gave identical and correct results when analyzing tank air of known concentration, using working standards that consisted of real air. Only when artificial air mixtures (specified concentrations of CO_2, nitrogen, oxygen, and argon) were used as working standards, did the URAS results increase by 0.3 ppm for the tank of known concentration. The Siemens analyzer officially replaced the URAS analyzer in September. Further tests are being carried out to determine if, and for what period, corrections to the URAS record will be necessary.

The calibrations of CO_2-in-air reference gas tanks continued in 1987; on 133 days, 266 tanks were calibrated. There was an accidental loss of one of the NOAA secondary reference gases during shipment to SIO for calibration. These gases define our link to the WMO calibration scale; therefore, this program is somewhat undercalibrated in this respect because of a lack of redundancy. Fifteen large (225 ft^3 STP capacity) aluminum tanks have now been acquired for the backup and eventual replacement of our present set of secondary gases. The new tanks will be filled with dry air at Niwot Ridge, Colorado.

Table 4.1. Provisional Monthly and Annual Mean CO_2 Concentrations (ppm, Relative to Dry Air-X85 Mole Fraction Scale) From the Continuous Analyzers in 1987

	BRW	MLO	SMO	SPO
Jan.	352.36	348.23	346.68	345.72
Feb.	352.72	348.50	346.88	345.55
March	353.90	349.58	346.84	345.54
April	353.85	351.10	346.38	345.72
May	354.44	351.87	347.92	345.95
June	352.19	351.46	347.81	346.41
July	346.45	349.80	348.21	346.92
Aug.	340.38	347.73	347.76	347.47
Sept.	340.54	346.38	347.91	347.94
Oct.	348.38	346.49	348.03	348.02
Nov.	349.50	347.71	348.23	348.17
Dec.	352.57	348.93	348.79	348.10
Annual	349.77	348.98	347.62	346.79

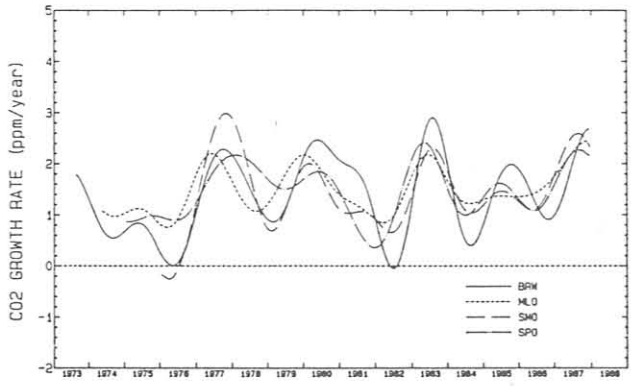

Fig. 4.1. Long-term trends of CO_2 concentration at the four GMCC observatories obtained by digital-filtering of the daily data. The seasonal cycles have been removed by the filtering.

4.1.2. Flask Sample CO_2 Measurements

Measurements of the global distribution of atmospheric CO_2 continued during 1987. Whole air samples were collected in glass flasks at the sites of the NOAA/GMCC cooperative flask sampling network. The network consisted of the same 26 sites as in 1985-1986 [*Schnell and Rosson*, 1986]. The provisional annual mean CO_2 concentrations for 1985-1987 are given in Table 4.2. The annual mean concentrations for 1987 are plotted in sine of latitude coordinates in Figure 4.2, extending a series of latitude plots given in *Schnell and Rosson* [1986, 1987].

In a continuing effort to find a replacement for the greased ground-glass stopcocks currently in use on the 0.5-L flasks, various O-ring stopcocks, with Viton, Buna, and Teflon O-rings were tested. Teflon was most promising, so several hundred Teflon O-ring stopcocks were purchased and installed on flasks. Larger scale laboratory and field tests are in progress to ensure that changing stopcocks will not adversely affect the time series for CO_2 flask data.

Analysis of the statistical uncertainty and some of the systematic biases of flask sampling continued. Biases may arise from the time of day of sampling and from the data selection that results from the rejection of outliers that have residual deviations from a smooth curve fit of more than 3 standard deviations. The biases depend on the method used to produce a smooth curve fit. A preferred method was selected that fits a sum of harmonics to represent the average seasonal cycle and

Table 4.2. Provisional Annual Mean CO_2 Concentrations From the Flask Network Sites

Code	Station	1985	1986	1987
ALT	Alert, N.W.T., Canada	--	348.0	349.5
AMS	Amsterdam Is.	344.1	345.0	[ ]
ASC	Ascencion Is.	345.0	345.8	348.1
AVI	St. Croix, Virgin Is.	345.4	346.4	348.2
AZR	Terceira Is., Azores	346.0	348.7	348.7
BRW	Pt. Barrow, Alaska	346.5	348.6	349.5
CBA	Cold Bay, Alaska	347.2	348.1	349.7
CGO	Cape Grim, Tasmania	343.7	344.6	346.5
CHR	Christmas Is.	345.9	346.3	348.5
CMO	Cape Meares, Oreg.	347.4	347.8	350.8
COS	Cosmos, Peru	[ ]	[ ]	[ ]
GMI	Guam, Mariana Is.	346.2	347.4	349.4
HBA	Halley Bay, Antarctica	344.2	[ ]	347.2
KEY	Key Biscayne, Fla.	346.7	347.6	349.5
KUM	Cape Kumukahi, Hawaii	345.6	346.5	348.5
MBC	Mould Bay, Canada	346.7	348.6	349.8
MID	Midway Is.	--	347.6	349.7
MLO	Mauna Loa, Hawaii	345.3	346.3	348.5
NWR	Niwot Ridge, Colo.	346.1	346.4	348.6
PSA	Palmer Station, Antarctica	343.9	344.7	347.0
SEY	Mahe Is., Seychelles	344.8	346.0	349.0
SGI	South Georgia Is.	--	[ ]	[ ]
SHI	Shemya Is.	--	348.9	350.0
SMO	American Samoa	344.7	345.2	347.1
SPO	South Pole, Antarctica	343.6	344.6	346.8
STM	Station M	346.0	347.2	348.8

Square brackets indicate no flasks received.
Dashes indicate no ongoing program.

uses a digital filter to establish the trend and seasonal anomalies from the residuals. Our estimate of the depth of the summer photosynthetic drawdown of CO_2 at high northern latitudes has increased somewhat compared with earlier work [*Conway et al.*, 1988].

Regular flask samples are obtained from a commercial container ship sailing on a 6-wk round-trip schedule between the west coast of North America and New Zealand. The samples are obtained in pairs at approximately every 5° of latitude by exposing evacuated 2.5-L flasks to ambient air. The sample collection is performed by the deck officers of the *Southland Star* of the Blue Star Line. The project is intended to provide higher resolution data than is available from our network of land-based sampling sites, so that the spatial and temporal variations of CO_2 and CH_4 over the Pacific Ocean can be better determined.

Thus far, 11 round-trip voyages have been completed between December 14, 1986, and May 20, 1988. Preliminary plots of concentrations vs. latitude show the ever-changing variations of atmospheric CO_2 with both latitude and time. However, the seasonal variations at the 5° lattitude intervals are not as well defined as those from the GMCC Pacific Basin flask sampling network sites, as there is only one sample every 3 weeks instead of one per week. Some samples must also be rejected because of poor pair agreement. How well this series of samples characterizes Pacific open-ocean background conditions should become apparent when a project to monitor the CO_2 continuously with an infrared analyzer is carried out on voyage 159 in July 1988.

4.1.3. Model Development

A deeper understanding of the present global carbon budget and its response to climatic changes is a necessary condition for any credible predictions of future levels of CO_2. One of the original purposes of obtaining the GMCC flask data is to deduce the globally significant sources and sinks of atmospheric CO_2 from the observed spatial and temporal gradients. An atmospheric transport model is needed to interpret the observations in terms of sources and sinks.

The Carbon Cycle Group has constructed and used for this purpose a two-dimensional (latitude and height) model that uses the advective and diffusive transport fields derived by *Plumb and Mahlman* [1987] from the GFDL three-dimensional model. This model was used to deduce from the atmospheric measurements the existence of a seasonal cycle in the uptake of CO_2 in the southern oceans and also in the tropical source of CO_2. The model calculations illustrate that in the northern hemisphere the source deduction problem is very hard to solve without measurements over the great continental areas [*Tans et al.*, 1989].

A global three-dimensional transport model is being constructed and tested. It is a Lagrangian type model, in which parcels of air are followed around the globe. The transport is based on ECMWF-observed and -interpolated wind fields. The model can either be stochastic, based on the statistical properties of the ECMWF fields, or it can use the ECMWF fields directly.

4.1.4. Flask Sample Methane Measurements

The measurement of methane in flask air samples returned from the NOAA/GMCC cooperative flask sampling network continued in 1987. Records of these data for SPO and MLO are shown in Figure 4.3. The larger degree of scatter in the MLO data is typical of locations in the northern hemisphere [*Steele et al.*, 1987]. The average growth rate for 1983-1987 at SPO is

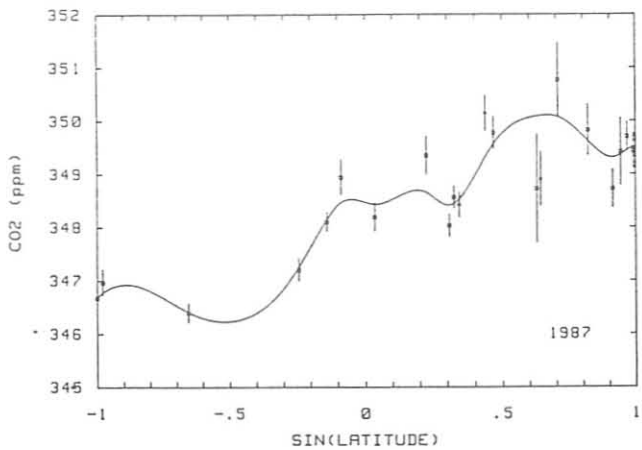

Fig. 4.2. Annual mean CO_2 concentrations vs. sine of latitude for the GMCC flask sampling network. Data plotted with the symbol (+) were not included in the smoothed curve fit.

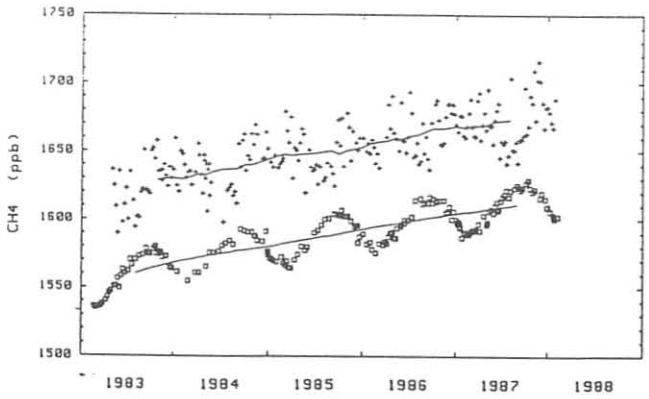

Fig. 4.3. Flask methane data at SPO (boxes) and MLO (pluses). In each case the solid line results by joining adjacent values of the 12-mo running-mean methane concentrations, which are plotted at the midpoint of the appropriate 12-mo interval.

12.1 ± 0.1 ppb yr^{-1}, while at MLO it is 12.2 ± 0.3 ppb yr^{-1}. Growth rates were determined by a linear fit to the 12-mo running-mean concentrations. The growth rates at both of these sites are now lower than they were just 1 year ago: for 1983-1986 at SPO, the average growth rate was 12.5 ± 0.1 ppb yr^{-1} [*Robinson et al.*, 1988], and for 1983-1986 at MLO it was 12.6 ± 0.3 ppb yr^{-1}.

4.1.5. In Situ Methane Measurements At BRW

These measurements continued during 1987 with few interruptions. As in 1986 highly elevated methane concentrations were often observed when the winds had a westerly component. These elevated concentrations are clearly associated with local human activities to the west of the observatory site.

More intriguing are the occurrences of elevated methane concentrations when the winds are from the east, particularly during the Arctic spring. During 1986 these elevations in methane were correlated with elevations in carbon dioxide [*Conway and Steele*, 1988] and aerosol black carbon [*Hansen et al.*, 1988], suggesting a common source or source region for all three species. This finding was confirmed for methane and carbon dioxide during 1987 and is illustrated in Figure 4.4 where scatterplots of hourly average methane versus hourly average carbon dioxide are shown for March 1986 and March 1987. The data shown in Figure 4.4 satisfy the restrictions that the corresponding hourly average wind speed was greater than 5 m s^{-1}, and that the hourly average wind direction was within the sector 20°-110°. Linear fits to the data give slopes of 21.1 ± 0.4 ppb CH_4 per ppm CO_2 for March 1986 and 18.1 ± 0.8 ppb CH_4 per ppm CO_2 for March 1987. It appears that this correlation between CH_4 and CO_2 concentrations is a recurring phenomenon during the Arctic spring.

4.1.6. In Situ Methane Measurements At MLO

During April 1987 an automated gas chromatographic system for the in situ measurement of atmospheric methane was installed at MLO. The chromatograph (Hach-Carle model 04270-A) has a flame ionization detector, and the output is fed to a Hewlett-Packard 3393A integrator. Data are stored on 3.5-in discs that are mailed to Boulder for processing. An ambient air sample is analyzed every 24 minutes, and samples of calibration gas are analyzed before and after every ambient sample. All air samples are dried before analysis. The ambient air is sampled from the top of the walk-up tower. The methane concentrations for the ambient samples are printed out at the site.

The Weiss-designed gas chromatograph was removed from the observatory in late April 1987 after a demonstration that over a period of 12 days the methane concentrations produced by this instrument were essentially identical to those generated by the Hach-Carle-based system.

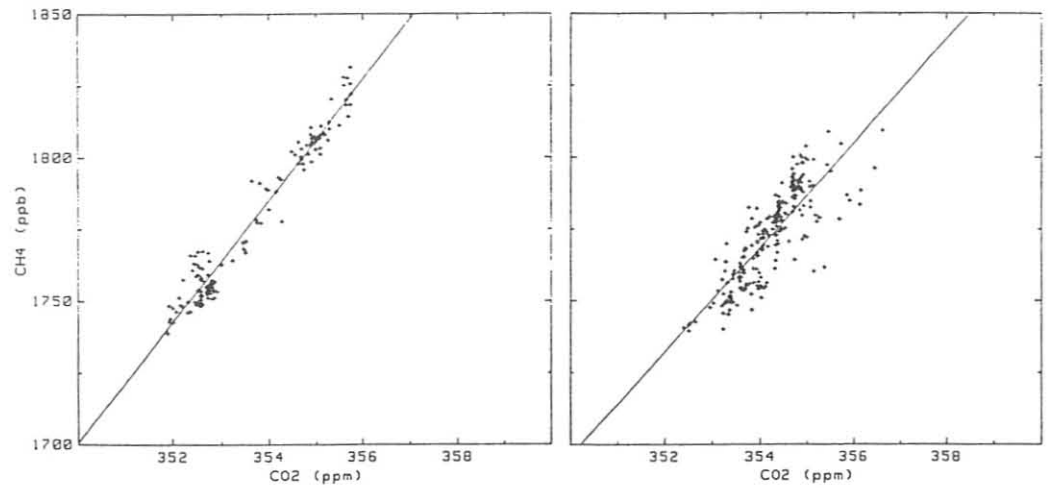

Fig. 4.4. Scatterplots of hourly average methane concentrations versus the corresponding hourly average carbon dioxide concentration at BRW during March 1986 (left) and March 1987 (right). Data are shown only for those times when the hourly average wind speed was greater than 5 m s^{-1} and the hourly average wind direction was within the sector 20°-110°.

The in situ data show some interesting features. During upslope conditions the methane concentrations generally increase. This is opposite to the behavior seen for some other trace gases such as carbon dioxide and ozone. The increase in methane concentrations is consistent with the existence of a vertical gradient in methane, in which lower concentrations are measured at higher altitudes most of the time. Comparison of the MLO in situ data with flask-sample data taken near sea level at Cape Kumukahi shows this vertical gradient quite clearly. However, during October-November there were times when higher concentrations were measured at the observatory than at Cape Kumukahi. Perhaps the most intriguing feature of the in situ data is illustrated in Figure 4.5 which shows the daily average methane concentrations during 1987. The two gaps in the data were due to instrument malfunctions. These daily average concentrations are observed to change by as much as 50 ppb over as little as a few days. A power spectrum of the daily data shows a prominent peak corresponding to a period of 12-14 days. The origin of these fluctuations is still not known.

4.2. Special Projects

4.2.1. SAGA II Expedition

The Carbon Cycle Group, in collaboration with the GMCC NOAH Group, participated in the SAGA II expedition aboard the Soviet research vessel *Akademic Korolev*. Data were obtained by gas chromatography on CO_2 and CH_4 in the atmospheric boundary layer and the sea surface waters between the Kamchatka Peninsula, U.S.S.R., and Wellington, New Zealand.

4.2.2. Egypt Project

In October the Carbon Cycle Group participated in a project that was organized by the National Geographic Society [*El-Baz*, 1988] in collaboration with the Egyptian Antiquities Organization. In 1954 two tombs were discovered adjacent to Cheops' pyramid in Giza. One of them was opened and found to contain all the parts of a remarkably well preserved boat. The boat was reconstructed and is now on display at the site. It was reported that upon opening the first pit the researchers could smell cedar, which would suggest that there had been a very tight seal. It appeared therefore that the second tomb presented a chance to obtain large samples of "old" air.

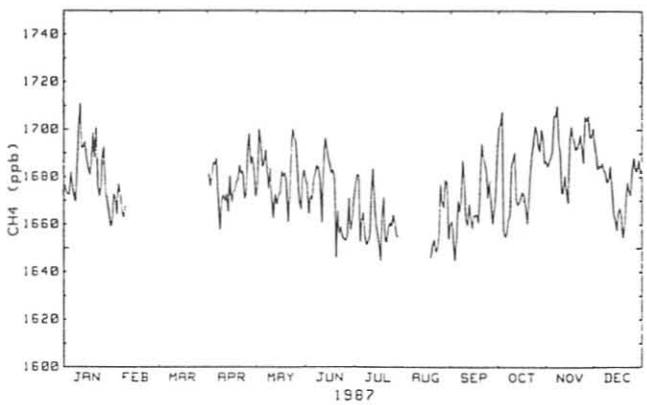

Fig. 4.5. Daily average methane concentrations at MLO during 1987. Data for January and February are from the Weiss-designed chromatograph. Data from April onward are from the Hach-Carle-based system. Gaps in the record are due to instrument malfunctions.

A special airlock assembly was designed by an engineer at Black and Decker, to allow drilling through the 6-ft-thick limestone roof of the chamber and extract air samples, without exchange of outside air with the air in the chamber. The hole was also used for the insertion of video and photography equipment to study the contents of the pit, as well as the insertion of a temperature and humidity monitor. Pieces of a ship similar to the first one were found, but no old air [*Tans et al.*, 1988]. During the sampling of the air inside the chamber it became clear that there was communication between the inside and outside air. This was later confirmed by the measurements of the concentrations of modern industrial gases inside, such as the chlorofluorocarbons CFC-11 and CFC-12. The second boat appeared to be in much worse condition than the first, but the reason for the difference is not understood. A complete and colorful description of the project was given by *El-Baz* [1988]

4.3. References

Conway, T.J. and L.P. Steele, Carbon dioxide and methane in the Arctic atmosphere, *J. Atmos. Chem.*, in press, 1988.

Conway, T.J., P.P. Tans, L.S. Waterman, K.W. Thoning, K.A. Masarie, and R.H. Gammon, Atmospheric carbon dioxide measurements in the remote global troposphere, 1981-1984, *Tellus, 40B*, 81-115, 1988.

El-Baz, F., Finding an Ancient Pharaoh's Barque, *National Geographic, 173*, 513-533, 1988.

Hansen, A.D.A., T.J. Conway, L.P. Steele, B.A. Bodhaine, K.W. Thoning, P. Tans, and T. Novakov, Correlations among combustion effluent species at Barrow, Alaska: Aerosol black carbon, carbon dioxide, and methane, *J. Atmos. Chem.*, in press, 1988.

Komhyr, W.D., T.B. Harris, L.S. Waterman, J.F.S. Chin, and K.W. Thoning, Atmospheric carbon dioxide at Mauna Loa Observatory: NOAA/GMCC measurements with a nondispersive infrared analyzer, 1974-1985, *J. Geophys. Res.*, in press, 1988.

Plumb, R.A., and J.D. Mahlman, The zonally averaged transport characteristics of the GFDL general circulation/transport model, *J. Atmos. Sci., 44*, 298-327, 1987.

Robinson, E., B.A. Bodhaine, W.D. Komhyr, S.J. Oltmans, L.P. Steele, P. Tans, and T.M. Thompson, Long-term air quality monitoring at the South Pole by the NOAA program Geophysical Monitoring for Climatic Change, *Rev. Geophys., 26*, 63-80, 1988.

Schnell, R.C., and R.M. Rosson, Geophysical Monitoring for Climatic Change No 14: Summary Report 1985, NOAA Air Resources Laboratory, Boulder, Colo., 1986.

Schnell, R.C., and R.M. Rosson, Geophysical Monitoring for Climatic Change No 15: Summary Report 1986, NOAA Air Resources Laboratory, Boulder, Colo., 1987.

Steele, L.P., P.J. Fraser, R.A. Rasmussen, M.A.K. Khalil, T.J. Conway, A.J. Crawford, R.H. Gammon, K.A. Masarie, and K.W. Thoning, The global distribution of methane in the troposphere, *J. Atmos. Chem., 5*, 125-171, 1987.

Tans, P.P., J.W. Elkins, and D.R. Kitzis, Air sampling procedures and measurements of the air composition of the second boat pit of Khufu's pyramid, *NOAA Tech. Memo. ERL ARL-163*, NOAA Air Resources Laboratory, Silver Spring, Maryland 1988.

Tans, P.P., T.J. Conway, and T. Nakajawa, Latitudinal distribution of the sources and sinks of atmospheric carbon dioxide derived from surface observations and an atmospheric transport model, *J. Geophys. Res.*, in press, 1988.

Thoning, K.W., P.P. Tans, and W.D. Komhyr, Atmospheric carbon dioxide at Mauna Loa Observatory: II. Analysis of the NOAA/ GMCC data, 1974-1985, *J. Geophys. Res.*, submitted, 1988.

5. Monitoring Trace Gases Group

5.1. Continuing Programs

5.1.1. Total Ozone

Routine Observations

Routine total ozone observations were made with Dobson spectrophotometers during 1987 at 16 stations that constitute the U.S. total ozone station network (Table 5.1). Of the 16 stations, 5 are operated by GMCC personnel, 4 are foreign cooperative stations, 3 are domestic cooperative stations, and 4 are operated by the NWS.

Daily 1987 total ozone amounts applicable to local apparent noon for stations in the U.S. Dobson instrument network have been archived by the WMO, World Ozone Data Centre, 4905 Dufferin Street, Downsview, Ontario M3H5TH, Canada, in *Ozone Data for the World.* Table 5.2 lists provisional monthly mean total ozone amounts for 1987 for the NOAA observatories and the cooperative stations.

1986 International Dobson Spectrophotometer and Brewer Spectrometer Intercomparisons

An international comparison of Dobson ozone spectrophotometers and Brewer spectrometers was conducted by NOAA/GMCC Ozone Project personnel in Arosa, Switzerland, in August 1986. A total of 16 Dobson and 3 Brewer instruments participated. The reference standard instrument for the

TABLE 5.1. U.S. Dobson Ozone Spectrophotometer Station Network for 1987

Station	Period of Record	Instrument No.	Agency
Bismarck, N. Dak.	Jan. 1, 1963-present	33	NOAA
Caribou, Maine	Jan. 1, 1963-present	34	NOAA
Wallops Is., Va.	July 1, 1967-present	38	NOAA; NASA
SMO	Dec. 19, 1975-present	42	NOAA
Tallahassee, Fla.	May 2, 1964-present	58	NOAA; Fla. State Univ.
Boulder, Colo.	Sept. 1, 1966-present	61	NOAA
Poker Flat, Alaska	March 6, 1984-present	63	NOAA; Univ. of Alaska
Lauder, New Zealand	Jan. 29, 1987-present	72	NOAA; DSIR
MLO	Jan. 2, 1964-present	76	NOAA
Nashville, Tenn.	Jan. 2, 1963-present	79	NOAA
Perth, Australia	July 30, 1984-present	81	NOAA; Australian Bureau Meteorol.
SPO	Nov. 17, 1961-present	82	NOAA
Haute Provence, France	Sept. 2, 1983-present	85	NOAA; CNRS
Huancayo, Peru	Feb. 14, 1964-present	87	NOAA; IGP
BRW	June 6, 1986-present	91	NOAA
Fresno, Calif.	June 22, 1983-present	94	NOAA

TABLE 5.2. Provisional 1987 Monthly Mean Total Ozone Amounts (m-atm-cm)

Station	Jan.	Feb.	March	April	May	June	July	Aug.	Sept.	Oct.	Nov.	Dec.
Bismarck, N. Dak.	370	358	373	350	334	335	313	314	297	295	307	325
Caribou, Maine	377	427	380	375	399	369	347	335	333	328	335	340
Wallops Is., Va.	328	335	374	397	384	344	336	327	322	312	289	301
SMO	238	221	240	238	247	248	243	257	253	265	257	254
Tallahassee, Fla.	302	283	342	365	360	314	320	315	323	288	280	263
Boulder, Colo.	328	339	352	342	352	326	317	302	299	287	293	299
Poker Flat, Alaska			406	424	405	360	326	303	309	311		
Lauder, New Zealand	289	287	274	286	301	325	314	329	368	365	335	306
MLO	249	239	263	278	294	292	280	267	262	248	249	237
Nashville, Tenn.	329	320	363	387	352	338	329	326	325	314	291	285
Perth, Australia	275	265	274	274	273	273	293	307	315	325	312	287
SPO	287	278		246	243	241	253	257		141	184	312
Haute Provence, France	329	366	398	385	411	372	346	333	308	298	308	298
Huancayo, Peru			254	246	238	241		254	257	257	251	247
BRW			443	410	400	360	335	305	333	321		
Fresno, Calif.	327	340	352	355	366	347	334	316	310	285	300	303

TABLE 5.3. Results of Calibrations of Foreign Dobson Spectrophotometers With U.S. Primary Standard Dobson Instrument No. 83, Expressed as Mean Total Ozone Differences (%) for Various Air Masses (μ)

Dobson Inst. No.	Country	Calibration Date, 1986	μ = 1.15-1.5	μ = 1.5-2.0	μ = 2.0-2.5	μ = 2.5-3.2	μ = 3.2-4.0	μ = 1.15-3.2
13	Portugal	Aug. 15	-1.13	-2.36	-3.27	-5.80	16.34	-2.41
15	Switzerland	Aug. 15	-1.69	-2.06	-1.80	-2.94	-7.53	-1.99
40	Belgium	Aug. 15	2.39	1.49	0.95	1.16	0.65	1.84
51	Switzerland	Aug. 15	-0.78	-1.62	-1.59	-1.69	-1.63	-1.22
56	Norway	Aug. 15	-1.02	-0.91	-0.55	-0.62	-1.01	-0.89
64	G.D.R.	Aug. 21	-0.16	0.51	0.27	-0.06	-0.21	0.11
71	G.D.R.	Aug. 15	1.69	1.78	2.73	2.49	0.98	1.94
74	Czechoslavakia	Aug. 15	-1.73	-1.25	-1.11	-1.16	-0.61	-1.46
83	United States				Reference Dobson Spectrophotometer			
84	Poland	Aug. 15	3.22	1.70	0.91	0.58	-0.10	2.22
85	France	Aug. 21	-0.17	-0.33	-0.43	-0.05	0.13	-0.23
92	Denmark	Aug. 15	2.04	1.21	0.25	0.07	-1.28	1.34
96	Egypt	Aug. 15	1.69	0.61	0.33	-0.93	-2.82	0.85
101	Switzerland	Aug. 15	-2.63	-2.62	-2.29	-3.42	-4.96	-2.73
104	F.R.G.	Aug. 6	3.78	1.36	0.34	0.34	-0.34	2.41
120	Spain	Aug. 15	2.15	0.70	-0.15	-0.26	-0.20	1.19

Foreign minus Dobson instrument no. 83 percent ozone differences are shown. The Dobson instrument values are derived from observations on AD wavelengths.

comparisons was World Primary Standard Dobson instrument no. 83, maintained by NOAA/GMCC in Boulder, Colorado.

Table 5.3 lists results of preliminary calibrations of the various Dobson instruments relative to instrument no. 83, as a function of the air mass μ. Results of preliminary calibrations of the Brewer spectrometers are shown in Table 5.4. More detailed information regarding the comparisons is available in *Komhyr et al.* [1988a].

Calibration of Portuguese Dobson Instrument No. 13 in Boulder

During 1987 GMCC continued the program that began in 1977 to upgrade foreign Dobson spectrophotometers under the auspices of the WMO Global Ozone Research and Monitoring Project. At the Arosa Dobson instrument comparisons, Portuguese Dobson instrument no. 13 was found to be highly μ dependent. Major repairs were made to the instrument in Boulder in May 1987. The instrument was then optically aligned, calibrated relative to Dobson spectrophotometer no. 83, and returned to Portugal.

Calibration Checks on Dobson Instruments in the Global Network

Komhyr et al. (1981) devised a standard lamp method for identifying Dobson instruments that have gross calibration errors. In an ongoing program by NOAA/GMCC to upgrade the calibrations of Dobson spectrophotometers throughout the world, seven standard lamp units, each consisting of two calibrated lamps and a stable power supply, were fabricated in 1981. The global Dobson instrument station network was then divided into seven areas, each containing 5 to 17 instruments, and a lamp unit was shipped to each area for checking the calibration of the Dobson instruments there. Results of the

TABLE 5.4. Results of Calibrations of Brewer Spectrometers With U.S. Primary Standard Dobson Instrument No. 83, Expressed as Mean Total Ozone Differences (%) for Various Air Masses (μ)

Dobson Inst. No.	Country	Calibration Date, 1986	μ = 1.15-1.5	μ = 1.5-2.0	μ = 2.0-2.5	μ = 2.5-3.2	μ = 3.2-4.0	μ = 1.15-3.2
10	F.R.G.	Aug. 15	0.0	-0.5	-1.1	-0.9	-0.4	-0.6
5	Greece	Aug. 21	0.0	-0.1	-0.6	-0.9	-0.3	-0.4
10	F.R.G.	Aug. 21	0.3	0.2	-0.4	-0.5	0.2	-0.1
17	Canada	Aug. 21	1.1	0.8	0.3	0.4	0.2	0.7

Brewer minus Dobson instrument no. 83 percent ozone differences are shown. The Dobson instrument values are derived from observations on AD wavelengths.

TABLE 5.5. Results of 1985-1987 Calibration Checks on Dobson Spectrophotometers Using Traveling Standard Lamps

Station	Inst No.	Date of Calib. Check	Inst. Calib. Error (%)*
Area 1-North America			
Toronto, Canada	77	May 31, 1985	-0.29
Resolute, Canada	59	Dec. 30, 1985	-0.81
Churchill, Canada	60	Feb. 12, 1986	+1.10
Goose Bay, Canada	62	July 13, 1985	+0.08
Edmonton, Canada	102	Nov. 14, 1985	+0.15
Reykjavik, Iceland	50	June 10, 1986	+0.15
SPO	82	Feb. 2, 1988	+0.15
Bismarck, N. Dak.	33	July 28, 1986	-2.35
Caribou, Maine	86	Oct. 6, 1986	-0.15
Wallops Is., Va.	38	Oct. 10, 1986	-0.22
Tallahassee, Fla.	58	Dec. 31, 1986	-0.29
Nashville, Tenn.	79	Jan. 9, 1987	+1.17
Poker Flat, Alaska	63	Jan. 13, 1987	-1.10
MLO	76	May 24,1987	+1.47
SMO	42	July 15, 1987	+1.61
BRW	91	Jan. 29, 1988	+0.30
Fresno, Calif.	94	May 5, 1987	+1.18
Boulder, Colo.	61	April 11, 1985	-1.03
Boulder, Colo.	65	April 11, 1985	-1.25
Boulder, Colo.	34	Jan. 27, 1988	+0.22
Boulder, Colo.	80	Jan. 13, 1988	+1.40
Area 2-South America, Africa			
Mexico City, Mexico	98	May 22, 1985	+1.32
Huancayo, Peru	87	April 1, 1985	-0.37
Cachoeira Paulista, Brazil	114	June 6, 1986	±0.00
Natal, Brazil	93		
Buenos Aires, Argentina	97	Nov. 4, 1985	-0.52
Buenos Aires, Argentina	99	Nov. 6, 1985	+0.15
Nairobi, Kenya	18		
Area 3-Western Europe (1)			
Bracknell, U.K.	41		
Bracknell, U.K.	2	July 25, 1985	-0.52
Halley Bay, U.K.	123	Dec. 28, 1985	+3.67
Argentine Is., U.K.	31	Feb. 19, 1986	+0.37
Seychelles, U.K.	57	Aug. 26, 1985	-2.50
St. Helena, U.K.	35	Sept. 25, 1985	-0.59
King Edward Point, U.K.	103	Oct. 17, 1985	-1.32
Lerwick, U.K.	32	July 31, 1985	-2.28
Arosa, Switzerland	15	March 27, 1985	-2.57
Arosa, Switzerland	101	March 27, 1985	+4.55
Hohenpeissenberg, F.R.G.	104	April 22, 1985	+2.42
Cologne, F.R.G.	44		
Oslo, Norway	56	July 12, 1985	-0.66
Tromsø, Norway	14	July 5, 1985	-1.03
Spitzbergen, Norway	8	July 3, 1985	-0.22
Cambridge, U.K.	73	Sept. 9, 1986	-2.79
Area 4-Western Europe (2)			
Aarhus, Denmark	92	March 19, 1985	+3.60
Uccle, Belgium	40	April 5, 1985	+1.61
Biscarrosse, France	11		
Haute Provence, France	85	June 27, 1985	-1.25
Lisbon, Portugal	13	July 26, 1985	+0.66
El Arenosillo, Spain	120	Oct. 8, 1985	+0.66
Vigna DiValle, Italy	47	Nov. 27, 1985	+1.03
Brindisi, Italy	46	Nov. 23, 1985	+0.88
Sestola, Italy	48	Dec. 6, 1985	+1.10
Calgiari/Elmas, Italy	113	Nov. 16, 1985	-0.59
Casablanca, Morocco	106		
Cairo, Egypt	69	Feb. 6, 1986	-1.25
Cairo, Egypt	96	Feb. 11, 1986	+1.17
Area 5-Eastern Europe U.S.S.R.			
Leningrad, U.S.S.R.	108	April 2, 1985	+0.08
Belsk, Poland	84	May 23, 1985	+1.24
Hradec Kralové Czechoslovakia	74	June 26, 1985	-4.40
Budapest-Lorini, Hungary	110	July 31, 1985	-1.54
Bucharest, Romania	121	Sept. 5, 1985	+2.72
Potsdam, G.D.R.	64	Oct. 10, 1985	-0.52
Potsdam, G.D.R.	71	Oct. 10, 1985	+0.66
Area 6-India			
New Delhi, India	36	Aug. 9, 1985	+0.73
New Delhi, India	112	April 22, 1985	-0.52
Srinagar, India	10		
Varanasi, India	55	Aug. 22, 1985	-1.76
Mt. Abu, India	54		
Poona, India	39	Jan. 23, 1986	+1.54
Kodaikanal, India	45	July 5, 1985	+2.42
Quetta, Pakistan	43	July 22, 1986	+1.40
Quetta, Pakistan	100	July 19, 1986	+1.47
Bangkok, Thailand	90	Oct. 9, 1986	-1.17
Singapore	7	Dec. 18, 1986	+3.06
Manila, Philippines	52	June 22, 1987	+1.18
Area 7-Australia, Japan			
Sapporo, Japan	5704	July 15, 1985	-0.88
Kagoshima, Japan	5705	June 18, 1985	-0.22
Tateno, Japan	116	July 25,1985	-0.34
Naha/Kagamizu, Japan	5706	June 29, 1985	-0.44
Tateno, Japan	5703	Oct. 24,1985	-0.49
Sapporo, Japan	5702		
Tateno, Japan	122		
Xianghe, China	75	Feb. 3, 1987	+0.66
Kunming, China	3	June 16, 1987	-0.74
Melbourne, Australia	105	July 9, 1986	+0.52
Perth, Australia	81	June 16, 1986	+0.52
Brisbane, Australia	111	Jan. 5, 1986	+0.22
Hobart, Australia	12	March 16, 1986	+0.73
Macquarie Is., Australia	6		
Invercargill, New Zealand	17	Oct. 17,1986	-1.17
Lauder, New Zealand	72		
Seoul, Korea	124	Nov. 30, 1985	+1.17
Melbourne, Australia	115		
Melbourne, Australia	78		

*See text for significance of indicated calibration error. Positive error means that instrument yields ozone values that are too large.

calibration checks were presented at the 1984 Quadrennial Ozone Symposium (*Grass and Komhyr*, 1985).

We present here the results of similar Dobson instrument calibration checks conducted in 1985-1987. Of 95 operational instruments, only 14 stations failed to report sufficient data. Results are shown in Table 5.5. Deduced instrument calibration errors of absolute magnitude >2% were taken to signify that an instrument problem exists. According to this criterion, 13 of 81 instruments were identified as needing recalibration.

Calibration of Primary Standard Dobson Instrument No. 83, 1962-1987

Dobson spectrophotometer no. 83 was established in 1962 as a standard for total ozone measurements in the United States. In 1980, this instrument was designated by the WMO as the Primary Standard Dobson Spectrophotometer for the world. Since 1962, 15 domestic and 75 foreign instruments have been calibrated, many of them several times, either directly or indirectly relative to instrument no. 83.

Absolute calibrations of instrument no. 83 (relative to 1953 Vigioux ozone absorption coefficients for Dobson instrument A and D wavelength pairs) were performed by the Langley slope method at Sterling, Virginia, in 1962, and at Mauna Loa, Hawaii, in 1972, 1976, 1978, 1979, 1980, 1981, 1984, 1986, and 1987. Additionally, calibration checks on the instrument have been performed routinely since 1962 with a set of standard lamps. Analysis of results of the two types of calibrations has yielded data on the long-term ozone measurement precision of the instrument [*Komhyr et al.*, 1988b].

The most comprehensive calibration of instrument no. 83 was performed in 1976 at MLO when ozone observations were made during 90 one-half days. The standard error associated with the determination of the mean correction to the instrument values at that time was 0.0006, which corresponds to an uncertainty in the measurement of ozone of 0.07% for ozone values x = 300 DU and μ = 2. This calibration of instrument no. 83 resulted in establishment of an August 26, 1976, Calibration Scale for the intrument that has been used through 1987 in calibrating all domestic and foreign Dobson spectrophotometers.

The August 26, 1976, Calibration Scale was used to establish N values in 1976 for Dobson instrument no. 83 standard lamps 83A, 83B, W, X, Y, Z, 83Q1, and 83Q2, some of which had been run on the instrument since 1962. The lamp data were then used to establish a 1962-1987 Standard Lamp Calibration Scale for instrument no. 83, which, except for the 1976 tie in, is independent of the Langley slope calibrations of the instrument.

Table 5.6 compares ozone values x_1, determined with instrument no. 83 during 1962-1987 on the August 26, 1976, Calibration Scale, with similar values, x_2 incorporating Langley slope calibration corrections; with x_3 values measured on the 1976 Standard Lamp Scale; and with x_4 values determined on the 1976 Standard Lamp Scale with Langley slope calibration corrections applied. We draw three conclusions from the results. First, the August 26, 1976, Calibration Scale has remained unchanged to within an uncertainty of ±0.5% during 1972-1987. Second, because this scale has remained highly stable with time, additional calibration corrections are not needed for domestic and foreign Dobson instruments calibrated since 1976 with Dobson spectrophotometer no. 83. Finally, instrument no. 83 calibration observations made at MLO spanned a solar cycle sunspot maximum and two minima. Because the Langley slope and the standard lamp instrument calibrations gave essentially identical results, we conclude that if the extraterrestrial intensities of the Dobson instrument A and D wavelengths vary during the course of a solar cycle, the variations are not large enough to cause errors in ozone measurements greater than several tenths of a percent.

TABLE 5.6. Stability of the August 26, 1976, Calibration Scale for Dobson Instrument No. 83

Year	$\frac{100(x_1 - x_2)}{x_2}$ (%)	$\frac{100(x_1 - x_3)}{x_3}$ (%)	$\frac{100(x_1 - x_4)}{x_4}$ (%)
1962		-0.7	-1.0
1972	-0.1	-0.3	-0.1
1976	0.1	0.0	0.1
1978	0.0	0.0	0.0
1979	-0.2	-0.1	-0.2
1980	0.2	0.0	-0.4
1981	-0.3	-0.1	-0.7
1984	0.5	-0.1	0.1
1986	0.2	-0.5	-0.5
1987	0.2	-0.2	-0.1

x_1 ozone values: Based on the August 26, 1976, Calibration Scale and instrument optical wedge calibration of August 26, 1976. x_2 ozone values: As x_1 values, but corrected by the Langley slope calibration method. x_3 ozone values: Based on the Standard Lamp Calibration Scale established in 1976, and updated optical wedge calibrations. x_4 ozone values: As x_3 values, but corrected by the Langley slope calibration method.

Long-Term Changes in the SBUV/TOMS Relative to the Primary Standard Dobson Instrument No. 83

The SBUV and TOMS instruments on Nimbus 7 measured a decrease in total ozone between 1979 and 1986 of 6%, while the Dobson network reported only a 3% decrease during the same period, bringing the long-term calibration of SBUV/TOMS into question. SBUV and TOMS are independent instruments, except that they share the diffuser plate that is used for instrument calibration. The TOMS and SBUV ozone observations agree very well, except for a 3.0% bias.

The time dependence of the calibration of the satellite instruments has been determined by comparing ozone measured by TOMS with that measured by instrument no. 83 [*McPeters and Komhyr*, 1988] at MLO during the summers of 1979, 1980, 1981, 1984, 1986, and 1987. As indicated earlier, instrument no. 83 observations were made for the purpose of monitoring the calibration of that instrument [*Komhyr et al.*, 1988b].

The percent differences between TOMS and instrument no. 83 ozone values are plotted for each year in Figure 5.1. Two different results (data sets 2 and 3) are given for the Dobson instrument; they represent two slightly different calibrations of the instrument. For set 2 the Dobson data were reduced using the 1976 instrument optical wedge calibration for all years,

whereas for set 3 the data were reduced using updated wedge calibrations. The two sets of results are shown to provide some indication of the level of uncertainty in instrument no. 83 results.

Figure 5.1 shows that the TOMS instrument was relatively constant with respect to instrument no. 83 in the period 1979-1981, especially if the Dobson results for 1980 are downweighted because of known problems of observational technique that year. But by 1984 the difference in ozone measured by the two instruments was +0.5%, a 1.5% decline relative to the earlier period, and by 1987 the TOMS ozone values were 1.4% less than instrument no. 83 values, a decline of 3.4% from 1979-1981. The overall pattern is that the TOMS (and by implication SBUV) calibration was relatively constant relative to that of instrument no. 83 between 1979 and 1981, declined rapidly between 1981 and 1986, and appears to be declining less rapidly between 1986 and 1987. Our conclusion is that the diffuser plate used by both the SBUV and TOMS has suffered an uncorrected wavelength-dependent degradation, with most of the degradation occurring between 1983 and 1986.

This change in the TOMS instrument calibration relative to the calibration level of instrument no. 83 confirms the change noted earlier relative to many individual stations. Also plotted in Figure 5.1 is the yearly average TOMS-Dobson trend relative to an ensemble of 41 Dobson stations for the period 1979-1985. These data were used by *Fleig et al.* [1986] to calculate the 0.38% per year trend, but with data for 1985 comparisons added.

Long-Term Ozone Trends at MLO and SMO

Total ozone data obtained in the past at MLO and SMO, archived at the World Ozone Data Centre in Downsview, Canada, have been provisional. The MLO data record for 1964-1987 and the SMO data record for 1976-1987 were reprocessed on the August 26, 1976, Calibration Scale of Primary Standard Dobson instrument no. 83 [*Komhyr et al.*, 1988c]. Although some shortcuts were taken in reprocessing the data, it is unlikely that more detailed processing will give results over portions of the record that differ on average from current values by more than 1%.

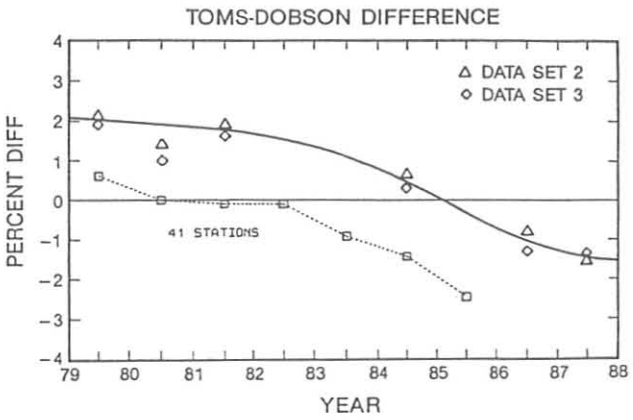

Fig. 5.1. Average ozone differences in percent measured at MLO by TOMS and Dobson instrument no. 83 during 1979-1987. Differences for an ensemble of 41 Dobson stations are also shown.

Figure 5.2 is a plot of ozone anomalies (i.e., deviations of ozone monthly means from monthly normals) at MLO for 1964-1987. Quasi-biennial oscillations in ozone are clearly evident in the record. Least-squares linear regression trend lines fitted to the data indicate that ozone at MLO increased on average at a rate of 0.37 ± 0.16% yr^{-1} during 1964-1974, but decreased at a rate of 0.35 ± 0.13% yr^{-1} during 1974-1987. (Indicated uncertainties are the 95% confidence intervals.) For the record as a whole, the mean ozone trend was -0.07 ± 0.06% yr^{-1}. Annual mean total ozone amounts at MLO were equivalent in 1964 and 1987, at 262 DU.

The SMO Dobson instrument total ozone record was similarly reprocessed. Ozone anomalies for SMO for 1976-1987 are shown in Figure 5.3. A least-squares linear trend line fitted to the data shows that, on average, total ozone has been decreasing at SMO at 0.40 ± 0.11% yr^{-1}. For 1976-1986, the downward trend in ozone was 0.35 ± 0.12% yr^{-1}.

A record low mean monthly total ozone amount of 221 DU was measured at SMO in February 1987, at the time of a deep minimum in the 1986-1987 tropical quasi-biennial oscillation in ozone. This value was 13% lower than the average total ozone amount for February months of 1976-1987. Although the value is subject to revision, it is unlikely to be too low by more than several percent.

Total Ozone at SPO

Total ozone amounts measured at SPO during September-November 1987 were the lowest on record. Figure 5.4 compares SPO total ozone data for 1986 and 1987. For the time interval January-May, the average total ozone amount in 1987 was larger than in 1986 by about 8%. During the polar night of both years, total ozone increased from about 245 DU in early June to 280-290 DU in August. Total ozone began to decrease rapidly during September of both years, to a low of 158 DU in early October 1986 but to an unprecedented low of 127 DU in early October 1987. Thereafter, the total ozone began to recover, but the recovery proceeded considerably more slowly (with a 3-wk delay) in 1987 than in 1986. Compared with the time of the springtime ozone increase at South Pole in 1978, as shown in Figure 5.4, the delay in the 1987 springtime ozone increase was 6 weeks. At year end for both 1986 and 1987, the total ozone amount at SPO was 315 DU.

The 1987 October (October 15-31) mean total ozone amount at South Pole was 138 DU. The previous October mean low of 161 DU occurred in 1985 [*Komhyr et al.*, 1986]. The average total ozone amount for October months at SPO during 1962-1979 (i.e., before onset of the ozone hole formation phenomenon in about 1980) was 292 DU.

The 1987 SPO November total ozone mean of 184 DU was also unusually low. The previous November mean low of 238 DU occurred in 1985. The 1962-1979 average total ozone amount for November months at SPO was 351 DU.

5.1.2. Ozone Vertical Distribution

ECC Ozonesonde Observations

Weekly ECC ozonesonde balloon flights sponsored by NESDIS continued in 1987 at Boulder, Colorado (51 flights),

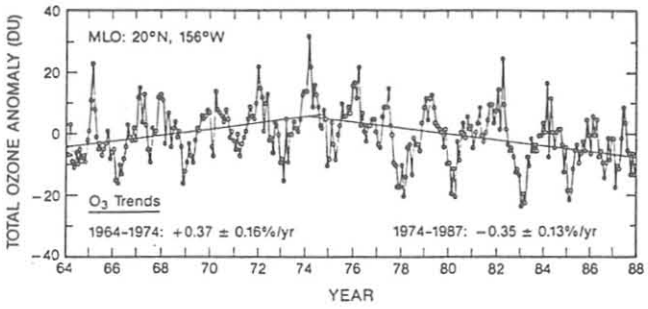

Fig. 5.2. Deviations of monthly mean total ozone amounts from monthly norms for the period of record at MLO (1964-1987). Least-squares regression trend lines are fitted to the data.

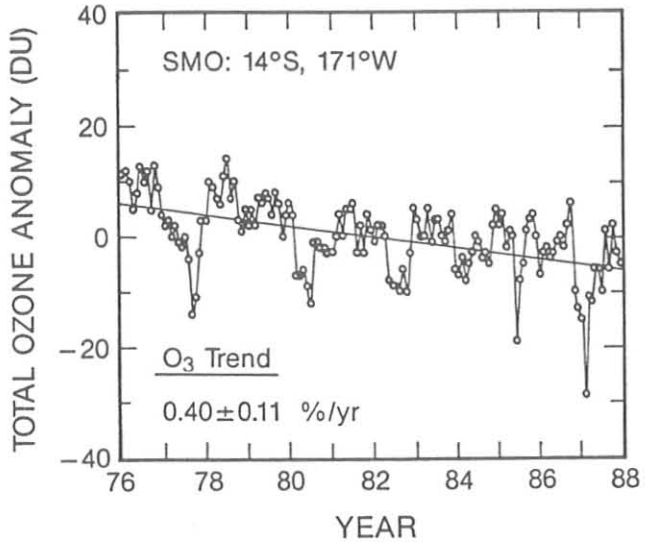

Fig. 5.3. Deviations of monthly mean total ozone amounts from monthly norms for the period of record at SMO (1976-1987). Least-squares regression trend lines are fitted to the data.

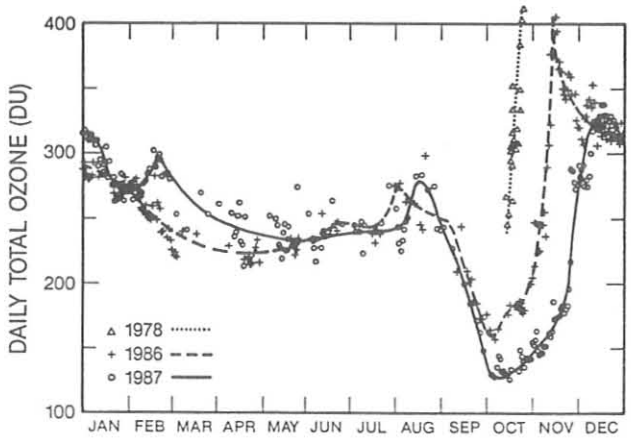

Fig. 5.4. Daily total ozone amounts at SPO in 1986 and 1987, and a portion of the 1978 total ozone record, showing the springtime ozone increase that occurs each year in Antarctica.

and Hilo, Hawaii (52 flights), extending the continuous record of weekly soundings to 3 years at these two sites (1985-1987). Mean Dobson normalization correction factors for these flights were 0.982 for Boulder and 0.984 for Hilo with standard deviations of 0.044 and 0.043, respectively. The data were forwarded to NESDIS to assist in their efforts to validate ozone data from the SBUV instrument on the NOAA F satellite.

At BRW and SMO, approximately weekly ECC ozone soundings were made in 1987, except for an increased launch frequency at BRW during March. Regular ozone soundings at BRW date from February 1986, and at SMO from April 1986, both programs depending for future continuance on the availability of funding.

Computer processing of ozonesonde data continued for the flight program operated by DSIR personnel at Lauder, New Zealand. Weekly ozonesonde releases were made at Lauder throughout the year, except twice-weekly during August-November months, for a total of 66 soundings [*Matthews et al.*, 1988]. This monitoring program provides an opportunity to assess the impact of ozone depletion in Antarctica on the ozone budget of the southern hemisphere at midlatitudes.

With support from NOAA and the NSF Division of Polar Programs, a successful campaign of 76 ECC ozonesonde flights was conducted in 1987 at SPO. From August through November, twice-weekly flights were conducted; during the remainder of the year, weekly soundings were made. Results were published by *Komhyr et al.*, [1988d].

Latitudinal Distribution of Ozone From ECC Ozonesonde Observations

ECC ozonesonde observations, made in recent years at nine U.S. and foreign stations whose locations range from the Arctic to Antarctica, have yielded a self-consistent data base from which the latitudinal distribution of ozone to 35 km altitude has been derived [*Komhyr et al.*, 1988e]. The stations are Resolute, Canada (74°N, 95°W); Point Barrow, Alaska (71°N, 156°W); Edmonton, Canada (53°N, 114°W); Boulder, Colorado (40°N, 105°W); Hilo, Hawaii (19°S, 155°W); American Samoa (14°S, 170°W); Lauder, New Zealand (45°S, 170°E); Syowa, Antarctica (69°S, 39°E); and South Pole, Antarctica (90°S, 24.8°W). Average seasonal and annual ozone vertical distributions have also been derived for the sites. The data should be useful for comparison with model calculations of the global distribution of atmospheric ozone, for serving as a priori statistical information in deriving ozone vertical distributions from satellite and Umkehr observations, and for improving the satellite and Umkehr ozone inversion algorithms.

Average December-January-February (DJF), March-April-May (MAM), June-July-August (JJA), September-October-November (SON), and annual (ANN) ozone profiles for the nine stations are plotted in Figure 5.5. Average seasonal and annual isopleths of ozone partial pressure to 35-km altitude, as a function of latitude, are presented in Figures 5.6 and 5.7, respectively. For 75°-90°N latitude, the isopleths were extrapolated, since the northernmost ozone data in the Arctic were obtained at Resolute at latitude 74°N.

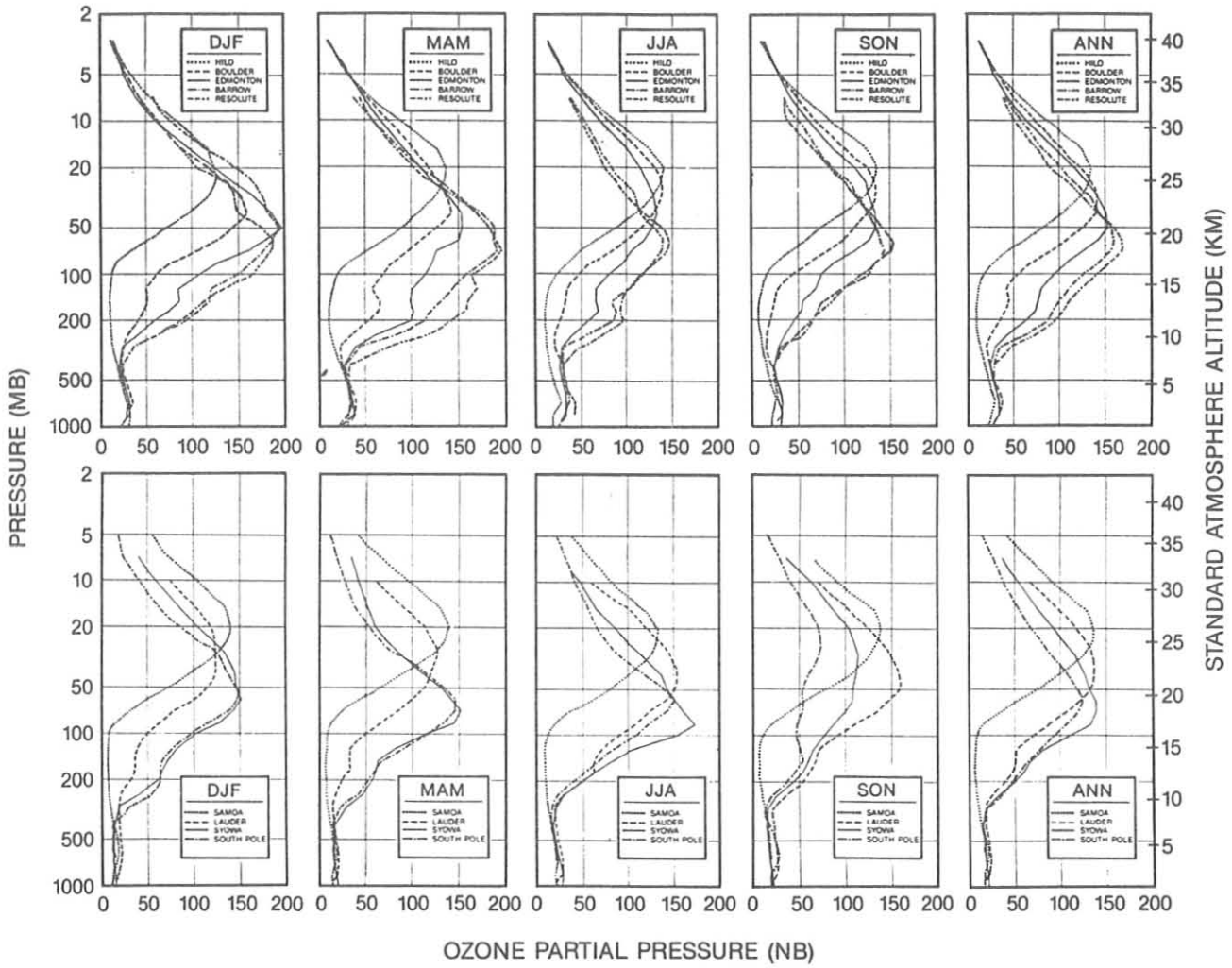

Fig. 5.5. Average seasonal and annual ozone profiles derived at nine stations from observations made in recent years with ECC ozonesondes.

Antarctica Springtime Ozone Depletion

Compared with the ozone depletion in the spring of 1986, the ozone hole at the south pole in 1987 formed more rapidly, was deeper in vertical extent, and lasted longer into the summer season [*Komhyr et al.*, 1988f]. A 4-km-thick atmospheric layer, centered on 17 km, was nearly completely depleted of ozone in early October. Select ECC ozonesonde data, comparing ozone hole formation at the south pole in 1986 and 1987, are shown in Figure 5.8.

In further contrast to the spring of 1986, colder stratospheric and warmer tropospheric temperatures in 1987 accompanied the deeper losses in ozone. The polar vortex broke down during late November-early December, 3 weeks later than it did in 1986. The enhanced ozone decrease at the south pole in the spring of 1987, compared with 1986, probably resulted largely from atmospheric circulation changes associated with the 1987 ENSO event. These changes augmented environmental conditions that promoted photochemical ozone destruction on polar stratospheric clouds and increased polar vortex stability, causing the springtime transport of ozone to Antarctica to be delayed.

Changes in South Pole Ozone Vertical Distributions Since the Early 1960's

A comparison of ozone vertical profile data obtained at SPO with Regener chemiluminescent ozonesondes in 1962-1965, and ECC ozonesondes in 1967-1971 and 1986-1987, has revealed a progressive ozone decrease with time for all seasons in the region of the ozone maximum centered at about 17 km (Figure 5.9), with the decrease rate accelerating in recent years during October months [*Komhyr et al.*, 1988g]. The altitudes of the ozone maxima, furthermore, exhibit an increase with time for all seasons. During summer months, a reduction in ozone with time has occurred in the stratosphere below 20 km, but an increase in ozone appears to have occurred above 20 km.

Umkehr Observations

In 1987, Umkehr observations were made with automated Dobson spectrophotometers [*Komhyr et al.*, 1985] at six stations: Boulder, Colorado (BDR, 40°N, 105°W); Mauna Loa Observatory, Hawaii (MLO, 20°N, 156°W); l'Observatoire de Haute Provence, France (OHP, 44°N, 6°E); Poker Flat Research Range, Alaska (POK, 65°N, 148°W); Perth Airport, Australia

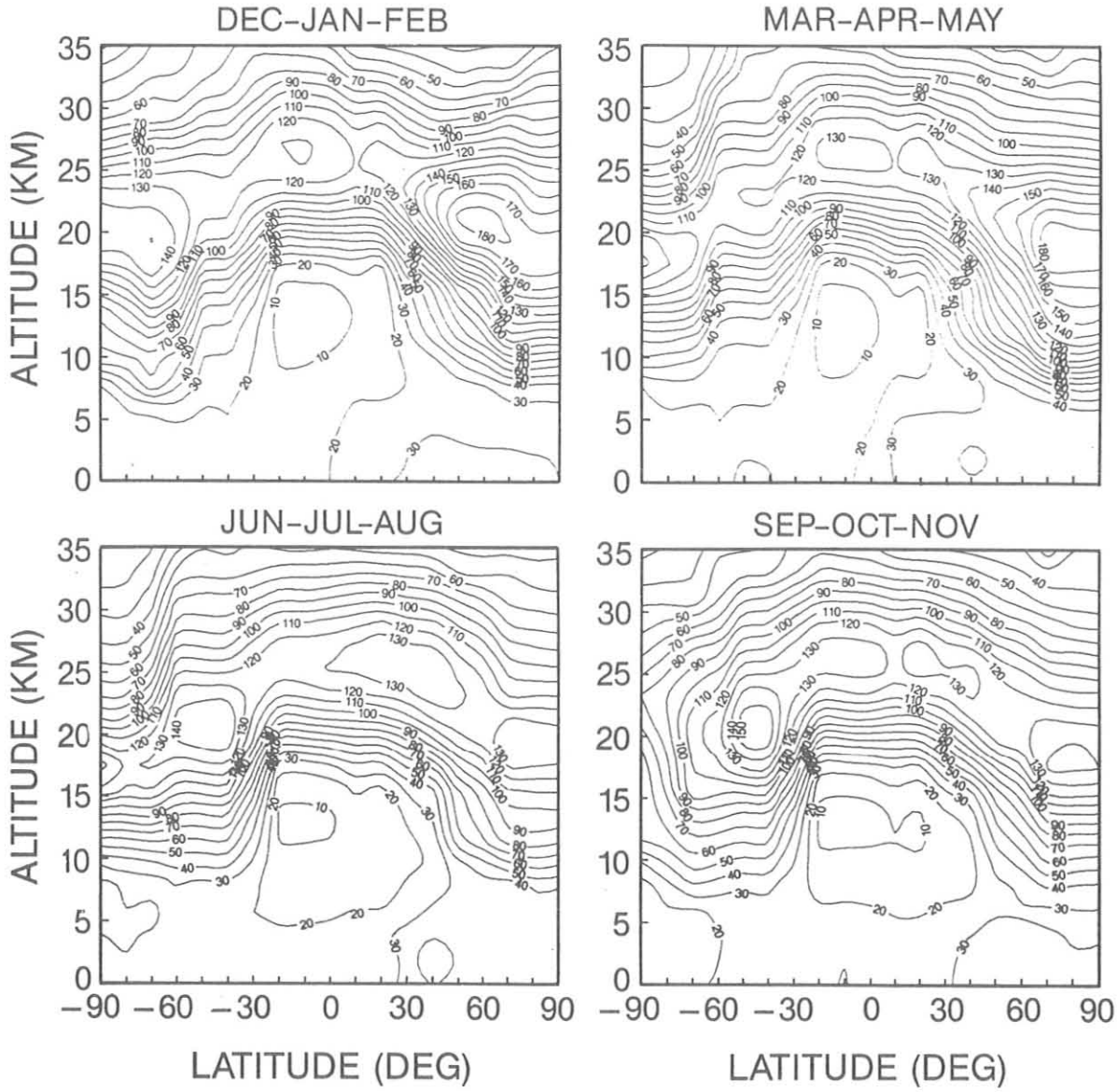

Fig. 5.6. Average seasonal isopleths of ozone partial pressure (nb) to 35 km altitude as a function of latitude, from ECC ozonesonde observations made in recent years at nine stations between 74°N and 90°S latitude.

(PTH, 32°S, 116°E); and Lauder, New Zealand (LDR, 45°S, 169°E). LDR became operational in February 1987. No serious instrument problems occurred at any of these stations. In 1987, 1298 usable ozone profiles were obtained. The Umkehr data are archived at the World Ozone Data Centre, Atmospheric Environment Service, Downsview, Ontario, Canada.

The Dobson instrument at Huancayo was operated manually throughout 1987 for total ozone observations only. Umkehr observations were not made, owing to malfunction of the automated instrument's computer system. A trip to the station was made in August to attempt to repair the system. A number of components were brought back to the United States for repair, and returned to the station, but the system remained down because of poor-quality main power. An isolation transformer was ordered for the system, but was not received by year's end.

A study was made [*Evans et al.*, 1988] of Umkehr profiles deduced by the conventional method [*Mateer and Dütsch* 1964] from data obtained at BDR, MLO, OHP, POK, and PTH during 1986 and 1987. By this time, stratospheric aerosols from the 1982 El Chichon eruption no longer affected the Umkehr observations adversely. Seasonal and annual Umkehr profiles for the five stations are shown for 1986 and 1987 in Figure 5.10. Differences in the profiles at each station for the 2 years are small. For annual means, no station shows a difference in any layer larger than the standard deviations associated with the means. This is generally repeated for the seasonal differences, except for the October-December MLO averages where

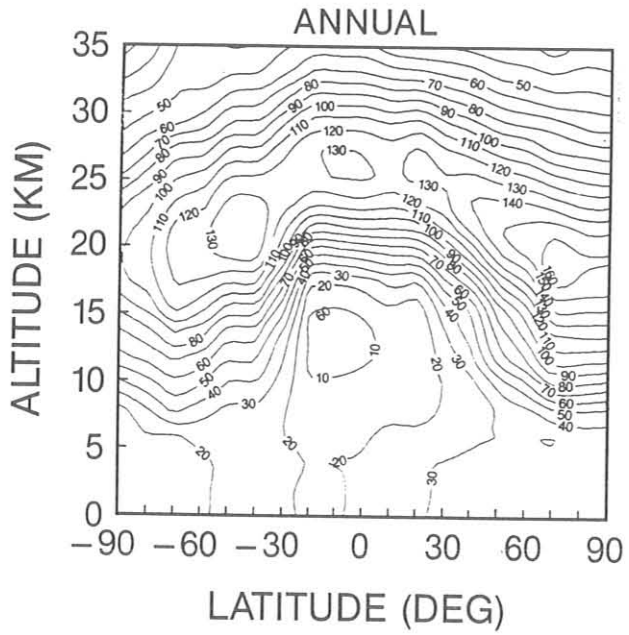

Fig. 5.7. Average annual isopleths of ozone partial pressure (nb) to 35 km altitude as a function of latitude, from ECC ozonesonde observations made in recent years at nine stations between 74°N and 90°S latitude.

significant differences have resulted from quasi-biennial oscillation effects. Classical features of the atmospheric ozone vertical distribution are exhibited by the profiles. The altitudes of the primary ozone maxima decrease as station latitude increases, and the maxima at higher latitude stations are broader than those at lower latitude. This broadening is greatest during winter seasons.

ECC Ozonesonde and Umkehr Profiles Compared

Ozone profiles obtained quasi-simultaneously from ECC ozonesonde and Dobson Umkehr observations at Boulder and at Hilo/MLO during 1985-1987 are given in Figures 5.11 and 5.12 respectively. The profiles show agreement [*Franchois et al.*, 1988] to within ±10% in Umkehr layers 4-6 (19-35 km). In layer 7 (35-40 km) the differences range from 15 to 25%, depending on season and station. Use of inadequate ECC ozonesonde pump efficiency corrections in Umkehr layer 7 most likely contributes to the observed differences in measured ozone. However, because the differences vary with station and season, it is most likely, also, that inadequacies in the inversion algorithm used in processing the Umkehr data contribute to the observed differences. The problem probably lies with the a priori information (first-guess profiles) used in the inversion algorithms.

5.1.3. Tropospheric Ozone

Prior to this report, GMCC tropospheric ozone research has concentrated on the four-station surface-based in situ ozone measurements. In 1985 ozone vertical profile measurements using ECC ozonesondes were begun on a weekly schedule at Boulder and Hilo. In 1986 ozonesonde programs were inaugurated at BRW, SMO, Lauder, (in cooperation with DSIR), and SPO. Although these soundings were begun primarily for stratospheric research, they provide a wealth of tropospheric data as well. Included here are results from the surface measurements as well as from the tropospheric portion of the ozonesonde profiles.

Although ozone amounts at the surface at MLO have been near the long-term mean in recent years, the overall 15-yr record shows a significant increase (Figure 5.13). This has been primarily a result of increases during the winter months. At BRW (Figure 5.13), on the other hand, which also shows a significant increase for the 15-yr period of observations, the largest increase is during the summer months.

In the southern hemisphere (Figure 5.14), the trend at SMO for all months is not significant, but during the seasonal minimum, which occurs during the austral summer, a large, significant decrease (1.9% yr^{-1}) has taken place. This is similar to the decrease seen at SPO during the same time of year (Figure 5.14). This is also the seasonal minimum in surface ozone at SPO. The low value for the seasonal minimum reported at SPO in 1987 [*Komhyr et al.*, 1988h] continued the downward trend reported last year [*Schnell and Rosson*, 1987]. The seasonal maximum was also much lower in 1987, reversing what appeared to be a number of years of increasing values.

On the basis of ozonesonde data from nine locations (the six GMCC sites described above as well as two Canadian sites and a Japanese station in Antarctica) stretching from 75°N to 90°S there is strong evidence that there is more tropospheric ozone in the northern hemisphere than in the southern hemisphere (Figure 5.15). On an average annual basis for all altitudes below 400 mb there is more ozone at all locations in the northern hemisphere than at any site in the southern hemisphere. This is not, however, always true on a seasonal or monthly basis. The reason for larger values in the northern hemisphere is probably both greater cross-tropopause fluxes of ozone from the stratosphere into the troposphere as well as possible production of ozone in the northern hemisphere troposphere there as a result of the emission of anthropogenic ozone precursors.

5.1.4. Stratospheric Water Vapor

Approximately monthly soundings of the water vapor content of the upper troposphere and stratosphere to about 25 km were continued in Boulder. In addition three soundings were attempted at McMurdo Station, Antarctica, during the austral spring. Because of problems with the balloon valving system, good descent data were not obtained on any of the flights. Several pieces of useful information were obtained from the ascent portion of the profiles, however. The McMurdo results [*Rosen et al.*, 1988] indicate that water vapor mixing ratios in the region between 15 and 20 km were approximately 2 ppmv. Because of the possibility of contamination from the balloon and instrument on balloon ascent, these data can only be construed as upper limits. To altitudes of about 70-80 mb (17-18 km), there is usually good agreement between ascent and descent data for flights made in Boulder. Above this altitude the amounts diverge, with the ascent data always higher.

Several instrument-related developments to the frost-point hygrometer are of note. Persistent noise problems that have

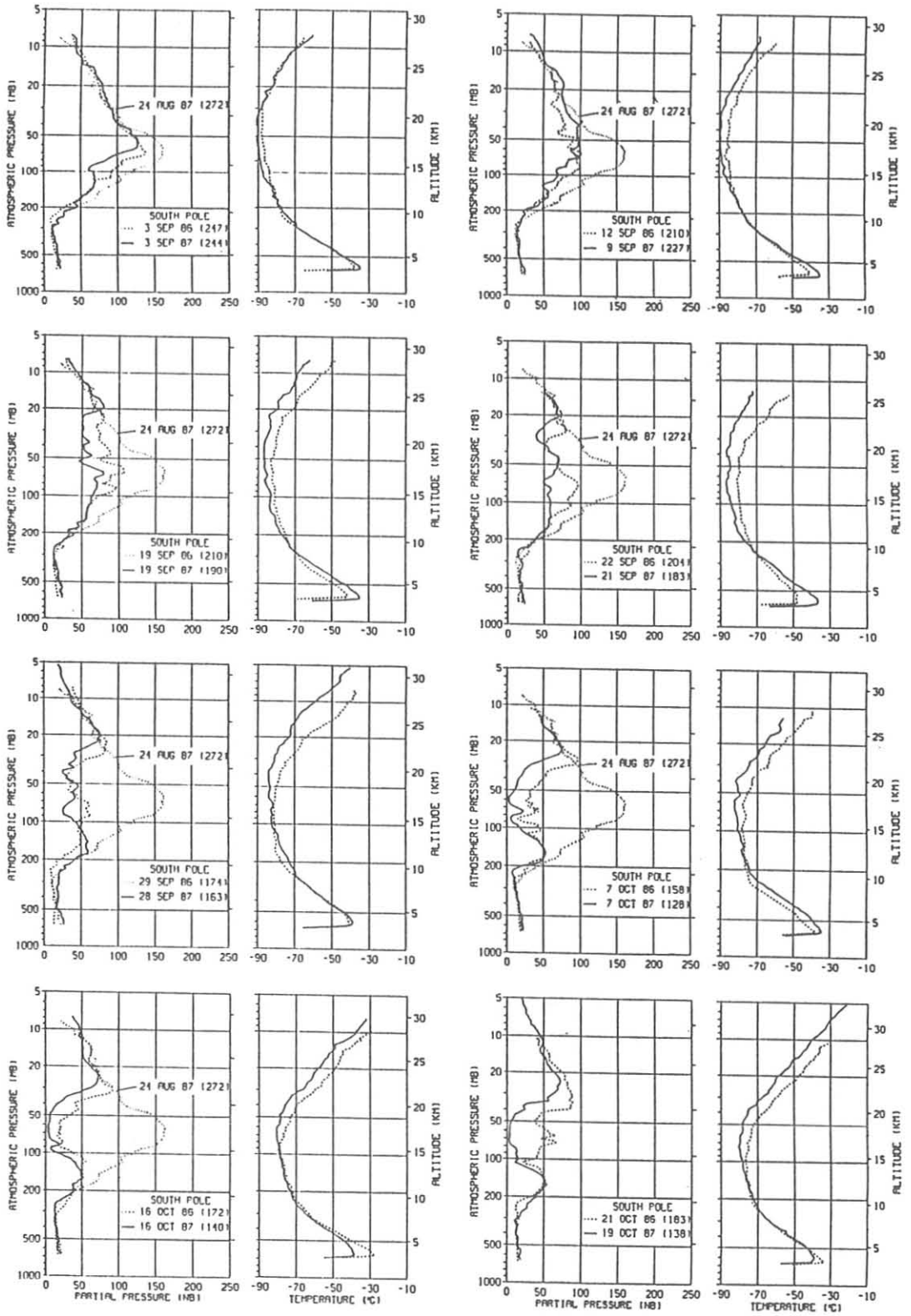

Fig. 5.8. Select ECC ozonesonde data showing ozone hole formation at the south pole in September and October 1986 and 1987. Values in parentheses in the legend boxes, and in the labels for the August 24, 1987, ozone profile shown for comparison, are total ozone amounts in Dobson units.

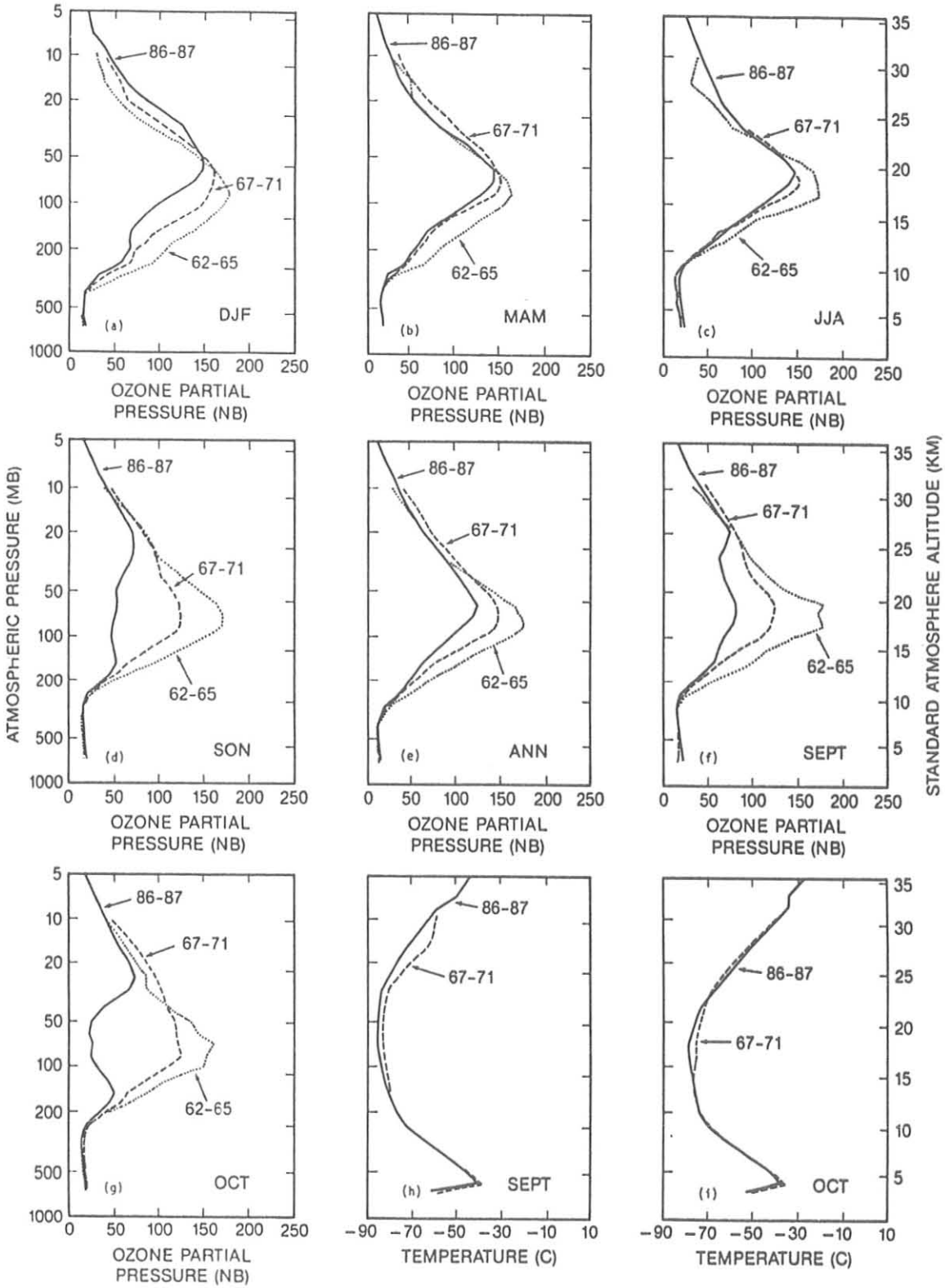

Fig. 5.9. (a)-(g) Comparison of average seasonal, annual, and September- and October-month ozone profiles for 1962-1965, 1967-1971, and 1986-1987. (h)-(i) Average temperature profiles, from September and October ozone soundings made in 1967-1971 and 1986-1987.

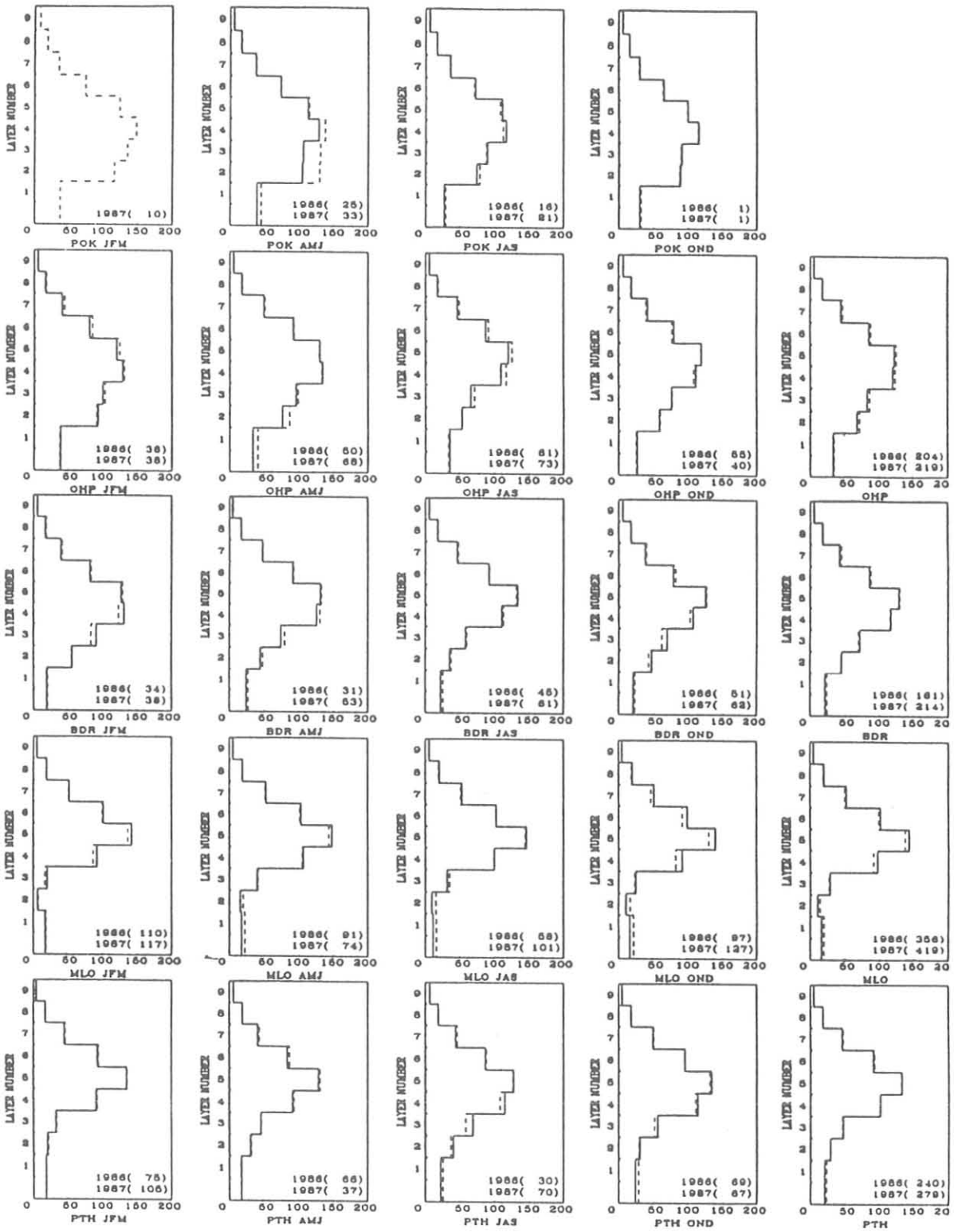

Fig. 5.10. Seasonal (columns 1-4) and annual (column 5) Umkehr layer average ozone partial pressures (nanobars) at five Umkehr observatories during 1986 and 1987. Solid-line profiles are from 1986; dashed-line profiles are from 1987. The values in parentheses after the dates indicate the number of profiles in the average.

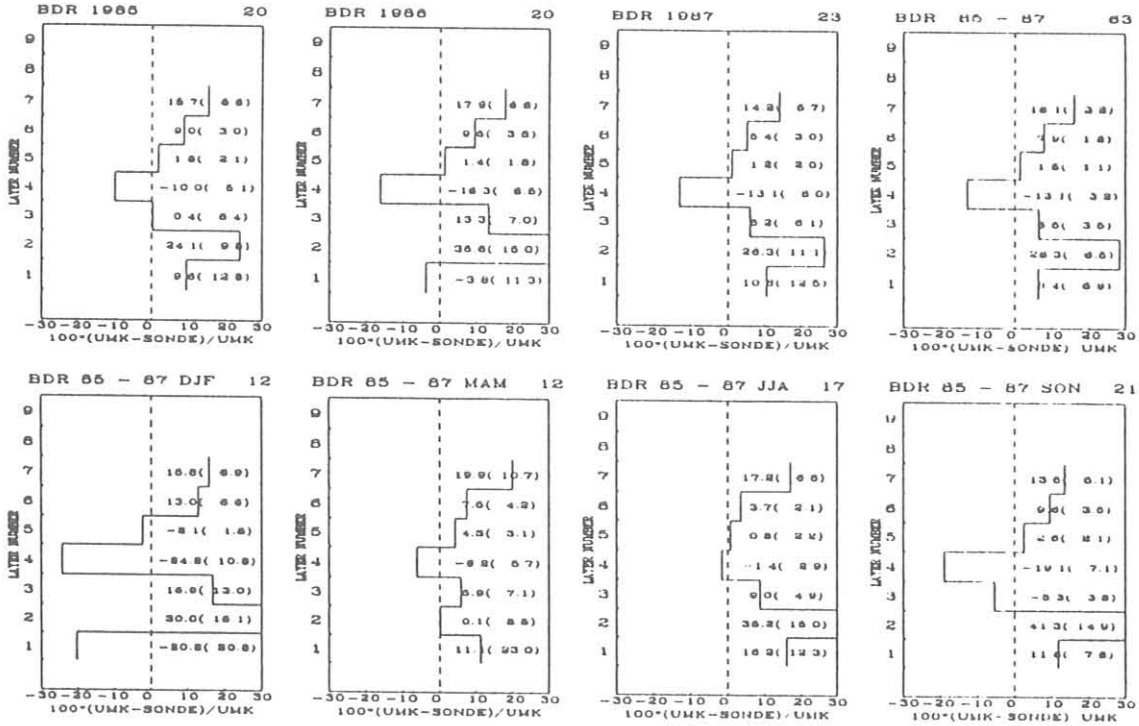

Fig. 5.11. Annual, long-term, and seasonal percentage ozone differences (determined by 100 [Umkehr-sonde]/Umkehr), by Umkehr layer for Boulder, 1985-1987. Values in parentheses are 95% confidence intervals.

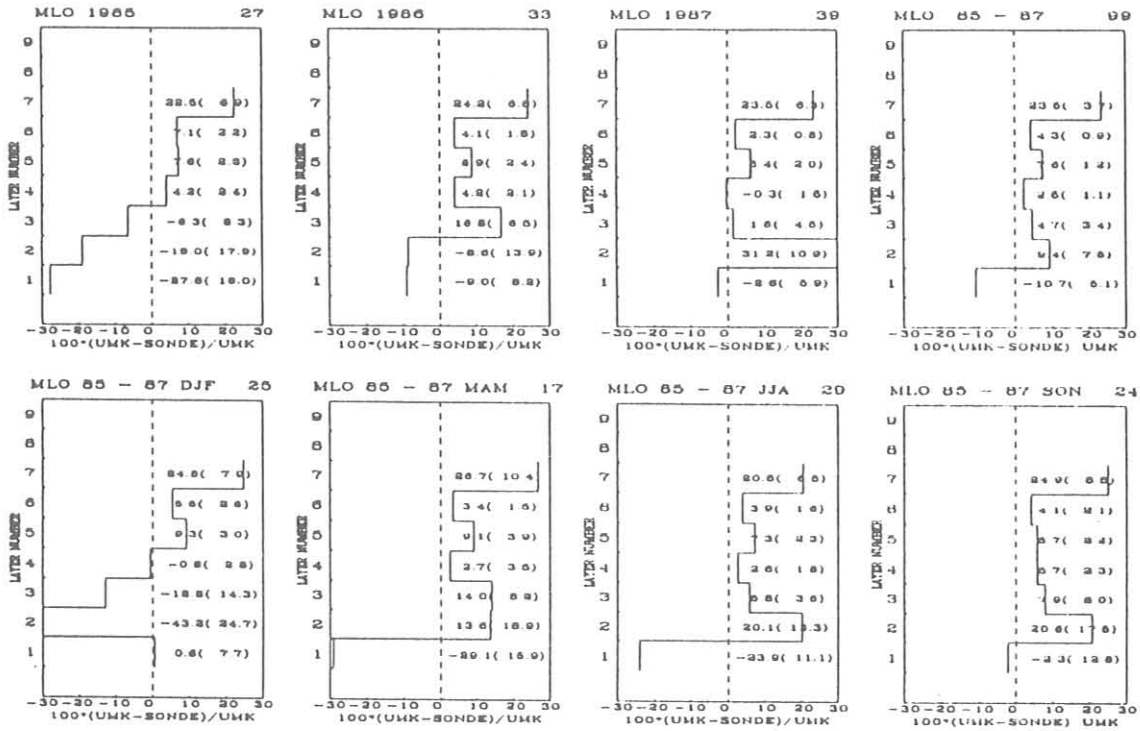

Fig. 5.12. Annual, long-term, and seasonal percentage ozone differences, as in Figure 5.11 but for MLO/Hilo, 1985-1987.

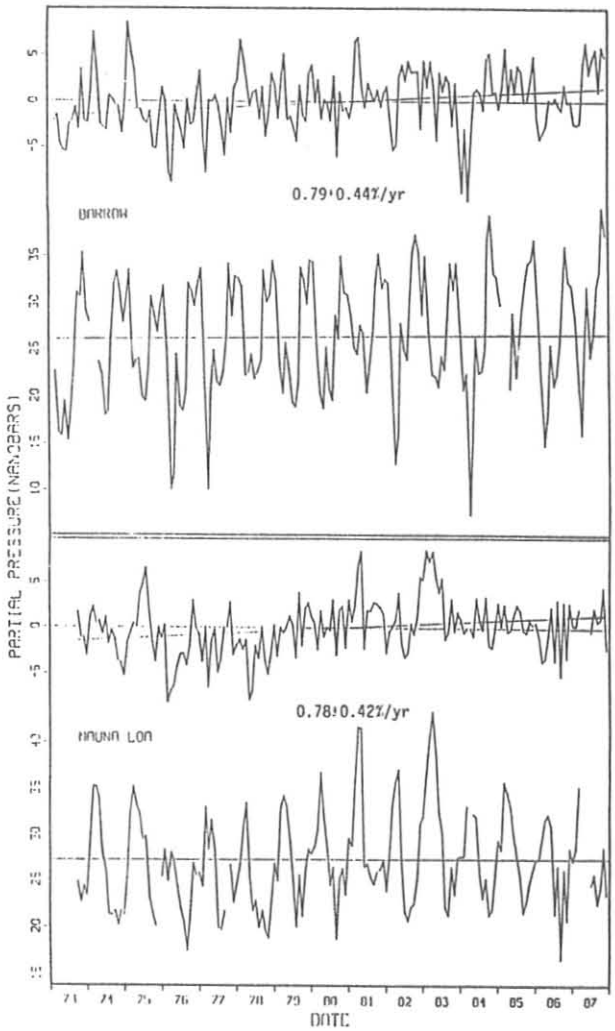

Fig. 5.13. Surface ozone monthly mean partial pressures (bottom plots) and anomalies (top plots) at BRW and MLO. The trends are linear-least-squares regressions of the monthly anomalies with 95% confidence interval.

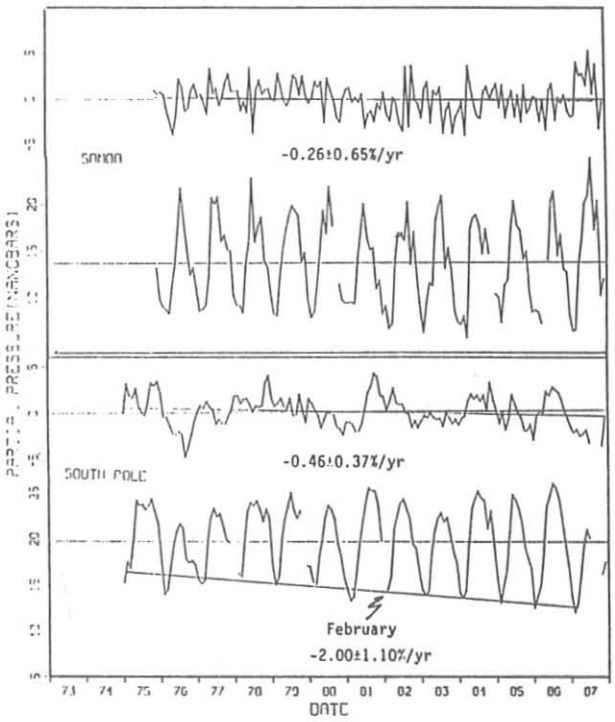

Fig. 5.14. Surface ozone monthly mean partial pressure anomalies, as in Figure 5.13 but for SMO and SPO.

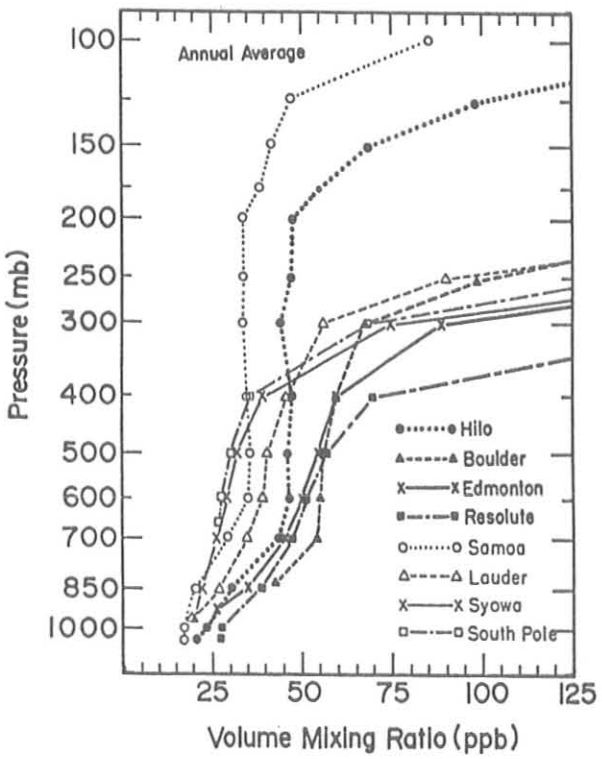

Fig. 5.15. Annual mean tropospheric ozone mixing ratio profiles from ozonesonde soundings.

periodically plagued the operation of the instrument over the years were identified as coming from the phototransistors that are part of the optics portion of the servo-control system [*Mendonca*, 1979]. In the past this problem was partially solved by selecting components with inherently low noise characteristics. This was very time consuming, and adequate performance could not always be attained. Modifications were made in the circuitry to electronically reduce the noise; recent tests indicate that these changes have improved the performance of the hygrometer.

As part of the recent tests to improve the performance of the instrument, it was discovered that a flaw existed in the calibration procedures. For calibration temperatures at 0°C the resistances measured were too low; because of the curve-fitting process used to determine frost-point temperatures colder than the lowest calibration value of -79°C, the frost-point temperatures colder than -79°C were too high. The error in resistance determination at 0°C leads to frost-point temperatures

that are too low by approximately 0.40°, 0.30°, 0.17°, and 0.06°C at 10, 20, 50, and 100 mb respectively. This leads to mixing ratios that are too low by about 7, 5, 3 and 1% at each of the pressures. The actual corrections for each sounding are slightly different because the correction depends on the magnitude of the thermistor resistance at 0°C. This correction applies to soundings made between August 1982 and December 1986.

5.2. REFERENCES

Evans, R.D., G.L. Koenig, W.D. Komhyr, J. Easson, and P. Marché, Umkehr observations at five automated Dobson spectrophotometer stations in 1986 and 1987, Proceedings of the 1988 Quadrennial Ozone Symposium, Göttingen, F.R.G., submitted, 1988.

Fleig, A.J., P.K. Bhartin, C.G. Wellemeyer, and D.S. Silberstein, An assessment of the long-term drift in SBUV total ozone based on comprisons with the Dobson network, *Geophys. Res. Lett., 13*, 1359-1362, 1986.

Franchois, P., G. Koenig, R.D. Evans, and W.D. Komhyr, Comparison of ECC ozonesonde and Umkehr profiles at Boulder, Colorado, 1985-1987, and Mauna Loa, Hawaii, 1985-1987, Proceedings of the 1988 Quadrennial Ozone Symposium, Göttingen, F.R.G., submitted, 1988.

Grass, R.D., and W.D. Komhyr, Traveling standard lamp calibration checks on Dobson ozone spectrophotometers during 1981-1983, in *Atmospheric Ozone*, Proceedings of the Quadrennial Ozone Symposium held in Halkidiki, Greece, September 3-7, 1984, Reidel, Dordrecht, Holland, 376-380, 1985.

Komhyr, W.D., R.D. Grass, and R.K. Leonard, WMO 1977 international comparison of Dobson ozone spectrophotometers, Proceedings of the Quadrennial International Ozone Symposium, August 4-9, 1980, Vol. I, edited by J. London, National Center for Atmospheric Research, Boulder, Colo., 25-32, 1981.

Komhyr, W.D., R.D. Grass, R.D. Evans, R.K. Leonard, and G.M. Semenink, Umkehr observations with automated Dobson spectrophotometers, in *Atmospheric Ozone*, Proceedings of the Quadrennial Ozone Symposium held in Halkidiki, Greece, September 3-7, 1984, D. Reidel, Dordrecht, Holland, 316-320, 1985.

Komhyr, W.D., R.D. Grass, and R.K. Leonard, Total ozone increase at South Pole, Antarctica, 1964-1985, *Geophys. Res. Lett., 13*, 1248-1251, 1986.

Komhyr, W.D., R.D. Grass, R.D. Evans, and R.K. Leonard, Results of international Dobson spectrophotometer and Brewer spectrometer intercomparisons, Arosa, Switzerland, 1986, Proceedings of the 1988 Quadrennial Ozone Symposium, Göttingen F.R.G., submitted, 1988a.

Komhyr, W.D., R.D. Grass, and R.K. Leonard, Dobson spectrophotometer no. 83: A standard for total ozone measurements, 1962-1987, *J. Geophys. Res.*, submitted, 1988b.

Komhyr, W.D., R.D. Grass, and R.K. Leonard, Calibration of primary standard Dobson spectrophotometer no. 83 and total ozone trends at Mauna Loa Observatory, Hawaii, and American Samoa, South Pacific, Proceedings of the 1988 Quadrennial Ozone Symposium, Göttingen F.R.G., submitted, 1988c.

Komhyr, W.D., P.R. Franchois, S.E. Kuester, P.J. Reitelbach, and M.L. Fanning, ECC ozonesonde observations at South Pole, Antarctica, during 1987, *NOAA Data Report ERL ARL-15*, 319 pp., NOAA Air Resources Lab., Boulder, Colo., 1988d.

Komhyr, W.D., S.J. Oltmans, P.R. Franchois, W. F. Evans, and W. A. Matthews, The latitudinal distribution of ozone to 35 km altitude from ECC ozonesonde observations, Proceedings of the 1988 Quadrennial Ozone Symposium, Göttingen F.R.G., submitted, 1988e.

Komhyr, W.D., R.D. Grass, P.J. Reitelbach, P.R. Franchois, M.L. Fanning, and S.E. Kuester, Total ozone, ozone vertical distributions, and stratospheric temperatures at South Pole, Antarctica, in 1986 and 1987, *J. Geophys. Res.*, submitted, 1988f.

Komhyr, W.D., S.J. Oltmans, R.D. Grass, P.R. Franchois, and R.K. Leonard, Changes in total ozone and ozone vertical distributions at South Pole, Antarctica, 1962-1987, Proceedings of the 1988 Quadrennial Ozone Symposium, Göttingen F.R.G., submitted, 1988g.

Komhyr, W.D., S.J. Oltmans, and R.D. Grass, Atmospheric ozone at South Pole, Antarctica, in 1986, *J. Geophys. Res., 93*, 5167-5184, 1988h.

Mateer, C.L, and H.U. Dütsch, Uniform evaluation of Umkehr observations from the World Ozone Network: Part I, Proposed standard evaluation technique, 105 pp., National Center for Atmospheric Reseach, Boulder, Colo., 1964.

Matthews, W.A., W.D. Komhyr, and P.R. Franchois, Vertical distribution and variation in atmospheric ozone over Lauder, New Zealand, Proceedings of the 1988 Quadrennial Ozone Symposium, Göttingen F.R.G., submitted, 1988.

McPeters, R.D., and W.D. Komhyr, Long-term changes in SBUV/TOMS relative to the world primary standard Dobson instrument, Proceedings of the 1988 Quadrennial Ozone Symposium, Göttingen F.R.G., submitted, 1988.

Mendonca, B.G., Geophysical Monitoring for Climatic Change, No. 7: Summary Report 1978, 131 pp., NOAA Environmental Research Laboratories, Boulder, Colo. 1979.

Rosen, J.M., D.J. Hofmann, J.R. Carpenter, J.W. Harder, and S.J. Oltmans, Balloon borne Antarctic frost point measurements and their impact on polar stratospheric cloud theories, *Geophys. Res. Lett., 15*, 859-862, 1988.

Schnell, R.C., and R.M. Rosson, Geophysical Monitoring for Climatic Change, No. 14: Summary Report 1987, 155 pp., NOAA Environmental Research Laboratories, Boulder, Colo., 1987.

6. Acquisition and Data Management Group

6.1. Continuing Programs

6.1.1. Station Climatology

The interpretation of measured values of aerosols, trace gases, and turbidity requires the measurement of meteorological variables to adjust gas measurements to standard conditions and to assess the influence of local pollution sources. Surface weather includes the measurements of wind direction, wind speed, station pressure, air and dewpoint temperature, precipitation amount and a determination of boundary layer stability. The current sensors used at GMCC stations were selected to withstand the extreme conditions of the environment at the two polar stations. The same sensors are used at all four stations, except the sensors measuring temperature at the South Pole. Wherever possible, WMO-recommended standards for exposure are used. A complete list of the sensors, model numbers, and heights appears in *Nickerson* [1986].

In 1984 the CAMS units were installed at all the stations; they increased the reliability of the data acquisition hardware and significantly reduced the quantity of missing data. The daily routine of printing hourly averages and comparing them with observed conditions improved the quality of the data as well. The DWR, which contains hourly average values for the individual meteorological variables for a 24-h period, served this purpose. The DWRs are sent to Boulder, checked, and stored on microfiche for future reference. *Herbert et al.* [1986a, b] presented a detailed discussion of the individual elements in the DWR and other CAMS printouts.

The global climatic trend for 1987 has been largely affected by the ENSO event. Many records and extremes were recorded at all four stations while the event was in the mature stage.

Barrow

A description of the BRW site, its surroundings, and climate can be found in previous GMCC Summary Reports [e.g., *DeLuisi,* 1981]. Wind roses of the hourly average resultant wind direction and speed are presented in 16 direction classes and 4 speed classes. The distribution of the wind by direction for 1987 (Figure 6.1) is consistent in general distribution with the average for the 1977-1986 period. The predominant wind direction is again from the "representative sampling sector" NE-SE (65%), and all other directions except westerly are less than 5%. Winds with a speed equal to or greater than 10 m s^{-1} were observed 16% of the time in 1987 as contrasted to 9% for the long-term average. The prevailing wind direction for January was from the WSW quadrant (Table 6.1), in contrast with the normal direction from ENE. The W direction logged the year's maximum wind speed of 19 m s^{-1} on February 25.

The most significant event of the year was the passage of a low-pressure system on July 22, which yielded 35.6 mm of rainfall in a 24-h period, and broke the 24-h precipitation record (25.4 mm, October 1926) that stood for nearly 61 years at Barrow village. Another record was broken on September 14 when 132.1 mm of snowfall accumulation was recorded in 24 h; this contributed to a new September record of 411.5 mm total snowfall accumulation. This unusually high amount of precipitation for BRW resulted in a 1987 total water equivalent of 130.6 mm, which is 10.2 mm above the normal.

The temperatures and pressures in 1987 were close to the long-term averages; the temperature was 0.4°C colder than normal and the pressure was 0.6 mb higher than normal. The minimum temperature for 1987 of -48.3°C occurred on February 17, breaking the 10-yr record of -47°C at BRW. The maximum pressures reported for June and August also broke the 10-yr

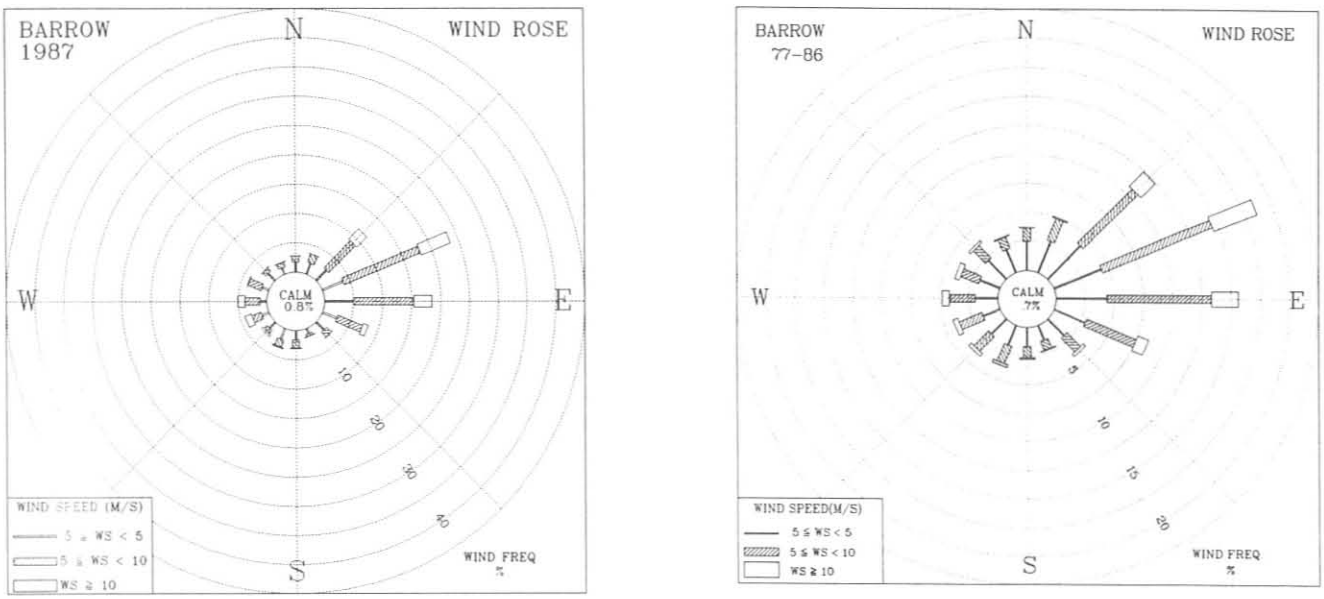

Figure 6.1. Wind rose of surface winds for BRW for 1987 (left) and 1977-1986 (right). The distributions of the resultant wind direction and speed are in units of percent occurrence for the year and 10-yr period, respectively. Wind speed is displayed as a function of direction in three speed classes.

TABLE 6.1. BRW 1987 Monthly Climate Summary*

	Jan.	Feb.	March	April	May	June	July	Aug.	Sept.	Oct.	Nov.	Dec.	1987
Prevailing wind direction	WSW	ENE	ESE	ENE	E	E	E	E	ENE	E	ENE	ENE	ENE
Average wind speed (m s^{-1})	6.5	6.4	5.7	6.3	6.8	7.1	6.3	7.4	7.3	6.6	9.0	6.2	6.8
Maximum wind speed† (m s^{-1})	18	19	13	13	13	13	13	15	17	17	19	17	19
Direction of max. wind† (deg.)	262	266	57	59	75	59	260	250	272	98	76	110	266
Average station pressure (mb)	1006.8	1019.1	1022.1	1016.7	1014.3	1011.3	1015.7	1017.3	1007.2	1008.8	1019.0	1008.4	1013.8
Maximum pressure† (mb)	1033	1040	1037	1033	1029	1031	1029	1030	1022	1022	1032	1034	1040
Minimum pressure† (mb)	978	998	1007	993	1002	996	1001	1007	993	977	1000	989	977
Average air temperature (°C)	-26.0	-30.3	-25.2	-21.6	-7.1	0.3	2.8	3.0	-2.0	-4.8	-20.7	-23.0	-12.6
Maximum temperature† (°C)	-6	-9	-4	-9	1	5	15	11	7	0	-10	-6	15
Minimum temperature† (°C)	-43	-48	-38	-33	-20	-5	-1	-2	-13	-14	-32	-36	-48
Average dewpoint temperature (°C)	-26.8	-31.2	-26.2	-23.0	-8.9	-2.0	0.8	1.1	-5.0	-6.4	-21.8	-23.7	-14.2
Maximum dewpoint† temperature (°C)	-7	-10	-6	-11	-1	1	10	9	3	-1	-12	-7	10
Minimum dewpoint† temperature (°C)	-44	-49	-39	-33	-20	-9	-3	-6	-17	-15	-33	-36	-49
Precipitation (mm)	0	0	1	0	4	2	45	24	15	1	1	0	92

*Instrument heights: wind, 17 m; pressure, 9.5 m (MSL); air and dewpoint temperature, 3 m. Wind and temperature instruments are on a tower 25 m northeast of the main building.

†Maximum and minimum values are hourly averages.

record. Lower pressures and colder temperatures characterized the BRW winter in 1987.

Mauna Loa

A description of the MLO site and its general climatology can be found in previous GMCC Summary Reports. The MLO 1987 monthly climate summary is shown in Table 6.2. Note that, for most variables, the average values are not representative of median values because of the bimodal distribution of the wind direction based on the time of day. The effect of Mauna Loa is to redirect stronger, predominantly easterly or westerly winds aloft down the slope with a more southerly component. The winds were again predominantly from the SSE (34%) in 1987, southerly wind speeds of less than 5 m s^{-1} occurring 8% of the time (Figure 6.2). Many spring storms, causing some flash floods at lower altitudes, were reported in 1987. On May 10 a storm passed MLO and caused the pressure to fall to 672 mb breaking the 10-yr record for May. The average temperature in May was also 1°C colder than normal for that month.

The ENSO event index reached its peak during April and May [*Wagner*, 1987] and can be associated with the change in MLO's climatic pattern for 1987. The equatorial central pacific, from the date line to 150°W, and from 15°N to 15°S, displayed positve sea surface temperature anomalies, which caused enhanced atmospheric convection in that area, which includes MLO. Associated with this convective area, an upper atmosphere anticyclone was centered with observations of negative outgoing longwave radiation anomalies [Freitag, 1987]. MLO's prevailing wind direction for June was from the NW direction. The normal SE wind direction for MLO was affected by strong equatorial westerly anomalies. Another interesting feature that was pointed out in the GMCC Summary Report for 1986, is the large number of storms and high wind speeds in December. More than half of the year's total precipitation occurred during December, and the year's maximum wind speed of 21 m s^{-1} was reported on December 18.

The average pressure for 1987 was 1.2 mb below the 10-yr average for the period 1977-1986. The average air temperature stayed the same as the long-term average, at 7.0°C. The precipitation amount of 557 mm was down 116 mm from the 1986 total, but was still 28% more than the 13-yr average reported by *Chin et al.* [1971].

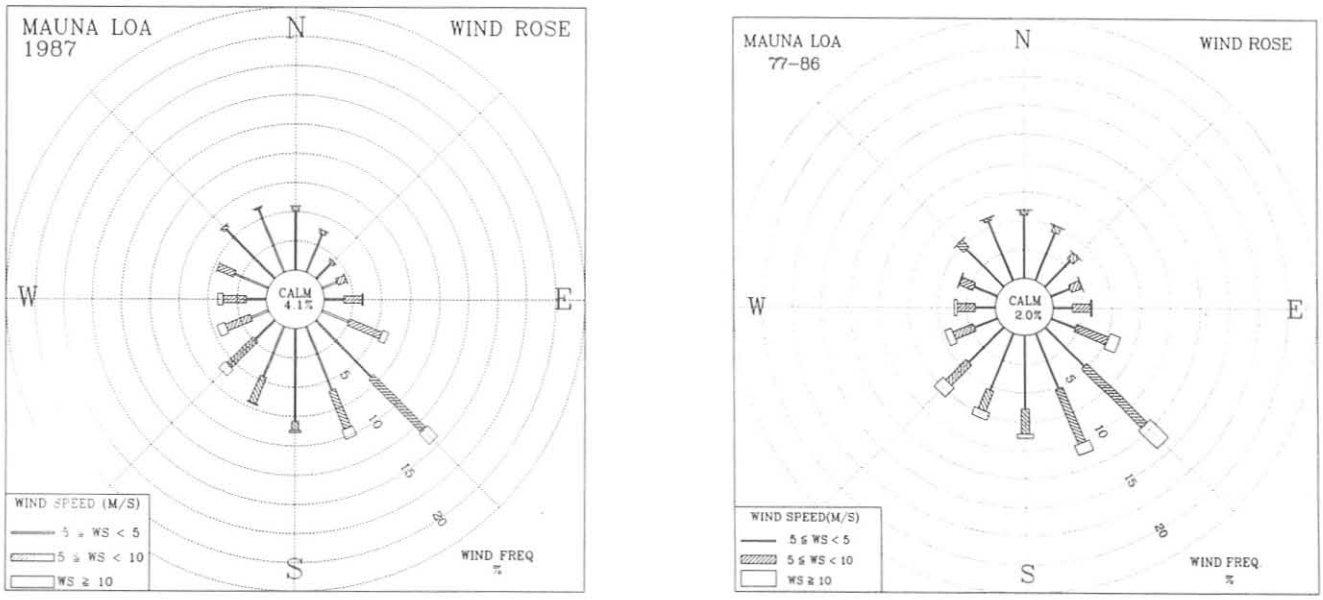

Figure 6.2. Wind rose of the surface winds for MLO for 1987 (left) and 1977-1986 (right). The distributions of the resultant wind direction and speed are units of percent occurrence for the year and 10-yr period, respectively. Wind speed is displayed as a function of direction in three speed classes.

TABLE 6.2. MLO 1987 Monthly Climate Summary*

	Jan.	Feb.	March	April	May	June	July	Aug.	Sept.	Oct.	Nov.	Dec.	1987
Prevailing wind direction	SE	SW	SE	SE	SW	NW	SE	SE	SE	SE	SE	SSE	SE
Average wind speed (m s^{-1})	4.4	5.3	6.1	4.5	5.3	3.6	3.7	3.8	3.7	3.6	5.3	4.4	4.5
Maximum wind speed† (m s^{-1})	12	13	17	13	14	13	19	13	10	13	15	21	21
Direction of max. wind† (deg.)	256	159	270	232	218	147	37		154	213	90	139	139
Average station pressure (mb)	679.4	677.2	679.0	679.5	678.4	681.0	680.7	680.6	680.8	680.6	680.8	679.8	679.8
Maximum pressure† (mb)	683	681	683	683	685	684	683	684	684	683	685	684	685
Minimum pressure† (mb)	672	670	673	674	672	677	678	677	678	678	676	673	670
Average air temperature (°C)	5.5	5.0	5.2	7.3	6.9	7.6	8.3	9.5	7.6	8.3	6.7	6.2	7.0
Maximum temperature† (°C)	15	16	14	17	18	17	17	17	16	17	15	14	18
Minimum temperature† (°C)	-2	-3	-2	-1	0	0	1	3	3	3	1	1	-3
Average dewpoint temperature (°C)			-13.9	-13.4	-9.8	-9.2	-4.3	-7.6	-1.0	-5.9	-10.8	-6.5	-8.4
Maximum dewpoint temperature† (°C)			4	5	6	6	19	14	8	8	6	22	22
Minimum dewpoint temperature† (°C)			-32	-38	-31	-23	-24	-24	-23	-23	-35	-32	-38
Precipitation (mm)	2	29	8	6	60	18	32	1	34	63	0	305	557

*Instrument heights: wind, 17 m; pressure, 3399 m (MSL); air and dewpoint temperature, 3 m. Wind and temperature instruments are on a tower located 25 m northeast of the main building.

†Maximum and minimum values are hourly averages.

Samoa

A comparison of the wind rose for 1987 with that for the preceding 10 years shows a very similar distribution except for the shift in the predominant wind direction to a more southerly component (Figure 6.3). A higher precentage (10%) of wind speeds equal to or greater than 10 m s^{-1} was also observed. This shifted distribution is almost identical to the 1986 wind rose, with the exception of higher velocity southerly winds in 1987. The SSE quadrant accounted for the highest percentage (37%) of the observed wind directions. The average wind speed for the year was 5.9 m s^{-1} (Table 6.3) , which was 1.5 m s^{-1} above the long-term average. New maximum wind speeds were observed for the months of February and April. The maximum wind speed recorded on February 3 of 18 m s^{-1} is the highest value for the year. The precipitation recorded in February was 600 mm, the highest monthly total for 1987. The winds from the NNW quadrant early in the year were associated with stormy periods accompanied by precipitation.

The main event for SMO in 1987 was the passage of tropical cyclone Tusi on January 17-18. This storm dropped the pressure to 987 mb and established a new record for minimum pressure in January. The storm's main swath passed 70 mi east of GMCC's site on Tutuila Island and hit Manu'a Island, causing enough destruction that President Reagan declared it a disaster area. The other extreme feature for SMO in 1987 was the effect the ENSO event had on the fall precipitation. An extreme drought for 6 months, from July to December devastated the island's lush vegetation. Precipitation amounts for September and November were 2 mm and 54 mm respectively, new minimum precipitation records for both months. The average monthly precipitation for the year of 143 mm was 70 mm below normal.

The average station pressure for the year was 1.4 mb higher than the long-term average, and the average temperature was 0.5°C lower than normal. The ENSO event that caused the drought in the fall may also be responsible for the high-pressure records during the fall drought. The maximum pressure record for September was broken on September 29 and 30 with measurements of 1008 mb.

South Pole

The most distiguishing feature of the distribution in the surface wind direction at SPO is that the predominant wind direction was grid ENE (20%) as compared with the long-term prevailing NNE direction (Figure 6.4). A very small percentage of these winds have speeds greater than 10 m s^{-1}. The prevailing wind direction was easterly in July-October in contrast to the normal, which has an associated northly component (Table 6.4). Another feature of the 1987 wind rose is the relatively large number of occurrences of wind speeds less than 5 m s^{-1} (50%). The average wind speed for the year of 5.3 m s^{-1} is identical to the long-term average. New maximum wind speeds were observed for the months of April and June (16 m s^{-1}).

The most significant weather event for the SPO station in 1987 was the colder-than-normal average air temperature for the year of -51.0°C. August was the coldest month ever on record (since 1957), having an average monthly temperature of -66.8° C. The recorded minimum hourly average temperature for this month was -80.4°C. It is interesting to note the change in the wind direction between May and August. During May and June the wind direction was predominantly from the north with associated high pressure and warm temperatures. The circulation pattern changed in July and August to a predominantly easterly flow. This triggered the colder air and lower pressures for the month of August.

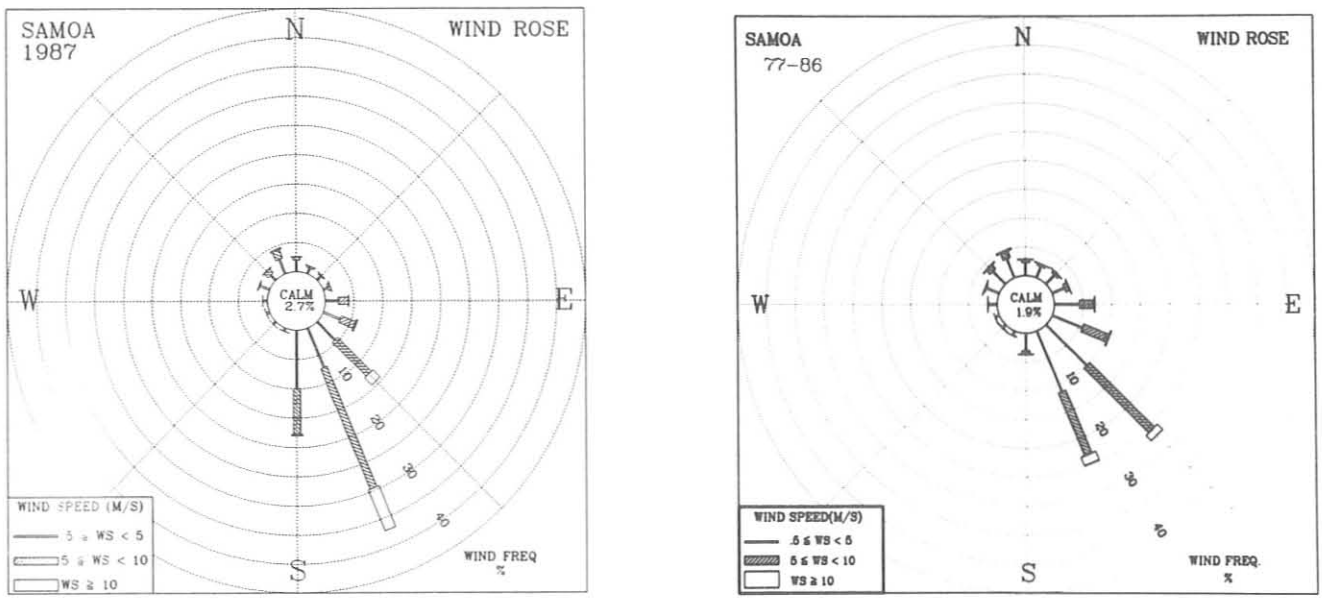

Figure 6.3. Wind roses of the surface wind for SMO for 1987 (left) and 1977-1986 (right). The distributions of the resultant wind direction and speed are in units of percent occurrence for the year and 10-yr period, respectively. Wind speed is displayed as a function of direction in three speed classes.

TABLE 6.3. SMO 1986 Monthly Climate Summary*

	Jan.	Feb.	March	April	May	June	July	Aug.	Sept.	Oct.	Nov.	Dec.	1987
Prevailing wind direction	NNW	SSE	SSE	SSE	S	SSE	SSE	SSE	SSE	SSE	SSE	SE	SSE
Average wind speed (m s^{-1})	3.7	4.0	3.8	6.5	5.9	5.5	7.3	8.6	6.2	8.0	5.4	5.5	5.9
Maximum wind speed† (m s^{-1})	15	18	13	17	15	15	13	14	11	13	11	14	18
Direction of max. wind† (deg.)	157	329	158	163	162	159	163	134	165	159	161	341	329
Average station pressure (mb)	997.3	996.8	1000.1	1000.0	1001.6	1002.2	1003.5	1003.1	1004.3	1003.1	1001.3	998.6	1001.0
Maximum pressure† (mb)	1003	1002	1004	1007	1005	1007	1008	1007	1008	1008	1004	1005	1008
Minimum pressure† (mb)	987	990	988	992	998	998	997	999	1000	999	998	992	987
Average air temperature (°C)	27.4	27.7	27.5	27.3	26.3	25.7	25.2	24.8	25.4	26.0	27.1	27.7	26.5
Maximum temperature† (°C)	31	32	32	31	31	29	29	28	30	30	33	33	33
Minimum temperature† (°C)	24	24	23	24	23	23	22	21	23	23	23	24	21
Average dewpoint temperature (°C)													
Maximum dewpoint temperature† (°C)													
Minimum dewpoint temperature† (°C)													
Precipitation (mm)	242	600	184	136	15	135	44	52	2	54	54	200	1718

*Instrument heights: wind, 14 m; pressure, 30 m (MSL); air and dewpoint temperature, 9 m. Wind and temperature instruments are on Lauagae Ridge, 110 m northeast of the main building. Pressure sensors are located in the main building.

†Maximum and minimum values are hourly averages.

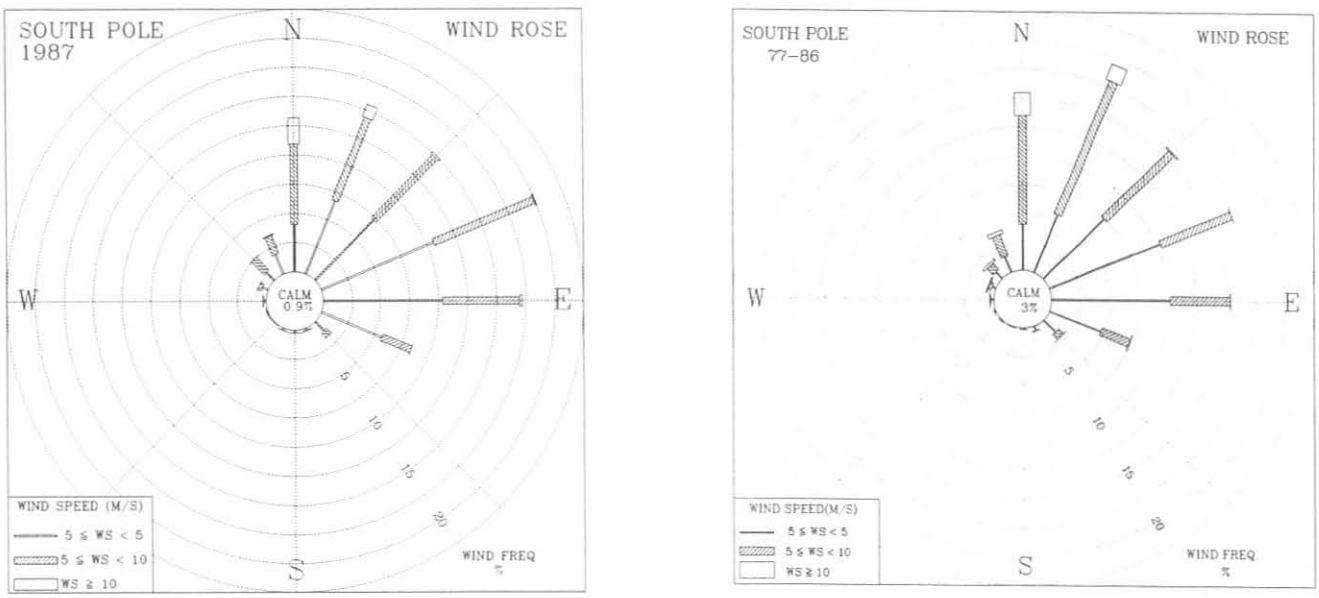

Figure 6.4. Wind roses of the surface wind for SPO for 1987 (left) and 1977-1986 (right). The disributions of the resultant wind direction and speed are in units of percent occurrence for the year and 10-yr period, respectively. Wind speed is displayed as a function of direction in three speed classes.

TABLE 6.4. SPO 1987 Monthly Climate Summary*

	Jan.	Feb.	March	April	May	June	July	Aug.	Sept.	Oct.	Nov.	Dec.	1987
Prevailing wind direction	N	NE	ENE	ENE	N	ENE	E	E	E	E	ENE	NNE	ENE
Average wind speed (m s^{-1})	4.1	4.6	6.4	5.6	5.6	6.2	6.6	5.1	6.2	5.4	4.6	3.1	5.3
Maximum wind speed† (m s^{-1})	8	9	13	16	14	16	13	11	15	13	8	8	16
Direction of max. wind† (deg.)	19	336	31	37	359	13	8	352	358	20	29	31	37
Average station pressure (mb)	695.7	683.4	681.8	680.1	679.9	683.0	681.1	665.6	680.2	675.0	677.8	686.3	680.7
Maximum pressure† (mb)	707	699	705	692	693	702	699	674	700	693	688	693	707
Minimum pressure† (mb)	678	667	664	669	669	658	667	655	657	661	666	677	655
Average air temperature (°C)	-25.7	-40.1	-49.8	-57.6	-58.0	-55.6	-59.9	-66.8	-60.4	-51.4	-39.3	-28.9	-51.0
Maximum temperature† (°C)	-20	-27	-35	-38	-42	-33	-39	-52	-43	-34	-29	-23	-20
Minimum temperature† (°C)	-31	-51	-68	-72	-73	-71	-74	-80	-72	-63	-52	-47	-80
Average dewpoint temperature (°C)													
Maximum dewpoint temperature (°C)													
Minimum dewpoint temperature (°C)													
Precipitation (mm)													

*Instrument heights: wind, 12 m; pressure, 2841 m (MSL); air temperature, 2 m. The anemometer and thermometer are on a tower 100 m grid east-southeast of CAF. Pressure measurements are made inside CAF.

†Maximum and minimum values are hourly averages.

6.1.2. Data Management

The automated data aquisition system (CAMS) continued operation through 1987 with no major problems. Table 6.5 shows the operations record for CAMS at the four observatories in terms of the number of blocks (data records) recorded for each possible block type. SPO and SMO had no unintentional down time for CAMS this year. BRW had 21 autorestarts and 1 BRAM loss, while MLO had 40 autorestarts and 3 BRAM losses. These down times reflect mostly power outages and some bad battery backed up memory boards (ZRAMs), which were replaced. In addition, a 12-V power supply failed and was replaced in BRW, a tape drive and an A-D board were replaced at SMO, and a tape drive and a ZRAM board were replaced at SPO. At every station, new clock boards and clock batteries were installed this year. Improvements were made in the software for the MO3 CAMS, among them a modification that fixed a bug in the Dasibi weekly calibration and that saves the results on tape.

In the summer of 1987, software (called the CAMS-VAX Data Management System) was developed and installed on the VAX computer that processes incoming CAMS cassettes and allows users to manipulate and display the data in various ways. GMCC users were trained on this software and have been accessing the CAMS data with this system. Because of this system, CAMS data arriving from the observatories can be made available to GMCC users within a week.

6.2. Special Projects

6.2.1. Atmospheric Trajectories

Computer models that calculate atmospheric trajectories on isobaric and isentropic surfaces have been developed within GMCC and have been available for use by GMCC and cooperative scientists for a number of years. Descriptions of trajectory model development and studies appear in the five previous GMCC Summary Reports. Methodology for the isobaric model is documented in *Harris* [1982] and for the isentropic model in *Harris and Bodhaine* [1983].

Table 6.6 lists most of the trajectories computed during 1987. These were provided for atmospheric researchers within GMCC and ARL as well as scientists at universities or research institutes of foreign governments affiliated with GMCC. In all, more than 45 station-years of trajectories were computed. Table 6.7 lists experiments supported in 1987.

TABLE 6.5. GMCC CAMS Operations Summary, 1987

Block Type	Description	Expected No. of Blocks yr^{-1}*	Blocks Recorded and [Blocks Missing]			
			BRW	MLO	SMO	SPO
A	Hourly aerosol data	2190	2162 [28]	2185 [5]	2191 [0]	2190 [1]
H	Daily aerosol data	365	364 [1]	365 [0]	367 [0]	366 [0]
S	Hourly solar radiation data	8760	8252 [108]	8745 [15]	8761 [0]	8758 [2]
C	Hourly CO_2 data	Variable	8127 [221]	8310 [45]	8392 [1]	8247 [7]
D	Daily CO_2 data	365	361 [6]	365 [0]	368 [10]	365 [0]
E	Hourly CO_2 calibration data	Variable	404	403	367	480
F	CO_2 calibration report	52	55	55	55	67
M	Hourly meteorological data	4380	4305 [74]	4361 [22]	4362 [19]	4328 [52]
O	Daily ozone data	365	368 [0]	366 [0]	354 [11]	365 [0]
W	Daily meteorological data	365	362 [3]	366 [2]	367 [0]	359 [6]
I	Meteorological caibration	365	361 [0]	368 [0]	364 [0]	364 [5]
N	Ozone calibration†	365	7	14	7	13

*Discrepancies between the expected number of blocks and blocks recorded + blocks missing are due to clock problems or autorestarts.
†New data block started when new MO3 PROMS were installed.

TABLE 6.6. GMCC Trajectories Calculated in 1987

Location	Dates
Norfolk, Va.	Feb., April 1985
Torres de Paine, Chile	1986
BRW	1986
MLO	1986
SMO	1986
SPO	Selected dates 1986, 1987
Little Rock, Ark.	Feb., April, July, Oct. 1987
Arctic (flight locations)	April 1983
Bermuda (climatology)	1983-1984
Ester Dome, Alaska	March-April 1986
Augustine Island	March-April 1986
Katherine, Australia	Sept. 1986-April 1987
Mount Lemmon, Ariz.	April 15-May 27
Amsterdam Island	1985-1986
Crozet Island	1985-1986
St. Francis, South Africa	1985
Niigata, Japan	May 1986
Yucatan, Mexico	June-Sept. 1986
Cape Hatteras, N.C. (climatology)	1982-1986
Charleston, S.C. (climatology)	1982-1986
Alert, Canada	March-April 1986
Buffalo, N.Y.	June 1987
State College, Pa.	June-July 1987
Saranac Lake, N.Y.	June-July 1987
Key Biscayne, Fla.	1985-1987
Adrigole, Ireland	1986
China	May-June 1987
Station M (climatology)	Nov.-April 1982-1987
Glasgow, Mont.	Jan.-March 1987
St. Cloud, Minn.	Jan.-March 1987

TABLE 6.7. Experiments Supported During 1987

Experiment	Dates	Organization
TOGA cruise	Dec. 1985-Feb. 1986	WPL
EMEX flight	Jan. 1987	AOML
Arctic flight	March-April 1983	Fraunhofter Inst.
AGASP-I, II	March-April 1983, 1986	GMCC
Researcher Cruise, RITS-1987	June 1987	AOML
ANATEX	Jan., Feb. 1987	GMCC
CURTAIN	Feb.-April, July-Oct. 1987	GMCC
PRECP V	June 1987	GMCC

The two data sets available for trajectory calculations consist of analyzed grids of meteorological data from the National Meteorological Center. Data on the northern hemisphere 65 × 65 grid cover the period 1975 to the present. Data on the global 2.5° latitude, longitude grids extend from 1977 to the present. Data are delivered from NCAR on a monthly basis and are available in house within 2 months of analysis time.

Improvements were made to the isentropic model this year to allow it to run on the 2.5° latitude, longitude data set. As a result, both isobaric and isentropic models now have global coverage. The isentropic programs were generalized to make changing of subgrids easier. Another improvement allows for the creation of up to five isentropic surfaces at a time. A new feature of the isentropic trajectory plots is shown in Figure 6.5. The lower plot shows the vertical path of the trajectory, and days from the destination along the x axis.

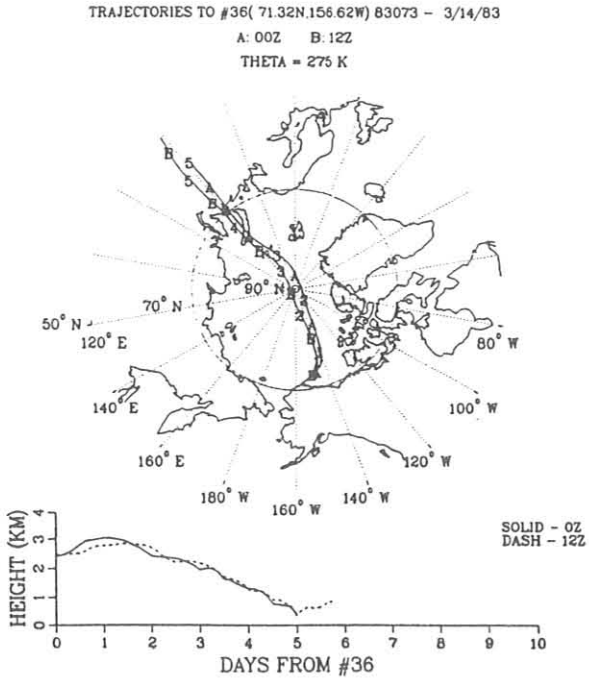

Fig. 6.5. BRW back trajectories arriving on March 14, 1983, on the 275-K isentropic surface. The lower plot shows the vertical paths of the trajectories.

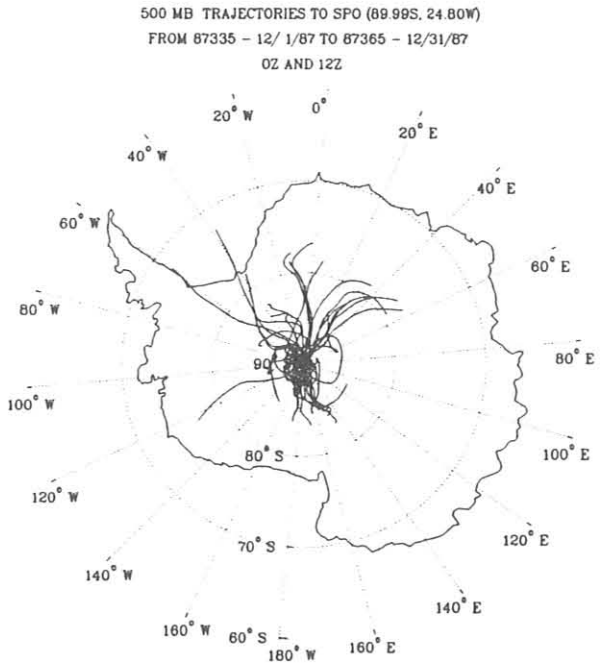

Fig. 6.7. SPO 2.5-day back trajectories arriving during December 1987 at the 500-mb level.

Atmospheric trajectories were provided in support of the 1987 SPO aerosol study. The first part of this investigation produced a monthwise trajectory climatology of 500-mb trajectories to SPO. This mandatory level was chosen since 500 mb is the first such level above the surface at SPO. To distinguish months in which long-range transport was possible from months in which winds were light and variable, the tracks were plotted for only 2.5 days back. This representation of the climatology pointed out a seasonal difference in the flow pattern to SPO. Figures 6.6 and 6.7 show trajectories for November and December. These plots can be contrasted to Figures 6.8 and 6.9, showing trajectories for July and August. During the austral summer months trajectories meander slowly and are confined to the continent. During the austral winter months of July and August trajectories indicate much higher wind speeds and more direct pathways for transport from lower latitudes. The faster trajectories result from well-organized storms off the coast that have been linked with episodic sea salt events in aerosol scattering extinction measured by the nephelometer at SPO [*Bodhaine et al.*, 1986]. Events associated with air flow from the north during July and from the south during August were studied in detail, but for expediency only the July case is discussed here.

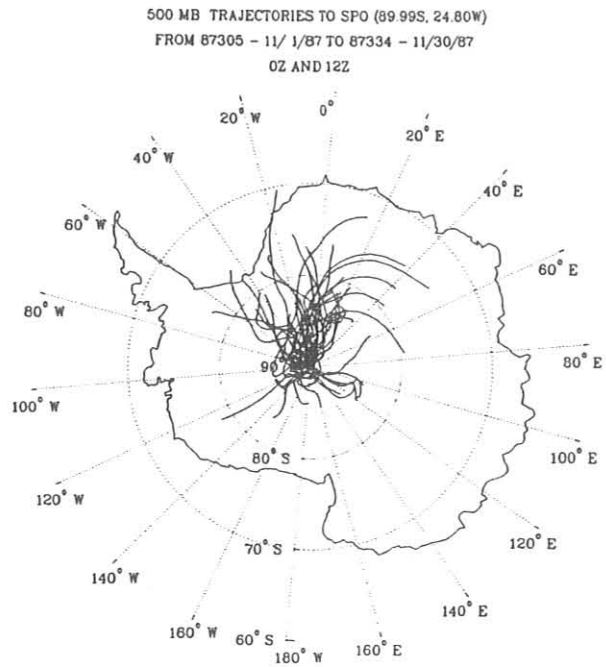

Fig. 6.6. SPO 2.5-day back trajectories arriving during November 1987 at the 500-mb level.

Nephelometer data collected at SPO for July 1987 (Figure 6.10) show a definite shift at the middle of the month that raises the level of the aerosol scattering extinction coefficients (σ_{sp}) an order of magnitude to about 10^{-6} m^{-1}. Individual 500-mb isobaric trajectories plotted daily for July likewise show a change in character at the middle of the month. Figure 6.11 shows 500-mb trajectories computed for July 10, 1987, characteristic of the first half of the month when winds were light to moderate, meandering around the continent. In contrast, Figure 6.12 shows a pattern typical of the latter half of July. Wind speeds at 500 mb during this time varied from 10 to 25 m

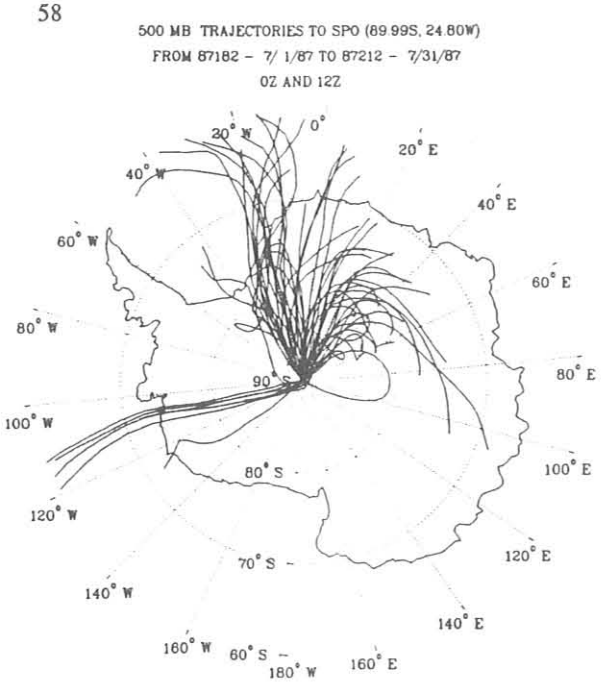

Fig. 6.8. SPO 2.5-day back trajectories arriving during July 1987 at the 500-mb level.

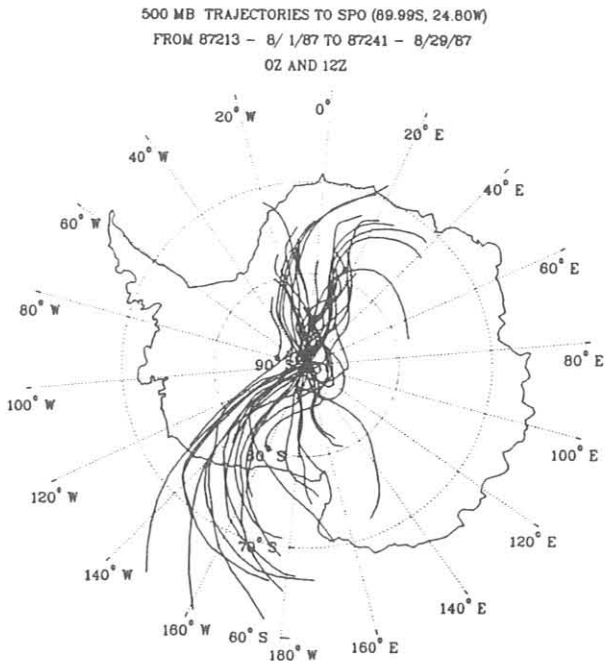

Fig. 6.9. SPO 2.5-day back trajectories arriving during August 1987 at the 500-mb level.

s^{-1}. Trajectories show travel from 70°S to SPO in 1-2 days. To investigate further the possibility that marine aerosol was transported to SPO during July and August 1987, isentropic trajectories were computed for the periods of interest. An example for July 20 is shown in Figure 6.13. The isentropic trajectories are similar in the horizontal to the isobaric ones; however they differ in the vertical in that the isentropic trajectories rise from near the ocean surface off the coast to approximately 550 mb above SPO. The slope of the isentropic surface could provide the mechanism for raising the marine aerosol from close to the surface to a level above the inversion at SPO. Transport to the surface at SPO is thought to occur during periods of warming, strong winds, or wind shear, which weaken the inversion.

The 500-mb heights for July 1987 (Figure 6.14) show a large storm that persisted to the grid northwest of SPO. High wind speeds developed in the area between the low and the ridge to the grid northeast that presumably provided the transport of marine aerosol to SPO.

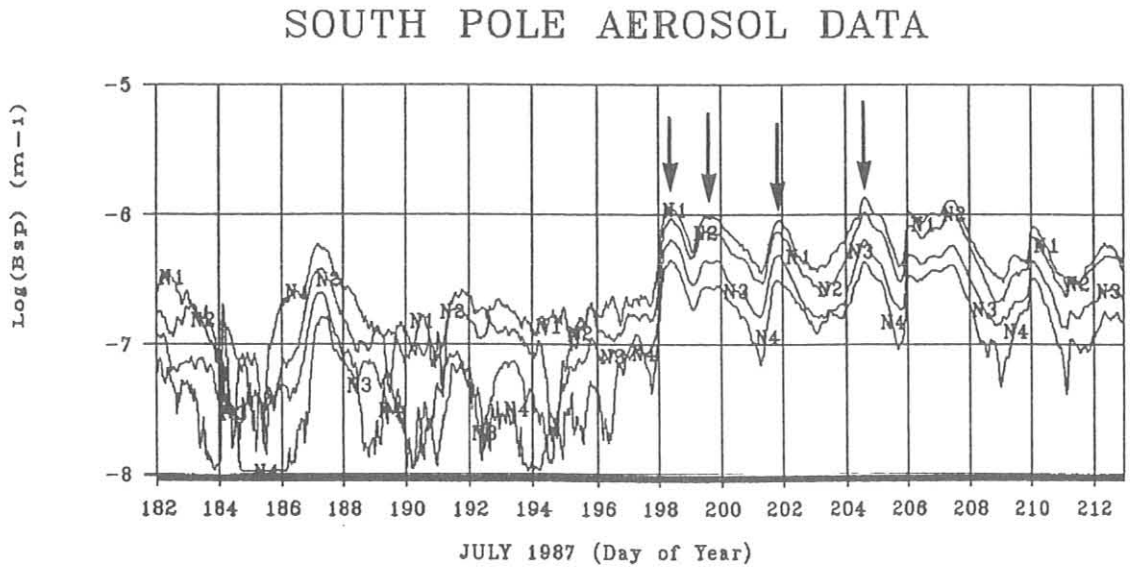

Fig. 6.10. Hourly geometric means of σ_{sp} at SPO for July 1987. σ_{sp} values are shown for 450 (N1), 550 (N2), 700 (N3), and 850 (N4) nm. Arrows indicate aerosol events studied.

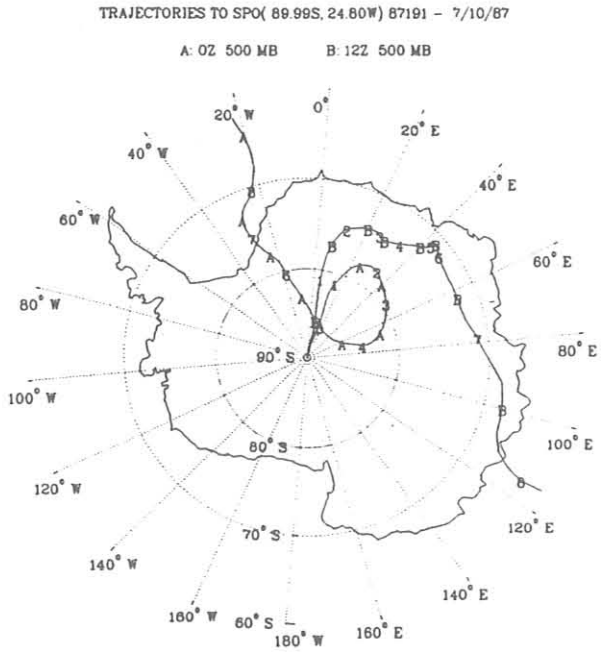

Fig. 6.11. SPO trajectories arriving on July 10, 1987, at the 500-mb level.

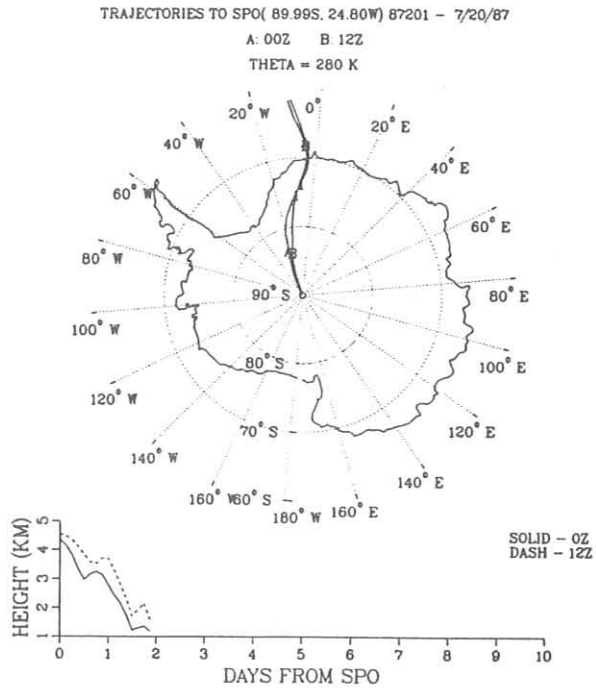

Fig. 6.13. SPO trajectories arriving on July 20, 1987, on the 280-K isentropic surface. The lower plot shows the vertical paths of the trajectories.

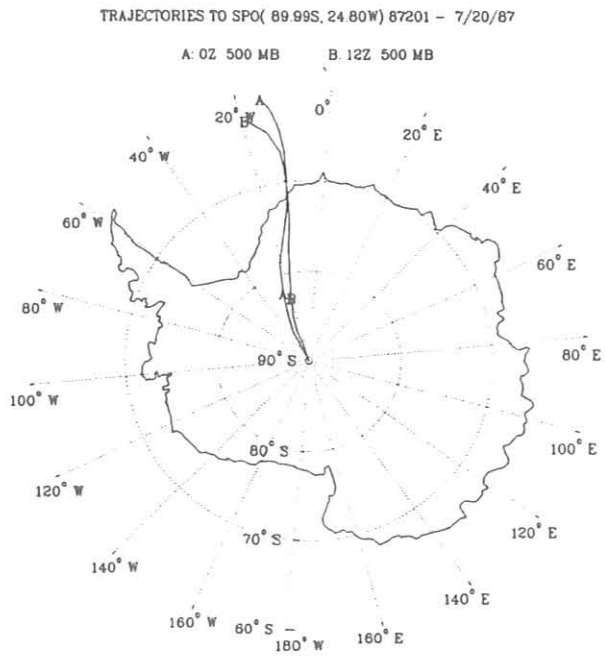

Fig. 6.12. SPO trajectories arriving on July 20, 1987, at the 500-mb level.

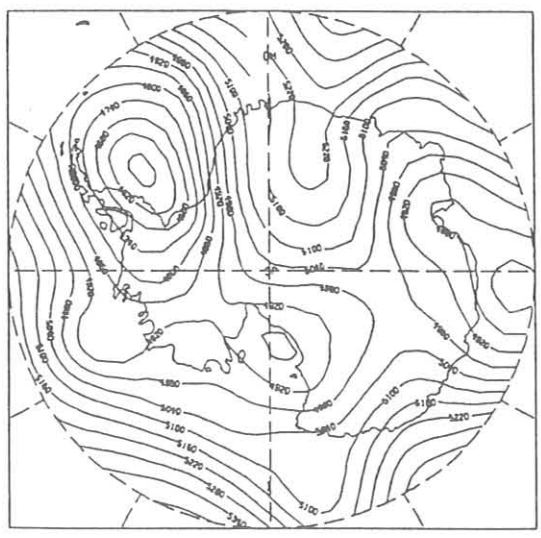

Fig. 6.14. Height in meters of the 500-mb pressure surface over Antarctica on July 19, 1987.

6.3. REFERENCES

Bodhaine, B.A., J.J. DeLuisi, J.M. Harris, P. Houmere, and S. Bauman, Aerosol measurements at the South Pole, *Tellus, 38B,* 223-235, 1986.

Chin, J.F.S., H.T. Ellis, B.G. Mendoca, R.F. Pueschel, and H.J. Simpson, Geophysical monitoring at Mauna Loa Observatory. *NOAA Tech. Memo. ERL APCL-13,* 34 pp., NOAA Environmental Research Laboratories, Boulder, Colo., 1971.

DeLuisi, J.J. (ed.), Geophysical Monitoring for Climate Change, No. 9: Summary report 1980, 163 pp, NOAA Environmental Research Laboratories, Boulder, Colo., 1981.

Frietag, P., Equatorial wind, temperature and pressure observations, *Climate Diagnostics Bulletins 1987,* 12 pp., NOAA/NWS/NMC Climate Analysis Center, Washington, D.C., 1987.

Harris, J.M., The GMCC atmospheric trajectory program. *NOAA Tech. Memo. ERL ARL-116,* 30 pp., NOAA Environmental Research Laboratories, Boulder, Colo., 1982.

Harris, J.M., and B.A. Bodhaine (eds.), Geophysical Monitoring for Climatic Change, No.11: Summary Report 1982, pp. 67-75, NOAA Environmental Research Laboratories, Boulder, Colo., 1983.

Herbert, G.A., E.R. Green, J.M. Harris, G.L. Koenig, and K.W. Thaut, Control and monitoring instrumentation for the continuous measurement of atmospheric CO_2 and meteorological variables, *J. Atmos. Ocean. Tech. 3,* 414-421, 1986a.

Herbert, G.A., E.R. Green, G.L. Koenig, and K.W. Thaut, Monitoring instrumentation for the continuous measurement and quality assurance of meteorological observations, *NOAA Tech. Memo. ERL ARL-148,* NOAA Environmental Research Laboratories, 44 pp., Boulder, Colo., 1986b.

Nickerson, E.C. (ed.), Geophysical Monitoring for Climate Change, No. 13: Summary Report 1984, 111 pp., NOAA Environmental Research Laboratories, Boulder, Colo., 1986.

Wagner, J.A., The global climate of March-May 1987: Moderately strong mature phase of ENSO with highly persistent monthly and seasonal temperature anomalies over the United States, *Mon. Wea. Rev., 115,* 3166-3187, 1987.

7. Air Quality Group

7.1. Continuing Programs

7.1.1. Introduction

AQG research during 1987 had three objectives: (1) to improve understanding of the mechanisms responsible for the formation of acidic aerosols; (2) to explain the effects of these aerosols and of trace gases on the formation, colloidal stability, optical properties, and chemical composition of clouds; (3) to supply observational data to validate and improve the acid deposition models now under development. AQG acquired data to satisfy these objectives using the NOAA King Air C-90 aircraft (Figure 7.1). Table 7.1 summarizes the research flights made by the King Air in support of our activities during 1987.

7.1.2. National Acid Precipitation Assessment Program

The Interagency Task Force on Acid Precipitation, created by Congress, sponsors NAPAP. This program consists of task groups entitled (A) Natural Sources, (B) Manmade Sources, (C) Atmospheric Processes, and (D) Deposition Monitoring. AQG continued its participation in NAPAP during 1986 by contributing to Task Groups A and C.

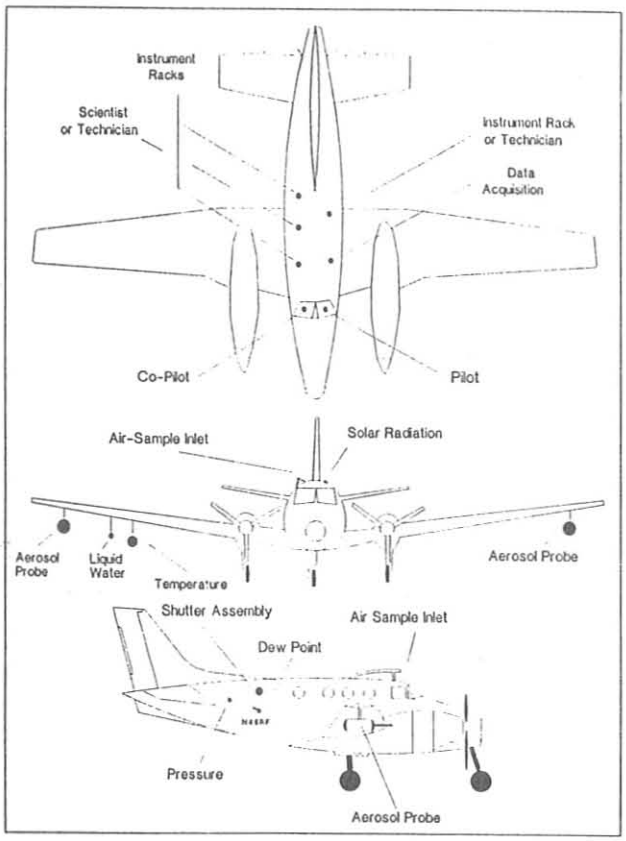

Fig. 7.1. The NOAA King Air C-90, configured for research.

7.1.3. Western Atlantic Ocean Experiment

WATOX data analysis continued during 1987. The purpose of the project was to quantify the flux of various trace species, notably sulfur and nitrogen, away from the United States.

7.1.4. Processing of Emissions by Clouds and Precipitation

The PRECP experiment made it possible for AQG to investigate the complex chemical transformations occurring in and near clouds. The NOAA King Air flew near to many active thunderstorms at selected altitudes during the 1987 period. Other flights were made to characterize the chemical state of the troposphere before the initiation of convection. A persistent "nose" profile of H_2O_2 with altitude was produced during the June flights. H_2O_2 concentrations were about 2 ppbv at the surface, increased to about 5 ppbv at the top of the planetary boundary layer, and decreased slowly above. SO_2 concentrations were at or near the instrument detection limits (1 ppbv) except during occasional anthropogenic plume encounters. Ozone concentrations were between 80 and 100 ppbv. Columbus, Ohio, was the site for a PRECP field effort during June 1987.

7.1.5. Central U.S. RADM Test and Assessment Intensives

CURTAIN was begun with two purposes in mind. One was to compare the observed concentrations of trace species along the western boundary of the RADM (a three-dimensional numerical model) with those predicted by the RADM. A second was to establish an observational data base along the western boundary of the RADM as an aid to model initialization in the future.

The field site for CURTAIN was Little Rock, Arkansas. Research aircraft flights were made north and south along the 91°30'W meridian. The plans for CURTAIN included field periods in February, April, July, and October 1987.

Each field period had two series, each consisting of a night flight and two day flights. One day flight was north to the Iowa border and the other south to the Gulf of Mexico. Each night flight was within 250 km of Little Rock.

Hydrogen Peroxide in Air During Winter Over the South-Central United States

H_2O_2 is important in atmospheric chemistry, both because it is an indicator of the recent concentrations of free radicals that were involved in photochemical reactions and because it plays an important role in the direct oxidation of sulfur species and other acid precursors. Several researchers have reported on H_2O_2 and organic peroxides in clouds and precipitation [*Zika et al.*, 1982; *Kelly et al.*, 1985; *McElroy*, 1986] and in polluted atmospheres [*Bufalini et al.*, 1972; *Kok et al.*, 1978].

TABLE 7.1. NOAA King Air Research Flights During 1987

Date 1987*	Time (LST) Start	End	Date 1987*	Time (LST) Start	End
	ANATEX				
Jan. 13-1	1342	1803	July 25	0928	1406
Jan. 13-2	2018	2346	July 26-1	0917	1348
Jan. 15-1	1420	1822	July 26-2	2229	2701
Jan. 15-2	2043	2333	Oct. 22	1138	1620
Jan. 18-1	0909	1347	Oct. 23	1440	1752
Jan. 18-2	1543	1758	Oct. 25	1313	1833
Jan. 20	1519	1922	Oct. 26	2257	0404
Jan. 23	0303	0709	Oct. 27	2113	0124
Jan. 26	1004	1334	Oct. 28	1022	1501
Jan. 28	0244	0625		*RADM Model Evaluation Experiment*	
Jan. 30	1430	1832			
Feb. 17	1133	1559	June 14	1420	2028
Feb. 18	0816	1226	June 17	1722	2121
Feb. 19	1601	1949	June 24	1202	1622
Feb. 20	0830	1210	June 28	1951	2302
Feb. 22	1136	1506	June 30-1	1131	1510
Feb. 24	1427	1912	June 30-2	1630	2044
Feb. 27	0820	0929		*PRECP-5*	
March 19	0220	0614			
March 21-1	1315	1411	June 3	1041	1421
March 21-2	1447	1838	June 4	1734	2151
March 24-1	0839	1018	June 6	1732	2154
March 24-2	1122	1319	June 8-1	1748	2010
March 26-1	1455	1842	June 8-2	2250	0147
March 26-2	2032	0031	June 9	1611	2031
	CURTAIN		June 12	1417	1619
			June 16	1640	2050
Feb. 5	1141	1612	June 18	1700	1949
Feb. 6-1	1351	1751	June 19	1906	2055
Feb. 6-2	2050	0044	June 20	2008	2318
Feb. 9	1127	1601	June 21	1821	2204
Feb. 10-1	1022	1501		*RITS*	
Feb. 10-2	2017	0056			
April 21	0931	1048	July 1*	0851	1255
April 22	1148	1620	July 16*	0906	1217
April 23-1	1315	1721	Jan. 8	1050	1437
April 23-2	2226	0246	Feb. 3	1057	1516
April 25	1042	1516	March 3	1008	1500
April 26-1	1021	1447	April 7	0918	1338
April 26-2	2147	0227	May 28	0943	1448
July 22	1104	1509	July 2	0940	1350
July 23-1	0930	1340	Aug. 4	0914	1345
July 23-2	2310	0301	Sept. 15	0938	1341

*Dates marked with an asterisk are 1986.

Only *Heikes et al.* [1987] reported on airborne measurements of H_2O_2, O_3, and SO_2, over an appreciable latitude range. They conducted a series of research flights during fall 1984 in which they made vertical profile measurements at selected locations from southern Alabama to upstate New York. They found H_2O_2 concentrations ranging from <0.2 to 4.1 ppbv, and an increase in concentrations from north to south at altitudes below 3000 m msl. They also reported an inverse relationship between H_2O_2 and SO_2, but found no relationship between H_2O_2 and O_3. The NOAA King Air made similar measurements during CURTAIN. The instrumentation aboard the aircraft measured O_3 and SO_2 concentrations, wind speed and direction, temperature, pressure, dewpoint, solar radiation, position, and heading. H_2O_2 was measured continuously using the method described by *Lazrus et al.* [1986] and an instrument built by K & K Enterprises, Boulder, Colorado.

Five-minute-average concentrations of H_2O_2 during the daytime flights of February 5, 6, and 10 (flights 1, 2, and 5) are shown in Figure 7.2, plotted versus latitude. The figure suggests ($r^2 = 0.7$) that the H_2O_2 concentration was increasing toward the south at about 0.046 ppbv per degree of latitude.

Heikes et al. [1987] reported a dependence of H_2O_2 concentration on altitude. Their measurements, designed to provide vertical profiles of the atmosphere at multiple locations, generally showed a positive correlation between altitude and H_2O_2 concentration, although with much variation, depending upon meteorological and pollution conditions. Since our flights consisted of long horizontal transects, direct comparison with the vertical profiling results of Heikes et al. is limited to the locations where we made altitude changes. These were usually at the ends of the transects. In order to provide the greatest validity to such a comparison, we used the average H_2O_2 concentrations within the 10 minutes of level flight immediately preceding and following an altitude change to show changes of concentration with respect to altitude. Figure 7.3 shows these concentration pairs.

In five of the seven examples, the change in concentration was positive (i.e., increasing upward); in the other two it was negative. Although the average profile derived from these examples is weakly positive, the confidence level is low. The establishment of a valid altitude profile awaits more data.

Research flights were made from Little Rock, to southern Iowa, and to the Gulf of Mexico during February 5-10, 1987. In five of the six flights, the H_2O_2 concentration range was <0.1 to 1.0 ppbv, and concentrations increased from north to south at 0.04-0.05 ppbv per degree latitude. Measurements made during the day and at night were not demonstrably different. The remaining flight was in an air mass that was transported from the vicinity of the U.S.-Canada border within the preceding 24 hours. The H_2O_2 concentrations within this air mass were about 0.1 ppbv.

The data suggest that latitude is a primary determinant of the H_2O_2 concentration, and meteorological transport is one of the most important features affecting variability in H_2O_2 concentrations at given altitudes. An increase in H_2O_2 concentration with

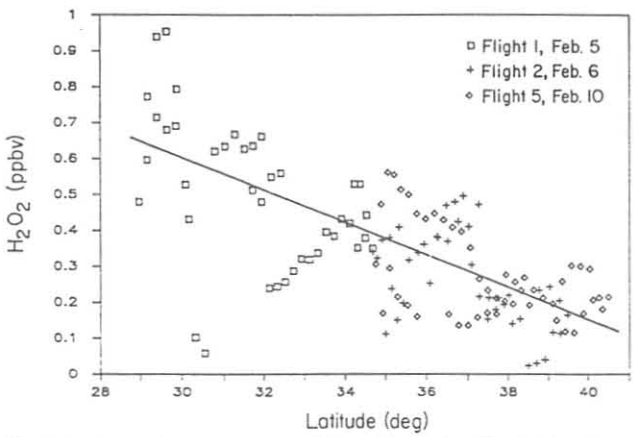

Fig. 7.2. Five-minute averages and linear regression ($r^2 = 0.7$) of H_2O_2 concentrations during flights 1, 2, and 5, versus latitude during CURTAIN.

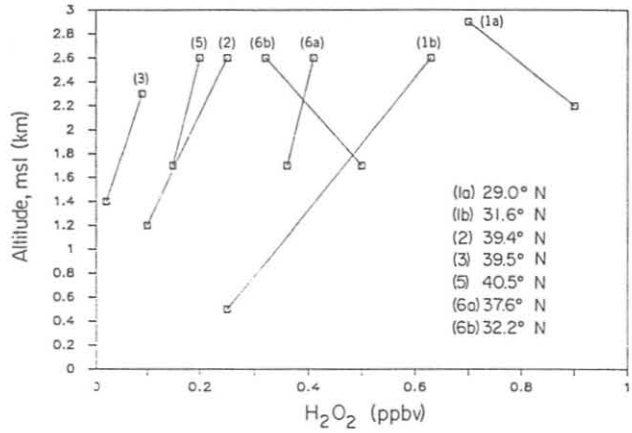

Fig. 7.3. Average H_2O_2 concentrations for the 10-min periods immediately preceding and following altitude changes during the CURTAIN flights indicated in parentheses. The latitudes where the altitude changes were made are listed. There were two altitude changes during flights 1 and 6.

altitude prevailed in five of seven cases investigated. However, the small number of examples and the weakness of the relationship requires further research. *Van Valin et al.* (1987b) gave a more complete description of these results.

7.1.6. Across North America Tracer Experiment

ANATEX was conducted during January-March 1987. The purpose of the experiment was to observe a plume of tracer material (perfluorocarbon) after release from Glasgow, Montana, and St. Cloud, Minnesota. Two research aircraft and a worldwide surface network accomplished this task. AQG used the NOAA King Air, based at Eden Prairie, Minnesota, to follow tracer plumes after their release from St. Cloud. Analysis is continuing, but two preliminary results are available:

1. The aircraft detected and characterized the tracer plume during nearly every flight. The plume was detected as far as 500 km from the release point.
2. Stable atmospheric conditions trapped the tracer plume at altitudes below 200 m above ground on several occasions. Numerical prediction models did not forecast the plume position well under these conditions.

7.1.7. RADM Evaluation Experiment

EPA contracted AQG and the NOAA King Air to provide further verification data for the RADM. Several research flights took place during late June 1987 from Columbus, Ohio to Saranac Lake, New York. These flights were coordinated with the Battelle Pacific Northwest Laboratory DC-3 research aircraft. The purpose of these flights was to document the chemistry of the lower troposphere in the Northeastern U.S. These data will be analyzed similarly to those of CURTAIN, as verification to the RADM. Some preliminary data analysis has occurred; results are not yet available.

7.1.8. Radiatively Important Trace Species

The RITS project monitors trace species that are important to the Earth's radiation budget. Certain atmospheric trace gases, notably CO_2, are known to absorb long-wave radiation from the Earth, thus preventing escape of the radiation to outer space. The capacity of these gases to trap long-wave radiation in the atmosphere plays an important role in the radiation balance of the Earth-atmosphere system. CO_2 is increasing in the atmosphere. Knowledge of this has led to speculation that the Earth-atmosphere system will experience a warming (the Greenhouse Effect) with serious environmental consequences.

Other trace gases such as CO and CH_4 are also known to be effective absorbers of long-wave radiation. However, they were considered much less important in the Earth-atmosphere radiation balance because of their low concentrations in the atmosphere. GMCC found that the concentrations of these gases were increasing at their observatories. This spawned concern that these gases (notably CO and CH_4) would soon become important contributors to the Greenhouse Effect along with CO_2. In order to supplement their surface measurements of these radiatively important trace species, GMCC deemed it important to obtain climatologically representative vertical profiles of them. The NOAA King Air made 10 research flights near Miami, Florida, to gather these data.

Preliminary analyses of the data suggest the following:

1. Measurement of CH_4 and CO from an aircraft is possible.
2. CH_4 and CO are altitude dependent. Surface concentrations do not characterize the troposphere.
3. CH_4 and CO are seasonally dependent.
4. CH_4 and CO are variable over short time and space intervals.

7.1.9. Use of an Airborne Air Sampling Platform for Regional Air Quality Studies

The need to investigate regional air quality issues motivated AQG to develop an airborne platform capable of providing complete air quality information using limited resources, on the one hand, but retaining the flexibility to operate anywhere within the North American continent, on the other hand. Since our objectives called for operation over areas affected by anthropogenic pollution, the analytical instrument package on board used commercially available units. These units may be less sensitive than experimental or developmental instrumentation but provide a higher degree of reliability. In early 1984, the AQG leased a Beechcraft King Air C-90 from the Department of Interior (DOI) and modified it for use as a regional air quality sampling platform. Ownership of the aircraft was later transferred from DOI to OAO, NOAA.

The Beechcraft King Air C-90 is a twin-engine aircraft equipped with 550 hp Pratt-Whitney PT-6A-20 turbine engines. The aircraft has a useful load of 1600 kg, a gross weight of 4380 kg, and was originally designed to carry a crew of two and up to seven passengers. Its fuel capacity is 1400 L and the consumption rate is 250 L h^{-1}. The range of the aircraft, fully fueled, is 2100 km at an average speed of 420 km h^{-1} and cruise altitude of 6400 m. The service ceiling of the aircraft is 7600 m. The outside dimensions are 10.8 m (length) by 15.3 m (wing span) by 4.3 m (vertical stabilizer height). The available cabin volume is 8.2 m^3 (excluding pilot compartment) with an additional 1.5 m^3 available in the baggage compartment at the rear of the cabin. The aircraft is fully equipped for operation under instrument flight rules (IFR), can be pressurized, and has complete deicing capability. When equipped as described below and with a crew of three (pilot, copilot, and scientist flight director) the aircraft weighs 3560 kg. This allows 820 kg of fuel and provides for a flight duration of about 4 hours.

The change from a passenger aircraft to an airborne laboratory required several major modifications to the aircraft. Aluminum research instrument racks were mounted, using the original floor track hardware [*Wellman*, 1982]. Power to the instruments (most of which require 110-VAC), is supplied by lightweight DC to AC inverters connected to the aircraft 28-VDC electrical system. The power pack consists of three 110-VAC (750 VA) 400-Hz inverters made by FliteTronics Co. Inc, two 110-VAC (1000 VA) 60-Hz units built by Avionics Instruments Inc., and an additional 28-VDC, 70-A power supply.

Spar doublers and torque boxes reinforced the end sections of the wings. This enabled the mounting of scientific instruments weighing up to 20 kg on each wing; wiring in the wings carried the power and signals for these instruments. To aid in sampling outside air, a stainless steel air intake system was installed in a reinforced portion of the fuselage above the right-hand side of the forward cabin. Three shutter assemblies were also installed, one on the top center and two on the right rear of the fuselage. They allow in situ or remote sensing, as needed.

A LORAN system determines the aircraft position accurately. This system (Advanced Navigation Inc. model 7000) enables determination of position to 0.5 km. A radar altimeter (King, KRA10) aids in maintaining constant altitude at low elevations (fewer than 760 m) and enhances flight safety at low-altitude.

The air intake system aboard the aircraft has different intakes for different applications. The WATOX, PRECP, RITS, and SAFE studies, used a five-tube stainless steel configuration. Three tubes pointed forward and two pointed vertically. One inlet tube, used for total aerosol sampling, was isokinetic at any flight sampling speed. Another inlet tube had an inner Teflon tube and supplied air for the gas monitors. A third tube supplied air to a cyclone particle separator described by *Boatman and Wellman* [1988]. Additional air samples, for intermittent sampling devices, are drawn from the vertical tubes and the sextant port at the top center of the fuselage.

A fully computerized data acquisition system digitizes the data from all continuous monitors, aerosol probes, mass flow meters, and navigation system (Algo, Inc.) and records it to magnetic tape. The onboard computer system displays the data during flight. Magnetic tape also records the data from the navigation system (Algo, Inc.). All magnetic tape data are later merged into one file for analysis using an HP 1000 computer system (Hewlett-Packard, Inc.).

The OAO operates the aircraft with an OAO pilot and copilot. The scientific personnel aboard include a mission scientist and, if required by the program, an instrument

operator-technician. An illustration of the aircraft as configured for scientific research is given in Fig. 7.1. Refer to *Boatman et al.* [1988] and *Wellman et al.* [1988] for a more detailed discussion of the aircraft platform.

7.2. Special Projects

7.2.1. Natural Sulfur Flux From the Gulf of Mexico: Dimethyl Sulfide, Carbonyl Sulfide, and Sulfur Dioxide

The emission of reduced sulfur compounds into the atmosphere through natural processes is well established. In recent years, however, a growing interest in the magnitude and composition has evolved, mainly because these compounds may make a significant contribution to the atmospheric loading of SO_4^{2-} aerosols. It is difficult to accurately assess the exact emission rate of S-containing compounds into the atmosphere; therefore, variations of 2 orders of magnitude between some estimates are not surprising [*Möller*, 1984b)].

It is widely believed that the primary atmospheric source of natural atmospheric S is dimethyl sulfide (DMS). *Andreae and Raemdonck* [1983] estimated that the global biogenic emission of S is about 10^3 Tg yr^{-1}, about half as DMS. Marine sources emit the most DMS (~75%), but continental areas also have a role [*Adams et al.*, 1981]. Other sources of biogenic S include hydrogen sulfide from biological decay 32-45 Tg (S) yr^{-1} [*Adams et al.*, 1981]. *Khalil and Rasmussen* [1984] put the biogenic emission of carbonyl sulfide (COS) and carbon disulfide (CS_2) at about 1 and 1.3 Tg (S) yr^{-1}. Other biogenic S compounds, such as methyl mercaptan, dimethyl sulfoxide, and dimethyl disulfide, contribute to the global S cycle in only a minor way [e.g., *Möller*, 1984b; *Adams et al.*, 1981; *Aneja et al.*, 1982; *Steudler and Peterson*, 1984]. An additional natural source of atmospheric S is sulfur dioxide (SO_2) from volcanic activity. *Cullis and Hirschler* [1980] estimated that SO_2 from volcanos is unlikely to contribute much more than ~5 Tg (S) yr^{-1}; *Cadle* [1980] estimated as much as 30 Tg (S) yr^{-1}, but other authors [e.g., *Möller*, 1984b] have placed the value at about 2 Tg (S) yr^{-1}.

Because the global natural emission of S is on the same order of magnitude as [*Cullis and Hirschler*, 1980] or somewhat larger than [*Möller*, 1984a] the anthropogenic emission, a program to investigate the contribution of natural S to the total S budget over North America was included in NAPAP. This appeared to be particularly advisable after *Reisinger and Crawford* [1980] reported SO_4^{2-} fluxes from areas southwest of central Tennessee that were as much as 2.3 times the fluxes of all the other sectors. As a part of this program, AQG conducted a series of research aircraft flights in June 1985 to determine the flux of S compounds into the North American continent from the marine atmosphere and from the zone extending inland as much as a few hundred kilometers.

Although there may be a large experimental uncertainty in the DMS measurements, the results of this study suggest that atmospheric DMS is surface derived, has a half-life commensurate with the boundary layer mixing time, and is very sensitive to the presence of trace atmospheric pollutants. Under clean atmospheric conditions in marine air masses, DMS concentrations over the Gulf of Mexico approached those typical of remote oceanic areas. A reduction in DMS by a factor of 4 occurred when the Gulf air was displaced by continental air.

There was no demonstrable diurnal cycle for DMS during the study; any possible diurnal cycle was within the noise level of the data. The very low concentrations at night, when admixture of continental air is suggested, support the importance of the recently proposed dark reaction between DMS and NO_3. COS concentrations were slightly higher in the boundary layer than above the boundary layer. The ratios between the concentrations of DMS and SO_2, and their reaction rates with HO, suggest that the oxidation of DMS is the principal source of SO_2 in the marine atmosphere. *Van Valin et al.* [1987a] gave a complete account of this work.

7.3. References

Adams, D. F., S. O. Farwell, E. Robinson, M. R. Pack, and W. L. Bamesberger, Biogenic sulfur source strengths, *Environ. Sci. Technol. 15*, 1493-1498, 1981.

Andreae, M. O., and H. Raemdonck, Dimethyl sulfide in the surface ocean and the marine atmosphere: A global view, *Science, 221*, 744-747, 1983.

Aneja, V. P., A. P. Aneja, and D. F. Adams, Biogenic sulfur compounds and the global sulfur cycle, *J. Air Pollut. Control Assoc., 32*, 803-807, 1982.

Boatman, J. F., and D. L. Wellman, An aerosol separator for use in aircraft, *Atmos. Environ.*, in press, 1988.

Boatman, J. F., D. L. Wellman, R. C. Schnell, K. M. Busness, M. Luria, and C. Van Valin, In-flight intercomparisons of some aircraft meteorological and chemical measurement techniques, *Global Biogeochem. Cycles, 2*, 1-11, 1988.

Bufalini, J. J., B. W. Gay, Jr., and K. L. Brubaker, Hydrogen peroxide formation from formaldehyde photooxidation and its presence in urban atmospheres, *Environ. Sci. Technol., 6*, 816-821, 1972.

Cadle, R. D., A comparison of volcanic and other fluxes of atmospheric trace gas constituents, *Rev. Geophys. Space Phys., 18*, 746-752, 1980.

Cullis, C. F., and M. M. Hirschler, Atmospheric sulphur: Natural and man-made sources, *Atmos. Environ. 14*, 1263-1278, 1980.

Heikes, B. G., G. L. Kok, J. G. Walega, and A. L. Lazrus. H_2O_2, O_3, and SO_2 measurements in the lower troposphere over the eastern United States during fall, *J. Geophys. Res., 92*, 915-931, 1987.

Kelly, T. J., P. H. Daum, and S. E. Schwartz, Measurements of peroxides in cloudwater and rain, *J. Geophys. Res., 90*, 7861-7871, 1985.

Khalil, M. A. K., and R. A. Rasmussen, Global sources, lifetimes and mass balances of carbonyl sulfide (OCS) and carbon disulfide (CS_2) in the earth's atmosphere, *Atmos. Environ. 18*, 1805-1813, 1984.

Kok, G. L., K. R. Darnall, A. M. Winer, J. N. Pitts, Jr., and B. W. Gay, Ambient air measurements of hydrogen peroxide in the California South Coast air basin, *Environ. Sci. Technol., 12*, 1077-1080, 1978.

Lazrus, A. L., G. L. Kok, J. A. Lind, S. N. Gitlin, B. G. Heikes, and R. E. Shetter, Automated fluorometric method for hydrogen peroxide in air, *Anal. Chem., 58*, 594-597, 1986.

McElroy, W. J., Sources of hydrogen peroxide in cloudwater, *Atmos. Environ., 20*, 427-438, 1986.

Möller, D., Estimation of the global man-made sulphur emission, *Atmos. Environ., 18*, 19-27, 1984a.

Möller, D., On the global natural sulphur emission, *Atmos. Environ., 18*, 29-39, 1984b.

Reisinger, L. M., and T. L. Crawford, Sulfate flux through the

Tennessee Valley region, *J. Air Pollut. Contr. Assoc., 30*, 1230-1231, 1980.

Steudler, P. A., and B. J. Peterson, Contribution of gaseous sulphur from salt marshes to the global sulphur cycle, *Nature, 311*, 455-457, 1984.

Van Valin, C. C., M. Luria, D. L. Wellman, R. L. Gunter, and R. F. Pueschel, Natural sulfur flux from the Gulf of Mexico: Dimethyl sulfide, carbonyl sulfide, and sulfur dioxide., *NOAA Tech. Rep. ERL 432-ARL 9*, Air Resources Lab., Boulder, CO, 14 pp., 1987a.

Van Valin C. C., J. D. Ray, J. F. Boatman, and R. L. Gunter, Hydrogen peroxide during winter in air over the South-Central United States, *Geophys. Res. Lett., 14*, 1146-1149,1987b.

Wellman D. L., M. Luria, C. C. Van Valin, and J. F. Boatman, The use of an airborne air sampling platform for regional air quality studies, NOAA Tech. Memo., in press, 1988.

Zika, R., E. Saltzman, W. L. Chameides, and D. D. Davis, H_2O_2 levels in rainwater collected in south Florida and the Bahama Islands, *J. Geophys. Res., 87*, 5015-5017, 1982.

8. Nitrous Oxide and Halocarbons Group

8.1. Continuing Programs

8.1.1. Samples

GMCC scientists have been analyzing flask samples for nitrous oxide (N_2O), and halocarbons CFC-12 (CCl_2F_2) and CFC-11 (CCl_3F) since 1977 at the GMCC baseline observatories and NWR. During 1987, air samples pressurized to about 8 psig were collected in a pair of 0.3-L Summa treated stainless steel cylinders each week at BRW, NWR, MLO, and SMO. Station personnel at SPO collected a pair of flask samples each week only during the Antarctic summer (November-January). These air samples were shipped back to Boulder for analysis by EC-GC.

Figure 8.1 shows plots of the average concentration from a flask pair versus time for N_2O, CFC-12, and CFC-11 at BRW, NWR, MLO, SMO, and SPO. Table 8.1 lists monthly concentration means for NOAA/GMCC flask pairs as mole fraction in dry air for N_2O, CFC-12, and CFC-11 collected from NOAA/GMCC baseline stations and NWR. Estimated secular trends and ±2 standard deviations at the 95% confidence level are also presented. Flask data are not included for May 1984 to February 1985, because the ECD response during this time was not linear. Figure 8.2 shows the strong latitudinal dependence, higher in the northern hemisphere than the southern hemisphere, and the accummulation rates of CFC-12 and CFC-11 from plots of the yearly mean concentration versus latitude since 1977. More information on experimental design and techniques used in data selection are described in *Thompson et al.* [1985].

Since 1983, a manually operated Shimadzu Mini-2 GC at SPO measured N_2O, CFC-12, and CFC-11 in situ twice a week. The monthly mean concentrations of N_2O, CFC-12, and CFC-11 from the in situ GC were compared with monthly means from flask samples and are shown in the bottom panel of Figure 8.1. The ECD on this GC became contaminated by February 1987, and analyses were stopped until a new detector arrived during the midwinter air drop in June 1987. The results from the flasks and in situ GC at SPO were so sporadic that it was decided to upgrade the existing in situ GC in early 1988. The upgraded GC system will include unattended, automated analyses, increased frequency of atmospheric sampling to once every 3 hours, and the additional sampling of new compounds, methyl chloroform (CH_3CCl_3) and carbon tetrachloride (CCl_4). An IBM PC clone computer will be used to store chromatographic information from two HP integrators, and to send this information back to Boulder via satellite each week for rapid analysis of data and for diagnosis of potential problems. These improvements may help resolve the question concerning the effects of vertical transport on the ozone hole. More technical information on GMCC's SPO N_2O and halocarbon measurements can be found in *Robinson et al.* [1988] and *Elkins et al.* [1988].

The calibration scales for GMCC's atmospheric measurements of CFC-12 and CFC-11 have been based since 1977 on the OGC scale of R. Rasmussen [*Rasmussen and Lovelock,* 1983]. NOAA primary calibration tank no. T3072, which was used exclusively from 1977 until 1985 when it was expended, was calibrated last in 1983. The current primary calibration tank no. T3088 was compared almost every 6 months between 1977 and 1985 with tank no. T3072 and replaced it in 1985. Because of concerns about the stability of CFC-12 and CFC-11 in the new tank, it was calibrated at OGC in December 1987. Drift was found to be about -4.5 ppt yr^{-1} for CFC-12 and negligible for CFC-11 during its 2 years of use. It was assumed that, before 1987, the drift of T3088 was identical to the drift of tank no. T3072, having drift rates of about -1.5 ppt yr^{-1} for CFC-11 and +5 ppt yr^{-1} for CFC-12. The new drift corrections

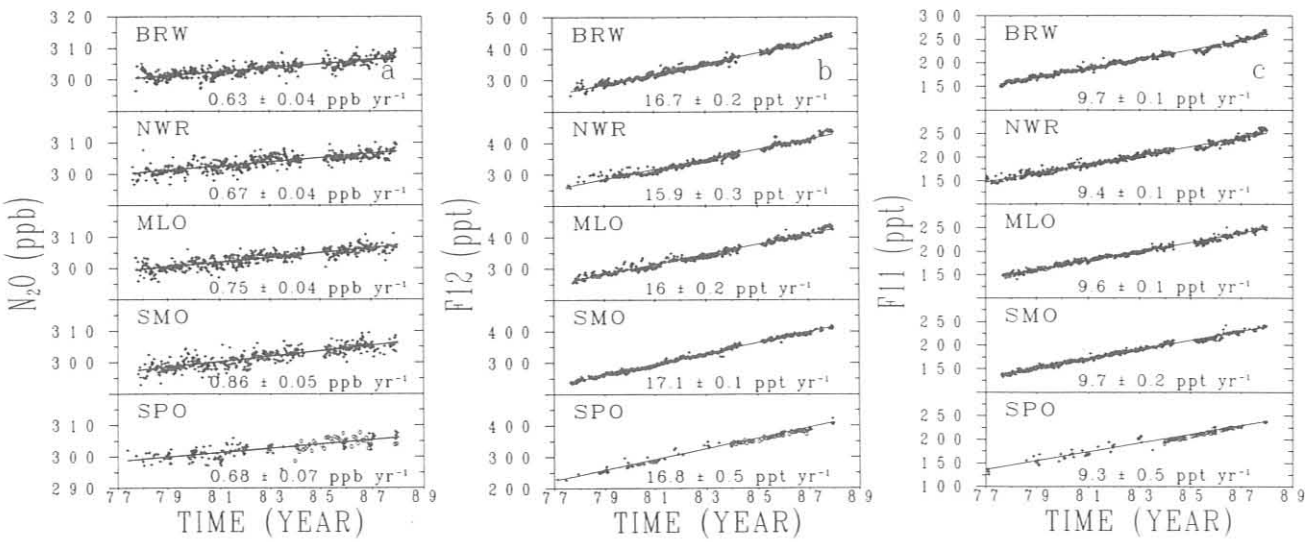

Fig. 8.1. Average concentration of (a) N_2O, (b) CFC-12, and (c) CFC-11 from measurements of paired flask samples versus time at BRW, NWR, MLO, SMO, and SPO. The trends and ± 2 s.d. errors are shown. The bottom panel (SPO) in each plot also shows the monthly means (o) from a manually operated GC.

TABLE 8.1. Monthly Concentration Means for NOAA/GMCC Flask Pairs for N_2O (ppb by mole fraction in dry air), CFC-12 (ppt), and CFC-11 (ppt) Collected From BRW, NWR, MLO, SMO, and SPO

	N_2O					CFC12					CFC11				
	BRW	NWR	MLO	SMO	SPO	BRW	NWR	MLO	SMO	SPO	BRW	NWR	MLO	SMO	SPO
JAN 77	---	---	---	---	---	---	---	---	---	---	---	157.1	---	---	137.4
FEB 77	---	---	---	---	---	---	---	---	---	230.2	---	153.8	---	---	129.4
MAR 77	---	---	---	---	---	---	---	---	---	---	---	147.6	---	---	---
APR 77	---	---	---	---	---	---	---	---	---	---	---	150.8	---	---	---
MAY 77	---	---	---	---	302.8	---	---	---	---	---	---	151.9	---	---	---
JUN 77	---	---	---	---	---	---	---	---	---	227.8	---	144.1	---	---	---
JUL 77	---	---	---	---	---	---	260.2	---	---	---	---	148.2	---	---	---
AUG 77	---	301.1	---	---	---	---	268.3	---	238.3	---	151.5	158.6	149.1	137.3	---
SEP 77	297.2	299.2	302.3	---	301.1	251.3	258.2	255.8	237.5	---	152.6	149.2	149.8	138.2	---
OCT 77	305.1	298.8	299.8	297.4	---	---	---	262.3	239.4	---	159.3	156.3	147.6	139.2	---
NOV 77	301.6	300.8	299.2	296.6	---	274.3	---	262.8	240.0	---	160.4	153.2	149.3	137.6	---
DEC 77	305.1	---	302.0	---	300.0	284.2	286.9	272.7	246.5	248.2	162.7	159.9	149.8	137.7	---
JAN 78	304.1	308.5	301.5	296.3	298.6	269.9	---	275.3	250.1	---	160.8	154.6	155.8	142.3	---
FEB 78	303.1	301.7	300.7	298.2	298.0	289.5	---	267.6	251.9	---	159.4	159.4	152.8	141.8	---
MAR 78	301.8	301.3	302.9	299.5	302.1	282.5	279.9	275.1	245.1	---	162.4	156.6	149.0	143.9	---
APR 78	301.9	302.1	299.7	299.1	298.2	260.3	---	277.9	261.0	---	164.3	---	154.1	146.3	---
MAY 78	302.0	301.7	298.8	300.8	301.1	267.4	---	---	255.4	---	161.9	166.6	154.5	146.8	---
JUN 78	301.6	301.1	300.1	300.1	301.6	---	298.6	282.3	255.6	---	162.4	157.7	154.8	145.8	---
JUL 78	300.9	300.2	299.5	299.3	301.5	273.7	302.5	280.6	253.1	---	163.6	163.5	154.0	145.6	156.6
AUG 78	300.3	300.2	299.5	298.5	---	---	301.0	279.3	254.4	---	164.8	165.8	158.2	148.0	---
SEP 78	302.0	301.4	300.6	298.8	299.2	285.7	---	277.7	257.8	---	168.4	170.8	160.4	147.9	---
OCT 78	301.6	301.4	300.2	298.4	---	290.6	296.5	277.6	258.5	249.7	169.0	165.4	158.4	149.6	---
NOV 78	301.7	302.2	300.5	299.4	300.3	293.8	293.8	281.6	262.1	251.4	174.0	167.6	159.8	152.5	165.4
DEC 78	301.7	302.6	300.4	298.8	300.7	292.4	---	291.0	262.0	257.5	171.3	164.8	159.8	151.4	154.8
JAN 79	301.2	302.4	301.0	300.8	300.6	287.6	283.9	290.4	269.3	258.9	168.7	164.5	162.8	154.4	151.1
FEB 79	301.7	299.7	301.9	299.4	300.9	290.0	292.5	283.3	268.5	253.4	171.3	163.7	164.3	158.1	157.9
MAR 79	302.4	303.4	301.0	298.4	---	296.2	---	286.6	268.1	---	174.1	173.7	164.3	154.5	---
APR 79	302.7	301.9	301.5	298.7	---	289.2	316.4	283.2	269.0	---	173.2	166.9	163.8	156.4	---
MAY 79	303.0	302.0	301.4	300.0	---	289.2	297.7	289.3	267.5	---	172.6	166.3	162.8	155.4	---
JUN 79	302.6	302.0	301.1	299.5	---	293.0	297.7	293.9	268.3	---	172.2	169.2	163.1	155.3	---
JUL 79	302.5	302.4	301.4	300.4	---	294.4	295.1	293.3	271.2	---	173.0	168.9	165.7	156.9	---
AUG 79	302.4	302.1	300.6	301.7	---	293.3	300.1	---	275.1	---	172.2	172.0	---	158.9	---
SEP 79	302.7	300.0	301.2	302.3	---	300.1	311.6	298.0	275.2	---	175.8	169.5	169.6	156.0	---
OCT 79	302.1	301.8	303.9	303.0	299.6	297.1	296.9	320.3	275.3	298.1	179.1	174.3	175.5	162.2	---
NOV 79	302.2	304.4	301.5	299.9	301.2	296.0	301.8	298.1	269.8	275.1	177.6	176.4	171.1	157.2	154.3
DEC 79	303.6	304.3	303.1	301.2	301.5	304.1	306.5	299.5	275.1	274.5	182.0	174.9	171.7	161.1	169.8
JAN 80	303.3	306.6	302.8	302.0	302.2	306.2	314.2	309.6	279.6	275.0	183.1	175.4	173.7	164.0	162.1
FEB 80	303.4	303.9	302.2	301.9	302.5	301.7	305.5	310.4	279.1	271.8	181.7	175.1	173.3	164.9	161.3
MAR 80	302.2	302.9	303.2	300.3	301.5	303.5	309.0	298.8	279.3	---	183.9	184.9	176.1	164.9	---
APR 80	300.1	303.4	301.1	298.0	301.4	309.0	304.1	304.2	282.5	276.9	182.3	179.0	177.9	165.9	167.5
MAY 80	302.2	302.8	302.6	299.2	303.1	309.0	310.8	292.8	281.1	277.3	181.9	183.4	172.5	165.9	174.9
JUN 80	302.3	304.3	302.0	300.9	299.9	306.9	301.6	309.2	283.7	281.8	183.4	180.1	177.1	168.1	163.4
JUL 80	301.7	301.4	301.0	300.0	299.1	303.2	301.3	316.8	284.5	279.6	182.8	182.1	179.4	166.7	---
AUG 80	304.3	303.6	301.9	299.5	304.2	307.1	301.6	300.6	283.6	---	188.4	195.2	179.7	166.9	---
SEP 80	302.1	303.2	301.7	300.6	---	312.3	309.7	301.2	288.1	300.6	186.4	184.7	176.7	170.6	---
OCT 80	300.9	302.0	303.5	300.4	300.1	311.1	304.6	310.9	287.4	286.3	184.5	182.3	181.7	168.4	177.1
NOV 80	301.7	303.4	301.3	298.0	301.1	319.8	305.0	309.3	286.7	284.3	192.8	185.4	183.1	168.8	165.5
DEC 80	303.7	302.2	300.8	297.3	300.1	327.9	308.8	306.0	290.5	286.9	189.4	181.3	178.5	169.5	168.3
JAN 81	303.1	303.3	301.3	300.9	299.8	315.1	309.5	303.8	291.5	286.2	188.8	184.6	179.1	171.3	170.3
FEB 81	302.8	303.0	301.7	303.3	301.3	315.4	307.6	310.6	298.3	291.8	193.4	184.3	182.8	177.1	---
MAR 81	303.3	304.2	303.0	300.6	303.4	319.0	315.5	310.3	298.3	---	188.0	186.7	183.8	172.3	---
APR 81	304.3	304.6	303.8	298.8	304.6	331.3	316.6	320.8	300.5	---	192.0	184.0	184.8	175.3	---
MAY 81	303.7	303.1	303.2	302.0	302.3	326.8	318.4	324.3	303.8	294.9	190.8	188.8	184.4	175.8	185.5
JUN 81	303.6	303.7	304.1	301.4	303.6	328.0	320.0	332.1	307.8	---	192.2	188.8	186.8	175.5	---
JUL 81	302.7	302.3	302.9	302.4	303.9	327.1	323.3	329.5	306.7	---	192.3	188.4	188.3	176.9	---
AUG 81	305.4	303.9	303.0	300.6	302.9	337.5	324.8	333.8	307.0	---	201.9	190.2	187.5	178.3	---
SEP 81	302.3	302.6	302.5	302.1	303.5	327.4	325.9	330.4	305.5	324.0	191.8	191.4	190.6	181.3	---
OCT 81	302.5	302.8	303.7	301.8	305.1	332.8	331.2	333.4	309.4	329.5	196.7	193.4	190.6	180.4	194.9
NOV 81	302.5	302.9	302.9	302.8	303.1	332.7	322.3	328.3	311.3	---	199.7	190.9	190.0	182.4	173.9
DEC 81	303.4	303.1	302.7	301.5	302.8	335.4	325.4	339.5	312.9	311.2	201.5	191.9	192.2	182.6	186.5
JAN 82	302.4	304.1	303.4	300.1	303.8	339.6	329.3	332.6	317.8	308.4	199.6	193.3	189.9	184.8	---
FEB 82	304.4	303.1	303.5	301.0	---	343.0	326.5	336.6	322.0	---	202.3	191.7	190.1	185.2	---
MAR 82	304.4	303.6	304.0	300.6	---	336.6	330.6	329.9	317.3	---	203.1	196.7	191.6	183.6	---
APR 82	305.5	305.9	304.7	303.7	---	339.8	339.9	330.1	320.4	---	201.4	197.9	192.2	186.7	---
MAY 82	305.3	305.0	304.5	303.6	---	340.0	333.0	332.6	320.2	---	199.6	197.2	194.5	186.4	---
JUN 82	304.9	305.2	304.4	304.4	---	334.6	337.1	330.9	318.6	---	198.4	197.6	192.9	187.7	---
JUL 82	304.4	305.1	304.2	302.6	---	340.3	345.3	330.4	321.0	---	201.6	201.1	192.2	187.3	---
AUG 82	304.1	306.5	305.8	302.6	---	341.6	339.8	334.1	322.5	---	201.8	198.1	195.8	189.1	---
SEP 82	304.1	305.0	304.0	304.2	---	343.2	339.3	337.9	323.3	---	203.6	199.5	197.5	189.1	---
OCT 82	303.9	304.5	304.9	302.9	---	348.1	343.1	339.3	325.7	---	205.1	199.7	198.5	190.2	---
NOV 82	304.6	305.8	304.5	303.0	303.1	351.2	343.5	339.7	325.0	337.6	206.8	204.3	197.7	190.5	202.2
DEC 82	304.9	305.4	304.3	302.5	303.8	350.9	343.2	342.5	325.2	---	208.0	204.6	197.2	189.8	201.8
JAN 83	305.2	306.0	304.6	304.1	303.7	353.4	344.1	337.1	330.1	340.0	209.8	202.3	198.9	194.9	203.1
FEB 83	305.9	306.5	305.3	303.1	---	353.9	347.1	342.3	330.9	---	209.1	205.7	200.0	191.8	---
MAR 83	305.3	306.2	305.4	303.0	---	352.8	349.1	343.1	334.5	---	209.9	208.4	201.5	196.1	---
APR 83	304.6	305.3	305.0	303.4	---	353.2	349.5	343.6	333.7	---	211.1	209.7	202.5	195.4	---
MAY 83	304.5	306.6	305.3	301.3	296.9	355.3	353.2	343.3	332.9	---	---	210.4	204.3	195.1	---
JUN 83	304.9	305.5	304.4	303.0	304.0	352.3	352.7	346.1	333.1	345.6	212.3	208.5	209.1	196.8	178.4
JUL 83	306.8	306.8	303.6	305.1	---	353.1	365.9	357.9	327.5	---	214.8	209.4	208.3	197.0	---
AUG 83	304.4	307.3	304.9	304.9	---	355.4	349.2	345.4	335.8	---	210.9	209.4	207.5	195.8	---
SEP 83	301.7	304.6	304.4	302.8	---	361.0	357.2	355.6	341.6	---	211.1	209.8	204.7	197.4	---
OCT 83	304.9	304.2	304.6	304.5	---	367.7	362.2	356.6	345.9	---	215.5	212.4	209.1	200.8	---
NOV 83	304.4	305.0	304.5	303.4	---	370.0	363.2	362.1	348.0	---	218.9	212.4	208.9	199.1	---
DEC 83	304.9	306.5	304.9	304.2	303.9	359.7	366.9	357.0	349.6	334.2	216.9	216.1	203.7	204.1	196.2
JAN 84	305.1	305.5	305.3	304.6	304.0	367.2	365.0	358.8	349.5	---	220.9	214.3	209.6	205.5	---
FEB 84	305.2	305.5	305.0	304.4	304.3	377.9	361.8	367.0	357.0	347.8	221.1	212.0	212.6	207.1	199.5
MAR 84	304.9	304.7	304.7	307.0	---	364.3	360.1	353.4	352.2	---	220.4	217.9	211.3	202.3	---
APR 84	305.6	305.8	306.5	304.2	---	375.3	368.4	368.8	360.8	---	217.4	215.8	212.7	207.1	---

TABLE 8.1. Continued

	N_2O					CFC12					CFC11				
	BRW	NWR	MLO	SMO	SPO	BRW	NWR	MLO	SMO	SPO	BRW	NWR	MLO	SMO	SPO
FEB 85	305.4	---	306.8	303.0	---	389.3	---	377.3	369.8	---	225.3	---	220.9	211.4	---
MAR 85	306.1	305.4	305.4	304.4	---	387.8	380.0	379.5	368.0	---	224.5	218.8	219.1	209.4	---
APR 85	306.6	306.0	305.7	305.5	---	389.7	379.9	375.4	369.4	---	227.8	219.2	217.2	210.7	---
MAY 85	307.5	307.2	305.4	304.7	---	392.5	384.8	382.4	373.0	---	225.5	222.0	220.3	210.9	---
JUN 85	306.3	305.0	306.0	306.8	---	394.6	385.0	390.5	373.5	---	222.4	219.5	220.6	208.8	---
JUL 85	303.7	306.5	304.6	304.9	---	388.1	386.1	382.7	375.7	---	222.0	218.4	217.4	210.4	---
AUG 85	304.4	305.7	304.4	305.4	---	393.4	393.4	384.5	373.7	---	227.5	221.0	219.0	211.0	---
SEP 85	305.0	306.0	305.9	304.4	---	400.8	406.6	396.0	379.8	---	227.9	230.6	222.4	214.4	---
OCT 85	305.4	306.0	306.4	305.8	---	404.0	401.6	398.6	381.5	---	233.4	229.6	226.7	215.1	---
NOV 85	305.7	306.7	306.7	304.7	304.4	406.8	403.7	392.3	375.6	375.1	235.7	230.3	224.9	214.3	214.6
DEC 85	305.3	305.8	306.7	305.9	305.1	408.3	397.1	398.3	383.6	377.6	236.1	229.0	231.1	218.0	220.9
JAN 86	305.5	306.1	306.5	303.8	306.4	407.0	396.7	395.1	383.9	381.0	236.8	228.3	223.5	217.2	---
FEB 86	305.8	306.2	305.8	306.4	---	408.4	396.1	400.0	388.8	---	236.6	226.3	227.2	216.2	---
MAR 86	305.9	306.1	307.2	305.5	---	409.6	398.4	398.4	386.6	---	233.9	227.2	228.4	218.6	---
APR 86	306.7	306.6	306.4	306.0	---	410.7	397.2	400.2	387.1	---	244.6	231.9	234.0	225.7	---
MAY 86	307.5	306.4	306.4	305.4	---	407.7	404.2	399.5	387.7	---	238.5	234.2	232.6	234.0	---
JUN 86	307.7	306.3	306.7	307.1	---	407.8	404.5	401.1	393.5	---	238.4	234.8	235.4	226.1	---
JUL 86	308.3	307.5	307.9	306.5	---	406.7	400.3	397.2	388.9	---	237.9	231.7	234.1	225.6	---
AUG 86	307.6	306.6	307.4	307.9	---	404.3	405.5	402.1	391.7	---	240.4	237.0	232.4	226.6	---
SEP 86	306.3	306.4	307.4	306.9	---	406.4	399.2	403.1	392.6	---	240.5	233.9	239.4	228.9	---
OCT 86	306.4	306.9	308.6	306.3	---	413.7	406.3	412.1	392.4	---	248.9	240.7	240.4	227.4	---
NOV 86	306.7	306.8	307.7	307.9	305.9	415.5	405.2	409.7	390.8	385.3	246.5	243.8	240.2	225.7	227.1
DEC 86	305.9	306.9	307.1	306.3	304.9	419.4	406.8	409.8	394.1	387.3	250.5	239.9	239.9	229.9	---
JAN 87	307.3	307.7	307.2	305.7	307.3	417.0	409.0	410.5	396.0	390.5	248.9	240.3	239.4	229.6	228.2
FEB 87	307.8	306.7	306.6	304.7	---	417.5	406.7	401.9	398.4	---	249.8	243.5	---	236.4	---
MAR 87	308.0	308.0	307.6	305.3	---	424.9	418.9	421.5	404.5	---	250.2	243.9	243.3	---	---
APR 87	307.2	307.3	305.2	303.9	---	422.6	418.3	412.6	408.1	---	253.3	242.8	---	235.0	---
MAY 87	309.1	307.5	307.5	---	---	430.9	---	---	---	---	253.9	247.4	---	---	---
JUN 87	308.1	307.5	307.0	301.5	---	429.1	433.0	423.1	400.5	---	253.1	249.7	244.9	232.0	---
JUL 87	307.3	305.5	305.6	304.2	---	434.4	432.3	422.2	408.0	---	255.1	248.8	242.2	232.9	---
AUG 87	307.7	307.0	307.2	---	---	433.1	429.2	426.5	---	---	256.5	251.1	246.2	---	---
SEP 87	308.3	305.3	305.5	304.9	---	439.5	438.4	435.8	---	---	259.0	254.5	249.8	239.2	---
OCT 87	308.4	307.9	307.2	304.8	---	443.5	441.3	435.9	409.1	---	262.7	260.8	254.5	236.5	---
NOV 87	307.7	308.4	308.4	304.8	307.6	444.1	439.0	436.0	413.0	407.8	265.5	258.3	252.7	239.9	238.1
DEC 87	309.4	310.1	307.7	305.2	307.2	444.9	438.9	429.0	413.5	410.9	265.9	260.0	248.5	241.1	237.4

Data presented for 1986-1987 are subject to change, pending final calibrations. See text for discussion of calibrations and gaps in data.

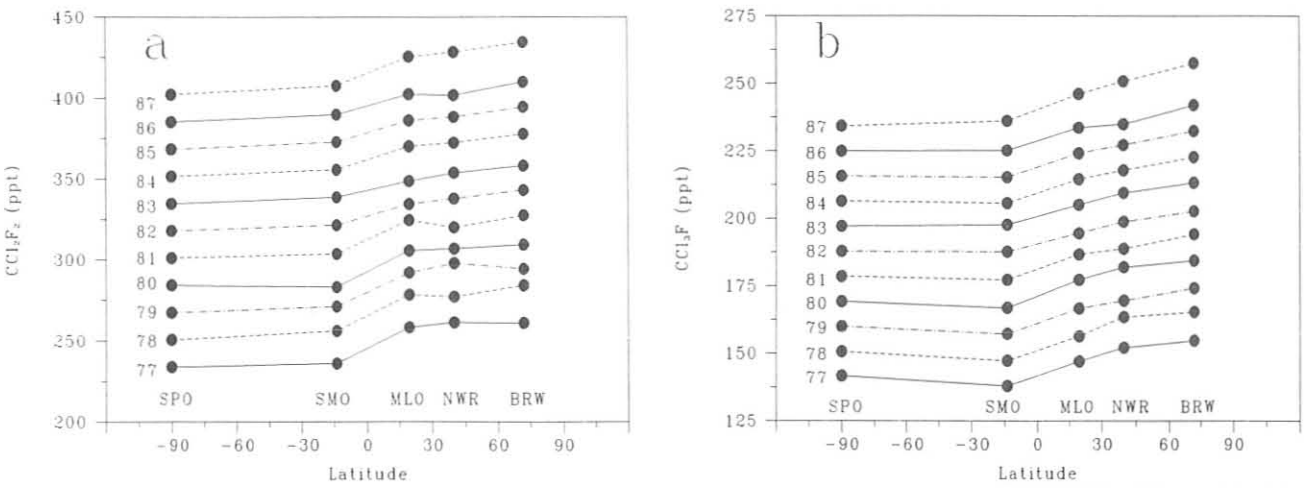

Fig. 8.2. Latitudinal dependence of yearly means for (a) CFC-12 and (b) CFC-11 concentrations at BRW, NWR, MLO, SMO, and SPO for 1977-1987. Yearly means for years 1977, 1984, and 1985 were calculated from the coefficients of the linear least-squares fit in Figure 8.1.

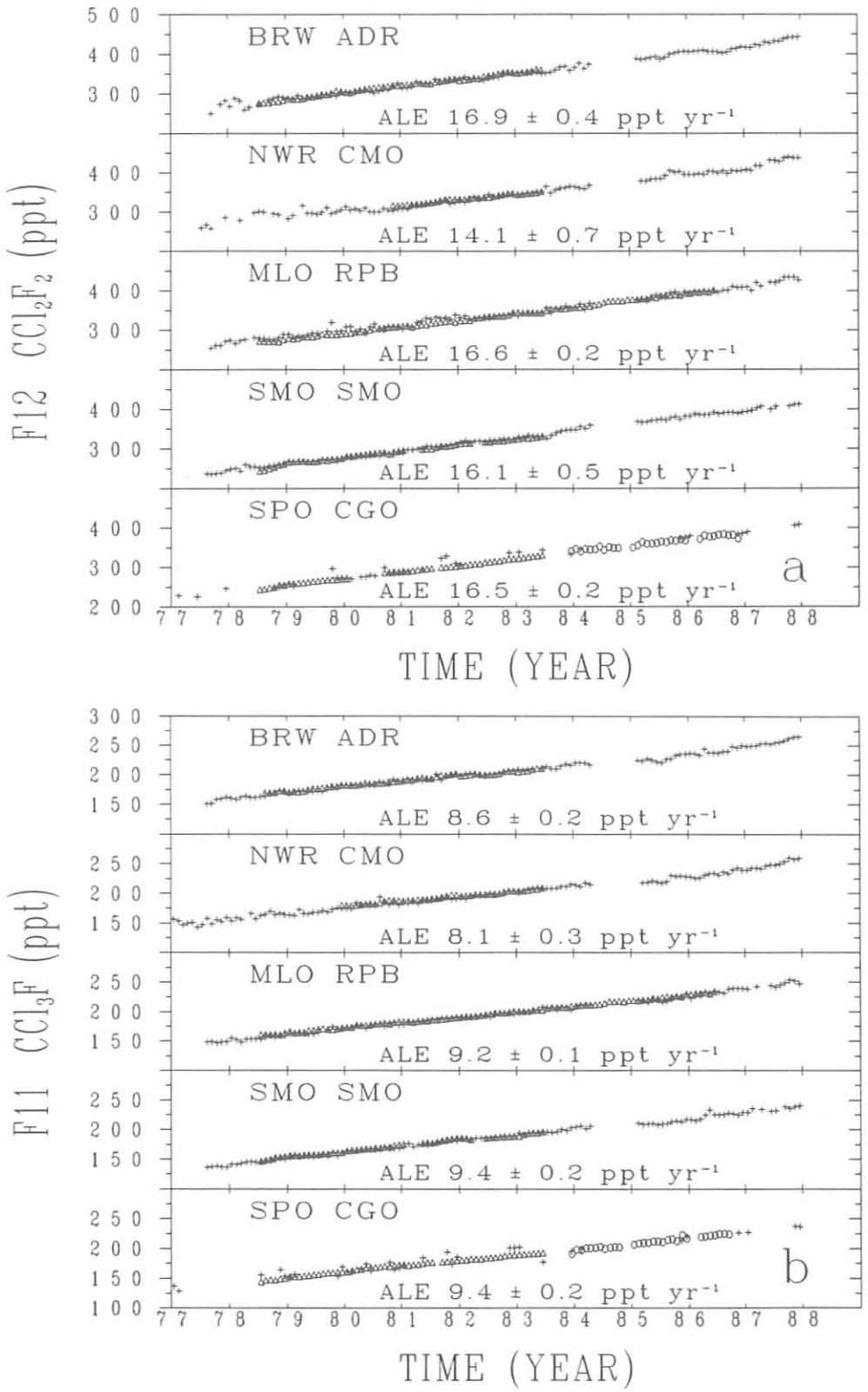

Fig. 8.3. Monthly mean concentrations for (a) CFC-12 and (b) CFC-11 from the NOAA/GMCC flask (+) and the ALE/GAGE (Δ) networks. The SPO plots also show monthly means (o) from the GMCC in situ GC. The ALE/GAGE data were from *Cunnold et al.* [1986], and some additional preliminary data for RPB were provided by P. Simmonds. The trends and ±2 s.d. errors are shown for the ALE/GAGE data.

to tank no. T3088 had the effect of reducing the concentration values of CFC-12 and CFC-11 in the last 3 years, yielding for CFC-12 and CFC-11 about a 1 and a 0.6 ppt yr^{-1} lower growth rate, respectively, than reported in *Schnell and Rosson* [1987].

Figure 8.3 shows monthly mean concentrations of CFC-12 and CFC-11 from the in situ GCs of the ALE/GAGE network, [*Cunnold et al.*, 1986] and the monthly means from GMCC's halocarbon flask network. Stations of comparable latitude from each network are plotted together. For example, CFC-11 and CFC-12 data from the RPB station of the ALE/GAGE network, which is partly supported by NOAA, at 13°N, 59°W in the North Atlantic Ocean is plotted with data from MLO. P. Simmonds from RPB has graciously provided further data, which are currently provisional and subject to change from mid-1985 to mid-1987. The comparison in growth rates for CFC-12 and CFC-11 between the two networks is very good at most locations, and excellent where the two networks share the same site at SMO.

The calibration scale used for GMCC's atmospheric N_2O measurements is the NBS SRM scale, prepared using gravimetric techniques [*Zielinski et al.*, 1986]. On average, this scale is 1 ppb lower than the gravimetric and dynamic dilution scale of *Komhyr et al.* [1988] and 1 ppb higher than the manometric scale of *Weiss et al.* [1981], and is acceptably within the experimental uncertainties of other techniques. The NBS N_2O scale is about 3 ppb lower than the Rasmussen scale currently used by the ALE/GAGE network.

8.1.2. RITS Continuous Gas Chromatograph Systems at GMCC Baseline Stations

The new RITS automated GC and data processing system was installed at MLO in June. This system joined others that were installed at SMO in June 1986 and at BRW in October 1986. Additions in 1987 to the systems included a separate backflush EC-GC for measuring N_2O without any interference from CO_2, a Supelco SP2100 column to separate CFC-113 from CFC-11, two calibration standards instead of one, and specially treated aluminum cylinders to enhance the stability of halocarbons in standards. The system consists of an HP model no. 5890 GC, a Shimadzu model no. GC-8AIE GC, two Nelson Analytical interfaces, an HP9816 computer, an HP9133 15-megabyte hard disk drive, and a printer. The system measures air concentrations of N_2O, CFC-12, CFC-11, CH_3CCl_3, and CCl_4 every 3 hours. Figure 8.4 shows a comparsion of flask samples with daily means from the in situ RITS GC for CFC-12 at BRW and SMO. The growth rate of CFC-12 in 1987 from BRW flask pairs appears to have increased from its average rate by about 8 ppt yr^{-1}, and this increase is also apparent from the in situ GC results at BRW. The reason for the increase is unknown and is being investigated for both real and experimental causes. Figure 8.5 shows results from the new back-flush N_2O GC at BRW and SMO. The N_2O concentration values from the flask pairs that include a correction for CO_2 and H_2O interference appear to be 1 to 2 ppb higher than those measurements from the in situ back flush GC's at the stations. This implies that our correction for the N_2O values from the flask pairs may need further refinement. Owing to regulator contamination problems, the data for CH_3CCl_3 and CCl_4 are very noisy. Changes will be made in 1988 to correct the contamination problems.

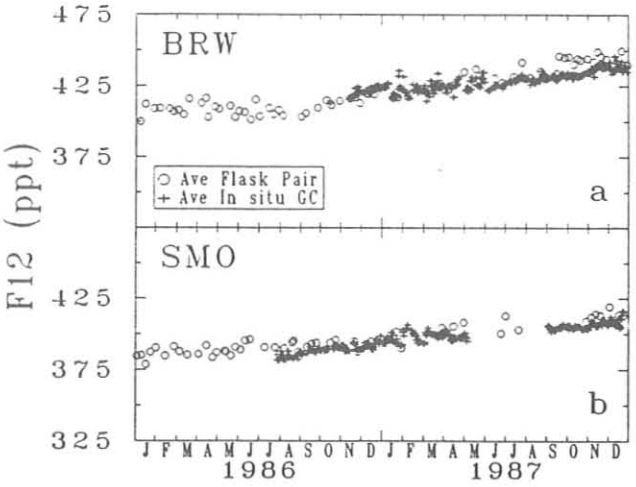

Fig. 8.4. CFC-12 concentrations from flask pair samples (o) and daily means from the in situ RITS GCs (+) versus time at (a) BRW and (b) SMO.

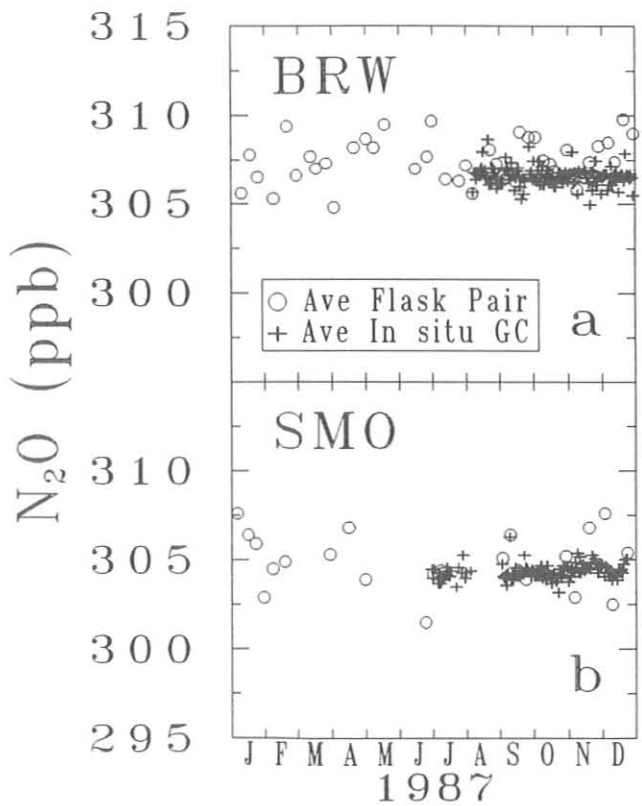

Fig. 8.5. N_2O concentrations from flask pair samples (o) and daily means from the in situ RITS GCs (+) (using Porapak Q in backflush mode) versus time at (a) BRW and (b) SMO.

8.1.3. Low Electron Attachment Potential Species

Considerable progress was made towards our goal in measuring the low electron attachment potential species (LEAPS). LEAPS are atmospheric gases which have a low response on an ECD either due to their low atmospheric concentration levels or their lack of sensitivity on the ECD. A literature review was completed on possible approaches for measuring the four gases: halons 1211 (CBrClF) and 1301 ($CBrF_3$), and halocarbons CFC-22 ($CHClF_2$) and CFC-113 (CCl_2F-$CClF_2$). Decisions were made by GMCC scientists concerning sample collection, concentration, and analysis, and the gas chromatograph and columns were chosen. The initial approach will involve preconcentrating samples onto tubes packed with adsorbent. The ultimate choice of collection temperature and adsorbent will depend on the results of ensuing tests. The tubes can then be brought to Boulder for analysis. The gases adsorbed to the tube packing will be thermally transferred to a cryogenic focusing trap, injected onto a wide-bore capillary column, and measured by temperature-programmed EC-GC. Pressurized Summa-treated stainless steel flasks also will be collected at baseline observatories and NWR, and shipped to Boulder for analysis by cryogenic focusing and capillary EC-GC.

It is planned to compare a number of columns, including the new PLOT columns, for their ability to separate these gases. These columns should be able to separate all of the gases without interference from oxygen. However, CFC-22 may require carrier-gas doping. If two columns are needed, the LEAPS GC is equipped with two independent channels for separate analyses. It also is apparent that it will be possible to obtain measurements of CFC-113 from the packed SP2100 columns on RITS station GCs. The problems that have been identified with the current CFC-113 analyses are contamination by the gas regulators and preparation of a long-lived standard. An investigation of possible solutions to these and other problems has begun, and it is anticipated that the first measurements of LEAPS gases will occur in 1988.

8.1.4. Gravimetric Standards

A gravimetric standards laboratory was completed at Boulder in 1987, and a CIRES research assistant was hired to prepare gravimetric standards. A custom Voland double-pan analytical balance, which is capable of weighing 10 kg cylinders (0.9 m tall by 0.3 m wide) to ±1 mg, was installed. For liquid phase halocarbons, like CFC-11, CFC-113, CH_3CCl_3, and CCl_4, a microbalance capable of weighing 4 g of a liquid in a glass tube to precisions of ±0.1 μg was also set up. Gravimetric standards of N_2O were compared against the OGC scale and the SIO scale, and the results were discussed at the end of section 8.1.1. Gravimetric standards of CFC-12 and CFC-11 were compared against the OGC scale. The results were in good agreement with the NOAA scales for CFC-12 and CFC-11 from gravimetric standards, and were found to be about 1 and 4% lower than the OGC scale, respectively. NOAA/GMCC will continue to report CFC-12 and CFC-11 values on the OGC scale until these small disagreements are resolved. Gravimetric standards for CH_3CCl_3, and CCl_4 were prepared, and the NOAA scale for these gases will be compared in the future to other international standards.

8.2. Special Projects

8.2.1. Soviet-American Gas and Aerosol Experiment

Objectives

The N_2O and Halocarbons group took the lead for GMCC's effort in SAGA II, a joint US/USSR research cruise that occurred from April to August 1987. This expedition involved the measurement of atmospheric and dissolved trace gases in and over the west Pacific and east Indian Oceans, and was conducted in conjunction with the Carbon Cycle group of GMCC, NOAA/PMEL, OGC, SIO, University of Washington, Washington State University, and University of Hawaii. The gases measured by GMCC were N_2O in the atmosphere, surface waters, and at depth, and CFC-11, CFC-12, CO_2, and CH_4 in the atmosphere and surface waters. Flask samples were also collected for subsequent analysis of CCl_4, CH_3CCl_3, CO_2, CH_4, and perhaps the LEAPS gases as well.

The cruise track is shown in Figure 8.6. GMCC scientists began the cruise at Hilo, Hawaii, sailed up to the Kamchatka Peninsula, down to Wellington, New Zealand, around Australia into the Indian Ocean, up to Singapore, and back to Hilo.

The objectives were (1) to test a highly precise technique for measuring N_2O under rigorous operating conditions, (2) to test a new, automated, headspace sampler for measuring dissolved N_2O, (3) to compare the latitudinal, atmospheric gradients with those indicated from our station sampling network, (4) to detect any sharp interhemispheric gradients of N_2O, CFC-11, CFC-12, CO_2, or CH_4 near the equator, (5) to evaluate the fluxes of these gases from the sea surface to the atmosphere along this transect,

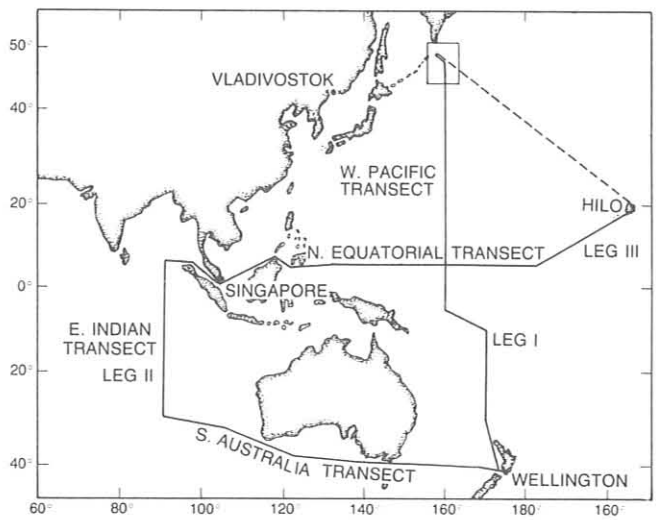

Fig. 8.6. Cruise track of the SAGA II experiment during April-July 1987 aboard the Soviet research vessel *Akademik Korolev*. The dashed line shows the shake-down leg.

(6) to observe any signals that may be associated with the recent ENSO event, and (7) to compare our atmospheric measurements with those from other shipboard investigators and from some of the ALE/GAGE network stations.

Results

More than 2000 measurements were made each for N_2O, CFC-11, and CFC-12 in the air and surface water and more than 600 measurements of N_2O at depth. The precision of the N_2O backflush technique, discussed by *Zielinski et al.* [1986], remained at less than ±0.2% for air samples; atmospheric CFC-12 and CFC-11 were measured with precisions of ±0.3% and ±0.5%. Relative error was less than ±1% for the equilibrated surface water and less than 2% for the automated headspace sampler. Substantial CO_2 and CH_4 data were obtained for most of the first leg, but the Weiss dual-catalyst FID GC never fully recovered from a breakdown near the equator.

Figure 8.7 shows the atmospheric, the surface water, and the difference between air and surface water concentrations for N_2O, CFC-12, and CFC-11 versus distance traveled. The average atmospheric N_2O concentration in the northern hemisphere was about 0.97 ppb higher than that for the southern hemisphere. This is essentially equivalent to results from our station network and very close to results reported by *Weiss* [1981]. Except for some apparently seasonal cooling effects in the middle-Southern latitudes, the surface waters were supersaturated with N_2O, with an overall mean of 2.5%. This is consistent with the concept of the ocean as a source of N_2O, but it is the lowest value reported to date. Although the area of coverage may have contributed in part to this lower value, the suppression of equatorial upwelling in the west Pacific in association with the 1987 ENSO event may have played a part as well. There may have been other ENSO effects, but they are more difficult to ascertain. The overall effect may have been significant, in that the mean surface concentration of N_2O did not differ significantly from that reported by *Weiss* [1978], in spite of an atmospheric increase of nearly 5 ppb during the past decade.

Although the equilibrator measurements of surface CFC-12 and CFC-11 required some filtering, owing to contamination by the ship, it is clear that seasonal warming and cooling predominated in determining surface saturations. The atmospheric profiles of CFC-12 and CFC-11 were virtually identical, underscoring their value as inert tracers. Small supersaturations (averaging between 4 and 6% above atmospheric levels) of CFC-12 and CFC-11 were found in the surface waters of the north Pacific ocean. On average, the oceans represent a small sink for the atmospheric CFCs; however, small supersaturations and undersaturations of dissolved CFCs can result due to the fact that the rate of thermal warming between the surface waters and the atmosphere is faster than the rate of gas exchange

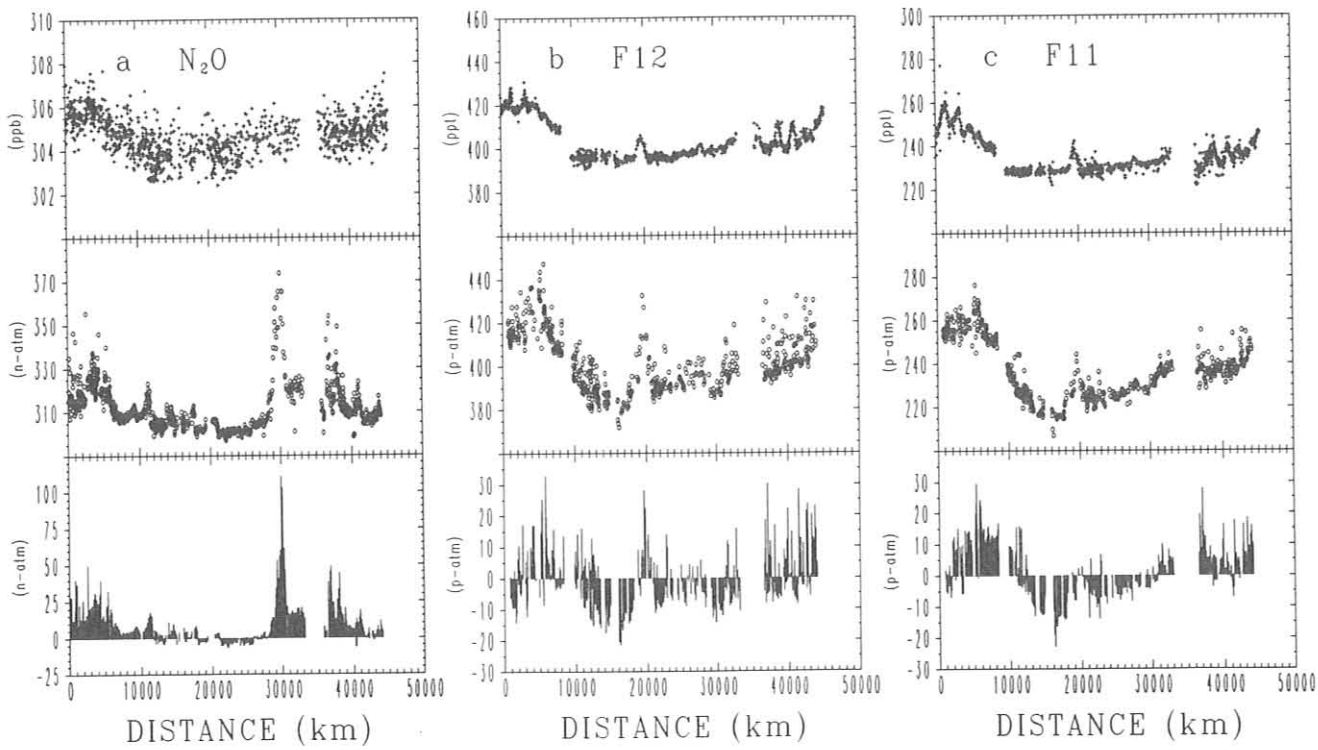

Fig. 8.7. Atmospheric concentrations (top panel), surface water concentrations (middle panel), and the saturation anomaly (bottom panel) for (a) N_2O, (b) CFC-12, and (c) CFC-11 versus distance traveled. The distance ranges for various sections were the following: Hilo to Kamchatka (0-4921 km), Leg I (4921-14770 km), Leg II (14785-33172 km), and Leg III (35706-45471 km).

between the atmosphere and surface waters. Along the west Pacific meridian, both gases decreased at a rate of 0.35 ppt deg^{-1} latitude in the northern hemisphere and remained virtually constant in the southern hemisphere. These gradients, as well as the absolute values shown in Figure 8.8, also corresponded well with results from the GMCC station network and measurements from other investigators. The CGO CFC-12 and CFC-11 provisional data were provided by P. Fraser of CSIRO, and the Khalil and Rasmussen CFC-12 and CFC-11 data were from the cooperative programs section 10.2 of this report.

As shown by others [*Yoshinari,* 1976; *Elkins et al.,* 1978], N_2O at depth from the SAGA II cruise correlated negatively with dissolved O_2 and positively with NO_3^-. Figure 8.9 shows dissolved N_2O and O_2, and NO_3^- concentrations over the Kuril Trench. The data from the headspace sampler were very consistent, giving us the most widespread data set of subsurface N_2O to date. The highest N_2O concentrations were in the intermediate waters of the northern hemisphere in both the west Pacific and east Indian Oceans. Waters bearing higher N_2O were found in the high northern latitudes, near the equator, and near other regions where surface currents diverge, including the ocean boundaries. Dissolved N_2O in waters of the southern hemisphere was much lower than that in the north, giving generally uneventful profiles. A strong temperature relation, similar to that discovered by *Elkins et al.* [1978], was found between the amount of dissolved N_2O produced (ΔN_2O) and the

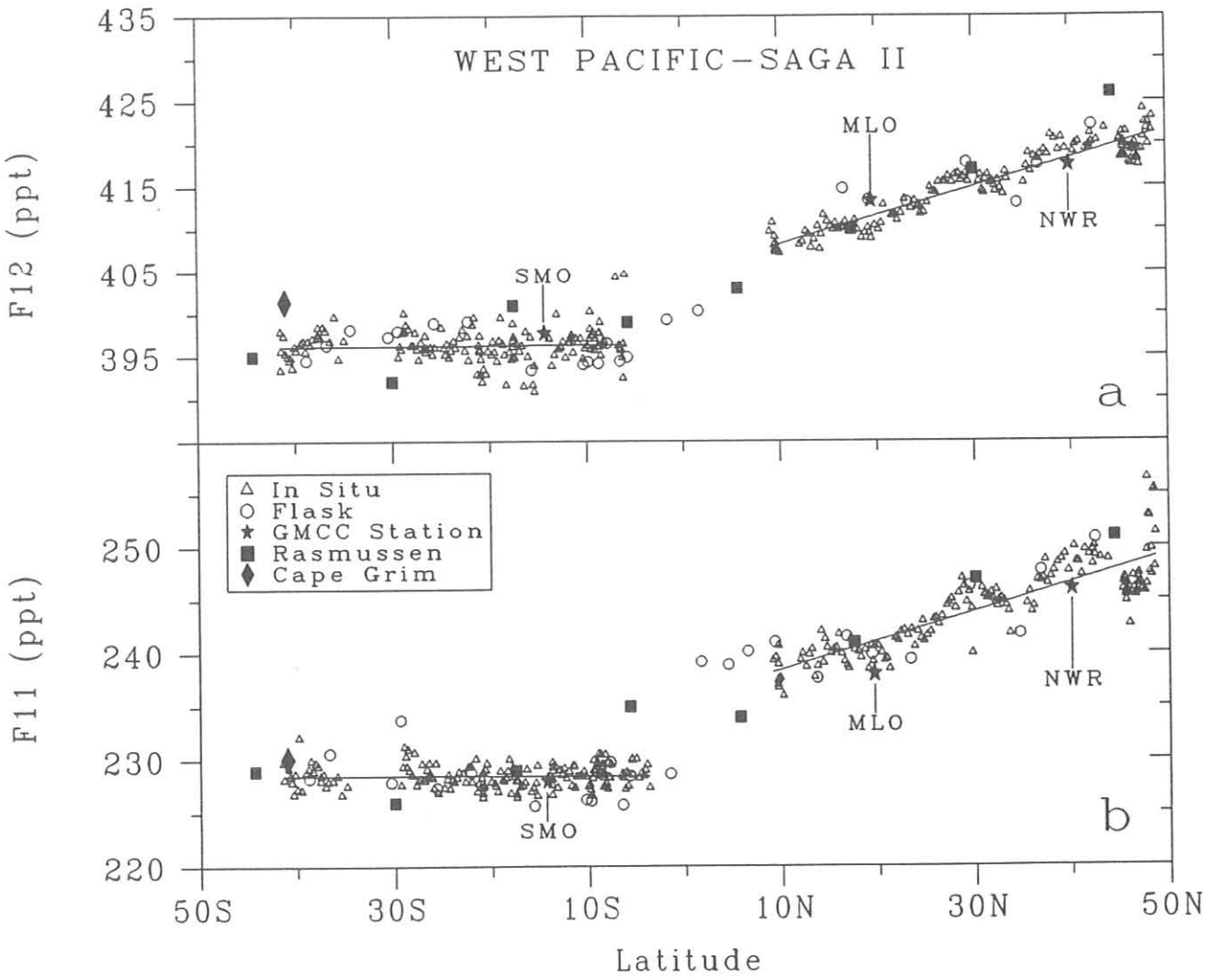

Fig. 8.8. Latitudinal dependence of (a) CFC-12 and (b) CFC-11 during Leg I of SAGA II from in situ GMCC GC (triangles) and GMCC flask analysis in Boulder (circles). Measurements are compared with SAGA II averages from the data presented in section 10.2 of this report (squares), GMCC stations (stars), and preliminary data from the CGO (diamonds) (P. Fraser, private communication).

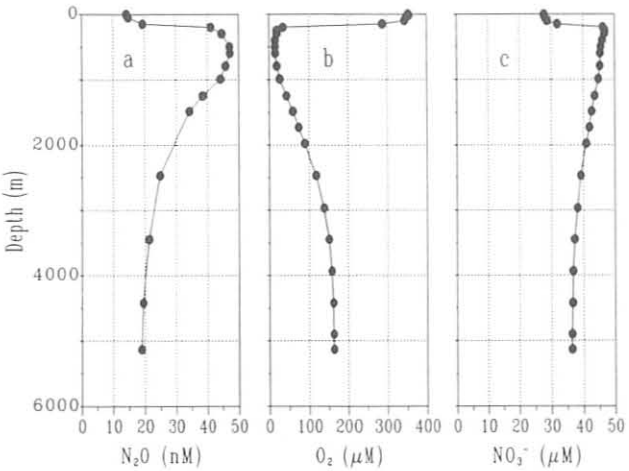

Fig. 8.9. Dissolved (a) N_2O and (b) O_2, and (c) NO_3^- concentrations versus depth over the Kuril Trench during the SAGA II experiment.

amount of dissolved oxygen consumed (AOU). It is apparent from these data that warmer water promotes a more rapid, subsurface production, which is consistent with laboratory studies of N_2O microbial production (Figure 8.10).

8.2.2. FT-IR Spectrometer Archive Project

A Nicolet FT-IR spectrometer was moved from NBS in Gaithersburg, Md., and installed in Boulder in RL-2. This instrument will be used to archive IR solar spectra for future analysis of compounds not currently analyzed by GMCC. Methods of analysis will be checked by comparing column densities determined by the FT-IR spectrometer against Dobson ozone measurements and other trace species measured by GMCC. The instrument was put to its first test on analyzing a flask sample for high levels of CO_2 from inside the second boat pit of Khufu's pyramid in Egypt (see section 4.2). Figure 8.11

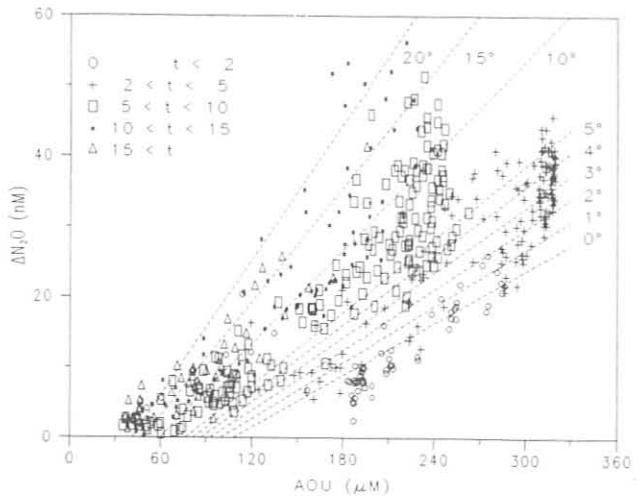

Fig. 8.10. ΔN_2O versus AOU (or dissolved oxygen consumed) as a function of temperature t for all SAGA II data for AOU > 35 µM. The equation, ΔN_2O = -13.3 + (0.124+0.0094t) AOU, was determined by a nonlinear, least-squares fit.

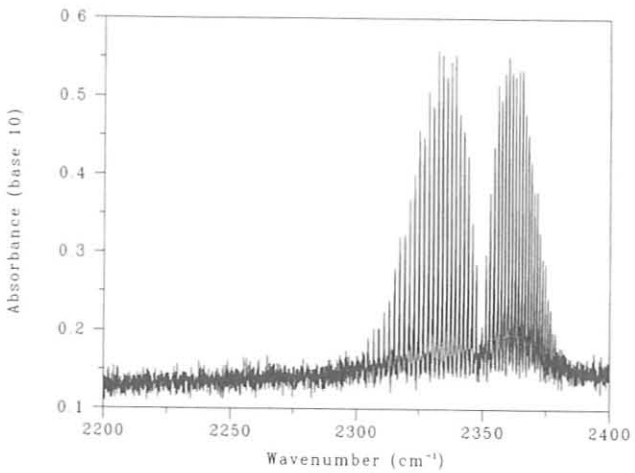

Fig. 8.11. FT-IR spectrum of the ν_3 band of CO_2 from a sample, SIS, that was taken in a tomb from Khufu's pyramid. The resolution of the FT-IR spectrometer was 0.06 cm^{-1} and the CO_2 concentration was measured at 745 ppm.

shows a spectrum of the ν_3 band of CO_2 in a 10-cm-long cell with KBr windows at 500-mm-Hg pressure. The measured concentration was 745 ppm compared with the Weiss dual-catalyst FID GC analysis of 750 ± 7 ppm (95% confidence level).

8.3. References

Cunnold, D.M., R.G. Prinn, R.A. Rasmussen, P.G. Simmonds, F.N. Alyea, C.A. Cardelino, A.J. Crawford, P.J. Fraser, and R.D. Rosen, Atmospheric lifetime and annual release estimates for $CFCl_3$ and CF_2Cl_2 from 5 years of ALE data, *J. Geophys. Res., 91(D10),* 10797-10817, 1986.

Elkins, J.W., S.C. Wofsy, M.B. McElroy, C.E. Kolb, and W.A. Kaplan, Aquatic sources and sinks for nitrous oxide, *Nature, 275,* 602-606, 1978.

Elkins, J.W., T.M. Thompson, B.D. Hall, K.B. Egan, and J.H. Butler, NOAA/GMCC halocarbons and nitrous oxide measurements at the South Pole, *Ant. J. U.S.,* submitted, 1988.

Komhyr, W.D., E.G. Dutton, and T.M. Thompson, A general gravimetric dilution technique for preparing trace calibration gases: N_2O calibration gas preparation, *Environ. Sci. Technol., 22,* 845-8488, 1988.

Rasmussen, R.A., and J.E. Lovelock, The Atmospheric Lifetime Experiment: 2, Calibration, *J. Geophys. Res., 88(C13),* 8369-8378, 1983.

Robinson, E., B.A. Bodhaine, W.D. Komhyr, S.J. Oltmans, L.P. Steele, P. Tans, and T.M. Thompson, Long-term air quality monitoring at the south pole by the NOAA program Geophysical Monitoring for Climatic Change, *Rev. Geophys., 26,* 63-80, 1988.

Schnell, R.C. and R.M. Rosson (Eds.), Geophysical Monitoring for Climatic Change, No. 15: Summary Report 1986, 155 pp., NOAA Air Resources Laboratory, Boulder, Colo., 1987.

Thompson, T.M., W.D. Komhyr, and E.G. Dutton, Chlorofluorocarbon-11, -12, and nitrous oxide measurements at the NOAA/GMCC baseline stations (16 September 1973 to 31 December 1979), *NOAA Tech. Rep. ERL 428-ARL 8,* 124 pp., NOAA Air Resources Laboratory, Boulder, Colo., 1985.

Weiss, R.F., Nitrous oxide in the surface water and marine atmosphere of the North Atlantic and Indian Oceans, *EOS, 59,* 1101, 1978.

Weiss, R.F., Surface water and atmospheric trace gas measurements during the NORPAX Hawaii-Tahiti shuttle experiment, *EOS, 62,* 894, 1981.

Weiss, R.F., C.D. Keeling, and H. Craig, The determination of tropospheric nitrous oxide, *J. Geophys. Res., 86(C8)*, 7197-7202, 1981.

Yoshinari, T., Nitrous oxide in the sea, *Marine Chem., 4*, 189-202, 1976.

Zielinski, W.L., E.E. Hughes, I.L. Barnes, J.W. Elkins, and H.L. Rook, High accuracy standards and reference methodology for carbon dioxide in air, *DOE Tech. Rep., TR033*, 74 pp., Department of Energy, Washington, D.C., 1986.

9. Director's Office

9.1. Alkaline Aerosols Program: Dust Emissions Modeling

9.1.1. Introduction

A model for the estimation of total dust production for the United States was discussed by *Gillette and Passi* [1988]. Its primary use was in constructing an inventory of alkaline elements for acid/base balance studies of atmospheric precipitation by the NAPAP. It has also been used for present estimates of soil aerosol generated by the wind and having the possibility of interacting with acids in the atmosphere.

9.1.2. Basis of the Dust Production Model

The model is a summation of the expected dust production caused by wind erosion for individual sampling units of the soil and land use inventory of the NRI compiled by the USDA. The model is based on a dust emission function derived theoretically and verified by experiment. Its form is

$$E = C \sum_{i=1}^{N} R_i\, g(L_i) A_i\, \Delta T \int_{U_{ti}}^{\infty} G(U)\, p_i(U) dU \qquad (1)$$

where E is the mass of dust emitted in the time period ΔT; C is a constant to be determined by calibration; i is the index of summation over N different erodible areas within the region of interest; R_i is effect of soil roughness; $g(L_i)$ is the effect of field length, L_i; A_i is the area of the land being considered; $G(U)$ is the vertical mass flux of dust (mass per unit area per time) as a function of wind speed, U; $p_i(U)$ is the probability density function of the wind speed during the time period of interest; and U_{ti} is the ith threshold wind speed for dust emission.

Owen's theory of suspension of dust that predicted that flux of dust should follow the fourth power of friction velocity was used (P.R. Owen, personal communication, 1987). $G(U)$ is integrated for all wind speeds above threshold, U_t, for each subarea of the region of interest; N such subareas are added together to obtain the total dust flux. The effects of live and dead vegetative protection of the surface, roughness of the soil, and soil moisture are largely built into the threshold wind speed. Experimentation has supplied values of this parameter for the calculation [*Gillette et al.*, 1980, 1982; *Gillette*, 1988]. The integral is multiplied by a function of field length, $g(L_i)$, that was set to unity in this evaluation; by a function of the roughness of an individual soil, R_i; by time duration ΔT; and by area of a given soil, A_i. The time ΔT for each integration for which the soil parameters are assumed to remain constant is 1 month.

Wind data used in the model were obtained from the WERIS for the years 1948-1978 [*Barchett*, 1982]. WERIS provided information on hourly mean winds by the month for 1432 locations in the United States. Precipitation data were obtained from the National Climatic Data Center. We used the USDA 1982 NRI [*Committee on Conservation Needs and Opportunities*, 1986] for soil information, land use, and wind erosion parameters including the roughness function, R_i. We organized our assignment of threshold parameters to the structure of the NRI data set. This data set contained over 350,000 individual point sampling units containing 841,860 records to give a detailed inventory of the land of the United States. Wind erosion data were obtained for point sampling units judged to have wind erosion potential. These supplementary wind erosion data consisted of 259,628 records.

Equation (1) was integrated using the method described by *Gillette and Passi* [1988]. Dust emission estimates were made for each MLRA, for each month of the 31-yr data set for winds.

9.1.3. Calibration of the Model

To evaluate C of Equation (1) for a scale appropriate to a national inventory, a large-scale area was chosen that could be effectively isolated and that had wind erosion data sufficient for our needs. This area is 1.25×10^5 km^2 (1.56% the area of the 48 contiguous United States). It constitutes MLRA 77 and 78 in the 1982 NRI data set and roughly includes the "panhandles" of Texas and Oklahoma and some bordering areas. The dust emission data used to calibrate the model were obtained from *Gillette et al.* [1978]. The data were total dust production estimates derived from dust concentrations measured in each dust cloud at several altitudes and locations multiplied by the volume of the dust cloud estimated from aircraft observations, meteorological charts, and ground-based observations. All of the major dust-producing events in the month of April for 1972, 1973, and 1975 were used for the calibration. Areas from which the dust originated were derived from data obtained from the USDA which compiled information on the dates of individual dust storms, area of erosion, and duration of erosion for eroding soils in a study area including Texas, New Mexico, and the Great Plains states.

9.1.4. Results of the Model

Plots of median dust flux values, 90th percentile flux, and 10th percentile flux are shown in Figures 9.1-9.3. The median flux in Figure 9.1 shows maxima in the dust bowl region, in the Red River Valley of North Dakota, and along the Montana-Canadian border. Maxima are much larger on the 90th percentile map in Figure 9.2, and the area of dust production is also larger although centered at about the same areas as on the median map. The features of the 10th percentile dust flux map in Figure 9.3 show much reduced dust fluxes; only small amounts of the most productive areas are still active, and much of the country has zero dust flux. Total dust fluxes for the median, 90th percentile, and 10th percentile maps are 3.8 million, 628 million, and 0.6 million t yr^{-1}.

The patterns of number of days for observed blowing dust shown in Figure 9.4 [after *Orgill and Sehmel*, 1972] shows agreement with the broad features of Figure 9.3 in the Great Plains, and Southern Plains area and the Red River Valley.

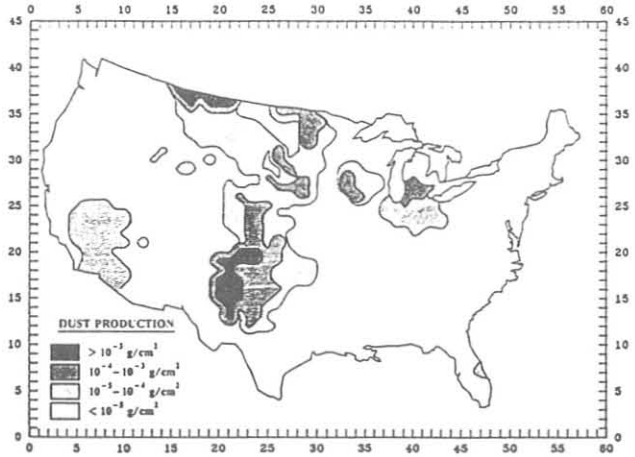

Fig. 9.1. Median flux of dust emission (g cm^{-2} yr^{-1}) for model runs.

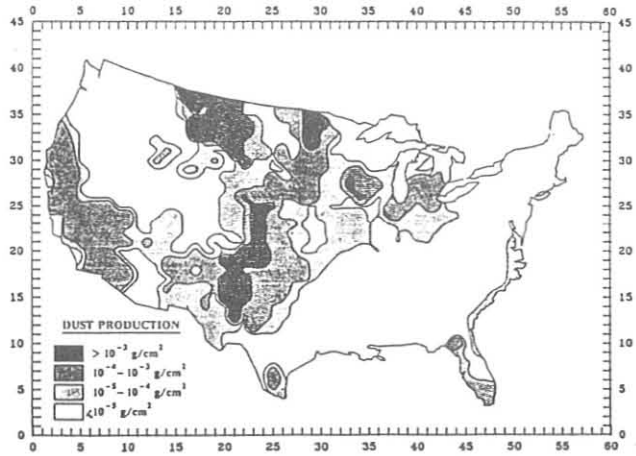

Fig. 9.2. The 90th percentile flux of dust emission (g cm^{-2} yr^{-1}) for model runs.

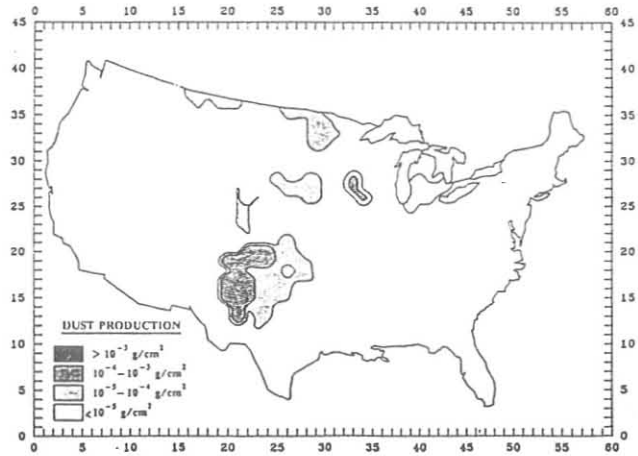

Fig. 9.3. The 10th percentile flux of dust emission (g cm^{-2} yr^{-1}) for model runs.

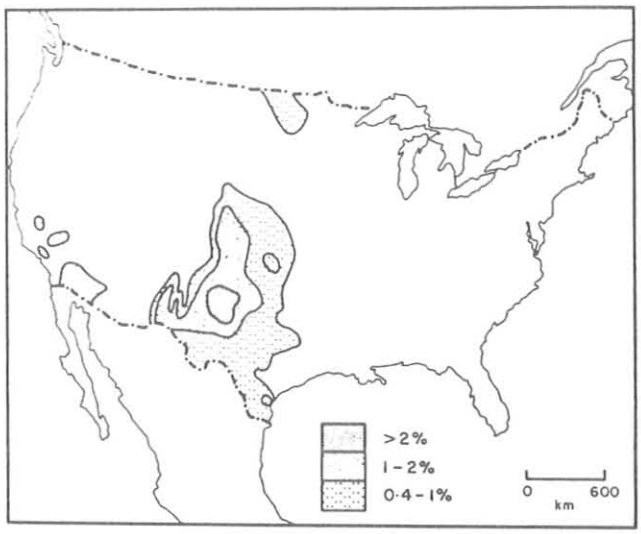

Fig. 9.4. Annual frequency of dust hours with visibility less than 11 km in the United States [from *Orgill and Sehmel*, 1976].

9.1.5. Conclusions

Areas of maximum dust production are in the panhandles of Texas and Oklahoma, and Nebraska, western Kansas, eastern Colorado, the Red River Valley of North Dakota, and northern Montana. Areas of minimal dust production are the southeastern United States, New England, and forested and mountainous areas.

9.2. Arctic Gas and Aerosol Sampling Program: Springtime Tropospheric Ozone Destruction in the High Arctic

9.2.1. Introduction

In the AGASP-I and AGASP-II flights in 1983 and 1986, ozone concentrations often showed a steep decline with decreasing altitude, beginning immediately beneath the top of the surface temperature inversion, to essentially zero values near the surface [*Raatz et al.*, 1985b; *Herbert et al.*, 1988; *Bridgman et al.*, 1988]. *Oltmans* [1981] noted that in the surface ozone record at BRW, ozone concentrations near zero may persist for periods of days during the spring in contrast to the remainder of the year when low ozone values are not observed.

Barrie et al. [1988a] presented strong evidence, based upon ozone and other chemical species measurements at Alert, NWT (82°N), that the springtime depletion of ozone is the result of photolytic reaction between ozone and gaseous bromine to form filterable bromine. Filterable bromine was defined by *Barrie et al.* [1988a] as the sum of particulate Br and gaseous HBr collected on filters. This sequence begins at polar sunrise and diminishes as summer approaches. At the end of the spring, both the precursor gaseous bromine reactants are depleted and the capping temperature inversion decreases in strength allowing enhanced downward mixing of ozone from above *Barrie et al.* [1988a].

9.2.2. Vertical Extent of the Ozone Depletion

The Arctic is often under the influence of strong temperature inversions that create stable conditions near the surface with little mixing of this layer with air from above the boundary layer [*Raatz et al.*, 1985a]. NOAA WP-3D aircraft profiles of springtime ozone concentrations above and upwind of BRW, over the deep Arctic ice pack, and over the ice upwind of the Alert Baseline Station [*Bridgman et al.*, 1988; *Herbert et al.*, 1988], show that the greatest ozone depletion is restricted to the atmosphere beneath the top of the surface temperature inversion. An ozone and temperature profile for a flight north of Alert at 82.5°N on April 14, 1986, is shown in Figure 9.5. In this figure, the gradient of ozone (1-min running mean) across the temperature inversion is essentially a step function. On 15 of 16 AGASP flights over ice in the Arctic in 1983 and 1986, ozone depletion was observed beneath the top of the surface temperature inversion. On the one remaining flight, strong southerly downslope flow from the Brooks Range, past BRW, out over the ice is thought to have mixed air of higher ozone content down to the surface.

9.2.3. Seasonal Pattern of Solar Insolation and Ozone Concentrations at BRW

During spring, solar insolation reaching the surface in the Arctic increases dramatically. This increase is shown in Figure 9.6B where the daily sum of the total global flux at BRW is plotted in relation to the BRW ozone record (Figure 9.6A). Beginning early in March, the solar flux begins a rapid rise, March and April being months with a high number of days with relatively clear skies. Although the radiative input continues to climb through May, there is a significant increase in cloudiness. This is indicated by the median falling well below the upper envelope that could be drawn through the 95 percentile values. As the period of 24-h daylight approaches (mid-May), cloudiness increases. The end of the period of near-zero surface ozone concentrations (Figure 9.6A) also coincides with the beginning of total daylight. By late May, the ground is no longer continuously covered with snow at BRW and the thermal stability in the near-surface air layer is much reduced.

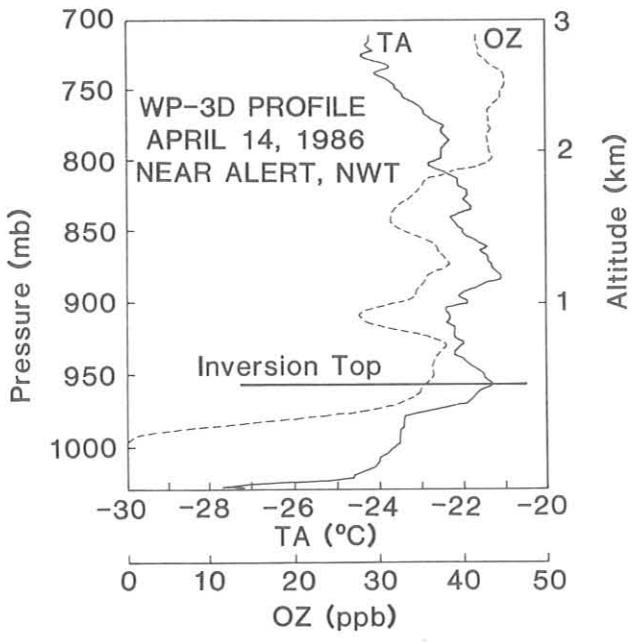

Fig. 9.5. An ozone (*OZ*) and air temperature (*TA*) profile showing ozone depletion below the top of the temperature inversion observed by the NOAA WP-3D aircraft north of Alert, NWT, April 14, 1986.

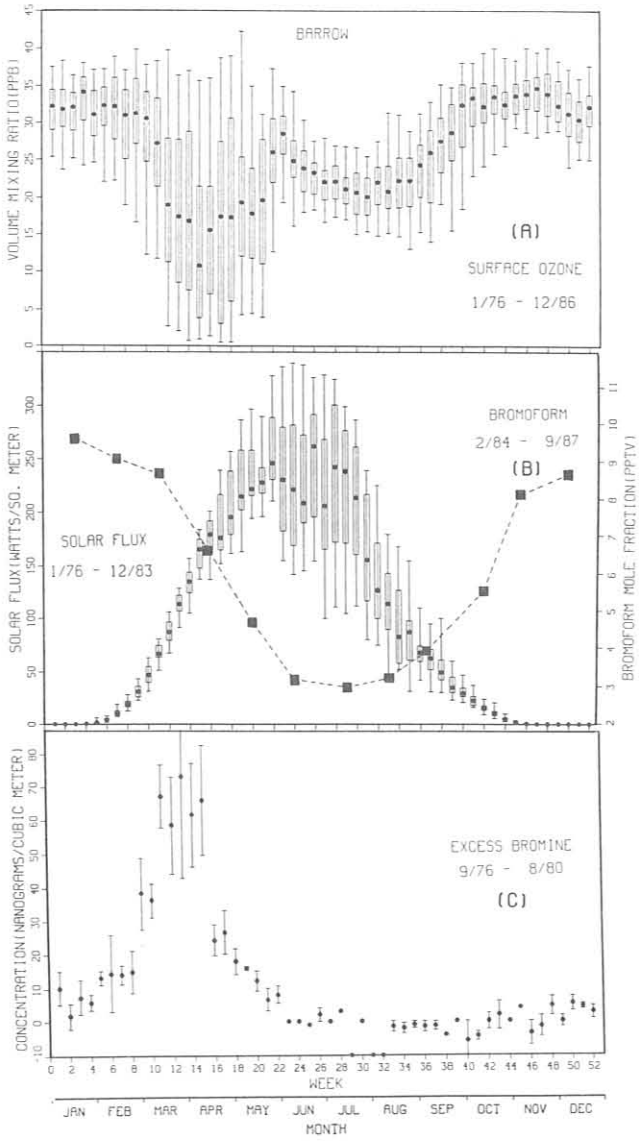

Fig. 9.6. (A) The seasonal ozone variation at BRW for 1976-1986. The medians (dots), the upper and lower quartiles (ends of the boxes), and upper and lower fifth percentiles (ends of lines) are shown. (B) Total global flux of solar radiation at BRW for 1976-1983 (as in A) and mean monthly bromoform mole fraction for 1984-1987 (squares) [*Cicerone et al.*, 1988]. (C) Weekly means and standard deviations of the excess filterable bromine at BRW for 1976-1980 [*Berg et al.*, 1983].

9.2.4. Ozone Destruction and Filterable Bromine Formation

Barrie et al. [1988b] showed that, at Alert during April, ozone concentrations were anticorrelated at 0.95 confidence level ($p < 0.05$) with the concentration of bromine sampled daily by filters. They attributed the ozone concentration minima to destruction by photochemical reactions of ozone with bromine-rich gases (mainly bromoform) to produce aerosol bromine collected on the filter. These reactions began at, and immediately following, polar sunrise at Alert and continued until about the beginning of the 24-h-daylight period.

Extensive filterable bromine measurements by *Berg et al.* [1983] at BRW during 1976-1980 (summarized in Figure 9.6C) indicate that during springtime, there also are extremely high values of filterable bromine relative to other times of the year. Since the sampling periods were 3-7 days, they do not facilitate correlation with the sharp day-to-day fluctuations observed in the surface ozone data. The filterable bromine record (Figure 9.6C) exhibits a gradual increase in February, but dramatic increases do not take place until March. This is consistent with the surface ozone data that also begin seasonal plunges to nearly zero concentrations in March. By mid-May filterable bromine has declined to lower values, and the sharp drops in ozone have essentially ended. The transport of ozone from above down into the boundary layer proceeds more freely by mid-May as the frequency and strength of the inversions are reduced. Any bromine (being converted to filterable form) would probably be more thoroughly mixed into the lower troposphere at this time. A marine source of bromine gases in the atmosphere might also be weaker in this season, although this has not been proved.

That the appearance of sunlight in the spring is an important factor in the large seasonal plateau in filterable bromine concentrations is suggested by the data of *Berg et al.* [1983], and *Sturges and Barrie* [1988]. These data, obtained at four locations in the Arctic (Igloolik at 69.5°N, BRW at 70.5°N, Mould Bay at 76°N, and Alert at 82°N), cover about a 12° range in latitude. It should thus be possible to distinguish a difference in the seasonal cycle of filterable bromine, particularly an earlier appearance in the springtime rise in concentrations at the lower latitudes. That this is indeed the case can be seen from Figure 9.7, which shows the monthly variation of the mean concentration of excess bromine at Igloolik and Alert, the two stations most widely separated in latitude. This average is based on 4-6 years of data depending on the location. Individual samples were collected weekly. It is clear that at the more southerly site (Igloolik) the seasonal increase begins sooner than at the more northerly site (Alert). The other two sites (BRW and Mould Bay) fall between these two in time of spring rise. The rate of falloff from the peak does not display this same latitudinal dependence.

9.2.5. Vertical and Areal Distribution of Filterable Bromine in the Arctic

Figure 9.8 shows the amount of excess filterable bromine (Br_{xs}) in the aerosol for all nonstratospheric filter samples collected during AGASP-I and AGASP-II aircraft flights

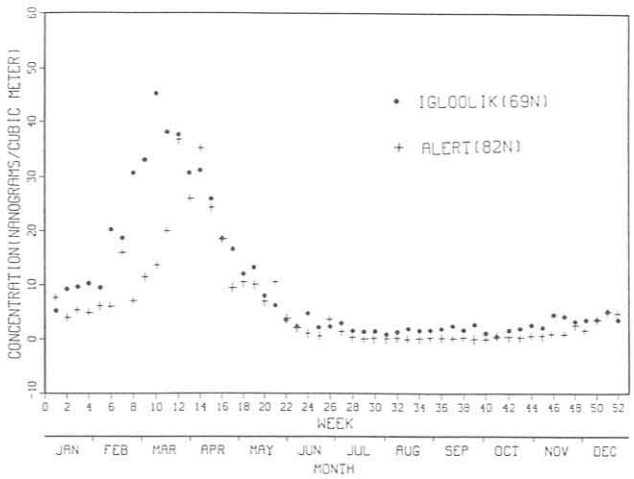

Fig. 9.7. Weekly means of the excess filterable bromine at Igloolik and Alert, 1979-1984 [*Sturges and Barrie,* 1988].

covering the Arctic from Alaska to Greenland to Norway. Elemental analyses of the 1983 AGASP filter data are published eleswhere [*Sheridan,* 1986; *Sheridan and Zoller,* 1988]. Samples were classified as containing significant marine aerosol contributions (*M*), when collected at low altitude over open ocean, or as having been collected over the pack ice in tropospheric air (*T*) at least 200 km from open ocean. Samples were plotted according to the weighted mean ambient pressure during sample collection as an approximate measure of altitude. Since we wanted to emphasize findings from aerosol collected within the surface inversion over the ice, we included pressure ranges for the *T* samples to show the vertical extent of sampling. For *T* samples where no pressure range is shown, the limits lie within the sample symbol. Pressure ranges for *M* samples were not included, since none of these samples contained appreciable Br_{xs}.

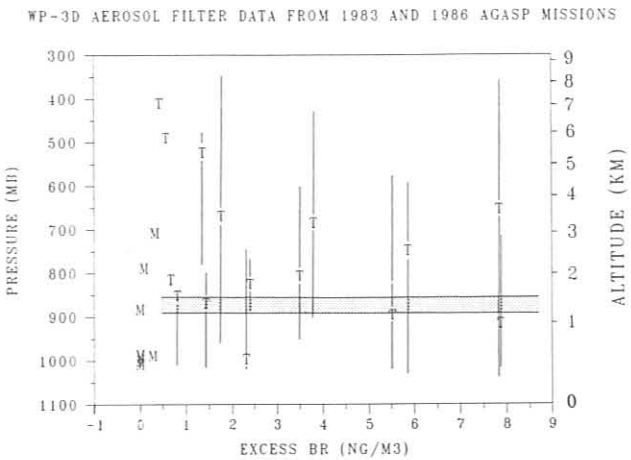

Fig. 9.8. Excess filterable bromine in the Arctic from AGASP aircraft samples. *M* = over ocean, marine sample ; *T* = over ice, tropospheric sample. The *M* and *T* symbols are plotted at the weighted mean ambient pressure of the sample, and the vertical bars indicate the sampling altitude range. The shaded section indicates the mean position of the temperature inversion over ice, observed in Arctic springs 1983 and 1986.

T samples collected wholly in the free troposphere generally show intermediate Br_{xs} concentrations (~0.5-2 ng m^{-3}). The remaining *T* samples in Figure 9.8 had significant aerosol contributions from below the temperature inversion layer. Most had sampling time near the surface at pressures >1000 mb. These samples contained elevated Br_{xs} concentrations. Three of the four largest Br_{xs} *T* samples were collected over pack ice north of Alert.

9.2.6. Discussion and Concluding Remarks

The work of *Barrie et al.* [1988a] suggests that bromine is important in the distribution of ozone near the surface at Alert in April. Our examination of the seasonal variation in ozone near the surface at several high Arctic stations suggests that both meteorology and photochemistry have significant roles in explaining the Arctic ozone-bromine cycle. The average behavior of atmospheric bromoform along with the ozone, solar radiation, and filterable bromine from BRW are shown together in Figure 9.6 to emphaze the regular timing of the seasonal patterns in these quantities.

To date, there has been little published concerning the causes of the high concentrations of filterable excess bromine. The excess bromine observed is much higher than can be explained by contributions from bulk seawater and leaded gasoline, although other air pollution sources cannot be ruled out. It is widely known though that many marine organisms, among them red benthic algae, contain high levels of brominated compounds, including bromoform [*Faulkner*, 1980]. A red algae source of bromoform in the Arctic was suggested by *Dyrssen and Fogelqvist* [1981], who measured bromoform levels in surface seawater north of Svalbard. This source has been endorsed by other researchers as a major contributor of atmospheric gaseous bromine to the Arctic [e.g., *Berg et al.*, 1983, 1984].

The character of the seasonal cycle in both ozone and filterable bromine at a number of locations in the Arctic suggests an important role for the appearance of sunlight in initiating the chain of events that leads to a drastic depletion of ozone in the boundary layer during the spring. The fact that the ozone loss is a springtime rather than an equinoctial event is compatible with the proposed interaction with bromoform and the consequent appearance of filterable bromine. In the autumn as the sunlight declines there is little bromoform present [*Cicerone et al.*, 1988] and the concentrations do not begin to build up again until after the autumnal equinox when there is a rapid rise to the wintertime values.

The role of nitrogen oxides and other forms of nitrogen in the determination of the seasonal variations in the surface ozone in the high Arctic has not been included here. Limited measurements of these species are available for some Arctic locations [*Barrie et al.*, 1988b; *Logan*, 1983, 1985]. Seasonal measurements of the nitrogen compounds are not available at Barrow. Because of the generally low levels of the nitrogen oxides as well as the lack of wintertime sunlight, *Levy et al.* [1985] found a tendency for only limited ozone production at high latitudes. A final determination of the role of photochemically produced ozone in the high Arctic, however, awaits the routine knowledge of the behavior of these nitrogen compounds as well as an understanding of the details of bromine chemistry. A much better knowledge of the possible ocean sources and the processes that produce the organic bromine gases is also required.

9.3. References

Barchett, W.R., Wind energy resource information system: system operation, Technical Memorandum prepared for the U.S. Department of Energy under Contract DE-AC06-76RLO 1830, Battelle Pacific Northwest Laboratory, Richland, Wash., 1982.

Barrie, L.A., J.W. Bottenheim, R.C. Schenll, P.J. Crutzen, and R.A. Rasmussen, Ozone destruction and photochemical reactions at polar sunrise in the lower Arctic atmosphere, *Nature, 334*, 137-141, 1988a.

Barrie, L.A., G. den Hortog, J.W. Bottenheim, and S. Lansberger, Anthropogenic aerosols and gases in the lower troposphere at Alert, Canada in April, *J. Atmos. Chem.*, in press, 1988b.

Berg, W.W., P.D. Sperry, K.A. Rahn, and E.S. Gladney, Atmospheric bromine in the Arctic, *J. Geophys. Res., 88*, 6719-6736, 1983.

Berg, W.W., L.E. Heidt, W. Pollock, P.D. Sperry, and R.J. Cicerone, Brominated organic species in the Arctic atmosphere, *Geophys. Res. Lett., 11*, 429-432, 1984.

Bridgman, H.A., R.C. Schnell, G.A. Herbert, B.A. Bodhaine, and S.J. Oltmans, Meteorology and haze during AGASP-II, Part 2: Canadian Arctic flights 13-16 April 1986, *J. Atmos. Chem.*, in press, 1988.

Cicerone, R.J., L.E. Heidt, and W.H. Pollack, Measurements of atmospheric methyl bromide and bromoform, *J. Geophys. Res., 93*, 3745-3749, 1988.

Committee on Conservation Needs and Opportunities (M. Gordon Wolman, Chairman), *Soil Conservation: Assessing the National Resources Inventory, Vol 1*. 112 pp., National Academy Press, Washington, DC, 1986.

Dyrssen, D., and E. Fogelqvist, Bromoform concentrations of the Arctic ocean in the Svalbard area, *Oceanol. Acta, 4*, 313-317, 1981.

Faulkner, D.J., *Handbook of Environmental Chemistry*, Vol. I, Springer-Verlag, Berlin, 1980.

Gillette, D., Threshold friction velocities for dust production for agricultural soils, *J. Geophys. Res., 93*, 12,645-12,662, 1988.

Gillette, D. and R. Passi, 1988, Modeling dust emission caused by wind erosion, *J. Geophys. Res., 93*, 14,233-14,242, 1988.

Gillette, D., Clayton, R.N., Mayeda, T.K., Jackson, M.L., and K. Sridhar, Tropospheric aerosols from some major dust storms of the southwestern United States, *J. Geophys. Res. 87*, 9003-9015, 1978.

Gillette, D.A., J. Adams, A. Endo, and D. Smith, Threshold velocities for input of soil particles into the air by desert soils, *J. Geophys. Res., 85(C10)*, 5621-5630, 1980.

Gillette, D.A., J. Adams, D. Muhs, and R. Kihl, Threshold friction velocities and rupture moduli for crusted desert soils for the input of soil particles into the air, *J. Geophys. Res. 87*, 9003-9015, 1982.

Herbert, G.A., R.C. Schnell, H.A. Bridgman, B.A. Bodhaine, and S.J. Oltmans, Meteorology and haze structure during AGASP-II, Part 1: Alaskan Arctic flights, 2-10 April 1986, *J. Atmos. Chem*, in press, 1988.

Levy H., J.D. Mahlman, W.J. Moxim, and S.C. Lim, Tropospheric ozone: The role of transport, *J. Geophys. Res., 90*, 3753-3772, 1985.

Logan, J.A., Nitrogen oxides in the troposphere: Global and regional budgets, *J. Geophys. Res., 88*, 10,785-10,807, 1983.

Logan, J.A., Tropospheric ozone: Seasonal behavior, trends and anthropogenic influence, *J. Geophys. Res., 90*, 10,463-10,482, 1985.

Oltmans, S.J., Surface ozone measurements in clean air, *J. Geophys. Res., 86*, 1174-1180, 1981.

Orgill, M., and G. Sehmel, Frequency and diurnal variation of dust storms in the continental United States, *Atmos. Environ., 10*, 813-8252, 1976.

Raatz, W.E., R.C Schnell, B.A. Bodhaine, S.J. Oltmans, and R.H. Gammon, Air mass characteristics in the vicinity of Barrow, Alaska, 9-19 March 1983, *Atmos. Environ., 19*, 2127-2134, 1985a.

Raatz, W.E., R.C. Schnell, M.A. Shapiro, S.J. Oltmans, and B.A. Bodhaine, Intrusions of stratospheric air into Alaska's troposphere, March 1983, *Atmos. Environ., 19*, 2153-2158, 1985b.

Sheridan, P.J., The use of analytical electron microscopy for the individual particle analysis of the Arctic haze aerosol, Ph.D. dissertation, 281 pp., University of Maryland, College Park, 1986.

Sheridan, P.J., and W. H. Zoller, Elemental composition of particulate material sampled from the Arctic haze aerosol, *J. Atmos. Chem.*, in press, 1988.

Sturges, W.T., and L.A. Barrie, Chlorine, bromine and iodine in Arctic aerosols, *Atmos. Environ., 22*, 1179-1194, 1988.

10. Cooperative Programs

Aerosol Black Carbon Measurements at the South Pole: Initial Results, 1986-1987

A.D.A. HANSEN

Lawrence Berkely Laboratory, Berkely, California 94720

B.A. BODHAINE AND E.G. DUTTON

NOAA/GMCC, 325 Broadway, Boulder, Colorado 80302

R.C. SCHNELL

University of Colorado, CIRES, Boulder, Colorado 80306

1. INTRODUCTION

The combustion of carbonaceous fuels results in the discharge to the atmosphere of both the major species, carbon dioxide and water vapor, and of minor or trace effluents. One of these trace effluents is graphitic or "black" carbon emitted as submicrometer aerosol particles. This material is a good tracer for combustion emissions, and may have a long lifetime in the atmosphere. It has been found in all studies in urban and regional locations as well as in the Arctic haze and in remote oceanic locations. Its detection in the Arctic implies transport paths exceeding 8000 km [*Bridgman et al.*, 1988].

Aerosol black carbon is a tracer for combustion emissions as well as a species of chemical and physical consequence in its own right. It has a large optical absorption cross section, it may act as a condensation nucleus, and its surface may act as a site for the destruction of ozone [*Stephens et al.*, 1986]. Its widespread distribution in the troposphere may lead to its eventual presence in the stratosphere [*Chuan and Woods*, 1984].

Graphitic carbon has been measured in the Antarctic snowpack in the vicinity of SPO [*Warren*, 1988], clearly indicating the effects of local sources on the areas downwind of the station. In December 1986 an aethalometer was installed at SPO to measure concentrations of aerosol black carbon with a time resolution of 1 hour. We present data covering a 1-yr period from December 1986 through November 1987 [*Hansen et al.*, 1988].

2. EXPERIMENTAL DETAILS AND RESULTS

The aethalometer draws the sampled airstream at a flow rate of approximately 20 SLPM through a 1.1-cm^2 active area of a quartz fiber filter while monitoring the transmission of light through the filter. The accumulation of aerosol black carbon on the filter causes this transmission to slowly diminish relative to a reference beam intensity. At the low concentrations encountered at the South Pole, the filter was changed approximately every 2 weeks. Data were recorded during the last 20 minutes of each hour and stored on magnetic tape.

We first scanned the hourly data to identify abnormal events, which were clearly evident above a threshold set at 25 ng m^{-3}. Thirteen such local contamination events were identified in the data during 1987 and were extracted for separate examination; these events were not included in the subsequent analysis of background data. We separated the periods when measurements were contaminated by local combustion sources (0.4% of the time) from periods when measurements represented large-scale background conditions (99.6% of the time). We calculated 1-d averages for the background data and used an exponentially declining weighted running mean on the hourly data to calculate a smoothed value for the concentration. Figure 1 shows these results. The points indicate the daily averages and the line shows the running mean calculated with a weighting function of 80-h half-width.

Figure 2 shows the hourly measurements during a local contamination event in which the black carbon concentration increased greatly above its background mean value (1.6 ng m^{-3} at that time), accompanied by a similar great increase of CN

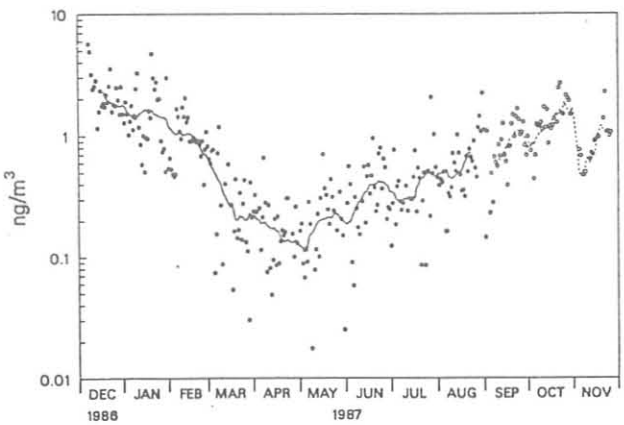

Fig. 1. Aerosol black carbon concentrations (ng m^{-3}) measured at SPO from December 1986 to November 1987. Data were recorded every hour; events of local contamination were removed. The solid points represent 24-h means; the solid curve was generated by a smoothing function of 80-h width. The open points represent data calculated from the operator's daily logsheets when hourly data were unavailable; the dashed curve shows a running average of 4-d width for these points.

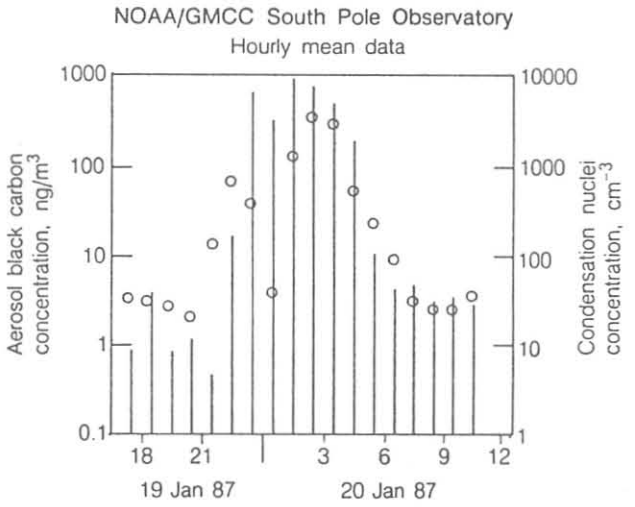

Fig. 2. Aerosol black carbon (vertical lines) and condensation nucleus data (circles) for a local contamination event occurring January 19-20, 1987, at SPO. Note the logarithmic scales. The mean smoothed value of background black carbon concentration at this time was 1.6 ng m^{-3}.

concentration. For 6 hours, carbon concentrations exceeded 160 ng m^{-3} (i.e. a greater than 100-fold increase over background). Other observations suggested that this event was due to contamination by local activities. The amount of carbon collected during these 6 hours was 50% greater than the total amount collected during the following 10 months of the study period, excluding other contamination events. It is important to note that such events are infrequent and can easily be detected by examining continuous hourly data.

3. Discussion

The results show that background aerosol black carbon concentrations generally ranged from 50 pg m^{-3} to 5 ng m^{-3} during the 1986-1987 sampling period at SPO, and that a pronounced minimum occurred in the early austral winter. This seasonal cycle is approximately in phase with that of the aerosol scattering extinction and the CN concentration [*Bodhaine et al.*, 1986]. We may compare the black carbon concentrations with the following ranges measured at other locations: 10-100 μg m^{-3}, winter coal heating season in European cities; 1-10 μg m^{-3}, annual averages for U.S. urban areas; 0.1-1 μg m^{-3}, annual averages for U.S. regional areas, and concentrations found in Arctic haze layers; and 10-100 ng m^{-3}, remote middle-latitude ocean area [*Goldberg*, 1985]. The concentrations at SPO are therefore much smaller than concentrations measured at any other location, but are nonetheless detectable. The material reaching the South Pole is the most long-lived fraction of the global background aerosol, and we may estimate a lower limit for the concentration of its black carbon component of about 10 pg m^{-3}.

We also note the essential attribute of real-time data in distinguishing local influences at a remote sampling location. The example illustrated in Figure 2 shows that the amount of carbon collected during only a few hours of local contamination could exceed that collected during an entire year of background sampling at such a remote location. Consequently, results derived from the analysis of filter samples operated for long periods of time may be seriously misleading if contaminating events are sampled. When sufficient data are available from several years of continuous sampling, it will be possible to study the statistics of local aerosol black carbon contamination events superimposed on background measurements at the South Pole. The real-time nature of aethalometer data allows for this examination in a manner that filter sample analyses do not.

4. Summary

Measurements of aerosol black carbon in background air at the South Pole for December 1986 to November 1987 show daily concentrations of this combustion-derived pollutant ranging generally from 50 pg m^{-3} to 5 ng m^{-3}, and having a minimum in the early austral winter. These concentrations are many orders of magnitude lower than those measured at less remote locations, and imply extremely long-range transport of energy-related anthropogenic emissions. The 1-h time resolution of the measurements allows for the identification of local source contamination events.

Acknowledgments. This work was supported by the Director, Office of Energy Research, Office of Health and Environmental Research of the U.S. Department of Energy under contract DE-AC03-76SF00098, and by the National Oceanic and Atmospheric Administration under contracts 40RANR730071 and 40RANR705255. The South Pole Observatory is funded and operated by the National Science Foundation.

References

Bodhaine, B. A., J. J. DeLuisi, J. M. Harris, P. Houmere, and S. Bauman, Aerosol measurements at the South Pole, *Tellus, 38B*, 223-235, 1986.

Bridgman, H. A., R. C. Schnell, J. D. Kahl, G. A. Herbert, and E. Joranger, A major haze event near Point Barrow, Alaska, during AGASP-II, 2-3 April 1986: Meteorological analysis of probable source regions and transport pathways, *Atmos. Environ.*, submitted, 1988.

Chuan, R. L., and D. C. Woods, The appearance of carbon aerosol particles in the lower stratosphere, *Geophys. Res. Lett., 11*, 553-556, 1984.

Goldberg, E. D., *Black Carbon in the Environment*, 196 pp., Wiley, New York, 1985.

Hansen, A.D.A, B.A. Bodhaine, E.G. Dutton, and R.C. Schnell, Aerosol black carbon measurements at the South Pole: Initial resuls, 1986-1987, *Geophys. Res. Lett., 15*, 1193-1196, 1988.

Stephens, S., M. J. Rossi, and D. M. Golden, The heterogenesis reaction of ozone on carbonaceous surfaces, *Int. J. Chem. Kinetics, 18*, 1133-1149, 1986.

Warren, S. G., Optical properties of Antarctic snow, *Ant. J. U.S.*, in press, 1988.

Global Distributions of Anthropogenic Chlorocarbons: A Comparison of CFC-11, CFC-12, CFC-22, CFC-113, CCl_4, and CH_3CCl_3 From an Ocean Cruise and From Land-Based Sampling Sites

M.A.K. KHALIL AND R.A. RASMUSSEN

Institute of Atmospheric Sciences, Oregon Graduate Center, Beaverton, Oregon 97006

1. INTRODUCTION

Between May and July 1987 OGC participated in a joint Soviet-American research program dealing with the effects of human activities on the global climate (SAGA II). Our experiments were conducted on the Soviet ship *Akademik Korolev*. The ship sailed from Hilo, Hawaii, to high northern latitudes to the Kamchatka peninsula, and then sailed south to New Zealand, westward to Tasmania, north to Singapore, and finally returned to Hilo. From this long trek we obtained flask samples from latitudes between about 50°N and about 45°S.

2. SAMPLING

Here, we report on the concentrations of six anthropogenic chlorine-containing trace gases including CFC-11 (CCl_3F) and CFC-12 (CCl_2F_2), two of the main chlorofluorocarbons implicated in the depletion of the stratospheric ozone layer. Of the six, CFC-113 ($C_2Cl_3F_3$) has been increasing most rapidly in the atmosphere in recent years, reflecting its growing use as a degreasing solvent in the high-technology electronics industry [Khalil and Rasmussen, 1986]. Methylchloroform (CH_3CCl_3) is also a degreasing solvent, but its uses are not growing as fast, so the rates of increase now are much less than in previous years [Rasmussen and Khalil, 1986]. All these chlorocarbons are much more concentrated in the northern hemisphere than in the southern hemisphere because most of their sources are in the industrialized middle northern latitudes.

In addition to taking measurements on ocean cruises such as SAGA II, we have obtained air samples, for nearly a decade, from sites distributed in latitudes from the Arctic Circle to the South Pole. The sites are located at Barrow, Alaska, inside the Arctic Circle; Cape Meares, Oregon, near our laboratory; Mauna Loa Observatory and Cape Kumukahi, Hawaii; American Samoa; Cape Grim, Tasmania; and the South Pole. At all the sites, except Cape Meares and Cape Grim, samples are collected for us by NOAA/GMCC. The weekly samples from these sites obtained at the same time as samples from the cruise of the *Akademik Korolev* can be compared with each other. Such a comparison shows very good agreement, demonstrating that the flask-sampling sites accurately reflect the concentrations of these trace gases, and many others not discussed here, for the entire range of latitudes represented by the sites.

3. RESULTS

The main results are summarized in Figure 1 and Table 1. Figure 1 shows the concentrations of the chlorocarbons obtained on the *Akademik Korolev* and the concentrations during the same time at the flask sampling sites. The shipboard measurements were averaged over latitudinal bands of 0.2 in the sine of latitude. So, for example, the point plotted at 0.5 in the sine of latitude is the average concentration in the latitude band spanning 0.4 and 0.6 in sine latitude or between 23° and 37°. We use sine of latitude as a standard unit of horizontal extent since equal divisions of sine latitude represent equal amounts of surface area on the earth. The vertical bars represent the 90% confidence limits of the mean concentrations. The solid line is an empirical fit to the average concentrations from the ship measurements. The empirical relation is expressed as

$$\frac{dC}{d\mu} = b(a-C)\,(C-d) \qquad (1)$$

where C is the concentration (pptv), μ is the sine of latitude, and a, b, and d are constants. The constant a represents the upper limit of concentrations at high northern latitudes, d is the lower limit in the southern hemisphere, and b is a parameter that expresses the rapidity and the magnitude by which concentrations fall as one moves from the northern hemisphere to the southern hemisphere. This is a logistic equation that has been applied to many natural processes in which limited changes are expected. The solution of this equation is given by

$$C = \frac{d + aK\,e^{\lambda\mu}}{1 + K\,e^{\lambda\mu}} \qquad (2)$$

where K is the constant of integration and $\lambda = b(a-d)$. The parameters to be fitted are a, b, d, and K, which we list in Table 2. Table 1 also contains the data on the average concentrations measured in each latitudinal band. The empirical function for the latitudinal distribution can be used to determine the average concentrations in any latitudinal band.

4. CONCLUSIONS

The current latitudinal distributions are shown of six anthropogenic chlorine-containing trace gases in the atmosphere that are implicated in the destruction of the stratospheric ozone layer. At present the most effective in this role are CFC-11 and CFC-12. The primary data are from the cruise of the Soviet ship *Akademik Korolev*. Simultaneous measurements taken at the sites of our global network are shown to agree with the results from the cruise

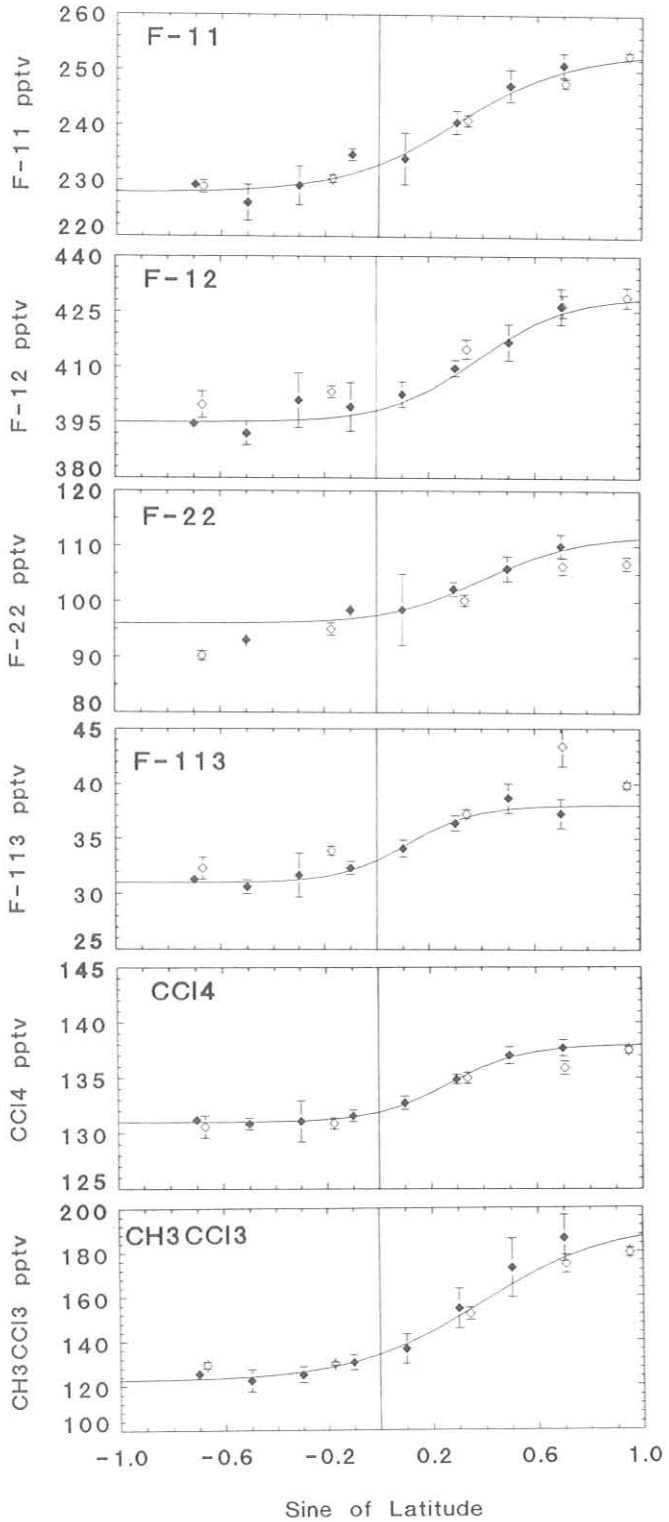

Fig. 1. The latitudinal distributions of six anthropogenic chlorocarbons obtained from a ship cruise (SAGA II - filled diamonds) and from systematic flask sampling sites (open diamonds). The vertical bars are the 90% confidence limits of the mean values. The solid line is an empirical fit of the data to a logistic model described in the text.

TABLE 1. The Latitudinal Distribution (pptv) of Six Anthropogenic Chlorocarbons Obtained Onboard the Cruise of the *Akademik Korolev* (SAGA II)*

sin μ	CFC-12	CFC-11	CFC-113	CH_3CCl_3	CCl_4	CFC-22
0.7	426	251	37	186	138	110
0.5	417	247	39	173	137	106
0.3	410	241	36	155	135	102
0.1	403	234	34	136	133	99
-0.1	399	235	32	130	132	98
-0.3	401	229	32	125	131	
-0.5	392	226	31	122	131	93
-0.7	395	229	31	125	131	

*The concentrations are averaged over latitudinal bands of ± 0.1 in sine of latitude surrounding the average location in the sin μ column.

TABLE 2. Values of Variables for the Empirical Logistic Model Fitted to the Latitudinal Data in Table 1

Variable	CFC-12	CFC-11	CFC-113	CH_3CCl_3	CCl_4	CFC-22
d	395	228	31	122	131	96
a	429	253	38	192	138	112
K	0.10	0.25	0.40	0.20	0.15	0.10
b	0.18	0.18	1.10	0.06	1.00	0.35

data. These results validate the shipboard measurements and show that measurements taken at the land-based sites represent the latitudes in which the sites are located. The data are fitted to an empirical logistic formula to represent the global latitudinal data by four parameters (*a, b, d,* and *K*) listed in Table 2. OGC is continuing the research based on the samples from the SAGA II program to analyze data on these and many other trace gases, both in the atmosphere and in the sea water, to determine the global mass balances of some 20-30 atmospheric trace gases.

Acknowledgments. We thank John A. Rau, a Senior Research Associate at the Institute of Atmospheric Sciences of the Oregon Graduate Center, who collected gas and aerosol samples on board the *Akademik Korolev,* including the samples on which the results of this paper are based. Financial support was provided by National Science Foundation Grant # ATM-8414020. We thank NOAA/GMCC for collecting the samples for our land-based, long-term flask sampling program. Additional support for this program was obtained from the resources of the Biospherics Research Corporation and the Andarz Company.

REFERENCES

Rasmussen, R.A., and M.A.K. Khalil, Atmospheric trace gases: Trends and distributions over the last decade, *Science, 232,* 1623-1624, 1986.

Khalil, M.A.K., and R.A. Rasmussen, Trichlorotrifluoroethane (F-113): Trends at Pt. Barrow, Alaska, in *Geophysical Monitoring For Climatic Change, No. 13: Summary Report 1984,* E.C. Nickerson (ed.), NOAA Environmental Research Laboratories, Boulder, CO, 91-93, 1986.

Some Characteristics of Aerosol Size Distributions at MLO

ANTONY D. CLARKE

Hawaii Institute of Geophysics, University of Hawaii, Honolulu, Hawaii 96822

1. INTRODUCTION

In-situ measurement of the aerosol size distribution was initiated at MLO in 1986 and was resumed in late 1987 through March 1988 as part of NASA/GLOBE in order to characterize aerosol properties of importance to the LAWS program. Previous experiments have demonstrated that aerosols measured under clean downslope flow at MLO undergo an annual cycle dominated by the springtime (February-June) transport of Asian dust and continental aerosol in the free troposphere [*Bodhaine et al.*, 1981; *Parrington et al.*, 1983]. The rest-of-the-year average mass concentration is an order of magnitude lower. However, previous data were often averages over a week or so; therefore, short-term variability in aerosol concentrations or properties was obscured. The poor size descrimination also limited information on particle number and mass distributions. This information is necessary to NASA/LAWS in order to relate aerosol microphysics to the existing MLO aerosol scattering extinction data so that aerosol backscatter at the 10.6 μm CO_2 wavelength can be better modeled, based on the nature and variability of low aerosol concentrations in the marine free troposphere.

2. MEASUREMENTS AND RESULTS

A measurement program was initiated at MLO using a modified LOPC with 254 size channels between 0.15 and 7.0 μm. The LOPC operated under microcomputer control and accumulated data continuously over 3-h intervals. Aerosols entering the LOPC first passed through a thermal conditioning system that heated them to 40°C, 150°C, and 340°C in separate channels. At 150°C sulfuric acid was driven off, and at 340°C all sulfates were volatilized to leave refractory components (e.g., soot, salt, dust), as shown in Figure 1 [*Clarke et al.*, 1987]. Sulfates have been identified as the major noncrustal downslope aerosol at MLO [*Bigg*, 1977], and this interpretation also appears appropriate here.

The 2.5-cm-ID sample inlet line was situated at about the 24-m level of a tower that was about 13 m from the enclosed sampling building. Calculated particle losses for the turbulent flow become significant at about 4 μm. Since other investigators [*Shutz*, 1980] and our own data from 1981 and 1982 (unpublished) find a mass mean diameter during dust events of between 3.0 and 4.0 μm after about 6000 km of transport, we

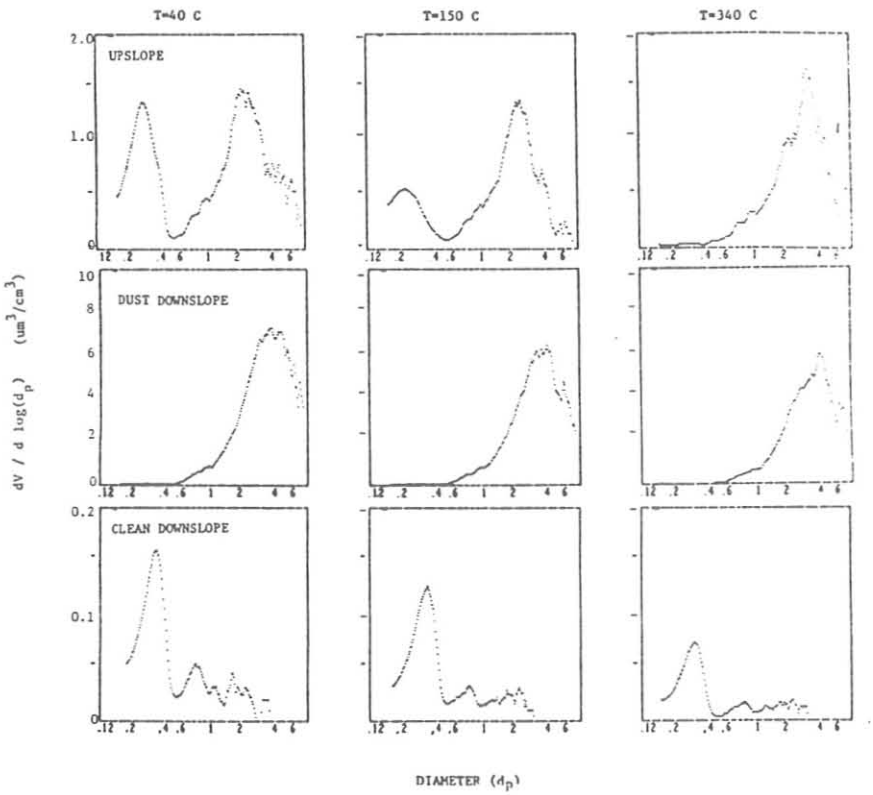

Fig. 1. Three volume size distributions of aerosols with diameters between 0.15 and 7.0 μm measured at MLO with the LOPC at 40°C, 150°C, and 340°C. The top row shows upslope air from the boundary layer; the middle row shows an Asian dust event (March 11, 1988); and the bottom row shows clean downslope air.

estimate that our coarse particle mass data may be 30% low but coarse number count will be at most a few percent low.

Several examples of the LOPC size distributions are shown in Figure 1 for each temperature. The top row is an example of a daytime upslope aerosol mass distribution from the marine boundary layer and illustrates the typical volatile component below 0.5 μm diameter (fine particles, sulfate) and refractory sea salt or dust at larger diameters (coarse particles) [*Clarke, et al.*, 1987]. The second row shows the character of the aerosol under downslope flow for March 11, 1988, when Asian dust was present in the troposphere above MLO. The 15% decrease in mass at 150°C and 25% decrease at 340°C for this case are attributed largely to higher coarse particle losses in the heated channels. Corrections for these decreases are applied to all of the data that follow. The bottom row of data is a characteristic distribution during downslope flow for the "clean" periods at MLO (note scale change) and shows the much reduced coarse-particle fraction and refractory fine fraction. Although concentrations are very low in comparison with the mixed layer, the presence of a significant fine mode (<0.4 μm diameter)

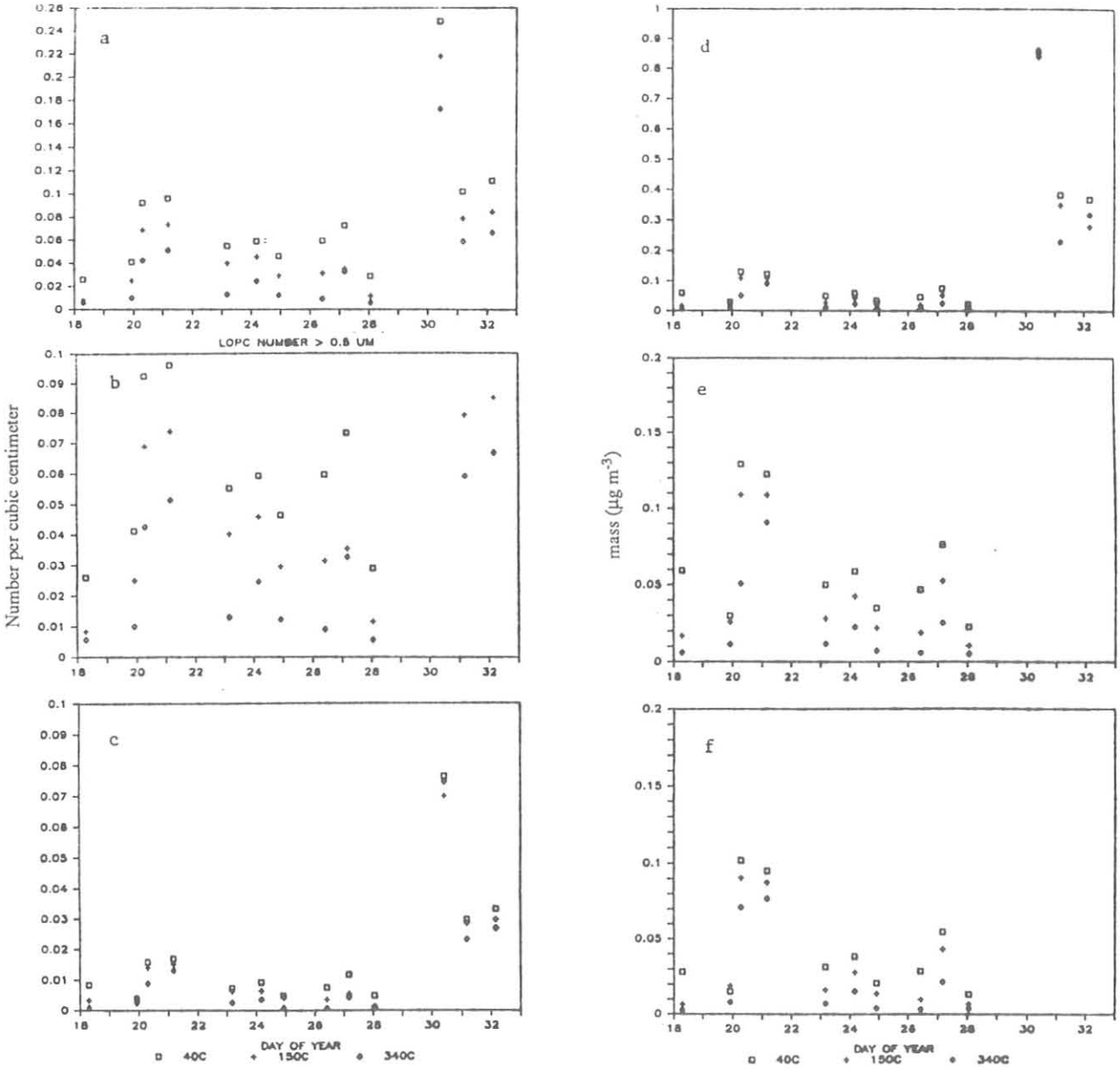

Fig. 2. Time series of coarse aerosol mass and number concentrations, measured with the LOPC at 40°C, 150°C, and 340°C, for downslope periods discussed in the text. Shown are (a) the number of particles greater than 0.5 μm diameter; (b) the same as (a), but rescaled to show lower values; (c) the number of particles greater than 1.0 μm diameter; (d) the mass (μg m^{-3}) of particles greater than 0.5 μm diameter; (e) the same as (d), but rescaled to show lower values; (f) the mass at particles greater than 1.0 μm diameter.

refractory component at 340°C is characteristic of a continental combustion source. A similar component has not been found in association with either high sea salt or high dust concentrations, but it has been observed when high soot concentrations were measured in remote polluted air [see *Clarke,* 1987]. A recalibration of the LOPC for soot instead of sulfate would reduce this refractory component by about a factor of 3 in apparent concentration, down to about 10 ng m^{-3}, similar to soot concentration values estimated from light absorption measurements at MLO in 1981-1982 [*Clarke and Charlson,* 1985].

Thirteen nights, in the period January 18 to February 1, 1988, were chosen for clean conditions based upon low CN counts and wind directions that did not favor transport of aerosol from the Mauna Loa caldera south of MLO. These data were then selected for the lowest aerosol concentrations observed, occurring generally between 0100 and 0400 LST. Figure 2 presents time series of integrated mass and number concentrations for particles greater than 0.5 and 1.0 μm diameter. Minimum and maximum concentrations in mass or number range over 2 orders of magnitude even though the highest dust concentration (January 30) is an order of magnitude lower than that illustrated for the large dust event shown in Figure 1 (March 11). The data points at 40°C, 150°C, and 340°C reveal the decrease of volatile particles and mass upon heating and were corrected for losses mentioned earlier. This response suggests that the sulfuric acid and ammonium sulfate/bisulfate [*Clarke et al.,*1987] present in these coarse particles can account for more than 80% of their mass at times of low concentrations of coarse aerosol but drop to a negligible fraction during the dustiest of these nights (e.g. January 30). The lowest concentrations obtained during this period, show that the number (mass) of coarse particles with diameters greater than 1.0 μm were usually less than 0.01 cm^{-3} (0.03 μg m^{-3}).

The interpretation of the above data in terms of backscatter at 10.6 μm CO_2 laser wavelength (BCO2), is of interest to the NASA GLOBE/LAWS programs. Here we estimate the various contributions to BCO2 from each component as a lognormal distribution in number centered at a particular diameter. These contributions are based upon the BCO2 per particle per cubic centimeter calculated for lognormal distributions of various components, a dust aerosol lognormal number peak at 1.0 μm, an ammonium sulfate coarse aerosol number peak at 0.6 μm, and an ammonium sulfate fine-particle number peak at 0.16 μm. These relative contributions to BCO2 are shown in Figure 3 as a histogram for each of the 13 sequential periods. A clear change can be seen in the relative contributions to BCO2 as the transition to a higher dust concentration takes place. The low-dust periods show contributions to BCO2 from dust of about 15-25% compared with 50-70% for minor dust incursions (periods 11, 12, 13). With one exception, the fine-particle sulfate contribution decreases from about 40% to 15% of the total. Coarse volatile sulfate tends to dominate the contribution to BCO2 during low-dust periods and remains significant even for the increasing dust concentrations seen in periods 11, 12, 13.

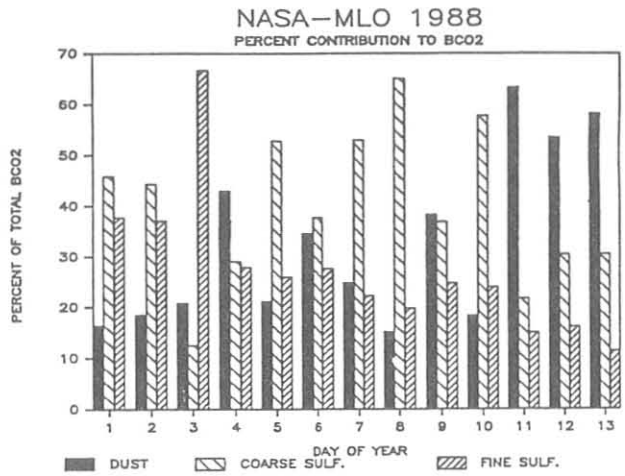

Fig. 3. Histogram of estimated percent BCO2 backscatter attributed to coarse (d_p > 0.5 μm) refractory aerosol (dust), coarse sulfate aerosol, and fine (d_p < 0.5 μm) sulfate aerosol for each sample interval.

REFERENCES

Bigg, E.K., Some properties of the aerosol at Mauna Loa Observatory, *J. Appl. Meteorol. 16,* 262-267, 1977.

Bodhaine, B.A., B.G. Mendonca, J.M. Harris, and J.M. Miller, Seasonal variations in aerosols and atmospheric transmission at Mauna Loa Observatory, *J. Geophys. Res., 86,* 7395-7398, 1981.

Clarke, A.D., Size distributions of volatile and refractory Arctic haze aerosol compnents measured at Barrow during AGASP-II 1986, in *Geophysical Monitoring for Climatic Change, No. 15: Summary Report 1986,* edited by R.C. Schnell and R.M. Rosson, pp. 115-119, NOAA Environmental Research Laboratories, Boulder, Colo., 1987.

Clarke, A.D., and R.J. Charlson, Radiative properties of the background aerosol: Absorption component of extinction, *Science, 229,* 263-265, 1985.

Clarke, A.D., N.C. Ahlquist, and D.S. Covert, The Pacific marine aerosol: Evidence for natural acid sulfates, *J. Geophys. Res., 92,* 4179-4190, 1987.

Parrington, J.R., W.H. Zoller, and N.K. Aras, Asian dust: Seasonal transport to the Hawaiian Islands, *Science, 220,* 195-197, 1983.

Shutz, L., Long range transport of desert dust with special emphasis on the Sahara, *Ann. N.Y. Acad. Sci., 338,* 515-532, 1980.

Snowfall Measurements in the Arctic

GEORGE CLAGETT

Soil Conservation Service, Anchorage, Alaska 99501

1. INTRODUCTION

Arctic winters are characterized by months of very low temperatures, infrequent and light-density snowfall, and incessant wind, the sum of which precludes much hope of accurate snowfall measurements using traditional methods. A precipitation gauge without artificial windshielding has little chance of catching a correct amount of new moisture falling out of a wind-driven Arctic snowstorm. In the mid-1970's, the University of Wyoming produced a windshield after 7 years of research that included tests in a wind tunnel [*Rechard,* 1975]. It provided snowfall catch in an exposed, windy area that was within 7% of the catch in a forest-protected area. This report compares snowfall catches using Wyoming windshielded gauges with catches using NWS nonshielded gauges at Barrow and Barter Island on Alaska's Arctic Coast for the last 12 years. These measurements are also compared with nearby measurements of the tundra snow-water equivalent (SWE).

2. METHODS

The Wyoming windshield consists of two concentric rings of snowfences surrounding the precipitation storage can orifice. A solid framework elevates the 1.2-m tall snowfence mesh. The outer circle is 3 m off the ground and 5.1 m in diameter; the inner circle is 2.4 m off the ground and 3 m in diameter. The rings of fencing are canted inward at the bottom, 30° from the vertical for the outer ring and 45° for the inner ring, to form a cup or funnel effect. The level of the storage can orifice is 2.4 m above the ground surface (i.e., level with the top of the inner ring of fencing).

The funnel shape is a critical part of the design, since wind hitting the leading edge of the fencing is forced downward and underneath the gauge rather than over the top. This causes air speed below the gauge to increase slightly in order for the larger air volume to pass. With the increased air speed below the fencing, a downward pressure gradient is created within the fencing, causing snow particles clearing the top of the gauge to settle out within the fencing and to fall into the can. Research suggests that the snow passing under the gauge is primarily drift material and snow at the 3-m elevation is primarily new snowfall.

The precipitation cans mounted within the Wyoming windshields are storage devices with an antifreeze solution and an evaporation-inhibiting oil layer. The storage-type gauge is a basic requirement of remote, seldom-visited locations, which constitute the bulk of the network of 23 active Wyoming windshields in Alaska monitored by the SCS. Frequency of readings generally ranges from twice monthly at Barrow to nine times annually at Barter Island. Contents of the 20.3-cm-diameter by 0.9-m-tall storage cans are weighed with an open-face dairy scale read to the nearest 0.25 cm. In 1984, a larger 30.5-cm-diameter by 2.4-m-tall can was installed at Barter Island, along with the attachment of a float-driven fluid-level recording system, whose accuracy is also to the nearest 0.25 cm. This level of resolution makes accurate evaluation of small increments over short time periods impossible, especially in the Arctic where many small events are often required to meet the smallest recordable increment. Therefore, monthly totals are used for the evaluation period of this report.

The Barrow gauges are separated by 7 km: the NWS gauge is near town center, which affords some disruption of air flow past the gauge; the Wyoming gauge is northeast of town near the NOAA-GMCC facility. GMCC services the Wyoming gauge. At Barter Island, the Wyoming gauge was originally 1.6 km south of town; however, it was difficult to get consistent readings by local observers, so the gauge was moved closer to town in June 1983. The new location is only 230 m from the NWS gauge which is about 60 m beyond the Barter Island DEW Line barracks. Readings are currently being made by the U.S. Fish and Wildlife Service.

3. COMPARISON OF DATA

NWS has staffed a first-order weather station for 67 years at Barrow and for 40 years at Barter Island. Published precipitation averages (30-yr period) for the two sites are 12.06 cm annually and 6.45 cm during the September-May winter months for Barrow, and 16.48 and 9.70, respectively, for Barter Island. Scientists have recognized that these averages are not accurate winter precipitation levels [*Black,* 1954; *Benson,* 1982]. Benson constructed two of the first three Wyoming gauge installations in Alaska at these two villages in the fall of 1975. By the end of the 1987 wateryear, 11 years of matching records were collected at Barrow and 8 years at Barter Island. Table 1 lists the average monthly catches over the last 12 years for both the NWS unshielded and Wyoming shielded gauges. NWS figures in the table correspond to the same periods that are available for the Wyoming gauge. For Barrow, the 1982 wateryear is missing because the Wyoming gauge was damaged; for Barter Island 1978, 1980, 1982, and portions of 1976 and 1981 wateryears are missing.

In Table 2 we combined the monthly totals by periods of the year for matching periods during 1976-1987. The shielded gauges yielded an overall catch 2 times that of unshielded gauges during the 9-mo winter season. However, the factor is 3 times during the November-April coldest months. Although the windshield is the probable reason for these discrepancies during the winter months, a windshield does not seem to provide any significant additional benefit during the three summer months.

TABLE 1. Average Monthly Precipitation (cm) at Barrow and Barter Island

	Barrow			Barter Island		
Month	NWS 1976-1987 Average*	NWS 30-yr Average†	Wyoming 1976-1987 Average*	NWS 1976-1987 Average‡	NWS 30-yr Average†	Wyoming 1976-1987 Average‡
Sept.	1.96	1.50	1.73	1.40	2.03	2.13
Oct.	1.02	1.40	1.55	1.40	2.06	2.36
Nov.	0.43	0.76	1.34	0.56	1.02	1.37
Dec.	0.28	0.46	1.14	0.64	0.58	1.57
Jan.	0.30	0.53	1.19	0.56	1.27	1.52
Feb.	0.36	0.43	0.96	0.25	0.68	1.35
March	0.23	0.43	0.96	0.48	0.61	1.52
April	0.33	0.53	0.64	0.30	0.56	1.32
May	0.28	0.41	0.53	0.43	0.89	0.84
June	0.66	0.94	1.14	0.81	1.42	1.37
July	2.03	2.18	2.08	1.90	2.62	2.26
Aug.	2.11	2.49	2.13	2.41	2.74	3.05

*Does not include 1982 wateryear.
†For the period 1951-1980.
‡Does not include 1978, 1980, 1982, and portions of 1976 and 1981 wateryears.

Table 1 points out another peculiar discrepancy. The NWS monthly average data over the last 12 years are consistently far below published 30-yr long-term averages (for the period 1951-1980). *Benson* [1982] noted that the Barrow station was moved in 1955 and again in 1966 and that these moves or possibly the addition of an Alter shield to the gauge had a profound effect on the recorded precipitation. After 1955 the gauge caught 1.4 times as much as before the move, but after 1966 it caught only 0.63 as much. The result is that most years since 1966 have precipitation data far below the inflated average. Barter Island also recorded a higher rate of precipitation during the period 1956-1967 than afterward. A sharp break occurred in 1967 on the double mass plot to 0.67 as much precipitation, even though the gauge was not moved, leading one to suspect that the Alter windshield was removed from both Barrow and Barter Island gauges at that time. Benson states that the site histories for both sites mention the use of Alter shields, but do not give details. It is known, however, that gauges have been unshielded since 1966 at Barrow and 1967 at Barter Island.

TABLE 2. Monthly Snow Catch Total (cm), Combined Into Period of the Year, for Matching Periods During 1976-1987

	Barrow			Barter Island		
	NWS	Wyoming	Factor	NWS	Wyoming	Factor
Wateryear Oct. 1-Sept. 30	9.98	15.42	1.54	11.15	20.67	1.85
Winter Season Sept. 1-May 31	5.18	10.06	1.94	6.02	14.00	2.32
Mid-Winter Nov. 1-April 30	1.93	6.25	3.24	2.79	8.66	3.10

The NWS measurement technique creates another problem. Precipitation increment is measured four times per day by exchanging the can each 6 hours with another one. The catch for the previous 6 hours is thawed, then measured to determine the new increment. If the catch is less than 0.13 mm, it is recorded as a trace. The can is then dried to be ready for its next 6-h shift. Since Arctic snowfall generally comes in small amounts, is of light density, and is wind driven, this technique of discounting even 0.13 mm four times a day becomes significant, as the unshielded gauge appears to be catching only a fraction of the small natural snowfall increments. This results in an extraordinary number of trace readings in the record. *Benson* [1982] reported that traces in the winter record go as high as 80% of all precipitation entries. Accumulation of precipitation over time in a storage gauge eliminates this problem.

Tundra snow measurements provide more data for comparisons (Table 3). The USGS team made reconnaissance snow measurements on the Arctic Slope during the spring of the year, just prior to the breakup season, in five different years (1977, 1978, 1979, 1982, and 1983). In 1979, however, they were late, as spring thaw was well under way in much of the region.

TABLE 3. USGS Tundra Snow-Water-Equivalent (SWE) Measurements Compared With Wyoming Shielded Gauges and NWS Unshielded Gauges

Year	Location	Date	Tundra SWE (cm)	Wyoming Gauge (cm)	NWS Gauge (cm)	Tundra SWE as % of Wyoming	NWS as % of Wyoming	NWS as % of Tundra
1977	Barrow	April 22	7.9	9.6	4.3	82%	45%	55%
1978	Barrow	April 17	7.4	9.1	4.1	80%	44%	55%
1982	Barter Is.	April 24	11.9		5.3			58%
1983	Barrow	April 25	6.1	8.6	3.6	70%	41%	58%
1983	Barter Is.	April 22	7.9	11.7	0.8	67%	6%	10%
Average (Barrow only)			7.11	9.14	4.06	73%	43%	56%

They landed a ski plane on the tundra at 24-40 sites over about a 1-wk period each year. Their transects avoided obvious deposition areas. Their reported figures represent an average of 40 individual random samples per site [*Sloan et al.*, 1979]. These surveys provide valuable insight into the variability of the snowpack across the slope.

Tundra snow measurements do not provide a precise comparison because of too many remaining unknowns, such as amount of wind exposure, representativeness of sample, or sublimation loss. But they do provide a starting point from which to make comparisons. For Barrow, the NWS gauge caught 56% of the precipitation remaining in the tundra snowpack. This is less than what fell, since a significant amount is blown away, according to the downwind drifts, and another portion is sublimated. The NWS gauge caught 43% of that caught by the Wyoming gauge, which is also probably less than what fell. (The values for Barter Island are much lower.)

Theoretically, the measurements from the two gauges and the tundra snow would be the same if snow always fell during calm air. However, wind is a dominant feature of the Arctic Coast. Long-term mean wind speed is 5.8 m s^{-1} at Barter Island and 5.4 m s^{-1} at Barrow [*Searby*, 1968] and calm air occurs only 2-3% of the time [*Wendler*, 1978]. It is probable that the principal difference in the two catches is attributable to wind-speed effect. The U.S. Forest Service's Rocky Mountain Forest and Range Experiment Station at Laramie, Wyoming, studied the Wyoming shield catch efficiency for 7 years and concluded that the catch efficiency drops off with increasing wind speed when the temperature is below -2°C [*Sturges*, 1984]. If the catch does drop off with increasing wind speed for a shielded gauge, it is probable that it drops much further with an unshielded gauge. The undercatch of a nonshielded gauge may be exemplified by comparison of a shielded catch with an unshielded catch at Barter Island in 1983 (Table 3): the unshielded gauge caught only 6% of that of the shielded gauge. At the same time, snow-on-the-ground water equivalent measurements by the USGS were 10 times greater than the unshielded gauge measurements.

Still another problem affects the comparison of shielded versus unshielded catches at Barrow and Barter Island: the Arctic Coast has a significant incidence of riming events in which supercooled fog coats everything, including the inside of the orifice of a precipitation can. NWS does not consider rime as true precipitation and effectively eliminates it from the record, since rime and precipitation events do not overlap and the gauge is serviced every 6 hours. Because the Wyoming shielded gauges are unstaffed and visited only once or twice a month, rime builds up from time to time, sometimes capping the orifice. This reduces or precludes further precipitation accumulation until the rime melts or is removed during maintenance visits. Therefore, the error is magnified, resulting in either a net loss due to the covered or reduced orifice or a net gain due to the rime melting into the can. Wyoming gauge observers are instructed to carefully remove rime from the can whenever it is found, in an attempt to be as similar as possible to NWS procedures. The field observers have frequently stated their belief that the riming error leans heavily to the net loss side. Some scientists argue that eliminating rime from the precipitation total is a mistake.

4. Conclusion

The accuracy of the data from the Wyoming windshielded gauge compared with true or total snowfall-water-equivalent is still somewhat unknown. The small amount of data presented here only indicate that the shield allows 2 to 3 times greater catch during the winter months compared with unshielded gauges along Alaska's Arctic coast. Unshielded gauges, in fact, catch only slightly more than half the snow-water equivalent of snow remaining on the tundra. Since accurate data is needed from locations offering no natural wind protection, there appears to be no viable alternative other than the use of a windshielded measuring device.

References

Benson, C.S., Reassessment of winter precipitation on Alaska's Arctic slope and measurements on the flux of wind-blown snow, Report UAG R-288, 26 pp., Geophysical Institute, Univ. of Alaska, Fairbanks, Alaska, 1982.

Black, R.F., Precipitation at Barrow, Alaska, greater than recorded, *Trans. Am. Geophys. Union. 35*, 203-206, 1954.

Rechard, P.A., Measurement of winter precipitation in wind-swept areas, *Proc. of Snow Management on the Great Plains*, Bismark, North Dakota, July 29, 1975, Great Plains Agriculture Council, Pub. 73, pp. 13-30, Agriculture Experiment Station, Univ. of Nebr., Lincoln, Nebr., 1975.

Searby, H.W., Climatology of the states, *ESSA climatology of the United States, No. 60-49*, U.S. Weather Bureau, 1968.

Sloan, C., D. Trabant. and W. Glude, Reconnaissance Snow Survey of the National Petroleum Reserve in Alaska, April 1977 and April-May 1978, *Water Resources Investigations Open-File Report, 79*, U.S. Geological Survey, Anchorage, Alaska, 1342. 1979.

Sturges, D.L., Comparison of precipitation as measured in gauges protected by an alter shield, Wyoming shield, and stand of trees, *52nd Proc., Western Snow Conference*, Sun Valley, Idaho, April 1984, pp. 57-67, 1984.

Wendler, G., Snow blowing and snowfall on the North Slope, Alaska, *Report UAG R-259*, 22 pp., Geophysical Institute, Univ. of Alaska, Fairbanks, Alaska, 1978.

Resolution and Geochemistry of Ionic Components in the Late Winter Aerosol at Barrow Station During AGASP-II

SHAO-MENG LI AND JOHN W. WINCHESTER

Florida State University, Tallahassee, Florida 32306-3048

Sixty-nine size-fractionated aerosol samples were taken day and night, March 16 to May 6, 1986, at BRW, during the AGASP-II project in order to identify components of the Arctic haze and their likely sources. In the experimental design, 12-hr samples were taken sequentially by two-stage stacked Nuclepore filters; 12 ionic species in the samples were measured by ion chromatography, and multivariate absolute principal component analysis (APCA) was used to resolve different components, each consisting of the ions sulfate $SO_4^=$, chloride Cl^-, bromide Br^-, nitrate NO_3^-, methanesulfonate MSA^-, formate Fo^-, acetate Ac^-, propionate Pp^-, pyruvate Py^-, potassium K^+, sodium Na^+, and ammonium NH_4^+ in different proportions. In applying APCA, linear physical mixing of components of fixed composition is assumed to cause the temporal variability in measured ionic concentrations, and goodness of fit is indicated by the fraction of data variance R^2 explained by the mixing model. The average absolute concentrations in air of the components and their ionic constituents, and standard deviations (s.d.), were then calculated by multiple linear regression. The results are summarized in Table 1.

Coarse and fine aerosol components exhibited both similarities and differences. Three components (C1, C2, and C3) explain more than 80% of the coarse concentration variance: sea-salt-contaminated C1, containing non-sea-salt (nss) $SO_4^=$ and nss K^+; a carboxylic acid anion component C2; and C3, containing most of the Br^-, NO_3^-, and MSA^-. Ion balances between cations and anions in all three components are close to unity, consistent with these components being internally mixed aerosols. The large amount of nss K^+ in C1 suggests aerosol from lower latitude combustion sources. C2, mainly carboxylic acid anions and some sea salt, may represent uptake of the acids by salt particles. C3 could be the product of gas phase reactions of marine organic compounds; its MSA^-/nss $SO_4^=$ ratio supports such an origin. A non-APCA component, found in seven coarse samples with the highest concentrations of Ac^- and sea salt, is identified by the combination of linear regression and APCA and does not belong to the communality of the rest of the data.

In the fine fraction four components (F1, F2, F3, and F4) explain 86% of the variance, with the compositions of F1, F2, and F3 resembling their coarse fraction counterparts. F1 is mainly a mixture of organic anions with additional NH_4^+ and Na^+, resembling C2 in composition. F2 is a contaminated sea-salt component similar in composition to the contaminated sea salt in C1; however, F2 contains smaller amounts of nss $SO_4^=$ and is not as deficient in Cl^-. F3, which exhibits a charge imbalance with an anion excess, has a composition similar to C3. Like C3, this component also contains the largest amount of MSA^-, with an MSA^-/nss $SO_4^=$ ratio similar to those reported for remote marine atmospheres. F4, apparently acidic, as indicated by an ion imbalance, is mainly nss $SO_4^=$ plus most of the NO_3^- and significant amounts of NH_4^+, and may be classified as ammonium bisulfate. F4 is uniquely a fine component and has no coarse-fraction counterpart.

These four aerosol types, consisting of the seven APCA components in the coarse and fine aerosol fractions, are attributed to different sources. The most prominent type is the contaminated sea salt coming from sea-salt scavenging of combustion products, as shown by the high content of nss K^+, and is considered to be transported to the Arctic as primary pollutants. The second contains the carboxylic acid anions, its internal relationships among the carboxylic acid ions suggesting natural vegetation emission sources. Lacking local winter Arctic sources, the carboxylic acid anions may have originated at lower latitudes as acid vapors and then been transported to the Arctic and condensed into aerosols at cold temperatures. The third, with the MSA^-/nss $SO_4^=$ ratios and the collection of Br^-, NO_3^-, small amounts of carboxylic acid anions, and sea salt, is demonstrated to be natural marine aerosols, and may be a collection of products from gas phase oxidation of precursors. Finally, a fine NH_4HSO_4 component is a likely product of SO_2 conversion in air and therefore a pollutant component. Most components have good charge balance, as indicated by their anion/cation ratios, reflecting extensive acid-base reaction in the components in aged aerosol systems with long atmospheric residence times.

We have attempted to partition by multiple linear regressions the total ionic concentrations as contributions from the stated natural and anthropogenic aerosol sources. Total inorganic ion concentrations are similar to previous data reported from the Arctic. The total coarse-plus-fine MSA^- average is 0.12 ± 0.02 nmol m^{-3}. High levels of Fo^- and Ac^- and traces of Pp^- and Py^- were found, which altogether account for 20% of the total aerosol mass: Fo^- 5.3 ± 0.7; Ac^- 12.4 ± 2.2; Pp^-, 0.3 ± 0.1; and Py^- 0.1 ± 0.04 nmol m^{-3}. With partitioning, about 10% of the carboxylic acid anions are associated with pollutants in the first aerosol type. The second type accounts for 80% of Fo^- and 60% of Ac^- in the Arctic aerosols. The third type in the marine aerosols, accounts for 18% of Fo^- and 10% of Ac^-. Thus, the carboxylic acid anions appear to be mostly natural; more than 90% of Fo^- and 70% of Ac^- from natural sources. In coarse aerosols, 67% of nss $SO_4^=$ is in the contaminated sea salt. In fine, 52% of nss $SO_4^=$ is connected to NH_4^+ and must be due to a secondary pollution source. Natural marine nss $SO_4^=$ is indicated

TABLE 1. Ionic Concentrations in Components of Both Fine and Coarse Aerosol Fractions, Based on 68 and 62 Samples, Respectively

Ion	Ionic Concentration (nmol m^{-3}), ± s.d.											R^2
Fine	Const.	s.d.	F1	s.d.	F2	s.d.	F3	s.d.	F4	s.d.	Total	
Fo^-	-0.19	0.14	2.01	0.05	0.20	0.03	0.27	0.09	0.11	0.03	2.40	0.96
Ac^-	0.82	0.29	2.26	0.11	0.25	0.06	0.23	0.18	-0.07	0.07	3.49	0.86
Pp^-	-0.06	0.02	0.09	0.01	0.02	0.00	0.04	0.01	0.01	0.00	0.19	0.77
Py^-	-0.03	0.06	0.11	0.02	0.04	0.01	0.03	0.04	0.00	0.02	0.07	0.28
MSA^-	0.00	0.02	0.00	0.01	0.01	0.00	0.06	0.01	0.01	0.00	0.08	0.27
Cl^-	1.84	0.66	0.84	0.26	3.48	0.15	4.25	0.43	-1.02	0.16	9.39	0.91
Br^-	0.03	0.02	0.02	0.01	0.03	0.01	0.23	0.02	-0.00	0.01	0.31	0.81
NO_3^-	-0.22	0.08	0.08	0.03	0.01	0.02	0.64	0.05	0.11	0.02	0.62	0.74
nss $SO_4^=$	0.66	0.30	0.22	0.12	0.28	0.07	1.04	0.19	2.41	0.07	4.61	0.94
Na^+	-1.01	0.55	2.04	0.21	3.37	0.12	1.31	0.35	1.18	0.13	6.89	0.94
NH_4^+	5.18	1.13	3.90	0.45	1.45	0.25	3.47	0.73	1.6	0.28	15.67	0.71
nss K^+	-1.08	0.23	0.93	0.09	1.17	0.05	0.25	0.15	0.45	0.06	1.72	0.92
Anion	3.43	0.96	6.12	0.38	4.91	0.22	7.93	0.61	4.08	0.23	26.47	
Cation	3.08	1.28	6.91	0.50	6.07	0.28	5.05	0.82	3.32	0.31	24.43	
A/C	1.12	0.56	0.89	0.08	0.81	0.05	1.57	0.28	1.23	0.13	1.08	
Mass	171.60		678.50		908.00		408.54		666.30		1727.57	
Coarse	Const.	s.d.	C1	s.d.	C2	s.d.	C3	s.d.			Total	
Fo^-	-0.35	0.19	0.40	0.06	1.97	0.08	0.69	0.11			2.71	0.92
Ac^-	0.76	0.28	0.45	0.08	2.02	0.12	0.40	0.17			3.63	0.84
Pp^-	-0.11	0.04	0.11	0.01	0.17	0.02	-0.02	0.02			0.15	0.74
Py^-	0.01	0.02	-0.00	0.01	-0.01	.01	0.05	0.01			0.03	0.27
MSA^-	0.01	0.02	-0.01	0.01	0.01	0.01	0.03	0.01			0.04	0.14
Cl^-	3.28	1.71	7.15	0.52	1.97	0.76	3.07	1.04			15.47	0.77
Br^-	-0.02	0.02	0.03	0.01	-0.00	0.01	0.18	0.02			0.19	0.73
NO_3^-	-0.03	0.13	0.01	0.04	0.25	0.06	1.01	0.08			1.24	0.77
nss $SO_4^=$	-0.08	0.54	2.23	0.16	0.78	0.24	0.41	0.33			3.34	0.76
Na^+	0.20	1.60	8.78	0.49	3.46	0.71	3.15	0.98			15.59	0.86
NH_4^+	2.72	0.93	3.47	0.28	3.55	0.41	2.36	0.57			12.10	0.80
nss K^+	-0.91	0.44	1.53	0.13	0.89	0.19	0.16	0.27			1.67	0.72
Anion	3.40	2.06	13.64	0.62	8.34	0.91	6.60	1.25			31.98	
Cation	2.01	1.90	13.97	0.58	7.97	0.84	5.74	1.17			29.69	
A/C	1.69	1.90	0.98	0.06	1.05	0.16	1.15	0.32			1.08	
Mass	126.60		1756.60		773.68		411.95				2039.47	

s.d., standard deviation; R^2, squared adjusted correlation coefficient; const., constant term; nss, non-sea-salt; A/C, anion-to-cation ratio.

by its association with MSA^- in both fractions. This marine-related nss $SO_4^=$ is about 20% of the total nss $SO_4^=$ measured.

These results show that natural compounds are important constituents in Arctic aerosols. Since Cl^- and Na^+ are natural sea salt, the proportion of products from natural sources may exceed the pollutant proportion. Hence, natural products cannot be ignored in future Arctic haze studies.

Acknowledgment. Support for this research was supplied in part by NSF grant ATM-86-01967.

The Global Precipitation Chemistry Project

WILLIAM C. KEENE AND JAMES N. GALLOWAY

Department of Environmental Sciences, University of Virginia, Charlottesville, Virginia 22903

GENE E. LIKENS

Institute of Ecosystem Studies, Cary Arboretum, Millbrook, New York 12545

JOHN M. MILLER

NOAA, Air Resources Laboratory, Silver Spring, Maryland 20910

1. INTRODUCTION

Anthropogenic emissions of SO_2 and NO_x have resulted in widespread acidification of precipitation and subsequent environmental damage in eastern North America and northern Europe. Of numerous research questions posed by this phenomenon, two are of special interest: (1) What was the composition of precipitation prior to the use of fossil-fuels? (2) To what degree does the long-distance transport of sulfur and nitrogen species influence the composition of precipitation in remote regions of the world? The GPCP was initiated in 1979 to address these questions. Principal objectives of the project are to measure the chemical composition of precipitation in remote areas of the world and to determine major processes controlling measured composition. Earlier reports of the GPCP compare the composition of precipitation in remote and impacted regions [*Galloway et al.*, 1982; 1984]; quantify the importance of, evaluate sources of, and intercompare measurement techniques for carboxylic acids in the atmosphere [*Keene et al.*, 1983, 1988; *Keene and Galloway*, 1984a,b, 1985, 1986]; assess factors controlling the chemical composition of precipitation at remote locations [*Jickells et al.*, 1982; *Church et al.*, 1982; *Galloway and Gaudry*, 1984; *Dayan et al.*, 1985; *Likens et al.*, 1987]; and present objective methods for differentiating sea-salt and non-sea-salt (nss) constituents in marine precipitation and aerosols [*Keene et al.*, 1986]. This report summarizes current research and reviews more recent contributions of the project.

2. MATERIALS AND METHODS

Samples of precipitation are collected, by event, in scrupulously washed polyethylene containers. Immediately after collection, pH is measured, samples are treated with $CHCl_3$ to prevent biological activity, and aliquots are subsequently sent to the University of Virginia for analyses for major organic and inorganic chemical constituents. To date we have analyzed samples of precipitation collected at 14 land-based sites and during nine oceanic cruises.

3. RESULTS AND DISCUSSION

3.1. THE CHEMISTRY OF PRECIPITATION ON AMSTERDAM ISLAND, INDIAN OCEAN

Between May 1980 and August 1985, 190 precipitation events were sampled on Amsterdam Island (37° 50′S, 77° 35′E) in the central Indian Ocean and samples were subsequently analyzed for major chemical constituents. Isobaric back trajectories were calculated for each event, and cluster analysis techniques were used to identify structure in the multivariate data sets for both chemistry and transport. Two chemical clusters (N_A = 141, N_B = 21) were identified. Storms in the smaller cluster occurred mainly in the spring and were associated with significantly greater depositions of H^+, NH_4^+, NO_3^-, and nss $SO_4^=$. Four distinct transport clusters revealed no significant differences for either concentrations or per-event depositions of any of the major chemical constituents, suggesting that transport is not an important factor in controlling the chemical composition of precipitation on the island. Although a continental influence on some air masses was suggested from both back trajectories and data for ^{222}Rn and CO_2, a signal in terms of major ions in associated precipitation events was not discernible from the marine background after the mean 3.5-day transport over the ocean. A significant seasonal signal in nss $SO_4^=$, NH_4^+ and H^+ is consistent with stronger source strengths of marine emissions and enhanced photochemistry during warmer months.

3.2. THE BIOGEOCHEMICAL CYCLING OF FORMIC AND ACETIC ACIDS THROUGH THE TROPOSPHERE

Despite remaining uncertainties, a general picture of the biogeochemical cycling of HCOOH and CH_3COOH is beginning to emerge [*Keene and Galloway*, 1988]. These acids are ubiquitous vapor- and aqueous-phase constituents of the global troposphere, contributing significant fractions of the natural acidity in precipitation and cloudwater, particularly in continental regions of the tropics and subtropics. The similarity

of concentrations in remote and impacted regions indicates that anthropogenic emissions of carboxylic acids or precursors are probably not important sources over broad geographical areas. In continental regions, seasonally varying emissions of acids and hydrocarbon precursors from vegetation are thought to represent major sources for both acids. In marine areas, the seasonality of wet deposition and apparent lack of transport from continents support the hypothesis of a marine biogenic source. Ratios of total (aqueous + vapor) concentrations of HCOOH versus CH_3COOH in clouds vary as a function of H^+. This observation is consistent with the hypothesis of a pH-dependent aqueous-phase source and sink for HCOOH in clouds, which may act to stabilize aqueous-phase ratios against shifts in solution H^+. Large diel periodicities in the concentrations of vapor-phase species over continents, together with a lack of evidence for long-distance transport, suggest that HCOOH and CH_3COOH have short atmospheric lifetimes, of several hours to a few (at most) days. Because they are important controllers of free acidity and represent a potentially large sink for aqueous-phase OH radicals, the cycling of carboxylic acids is expected to interact directly and indirectly in the chemical cycling of other atmospheric constituents.

3.3. Standard Error Calculations for Non-Sea-Salt Consituents in Marine Precipitation

Studies of pollutant transport and investigations of geochemical cycling often involve calculation of nss concentrations for various ionic constituents of precipitation and atmospheric aerosols. The nss concentrations are calculated from measurements of the concentrations of a reference species and the species of interest. Formulas for determining the accuracy of calculated nss concentrations are necessary because this accuracy can vary significantly from sample to sample within the same data set, as well as from one study to another. Formulas were derived demonstrating that the standard error of calculated nss concentrations is dependent on the nature and magnitude of the analytical errors made in measuring total concentrations. Application to a real data set indicates that this standard error is often greater than the calculated nss concentration, and that the standard error may vary by orders of magnitude for various samples in the same data set. The magnitude of the potential errors has important implications for the reliability of conclusions based on calculated nss concentrations, and the sample-to-sample variation of these errors complicates the process of determining the accuracy of summary statistics such as the volume-weighted concentration. In addition, these variations in accuracy can obscure the relationships between nss concentrations and other variables, both chemical and meteorological. This complicates investigations of source-receptor relationships and geochemical cycling, and may lead to faulty conclusions.

4. Ongoing Research

Research efforts currently under way within the GPCP include the following:

- Evaluation of shipboard data to determine factors controlling the atmospheric chemistry of the equatorial Atlantic Ocean during August and September 1986.
- Analysis of a 15-yr data record for precipitation chemistry at MLO.
- Determination of the speciation and overall importance of organic nitrogen in precipitation.

References

Church, T. M., J. N. Galloway, T. D. Jickells, and A. H. Knap, The chemistry of western Atlantic precipitation at the mid-Atlantic coast and on Bermuda, *J. Geophys. Res., 87*, 11,013-11,018, 1982.

Dayan, U., J. M. Miller, W. C. Keene, and J. N. Galloway, A meteorological analysis of precipitation chemistry from Alaska, *Atmos. Environ., 19*, 651-657, 1985.

Galloway, J. N., and A. Gaudry, The chemistry of precipitation on Amsterdam Island, Indian Ocean, *Atmos. Environ., 18*, 2649-2656, 1984.

Galloway, J. N., G. E. Likens, W. C. Keene, and J. M. Miller, The composition of precipitation in remote areas of the world, *J. Geophys. Res., 87*, 8771-8786, 1982.

Galloway, J. N., G. E. Likens, and M. E. Hawley, Acid precipitation: Natural versus anthropogenic components, *Science, 226*, 829-830, 1984.

Jickells, T. C., A. H. Knap, T. M. Church, J. N. Galloway, and J. M. Miller, Acid precipitation on Bermuda, *Nature, 297*, 55-56, 1982.

Keene, W. C., and J. N. Galloway, A note on acid rain in an Amazon rainforest, *Tellus, 36*, 137-138, 1984a.

Keene, W. C., and J. N. Galloway, Organic acidity in precipitation of North America, *Atmos. Environ., 18*, 2491-1497, 1984b.

Keene, W. C., and J. N. Galloway, Gran's titrations: Inherent errors in measuring the acidity of precipitation, *Atmos. Environ., 19*, 199-202, 1985.

Keene, W. C., and J. N. Galloway, Considerations regarding sources for formic and acetic acids in the troposphere, *J. Geophys. Res., 91*, 14,466-14,474, 1986.

Keene, W. C., and J. N. Galloway, The biogeochemical cycling of formic and acetic acids through the troposphere, *Tellus*, in press, 1988.

Keene, W. C., J. N. Galloway, and D. H. Holden, Jr., Measurement of weak organic acidity in precipitation from remote areas of the world, *J. Geophys. Res., 88*, 5122-5130, 1983.

Keene, W. C., A. A. P. Pszenny, J. N. Galloway, and M. E. Hawley, Sea-salt corrections and interpretation of constituent ratios in marine precipitation, *J. Geophys. Res., 91*, 6647-6658, 1986.

Keene, W. C., R. W. Talbot, M. O. Andreae, K. Beecher, H. Berresheim, J. C. Farmer, J. N. Galloway, M. R. Hoffman, S.-M. Li, J. R. Maben, J. W. Munger, R. B. Norton, A. A. P. Pszenny, H. Puxbaum, H. Westberg, and W. Winiwarter, An intercomparison of measurement systems for vapor- and particulate-phase concentrations of formic and acetic acids, *J. Geophys. Res.*, submitted, 1988.

Likens, G. E., W. C. Keene, J. M. Miller, and J. N. Galloway, The chemistry of precipitation from a remote terrestrial site in Australia, *J. Geophys. Res., 92*, 13,299-13,314, 1987.

Radioactivity in the Surface Air at BRW, MLO, SMO, and SPO

RICHARD LARSEN AND COLIN SANDERSON

U. S. Department of Energy, Environmental Measurements Laboratory, New York, New York 10014-3261

1. INTRODUCTION

Air filter samples are routinely collected by GMCC personnel at BRW, MLO, SMO, and SPO for the SASP. The primary objective of this program is to study the temporal and spatial distribution of specific natural and anthropogenic radionuclides in the surface air.

2. MATERIALS AND METHODS

High-volume air filter samples are continually collected on a weekly basis using Microsorban filter material. The air samplers move ~1500 m^3 of air per day through a 20-cm-diameter filter. The weekly filter samples collected at BRW and MLO are analyzed by compressing a section of the filter into a 1-2 cm^3 cylinder, which is analyzed by gamma-ray spectrometry using a high-purity germanium (HPGe) detector with a 1.5-cm-diameter well. For each site, sections of the weekly filter samples are added together to form a monthly composite sample. These composite samples are compressed into a 45-cm^3 plastic planchet, and are analyzed for gamma-ray-emitting nuclides using either HPGe n-type low-energy coaxial, or Ge(Li) or HPGe p-type coaxial high-resolution germanium detectors. The activities from specific gamma-ray-emitting radionuclides are determined by computerized analyses of the spectral data. Detailed information on SASP is periodically published [*Feely et al.*, 1985].

3. RESULTS

Table 1 presents the weekly surface air concentrations of ^{7}Be and ^{210}Pb at BRW and MLO during 1987. Table 2 presents the surface air concentrations of ^{7}Be and ^{210}Pb during 1987 in monthly composite filter samples from SPO and ^{7}Be monthly concentrations from SMO. The "less than" values for ^{7}Be at SPO result from its radioactive decay in the sample prior to analysis. These values are excluded from summary data tables. There were no announced atmospheric nuclear weapons tests or other significant releases of radioactive materials into the atmosphere during 1987, and the concentrations of the fission products ^{95}Zr, ^{137}Cs, and ^{144}Ce were below our lower limit for data reporting (0.5 fCi m^{-3}). The long-term mean monthly surface air concentrations of ^{7}Be and ^{210}Pb at BRW, MLO, SMO, and SPO are presented in Table 3. The mean values are reported along with the standard deviation at the 1σ level; the number of data points used to calculate each value is presented in parentheses.

4. DISCUSSION

The weekly concentrations of ^{7}Be and ^{210}Pb at BRW and MLO show a pronounced episodic behavior throughout 1987. ^{7}Be (half-life 53.2 days) is produced by cosmic-ray interactions in the upper troposphere and the stratosphere. ^{210}Pb (half-life 21 years) is a decay product of ^{222}Rn, which is a natural radionuclide emitted from soils. Because of their distinctly different source regions, these nuclides serve as excellent tracers for upper and lower tropsopheric sources and transport processes. We believe the three episodes of

TABLE 1. Surface Air Concentrations (fCi m^{-3}) of ^{7}Be and ^{210}Pb in Weekly Filter Samples Collected at BRW and MLO During 1987

Sampling Interval	^{7}Be	^{210}Pb	Sampling Interval	^{7}Be	^{210}Pb
		BRW			
1/ 1/87- 2/ 7/87			7/17/87- 7/24/87	15	2
2/ 7/87- 2/14/87	48	15	7/24/87- 8/ 4/87	13	1
2/14/87- 2/24/87	48	15	8/ 4/87- 8/10/87	6	< 1
2/24/87- 2/28/87	59	15	8/10/87- 8/14/87	10A	1A
2/28/87- 3/ 7/87	114	41	8/14/87- 8/21/87	17	1
3/ 7/87- 3/14/87	93	17	8/21/87- 8/28/87	14	2
3/14/87- 3/21/87	52	23	8/28/87- 9/ 8/87	34	2
3/21/87- 3/28/87	69	29	9/ 8/87- 9/14/87	13	1A
3/28/87- 4/ 4/87	69	15	9/14/87- 9/18/87	42	3
4/ 4/87- 4/11/87	98	14	9/18/87- 9/28/87	38	4
4/11/87- 4/21/87	113	19	9/28/87-10/ 3/87	36	3
4/21/87- 4/25/87	139	24	10/ 3/87-10/ 9/87	36	7
4/25/87- 4/28/87			10/ 9/87-10/17/87	18	3
4/28/87- 5/ 2/87	115	13	10/17/87-10/23/87	12	3
5/ 2/87- 5/ 9/87	68	8	10/23/87-10/30/87	60	7
5/ 9/87- 5/15/87	84	8	10/30/87-11/ 9/87	53	8
5/15/87- 5/26/87	58	6	11/ 9/87-11/16/87	52	13
5/26/87- 5/29/87	54	5	11/16/87-11/23/87	65	15
5/29/87- 6/ 3/87	48	5	11/23/87-12/ 4/87	39	13
6/ 3/87- 6/16/87	28	2	12/ 4/87-12/ 8/87	46	14
6/16/87- 6/22/87	17	1	12/ 8/87-12/14/87	35	16
6/22/87- 7/ 6/87	32	3	12/14/87-12/22/87	45	19
7/ 6/87- 7/13/87	41	3	12/22/87-12/29/87	38	12
7/13/87- 7/17/87	21	2A			
		MLO			
1/ 2/87- 1/ 8/87	173	4	7/ 1/87- 7/16/87		
1/ 8/87- 1/16/87	135	4	7/16/87- 7/22/87	176	6
1/16/87- 1/22/87	250	7	7/22/87- 8/ 1/87	104	4
1/22/87- 2/ 2/87	204	6	8/ 1/87- 8/ 7/87	638	< 1
2/ 2/87- 2/ 9/87	232	6	8/ 7/87- 8/14/87	220	5
2/ 9/87- 2/17/87	187	7	8/14/87- 8/21/87	167	7
2/17/87- 2/23/87	395	18	8/21/87- 9/ 1/87	90	7
2/23/87- 3/ 2/87	242	15	9/ 1/87- 9/ 8/87	163	5
3/ 2/87- 3/ 9/87	308	< 2	9/ 8/87- 9/15/87	184	7
3/ 9/87- 3/16/87	237	14	9/15/87- 9/22/87	262	10
3/16/87- 3/23/87	328	< 2	9/22/87-10/ 1/87	126	7
3/23/87- 4/ 1/87	219	13	10/ 1/87-10/ 8/87	174	7
4/ 1/87- 4/ 8/87	217	13	10/ 8/87-10/15/87	149	5
4/ 8/87- 4/15/87	294	15	10/15/87-10/22/87	157	4
4/15/87- 4/22/87	184	12	10/22/87-10/30/87	235	13
4/22/87- 5/ 1/87	291	9	10/30/87-11/ 6/87	117	4
5/ 1/87- 5/ 8/87	148	8	11/ 6/87-11/14/87	227	14
5/ 8/87- 5/15/87	201	10	11/14/87-11/21/87	155	4
5/15/87- 5/22/87	252	13	11/21/87-12/ 1/87	213	6
5/22/87- 6/ 1/87	278	10	12/ 1/87-12/ 8/87	258	9
6/ 1/87- 6/ 8/87	173	8	12/ 8/87-12/16/87	41?	2A
6/ 8/87- 6/15/87	233	11	12/16/87-12/22/87	61?	1A
6/15/87- 6/22/87	348	14	12/22/87-12/31/87	183	3
6/22/87- 7/ 1/87	217	11			

? doubtful values

Counting errors at 2σ are less than 20%, except A counting errors are between 20% and 100%.

TABLE 2. Monthly Surface Air Concentrations (fCi m^{-3}) of ^{7}Be at SMO and SPO, and ^{210}Pb at SPO During 1987

	^{7}Be		^{210}Pb		^{7}Be		^{210}Pb
Month	SMO	SPO	SPO	Month	SMO	SPO	SPO
Jan	68	130	2A	Jul	73	54	< 1
Feb	58	94	< 1	Aug	139	54	< 1
Mar	56	174A	2A	Sep	110	< 4	1A
Apr	58	59	< 1	Oct	114	103	< 3
May	82	77	< 1	Nov	72	190	< 1
Jun	112	< 8	1A	Dec	48	140	< 1

Counting errors at 2σ are less than 20%, except A counting error are between 20% and 100%.

TABLE 3. Long-Term Monthly Mean Concentrations (fCi m^{-3} ± 1σ) of ^{7}Be and ^{210}Pb at BRW, MLO, SMO, and SPO,

	^{7}Be				^{210}Pb		
Month	BRW	MLO	SMO	SPO	BRW	MLO	SPO
Jan	66±19 (12)	226±50 (16)	61±24 (11)	175±38 (17)	24± 7 (7)	8± 5 (10)	1± 1 (9)
Feb	64±20 (13)	198±52 (18)	57±15 (11)	157±62 (11)	23±10 (7)	9± 3 (11)	1± 1 (7)
Mar	74±20 (11)	224±43 (16)	54±13 (11)	147±58 (14)	22±10 (6)	12± 3 (9)	1± 1 (7)
Apr	75±20 (10)	209±48 (14)	50±10 (11)	111±36 (13)	19± 7 (5)	15± 5 (8)	1± 1 (6)
May	55±11 (12)	209±41 (16)	67±17 (12)	117±70 (14)	9± 4 (5)	16± 7 (8)	1± 1 (7)
Jun	26± 8 (12)	223±38 (16)	80±25 (12)	83±29 (15)	3± 1 (7)	14± 4 (9)	1± 1 (7)
Jul	25± 7 (11)	211±39 (15)	90±17 (12)	99±36 (15)	3± 1 (7)	10± 3 (9)	1± 1 (6)
Aug	19± 7 (11)	195±49 (16)	88±23 (11)	87±25 (17)	2± 1 (7)	9± 2 (10)	1± 1 (7)
Sep	27± 4 (13)	185±50 (16)	90±15 (11)	94±23 (16)	5± 2 (7)	8± 2 (10)	1± 1 (8)
Oct	42±12 (13)	182±31 (17)	79±21 (11)	101±17 (18)	9± 3 (8)	9± 4 (11)	1± 1 (8)
Nov	59±11 (12)	157±53 (17)	80±30 (12)	143±41 (15)	16± 8 (7)	7± 3 (12)	2± 2 (7)
Dec	53±20 (11)	214±52 (16)	59±16 (11)	175±47 (16)	21±10 (6)	8± 3 (9)	2± 1 (8)
Mean	48±24 (141)	202±49 (193)	72±24 (136)	123±52 (181)	13±10 (79)	10± 5 (116)	1± 1 (87)

elevated ^{7}Be with undetectable ^{210}Pb at MLO reported in 1987 (March 2-9, March 16-23, August 1-7) indicate periods when a significant descent of air masses from the upper troposphere or stratosphere may have occurred.

The monthly ^{210} Pb concentrations at SPO are low with no detectable seasonal variation, reflecting the distance of SPO from ^{210}Pb source regions. A seasonal cycle in the surface air concentrations of ^{7}Be occurs at BRW, SMO, and SPO, and a seasonal cycle in ^{210}Pb occurs at BRW and MLO. *Larsen and Feely* [1986] have related the seasonal variations of ^{7}Be and ^{210}Pb at BRW to the transport of air masses poleward during the winter, and the seasonal variations of ^{210}Pb at MLO to the transport of continental air masses to MLO during the spring. *Feely et al.* [1988] describe four factors that affect the surface air concentration of ^{7}Be at a number of the SASP sites.

Acknowledgment. We wish to thank the NOAA/GMCC staff at BRW, MLO, SMO, and SPO for the collection of air filter samples for the SASP.

REFERENCES

Feely, H.W., R.J. Larsen, and C.G. Sanderson, Annual report of the surface air sampling program, EML-440, U.S. DOE Environmental Measurements Laboratory, 82 pp., New York, 1985.

Feely, H.W., R.J. Larsen, and C.G. Sanderson, Factors that cause seasonal variations in Beryllium-7 concentrations in surface air, *J. Environ. Radioactivity*, submitted, 1988.

Larsen R.J. and H.W. Feely, Seasonal variation of ^{210}Pb and ^{7}Be at Mauna Loa and Barrow, in *Geophysical Monitoring for Climatic Change, No 14: Summary Report 1985*, edited by R.C. Schnell and R.M. Rosson, pp. 127-129, NOAA Environmental Research Laboratories, Boulder, Colo., 1986.

Precipitation Chemistry

R.S. ARTZ

Air Resources Laboratory, NOAA, Silver Spring, Maryland 20910

1. INTRODUCTION

Routine precipitation chemistry measurements continued at the 14 regional sites and at the four GMCC baseline stations. New daily monitoring protocol was instituted at three locations on the island of Hawaii and on the observatory roof in Samoa. A cooperative project, instituted through the University of Virginia and designed to measure organic acids in precipitation, continued with little change.

2. BASELINE MEASUREMENTS

Along with the initiation of the new collection protocol for the sites on Hawaii and Samoa, several other new projects were pursued at the background stations. Important events include the following:

To reduce equipment washing requirements at SMO, an automatic wet-dry Aerochem Metrics sampler was shipped and installed. Because of the drought and associated water problems at the laboratory, no samples were collected using that sampler until December 1987.

Several samples were collected by both the funnel and bottle collector, and the new Aerochem Metrics collector, during December at SMO. Preliminary indications from these samples and from paired samples similarly collected at MLO are that considerable dry deposition may be elevating precipitation ion concentrations, even with daily collection. To quantify such differences, a short-term intercomparison will be designed for studying the MLO samples.

Although the new Dionex QIC and the aging Dionex Model 10 are both currently operational, chloride data for SPO are not reported due to suspected column problems, and cations are not available (except for MLO) due to the current shortage of laboratory time. MLO monovalent cation values should be available in the next report after reanalysis.

Figures 1-5 summarize the precipitation chemistry data for 1987.

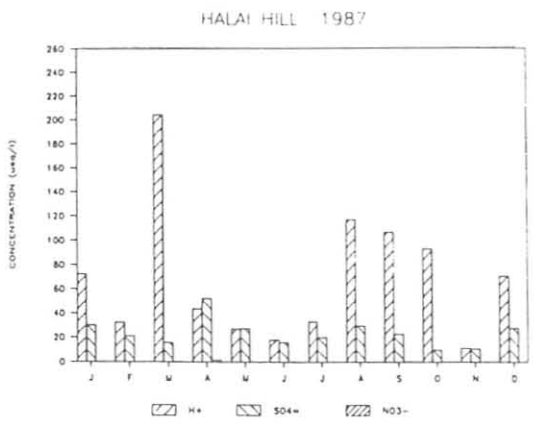

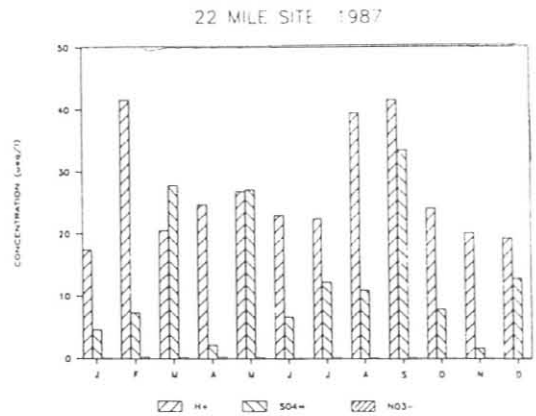

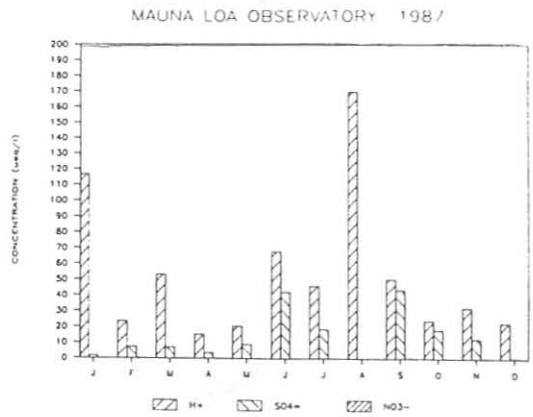

Fig. 1. Monthly precipitation weighted means for three sites on the island of Hawaii, 1987: Halai Hill, 22 Mile, MLO.

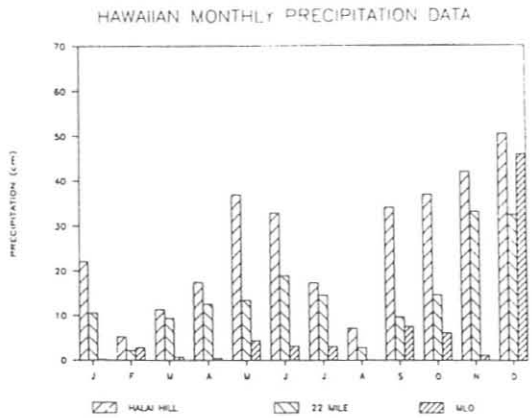

Fig. 2. Monthly precipitation at Hawaiian sites, 1987.

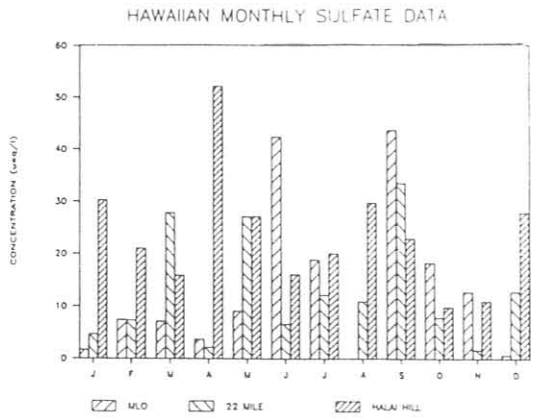

Fig. 3a. Monthly precipitation weighted sulfate means for the Hawaiian network, 1987.

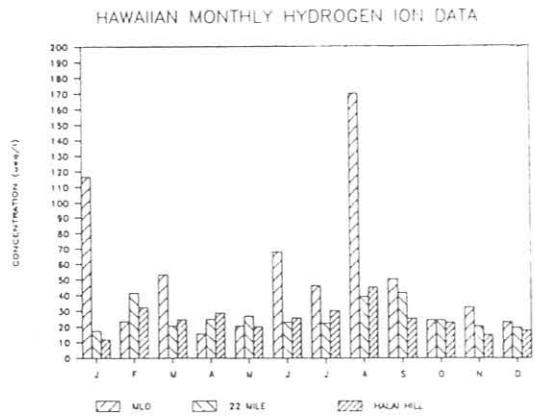

Fig. 3b. Monthly precipitation weighted hydrogen ion means for the Hawaiian network, 1987.

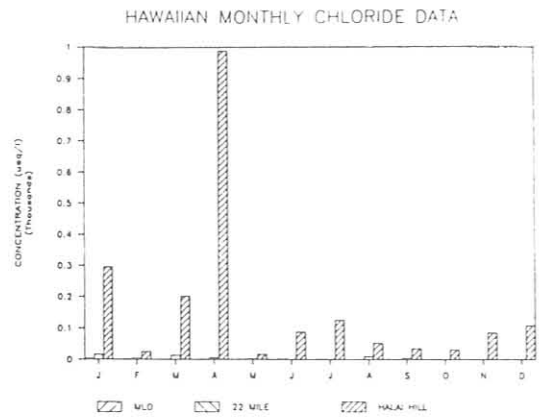

Fig. 3c. Monthly precipitation weighted chloride means for the Hawaiian network, 1987.

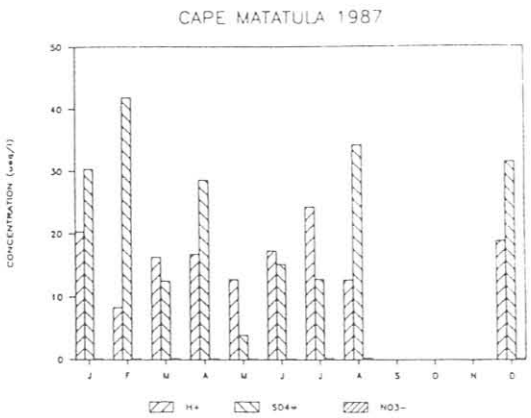

Fig. 4. Monthly precipitation weighted hydrogen ion, sulfate, and nitrate ion means for SMO, 1987.

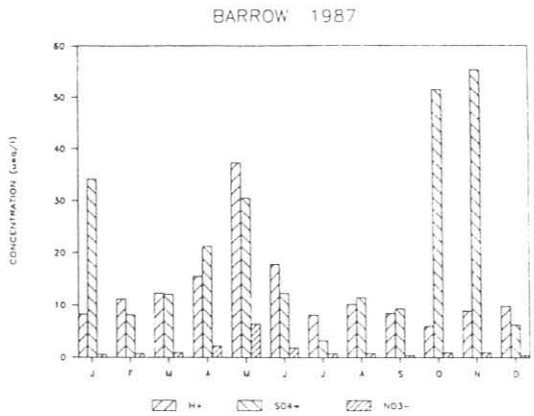

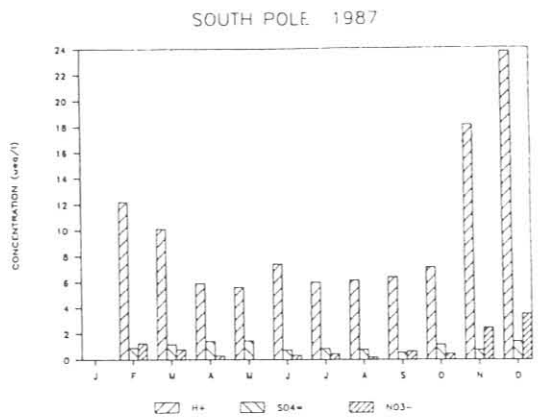

Fig. 5. Monthly average hydrogen ion, sulfate, and nitrate concentrations for snow samples collected at BRW and SPO, 1987.

3. Regional Measurements

A statistical comparison of precipitation data collected at the paired regional stations of Beeville and Victoria, Texas, and of Caribou and Presque Isle, Maine, was conducted for the purpose of determining whether stations violating siting protocols had different precipitation chemistry results than stations sited according to network rules. Small differences were found between both Maine and Texas pairs, although differences were seldom statistically significant. As a result of this study, two regional stations, Victoria and one of the Maine stations, will be closed at the end of fiscal year 1988.

UVB Monitoring Data From Mauna Loa, Boulder, and Rockville

DAVID L. CORRELL

Smithsonian Environmental Research Center, Box 28, Edgewater, Maryland 21037

Our laboratory has been continuously monitoring surface irradiance in a series of eight 5-nm band passes in the UVB at these three locations with high-precision, accurately calibrated, interference filter radiometers. Long-term data sets are now being screened and analyzed before publication and archiving. The data include 1976 to the present at Rockville, Maryland (39°N, 77°W); from July 1987 to the present at Boulder, Colorado (40°N, 105°W); and August 1984 to the present at MLO (16°N, 156°W).

Data file screening and editing include routine concerns, such as file format consistency; screening for data processing and file maintenance errors by testing for unreasonable ratios between channels, time of sunrise and sunset, and effects of cloud cover; corrections for calibration changes and equipment malfunctioning; and altered equipment design.

Until this process is completed, no data will be available. Requests for data or further information should be directed to David L. Correll, Acting Director, at the address above.

A new-generation 20-channel interference filter radiometer is under development and nearing completion. This new instrument features not only more optical channels and modern electronics, but improved PC-based data acquisition and PC-controlled choices of set gains over 3 orders of magnitude for different channels in the same operational instrument. Both present radiometers and radiometers under development operate as cosine collectors.

Nitric Acid and Aerosol Nitrate Variations at Mauna Loa

B.J. HUEBERT AND W.M. WARREN

Graduate School of Oceanography, University of Rhode Island, Narragansett, Rhode Island 02882-1197

1. INTRODUCTION

Much of the NO and NO_2 that is emitted into the atmosphere is converted to nitric acid vapor or aerosol nitrate before it is removed by dry or wet deposition. This conversion to nitrate is largely complete within a few days of the odd-nitrogen's emission; therefore, in remote areas such as at MLO, the total nitrate concentration (vapor plus aerosol) represents a fair estimate of the total odd-nitrogen concentration. It is possible that there may be similar amounts of PAN at high altitudes in clean air, but at this writing measurements are still too few to test this hypothesis.

With support from NSF, we measured nitrate concentrations at MLO for several years to help identify the important sources of odd-nitrogen compounds in remote parts of the globe [*Galasyn et al.*, 1987a, 1987b; *Robinson and Harris*, 1987]. In 1987 we initiated a program of sampling from the new walkup tower to minimize the effects of dry surface deposition of nitric acid on our nitric acid measurements.

2. MATERIALS AND METHODS

We use a teflon/nylon filter pack method for collecting atmospheric nitrate. The filter packs are exposed by a sequential sampler during 8-day visits to the site approximately every 2 months. Filters are returned to the laboratory for extraction and analysis by ion chromatography. Our final data are sorted using three criteria (wind direction, humidity, and CN count) to eliminate those samples that have been influenced by local sources on the island.

Our tower sampling was sporadic during 1987 because it had to be performed manually. The difficulties associated with nighttime filter changes limited our ability to observe diurnal changes from the tower. However, we have just finished fabricating and installing an automated sampler on the tower to facilitate such measurements in the future.

3. RESULTS AND DISCUSSION

3.1. DIURNAL VARIATION

At our earlier sampling site (about 1.5 m above the surface), we found a distinct diurnal cycle in nitric acid concentration, even when we removed the island-influenced samples. Nighttime concentrations were sometimes only half the daytime values. We believe this was the result of the rapid dry deposition of nitric acid vapor, which is resupplied from the free troposphere more rapidly in the daytime than at night.

Our preliminary tower sampling supports this idea, since the few day/night sampling data sets we collected at about 26 m show no apparent diurnal variation. We also found that nitric acid vapor concentrations decreased near the surface, while aerosol nitrate did not appear to have an altitude gradient. The nitric acid gradient was steepest during the stable nighttime hours. These observations are understandable in view of the rapid dry deposition of nitric acid vapor.

3.2. ANNUAL VARIATION

We have observed a sharp maximum in nitric acid and aerosol nitrate concentrations in the late summer. Possible reasons for this peak include reduced loss rates during this time period (which seems unlikely), increased natural sources (such as lightning in the ITCZ, which is closer in summer), and increased transport of anthropogenic material to MLO. One possible anthropogenic source is the North American continent, which is in the general direction of the origin of MLO back trajectories. We still have too little tower data to say what effect seasonal variations in surface deposition may have had in generating the annual variability we noted near the surface.

We hope that the study of the late-summer nitric acid maximum will lead to improvements in our ability to describe those coastal eddies and diurnal flows that are missed by trajectories using input winds from GCMs. The search for an explanation of the maximum continues to stimulate our research.

4. ONGOING RESEARCH

We are now making our routine measurements from the tower in an attempt to clarify the role of dry deposition and assess the actual variability of nitric acid in the free troposphere. We are planning to participate in a joint program with numerous other investigators during the spring of 1988 to study the clean troposphere's nitrogen cycle at MLO in much greater detail.

We are also trying to arrange for daily sampling throughout the year to see if the relatively high concentrations we observed in August were simply an infrequent "event" that may not be representative of the norm at MLO. To address this possibility we clearly must change to an *inclusive* sampling strategy, even though it will require some local assistance for weekly sample changes.

REFERENCES

Galasyn, J.F., K.L Tschudy, and B.J. Huebert, Seasonal and diurnal variability of nitric acid vapor and ionic aerosol species in the remote free troposphere at Mauna Loa, Hawaii, *J. Geophys. Res., 92*, 3105-3113, 1987a.

Galasyn, J.F., K.L. Tschudy, and B.J. Huebert, Authors' Reply to the Comment of Robinson and Harris, *J. Geophys. Res., 92*, 14868, 1987b.

Robinson, E., and J. Harris, Comment on "Seasonal and diurnal variability of nitric acid vapor and ionic aerosol species in the remote free troposphere at Mauna Loa, Hawaii," by J.F. Galasyn, K.L. Tschudy, and B.J. Huebert, *J. Geophys. Res., 92*, 14865-14867, 1987.

11. International Activities, 1987

During September 21-25, B. Bodhaine and R. Schnell traveled to Leningrad, U.S.S.R., to attend the *Arctic Aerosol Symposium* under the U.S.-U.S.S.R. bilateral agreement, Working Group VIII. This was the first opportunity for U.S. and U.S.S.R. scientists to work together on the Arctic haze problem. The symposium was held at the Arctic and Antarctic Research Institute in Leningrad, and was attended by eight members of the U.S. delegation and many Soviet scientists from Leningrad and Moscow.

B. Bodhaine, R. Schnell, and G. Herbert attended the *Fourth International Symposium on Arctic Air Chemistry* during September 29-October 2 at Hurdal, Norway. This meeting was hosted by the Norwegian Institute for Air Research and was devoted to the Arctic haze problem, particularly the question of long-range transport. Many of the results of the AGASP experiments were reported by scientists from many nations at this meeting.

On February 7-11, J. DeLuisi and three other U.S. representatives participated in a Working Group VIII meeting in the Soviet Union. The meeting was hosted by the Aerological Observatory at Moscow. The purpose was to provide a briefing by each side on the research being conducted on the stratospheric ozone depletion problem, and to suggest cooperative research projects that would involve combining scientific expertise and resources for solving experimental and theoretical research problems.

A cooperative South Pole Observatory lidar project was organized between the University of Rome, Italy, and GMCC. The University of Rome effort, headed by G. Fiocco, supplied a complete lidar system and trained the GMCC observers. The GMCC effort, coordinated by J. DeLuisi, provided the winter-over observers, modifications to the NSF Clean Air Facility roof (partly supplied by NSF), and a frost-proof window in the roof. The lidar measurement project will provide valuable data on cloud structure, aerosol structure, and polar stratospheric clouds.

In November, P. Franchois traveled to SPO to assist with ozonesonde flights and to install software for processing the sonde data on site. Upon his return trip, P. Franchois visited the DSIR Observatory in Lauder, New Zealand, where the use of similar software for processing ozonesonde data was implemented.

During the summer, optical adjustments were made in Boulder by R.D. Grass to Portuguese Dobson spectrophotometer no. 13, new electronics were installed into the instrument, and the instrument was recalibrated relative to World Primary Standard Dobson instrument no. 83.

During January and February, R. Evans installed automated Dobson spectrophotometer no. 72 at Lauder, New Zealand. The site is one of six NOAA and NOAA-foreign cooperative observatories where Umkehr observations are made routinely. R. Evans traveled to Huancayo Observatory, Peru, in August to repair automated Dobson spectrophotometer no. 87 located there, and to train observers in operation of the instrument.

P. Steele was appointed to the Source Gases Working Group of the Ozone Trends Panel. He wrote the section on atmospheric methane for the report of this panel. The report is due to appear in 1988 and updates *WMO Report No. 16: Atmospheric Ozone 1985*.

J. Butler and K. Egan participated in the SAGA-II experiment aboard the Soviet research vessel *Akademik Korolev* from May 30 to August 10. J. Elkins, T. Thompson, and T. Conway assisted J. Butler in setting up GC's on April 26 to May 2 before the *Korolev* left Hilo, Hawaii. J. Elkins discussed the cruise results with V. Koropolov and A. Shashkov in Hilo, Hawaii, near the end of SAGA-II from July 28 to August 1. The results of the cruise are discussed in section 8.2 of this report.

J. Elkins was a cochairman of the *International Workshop on Nitrous Oxide*, held September 15-16 in Boulder. T. Thompson and K. Egan attended the workshop and its special sessions. The purpose of the workshop, which was cosponsored by EPA, NOAA, USDA, and NASA, was to evaluate our current understanding of N_2O in the atmosphere and sources of N_2O from combustion.

J. Elkins, R. Schnell, M. Luria, and H. Sievering attended the *Sixth International Symposium on Global Atmospheric Chemisty* of the Commission on Atmospheric Chemistry and Global Pollution, Peterborough, Ontario, Canada, August 25-29. J. Elkins was a coauthor of a position paper on "Intercomparisons of Standards and Instruments" in the Global Trends and Distributions section following the CACGP meeting.

J. Elkins set up a cooperative program between the NOAH group and N. Trivett of the Atmospheric Environment Service Canada, to begin taking flask samples for N_2O, CFC-12, and CFC-11 at their Alert station in the Northwest Territories of Canada.

At the request of K. Higuchi of Atmospheric Environment Service Canada, G. Herbert participated in the *Arctic Regional Modeling Workshop* in Downsview, Ontario, May 24-26. He presented a paper titled "GMCC Long-Range Transport Models" at the workshop.

H. Bridgman of the University of New Castle, NSW, Australia, completed a 1-yr appointment at GMCC in August as a guest scientist. During this productive time in Boulder, he participated in analysis of AGASP and WATOX data, and coauthored more than ten manuscripts.

Attendees at the March GMCC Annual Meeting in Boulder included K. Higuchi, N. Trivett, S. Syminton, R. Bojkov, and G. Shah of Canada, H. Bravo of Mexico, G. Ayers of Australia, and K. Labitzke of Federal Republic of Germany.

A Soviet delegation represented by A. Frolov, V. Ivanov, A. Ivanovsky, and V. Rudakov visited GMCC under Working Group VIII during May-June. They received training on the use of ozonesondes, discussed Umkehr cooperative research, and planned further joint programs. J. Peterson attended the annual Working Group VIII planning meeting in Princeton, New Jersey, in November. At that time the protocol for 1988 was negotiated.

GMCC provided 60 ozonesonde systems to the U.S.S.R. under the WG VIII bilateral agreement. Soviet scientists were to fly the ozonesondes from their Antarctic base during 1988 as part of the Antarctic ozone hole research program.

12. Publications and Presentations by GMCC Staff, 1987

Aimedieu, P., W.A. Mathews, W. Attmannspacher, R. Hartmannsgruber, J. Cisneros, W. Komhyr, and D.E. Robbins, Comparison of in situ stratospheric ozone measurements obtained during the MAP/GLOBUS 1983 campaign, *Planet. Space Sci., 35(5)*, 563-585, 1987.

Boatman, J., and D. Henderson, Grand Canyon wind study aids in smoke management, *Park Sci., 6(4)*, 18-19, 1987.

Boatman, J.F., and D.L. Wellman, An aerosol separator for use in aircraft, paper A31B-14 presented at the AGU Fall Meeting, San Francisco, Calif., December 7-11, *EOS, 68*, 1221, 1987.

Bodhaine, B.A., Surface aerosol measurements at Barrow, Alaska, paper presented at the Arctic Aerosol Symposium, Leningrad, U.S.S.R., September 18-27, 1987.

Bodhaine, B.A., J.J. DeLuisi, J.M. Harris, P. Houmere, and S. Bauman, PIXE analysis of South Pole aerosol, *Nuclear Instr. Meth., B22*, 241-247, 1987.

Bodhaine, B.A., E.G. Dutton, J.J. DeLuisi, G.A. Herbert, G.E. Shaw, and A.D.A. Hansen, Surface aerosol measurements at Barrow during AGASP-II, paper presented at the Fourth Symposium on Arctic Air Chemistry, Hurdal, Norway, September 29-October 2, 1987.

Bridgman, H.A., G.A. Herbert, R.C. Schnell, A major haze event near Point Barrow, Alaska during AGASP-II, April 2-3, 1986, paper presented at the Fourth International Symposium on Arctic Air Chemistry, Hurdal, Norway, September 29-October 2, 1987.

Bridgman, H., B. Stunder, R. Artz, G. Rolph, R. Schnell, B. Bodhaine, and S. Oltmans, Meteorological and aerosol measurements from the NOAA WP-3D aircraft during WATOX-86, January 4-9, 1986, *NOAA Tech. Memo. ERL ARL-156*, 65 pp., NOAA Air Resources Laboratory, Silver Spring, Md., 1987.

Butler, J.H., K.B. Egan, J.W. Elkins, and T.M. Thompson, Nitrous oxide in the atmosphere, surface water, and at depth for the western Pacific and eastern Indian Oceans, paper A31B-02 presented at the AGU Fall Meeting, San Francisco, Calif., December 7-11, *EOS, 68(44)*, 1220, 1987.

Butler, J.H., R.D. Jones, J.H. Garber, and L.I. Gordon, Seasonal distributions and turnover of reduced trace gases and hydroxylamine in Yaquina Bay, Oregon, *Geochim. Cosmochim. Acta, 51(3)*, 697-706, 1987.

Chaumerliac, N., E. Richard, J.P. Pinty, and E.C. Nickerson, Sulfur scavenging in a mesoscale model with quasi-spectral microphysics: two-dimensional results for continental and maritime clouds, *J. Geophys. Res., 92*, 3114-3126, 1987.

Christofferson, R.D., and D.A. Gillette, A simple estimator of the shape factor of the two-parameter Weibull distribution, *J. Clim. Appl. Meteorol., 26*, 323-325, 1987.

De Foor, T. E., and E. Robinson, Stratospheric lidar profiles from Mauna Loa Observatory, Winter 1985-86, *Geophys. Res. Lett., 14*, 618-621, 1987.

Dickerson, R.R., G.J. Huffman, W.T. Luke, L.J. Nunnermacker, K.E. Pickering, A.C.D. Leslie, C.G. Lindsey, W.G.N. Slinn, T.J. Kelly, P.H. Daum, A.C. Delany, J.P. Greenberg, P.R. Zimmerman, J.F. Boatman, J.D. Ray, and D.H. Stedman, Thunderstorms: An important mechanism in the transport of air pollutants, *Science, 235*, 460-465, 1987.

Dutton, E.G., and J.J. DeLuisi, Aerosol opitcal depth and ratios of diffuse-sky to total solar irradiance measured from aircraft following the eruption of El Chichon, *NOAA Data Rep. ERL ARL-12*, 32 pp., NOAA Air Resources Laboratory, Silver Spring, Md., 1987.

Dutton, E.G., J.J. DeLuisi, and A.P. Austring, Measurements of solar radiation at Mauna Loa Observatory, 1978-1985, with emphasis on the effects of the eruption of El Chichon, *NOAA Data Rep. ERL ARL-13*, 35 pp., NOAA Air Resources Laboratory, Boulder, Colo., 1987.

Elkins, J.W., Measurement techniques for atmospheric nitrous oxide, paper presented at the International N_2O Workshop, Boulder, Colo., September 15-16, 1987.

Elkins, J.W., N_2O sources and sinks in aquatic ecosystems, paper presented at the International N_2O Workshop, Boulder, Colo., September 15-16, 1987.

Elkins, J.W., and M. Zahniser, Infrared measurements methods for nitrous oxide., in *EPA Research and Development Report EPA-600/8-86-035*, edited by W.S. Lanier and S.B. Robinson, 97-101, Energy and Environmental Research Corp., Chapel Hill, N.C., 1986.

Elkins, J.W., T.M. Thompson, K.B. Egan, J.H. Butler, and W.D. Komyhr, Nitrous oxide, halocarbons F-11 and F-12 from GMCC baseline stations, paper DT P 16 presented at Sixth International Symposium of the Commission on Atmospheric Chemistry and Global Pollution, Trent University, Peterborough, Ontario, Canada, August 23-29, 1987.

Feely, R.A., R.H. Gammon, B.A. Taft, P.E. Pullen, L.S. Waterman, T.J. Conway, J.F. Gendron, and D.P. Wisegarver, Distribution of chemical tracers in the eastern equatorial Pacific during and after the 1982-1983 El Niño/Southern Oscillation event, *J. Geophys. Res., 92*, 6545-6558, 1987.

Gaudry, A., T.J. Conway, and L.S. Waterman, Report on the intercomparison between the atmospheric CO_2 concentrations obtained at Amsterdam Island by the National Oceanic and Atmospheric Administration and the Centre des Faibles Radioactivites, Internal report of the Centre des Faibles Radioactivites, 15 pp., Gig-Sur-Yvette, France, 1987.

Gillette, D.A., W.D. Komhyr, L.S. Waterman, L.P. Steele, and R.H. Gammon, The NOAA/GMCC continuous CO_2 record at the South Pole, 1975-1982, *J. Geophys. Res., 92*, 4231-4240, 1987.

Herbert, G.A., GMCC long-range transport models, paper presented at the Canadian Workshop on Arctic Regional Modeling, Downsview, Ontario, Canada, May 25-26, 1987.

Herbert, G.A., H.A. Bridgman, J.M. Harris, B.A. Bodhaine, and R.C. Schnell, Meteorology and atmospheric tranport during AGASP-II, paper presented at the Fourth Symposium on Arctic Air Chemistry, Hurdal, Norway, September 28-October 2, 1987.

Herbert, G.A., H.A. Bridgman, R.C. Schnell, B.A. Bodhaine, and S.J. Oltmans, The analysis of meteorological conditions and haze distribution for the second Arctic Gas and Aerosol Sampling Program (AGASP-II), March-April 1986, *NOAA Tech. Memo. ERL ARL-158*, 67 pp., NOAA Air Resources Laboratory, Silver Spring, Md., 1987.

Herbert, G.A., E.R. Green, G.L. Koenig, and K.W. Thaut, Monitoring instrumentation for the continuous measurement and quality assurance of surface weather observations, paper presented at the Sixth Symposium on Meteorological Instrumentation, American Meteorological Society, New Orleans, La., January 12-16, 1987.

Komhyr, W.D., Ozone measurements to 40 km with ECC ozonesondes, *Promet*, Deütcher Wetterdienst, Schön and Wetzel GmbH, Frankfurt (Main), FRG, 29-31, 1987.

Komhyr, W.D., Vertical distribution of ozone at Hilo, Hawaii, 1982-1986, paper A51A-10 presented at the Fall AGU meeting, San Francisco, Calif., December 7-11, *EOS 68(44)*, 1232, 1987.

Komhyr, W.D., P.R. Franchois, B.C. Halter, and C.C. Wilson, ECC ozonesonde observations at South Pole, Antarctica, during 1986, *NOAA Data Rep. ERL ARL-11*, 213 pp., NOAA Air Resources Laboratory, Boulder, Colo., 1987.

Luria, M., C.C. Van Valin, J.F. Boatman, D.L. Wellman, and R.F. Pueschel, Sulfur dioxide flux measurements over the Western Atlantic Ocean, *Atmos. Environ., 21(7)*, 1631-1636, 1987.

Luria, M., C.C. Van Valin, D.L. Wellman, H. Sievering, J.F. Boatman, J.N. Galloway, and W.C. Keene, On the relationship between dimethyl sulfide and sulfate ions in the mid-Atlantic Ocean atmosphere, paper A12-10 presented at the AGU Fall Meeting, San Francisco, Calif., December 7-11, *EOS, 68*, 1212, 1987.

Mahfouf, J.F., E. Richard, P. Mascart, E.C. Nickerson, and R. Rosset, A comparative study of various parameterizations of the planetary boundary layer in a numerical mesoscale model, *J. Clim. Appl. Meteorol., 26*, 1672-1695, 1987.

Massey, D. M., T. K. Quakenbush, and B. A. Bodhaine, Condensation nuclei and aerosol scattering extinction measurements at Mauna Loa Observatory: 1974-1985, *NOAA Data Rep. ERL ARL-14,* 174 pp., NOAA Air Resources Laboratory, Silver Spring, Md., 1987.

Matthews, W.A., P. Aimedieu, G. Megie, J. Pelon, W. Attmannspacher, W. Komhyr, P. Marché, J. DeLa Noe, P. Rigaud, D.E. Robbins, and P.C. Simon, General comparison of ozone vertical profiles obtained by various techniques during the 1983 MAP/GLOBUS campaign, *Planet. Space Sci., 35(5),* 603-607, 1987.

Matthews, W.A., W.D. Komhyr, and P.R. Franchois, Ozonesonde observations at Lauder, New Zealand, during the spring and early summer of 1986, *PEL Rep. No. 960,* 156 pp., Department of Scientific and Industrial Research, Physics and Engineering Laboratory, Lower Hutt, New Zealand, 1987.

Nelson, D., R. Haas, J. DeLuisi, and G. Zerlaut, Results of the NRIP-7 intercomparison, November 18-21, 1985, *NOAA Tech. Memo. ERL ARL-161,* 108 pp., NOAA Air Resources Laboratory, Silver Spring, Md., 1987.

Newchurch, M.J., G.W. Grams, D.M. Cunnold, and J.J. DeLuisi, A comparison of SAGE 1, SBUV, and Umkehr ozone profiles including a search for Umkehr aerosol effects, *J. Geophys. Res., 92,* 8382-8390, 1987.

Peterson, J.P., Atmospheric greenhouse gases: recent trend, paper presented at the Eightieth Annual Meeting of the Air Pollution Control Association, New York, N.Y., June 21-26, 1987.

Ray, J.D., M. Luria, and C.C. Van Valin, Latitudinal changes of atmospheric hydrogen peroxide during summer, paper A12-02 presented at the AGU Fall Meeting, San Francisco, Calif., December 7-11, *EOS, 68,* 1212, 1987.

Reinking, R., and J.F. Boatman, Upslope precipitation events, in *Mesoscale Meteorology and Forecasting,* edited by P. Ray, American Meteorological Society, Boston, Mass., 437-463, 1987.

Reinsel, G.C., G.C. Tiao, A.J. Miller, D.J. Wuebbles, P.S. Connell, C.L. Mateer, and J.J. DeLuisi, Statistical analysis of total ozone and stratospheric Umkehr data for trends and solar cycle relationship, *J. Geophys. Res., 92,* 2201-2209, 1987.

Richard, E., N. Chaumerliac, J.F. Mahfouf, and E.C. Nickerson, Numerical simulation of orographic enhancement of rain with a mesoscale model, *J. Clim. Appl. Meteorol., 26,* 661-669, 1987.

Robinson, E., Book Review: R. E. Munn and H. Rodhe, Compendium of Meteorology, Volume II, Part 6, Air Chemistry and Air Pollution Meteorology, WMO No. 364, World Meteorological Organization, 209 pp., Geneva, Switzerland, 1985, *Water Air Soil Poll., 33,* 447-448, 1987.

Robinson, E., and T.E. DeFoor, Stratospheric aerosol conditions over Mauna Loa during recent volcanic interregnum periods, paper M2-67 presented at IUGG/IAMAP meeting, Vancouver, British Columbia, August 1987.

Robinson, E., and J. Harris, Comment on "Seasonal and diurnal variability of nitric acid vapor and ionic aerosol species in the remote free troposphere at Mauna Loa, Hawaii" by J.F. Galasyn, K.L. Tschudy, and B. J. Huebert, *J. Geophys. Res., 92,* 14865-14867, 1987.

Ruhnke, L.H., and R.C. Schnell, Arctic Haze, paper presented at the DOD Symposium and Workshop on Arctic and Arctic-Related Environmental Sciences, Washington, D.C., January 27-30, 1987.

Schnell, R.C., Arctic haze measurements from aircraft during AGASP I and II, paper presented at the Arctic Aerosol Symposium, Leningrad, U.S.S.R., September 18-27, 1987.

Schnell, R.C., Gas and aerosol distribution in the Arctic during AGASP-II, paper presented at the Fourth International Symposium on Arctic Air Chemistry, Hurdal, Norway, September 29-October 2, 1987.

Schnell, R.C., Long range transport of anthropogenic pollutants into the Arctic, paper presented at the Sixth International Symposium of the Commission on Atmosheric Chemistry and Global Pollution, Peterborough, Canada, August 23-29, 1987.

Schnell, R.C., Use of a NOAA WP-3D with multi-sensor gas and aerosol sampling systems: WATOX and AGASP-II, 1986, Proceedings, Second Airborne Science Workshop, p. 151, University of Miami, Miami, Fla., February 3-6, 1987.

Schnell, R.C., and R. M. Rosson, Geophysical Monitoring for Climatic Change, No. 15: Summary Report 1986, 155 pp., NOAA Air Resources Laboratory, Boulder, Colo., 1987.

Schnell, R.C., H.A. Bridgman, P.S. Naegele, and T. Watson, The NOAA WP-3D meteorological, aerosol, and gas systems and flight operations on WATOX-86, WATOX Special Issue, *Global Biogeochem. Cycles, 1,* 297-307, 1987.

Sheridan, P.J., and R.C. Schnell, Cascade impactor studies of aerosol collected during AGASP-II, flights 201-203, paper presented at the Fourth International Symposium on Arctic Air Chemistry, Hurdal, Norway, September 29-October 2, 1987.

Sievering, H., Comments on "Evaluation of accuracy with which dry deposition can be measured with current micrometeorological techniques", *J. Clim. Appl. Meteorol., 26,* 652, 1987.

Sievering, H., Dynamics of sulfur exchange at the air/forest canopy interface: A review of throughfall inferred deposition rates, *Global Biogeochem. Cycles, 1(3),* 233-249, 1987.

Sievering, H., Midwest/Western/Eastern U.S. precipitation and aerosol sulfate: Differences attributable to natural source inputs?, *Atmos. Environ., 21,* 2525-2530, 1987.

Sievering, H., Small particle eddy flux measurements at the BAO: Deposition under high windspeed conditions, *Atmos. Environ., 21,* 2179-2185, 1987.

Sievering, H., J. Boatman, H. Horvath, M. Luria, and C.C. Van Valin, Heterogeneous conversion of SO_2 to SO_4 in coarse fraction sea-derived aerosol, paper presented at AGU, San Francisco, Calif., December 7-11, 1987.

Sievering, H., J.F. Boatman, L. Gunter, H. Horvath, D. Wellman, and S. Wilkison, Size distribution of sea-source aerosol particles: A physical explanation of observed differences, nearshore vs. open sea, *J. Geophys. Res., 92,* 14850-14860, 1987.

Stearns, L.P., Aspects of the local circulation at the Grand Canyon during the fall season, *J. Clim. Appl. Meteorol., 26,* 1987.

Steele, L.P., P.J. Fraser, R.A. Rasmussen, M.A.K. Khalil, T.J. Conway, A.J. Crawford, R.H. Gammon, K.A. Masarie, and K.W. Thoning, The global distribution of methane in the troposphere, *J. Atmos. Chem., 5,* 125-171, 1987.

Steele, L.P., K.A. Masarie, P.M. Lang, and R.C. Martin, The distribution and growth rate of atmospheric methane, paper presented at the Sixth International Symposium of the Commission on Atmospheric Chemistry and Global Pollution, Trent University, Peterborough, Ontario, Canada, August 23-29, 1987.

Van Valin, C.C., and E. Ganor, Air pollution measurements at the Boulder Atmospheric Observatory, *Water Air Soil Pollut., 35,* 357-372, 1987.

Van Valin, C.C., H. Berresheim, M.O. Andreae, and M. Luria, Dimethyl sulfide over the Western Atlantic Ocean, *Geophys. Res. Lett., 14(7),* 715-718, 1987.

Van Valin, C.C., M. Luria, J.D. Ray, R.L. Gunter, D.L. Wellman, and J.F. Boatman, Seasonal variations of H_2O_2 as observed in CURTAIN, paper A12-03 presented at the AGU Fall Meeting, San Francisco, Calif., December 7-11, *EOS, 68,* 1212, 1987.

Van Valin, C.C., M. Luria, D.L. Wellman, R.L. Gunter, and R.F. Pueschel, Natural sulfur flux from the Gulf of Mexico: Dimethyl sulfide, carbonyl sulfide, and sulfur dioxide, *NOAA Tech. Rep. ERL 432-ARL 9,* 14 pp., NOAA Air Resources Laboratory, Boulder, Colo., 1987.

Van Valin, C.C., J.D. Ray, J.F. Boatman, and R.L. Gunter, Hydrogen peroxide in air during winter over the South-Central United States, *Geophys. Res. Lett., 14,* 1146-1149, 1987.

Van Valin, C.C., D.L. Wellman, and L.P. Stearns, Aerosol and cloudwater properties at Whiteface Mountain, New York, *Water Air Soil Pollut., 34,* 369-383, 1987.

Wellman, D.L., J.F. Boatman, C.C. Van Valin, S.W. Wilkison, R.L. Gunter, J.D. Ray, and M. Luria, Airborne sampling for validation of the regional acid deposition model-the CURTAIN experiment, paper A31B-09 presented at the AGU Fall Meeting, San Francisco, Calif., December 7-11, *EOS, 68,* 1220, 1987.

13. Acronyms and Abbreviations

ACR	active cavity radiometer
ADN	Automated Dobson Network
ADR	Adrigole, Ireland (ALE/GAGE station)
AES	Atmospheric Environment Service, Canada
AGASP	Arctic Gas and Aerosol Sampling Program
ALE	Atmospheric Lifetime Experiment
ANATEX	Across North America Tracer Experiment
AOML	Atlantic Oceanographic and Meteorological Laboratory, Miami, Florida (ERL)
AOU	apparent oxygen utilization
ARL	Air Resources Laboratory, Silver Spring, Maryland (ERL)
ARM	Aerosols and Radiation Monitoring Group, Boulder, Colorado (GMCC)
ASCS	Alaska Soil Conservation Service
ASR	Aerosols and Solar Radiation
AQG	Air Quality Group, Boulder, Colorado (GMCC)
BAPMoN	Background Air Pollution Monitoring Network
BRAM	battery random access memory
BRW	Barrow Observatory, Barrow, Alaska (GMCC)
CACGP	Commission on Atmospheric Chemistry and Global Pollution
CAF	Clean Air Facility
CAMS	Control and Monitoring System
CFC	chlorofluorcarbon
CFC-11	trichlorofluoromethane
CFC-12	dichlorodifluoromethane
CGO	Cape Grim Observatory, Australia, (CSIRO and ALE/GAGE station)
CIRES	Cooperative Institute for Research in Environmental Sciences, University of Colorado, Boulder, Colorado
C.L.	confidence level
CMO	Cape Meares, Oregon (ALE/GAGE station)
CN	condensation nuclei
CNC	condensation nucleus counter
CNRS	Centre National de la Recherche Scientifique
CRT	cathode ray tube
CSIRO	Commonwealth Scientific and Industrial Research Organization, Australia
CSU	Colorado State University
CURTAIN	Central United States RADM Test and Assessment Intensives
DEC	Digital Equipment Corporation
DEW	distant early warning
DMS	dimethyl sulfide
DOE	Department of Energy
DOI	Department of Interior
DSIR	Department of Scientific and Industrial Research, New Zealand
DOY	day of year, Julian
DU	Dobson unit
DWR	Daily Weather Report
EC	elemental carbon
ECC	electrochemical concentration cell
ECD	electron capture detector
EC-GC	electron capture gas chromatograph
ECMWF	European Center for Medium-Range Weather Forecasts
EG&G	Edgerton, Grier, and Germerhausen, Inc.
EKTO	(a commercial name for a prefabricated building)
EML	Environmental Measurements Laboratory (DOE)
ENSO	El Niño/Southern Oscillation
EPA	Environmental Protection Agency
ERL	Environmental Research Laboratories, Boulder, Colorado (NOAA)

FID	flame ionization detector
FIDO	(electronic bulletin-board system for IBM PC)
FRG	Federal Republic of Germany (West Germany)
FT	Fourier transform
FWNIP	filter wheel normal incidence pyrheliometer
GAGE	Global Atmospheric Gases Experiment
GC	gas chromatograph
GCM	general circulation model
G.E.	General Electric
GFDL	Geophysical Fluid Dynamics Laboratory, Princeton, New Jersey (ERL)
GLOBE	Global Backscatter Experiment
GMCC	Geophysical Monitoring for Climatic Change, Boulder, Colorado (ARL)
GPCP	Global Precipitation Chemistry Project
GSA	General Services Administration
GTE	General Telegraphic Electronics
HAO	High Altitude Observatory
HASL	Health and Safety Laboratory (EPA)
HP	Hewlett-Packard
IBM	International Business Machines
IGP	Instituto Geofisico del Peru
IR	infrared
ISWS	Illinois State Water Survey
ITCZ	inter tropical convergence zone
LAWS	Laser Atmospheric Wind Sounder
LEAPS	Low Electron Attachment Potential Species
LED	light-emitting diode
LOPC	laser optical particle counter
LST	local standard time
LORAN	long-range aid to navigation
MASC	Mountain Administrative Support Center, Boulder, Colorado
MLO	Mauna Loa Observatory, Hawaii (GMCC)
MO3	meteorology and ozone (CAMS unit)
MLRA	Major Land Resources Area
MSL	mean sea level
MTG	Monitoring Trace Gases Group, Boulder, Colorado (GMCC)
NADP	National Atmospheric Deposition Program
NAPAP	National Acid Precipitation Assessment Program
NARL	Naval Arctic Research Laboratory, Barrow, Alaska
NASA	National Aeronautics and Space Administration
NBS	National Bureau of Standards
NCAR	National Center for Atmospheric Research, Boulder, Colorado
NDIR	non-dispersive infrared analyzer
NESDIS	National Environmental Satellite, Data, and Information Service
NIP	normal incidence pyrheliometer
NOAA	National Oceanic and Atmospheric Administration
NOAH	Nitrous Oxide And Halocarbons Group, Boulder, Colorado (GMCC)
NRBS	non-Rayleigh backscatter
NRI	National Resource Inventory
NRIP	New River Intercomparison of Pyrheliometers
NSF	National Science Foundation
NWR	Niwot Ridge, Colorado
NWS	National Weather Service
NWT	Northwest Territories, Canada
NZARP	New Zealand Antarctic Research Program
OAO	Office of Aircraft Operations
OGC	Oregon Graduate Center, Beaverton, Oregon
PAN	peroxyacepyl nitrate
PC	personal computer

P.I.	Principal Investigator
PLOT	porous-layer, open tubular (columns)
PMEL	Pacific Marine Environmental Laboratory, Seattle, Washington (ERL)
PRECP	Processing of Emissions by Clouds and Precipitation Experiment
PROM	programmable read-only memory
P^3	Portable Pressurizer Pack (air sampler)
RADM	Regional Acid Deposition Model
RITS	Radiatively Important Trace Species
RL-2	Research Laboratory No. 2, Boulder, Colorado
RPB	Ragged Point, Barbados (ALE/GAGE station)
SAFE	Southeastern Alaska Flux Experiment
SAGA	Soviet-American Gas and Aerosol (Experiment)
SAGE	Stratospheric Aerosol and Gas Experiment
SASP	Surface Air Sampling Program
SBUV	solar backscattered ultraviolet (satellite ozone instrument)
s.d.	standard deviation
SEASPAN	SEAREX South Pacific Aerosol Network
SERI	Solar Energy Research Institute
SIO	Scripps Institution of Oceanography, La Jolla, California
SLPM	standard liters per minute
SMO	Samoa Observatory, American Samoa (GMCC)
SOLRAD	solar radiation
SUNYA	State University of New York at Albany
SPO	South Pole Observatory, Antarctica (GMCC)
SRF	Solar Research Facility
SRM	standard reference material
STP	standard temperature and pressure (0°C and 1 atm)
TOGA	Tropical Ocean Global Atmosphere
TOMS	Total Ozone Mapping Spectrometer
TSI	Thermo Systems Incorporated
UAF	University of Alaska, Fairbanks
UIC	Ukpiagvik Inupiat Corporation
UPS	uninterruptable power supply
URAS	(a commercial CO_2 analyzer)
URI	University of Rhode Island, Kingston, Rhode Island
USDA	United States Department of Agriculture
USGS	United States Geological Survey
UV	ultraviolet
WASC	Western Administrative Sevice Center, Seattle, Washington
WATOX	Western Atlantic Ocean Experiment
WERIS	Wind Energy Resource Information System
WMO	World Meteorological Organization, Geneva, Switzerland
WPL	Wave Propagation Laboratory, Boulder, Colorado (ERL)
ZRAM	"Z" random access memory
ZSCD	zenith-sky cloud detector

*U.S. GOVERNMENT PRINTING OFFICE:1994-673-018/00047